# Delineating the Mechanism of Heterotypic Multicomponent Phase Separation of Tau using Multicolor Fluorescence Imaging and Single-Molecule FRET

**SANDEEP KUMAR RAI**

*A thesis submitted for the partial fulfillment of the degree of*

***Doctor of Philosophy***

**Department of Chemical Sciences**

**Indian Institute of Science Education and Research Mohali**

**Knowledge City, Sector 81, SAS Nagar, Manauli PO, Mohali 140306, Punjab, India**

**May, 2024**

Dedicated to

my family

*“Education without values, as useful as it is, seems rather to make man a more clever devil.”*

*-C. S. Lewis*

# Declaration

The work presented in this thesis has been carried out by me under the guidance of Prof. Samrat Mukhopadhyay at the Indian Institute of Science Education and Research Mohali. This work has not been submitted in part or in full for a degree, a diploma, or a fellowship to any other universityor institute. Whenever contributions of others are involved, every effort is made to indicate this clearly, with due acknowledgement of collaborative research and discussions. This thesis is a bonafide record of original work done by me and all sources listed within have been detailed in the bibliography.

**Date:** **Sandeep Kumar Rai**

In my capacity as the supervisor of the candidate's thesis work, I certify that the above statements by the candidate are true to the best of my knowledge.

**Date:** **Prof. Samrat Mukhopadhyay**

# Acknowledgements

The successful accomplishment of this thesis is attributed to the remarkable support and collaboration extended by numerous individuals. I would like to seize this opportunity to convey my profound gratitude to everyone who has been with me throughout this journey. I sincerely appreciate every individual I have had the privilege of collaborating with, as your contributions have been instrumental in shaping the outcome. Your dedicated efforts have decisively influenced the trajectory, and I am genuinely pleased with the unfolding of events.

First and foremost, I would like to thank my Ph.D. supervisor and super mentor, Prof. Samrat Mukhopadhyay. I am immensely grateful for his unwavering support and invaluable guidance throughout this journey from day one. Under his mentorship, I discovered the realm of the scientific world, a pursuit that I never thought possible, and with each passing day, I became surer about what I wanted. I learned so many things from him, which is hard to mention here, though I will try to recount those. His consistent encouragement and the environment he provided in the lab propelled me to step outside my comfort zone and pushed me to explore and simulate various things that otherwise would not have been possible. I cannot express enough gratitude for his belief in my capabilities and the freedom he provides in the lab. He always corrected my faults and pushed me in the right direction. His relentless pursuit of understanding and intellectual curiosity has always inspired me to strive for excellence. The stimulating discussions with him on the lab projects, fluorescence, academic life, cricket, geography, and the science happening in the field, I enjoyed the most. In a few words, I can say that after my parents, who gave birth to me and seeded good manners and discipline, provided food and support throughout my academic career, Samrat truly shaped my personality and has had an immense impact on my character. Also, I will miss all kinds of sweets he carries to the lab after returning from foreign trips. I will try to continue his legacy in my entire career.

I sincerely thank my doctoral committee members, Dr. Sabyasachi Rakshit, and Dr. Sanchita Sengupta, for their support, annual evaluation, and valuable suggestions on my thesis work. They have provided phenomenal critiques of my work and progress.

The one person with whom I never overlapped on the working bench but was lucky enough to be guided in our every encounter is Dr. Mily Bhattacharya (#the First reviewer). I owe a special thanks to Dr. Mily for all the support and evaluation of my work progress, critically reviewing manuscripts, guidance, encouraging pep talks, and motivating punch lines, which she often put

on her WhatsApp status, which usually happened to be on a very tough day. I will always cherish those moments and acts. Thank you so much, Mily.

I want to sincerely thank Dr. Neha Jain for her constant moral support, encouragement, and belief in my capabilities, as well as for extra cookies and parties. I also want to take this opportunity to thank my "X" friend-cum-mentor, Dr. Subhabrata Maiti, for his intense scientific discussions as well as sometimes behind the story of any paper/grants/news, which has no boundary of traditional science. Neha and Subhabrata are the crucial catalysts of my academic career, and every opportunity of their interactions led me to pursue academia.

I want to thank all my colleagues outside and in the lab for their help, patience, and contribution to my thesis work. I thank Priyanka Singh, Adriana Savastano, Prof. Markus Zweckstetter (University of Göttingen, Germany), Roopali Khanna, Anusha Sarbahi, Anamika Avni, Ashish Joshi, and Ekta Shandilya for their contributions to my thesis work. I thank Prof. Elizabeth Rhoades (University of Pennsylvania, USA), Prof. Witold Surewicz (Case Western Reserve University, USA), and Prof. Deepak Sharma (CSIR-IMTECH, India) for their kind gifts of DNA plasmids. I acknowledge the Council of Scientific and Industrial Research (CSIR) for providing a doctoral fellowship and IISER Mohali for providing facilities and supporting the travel expenses that enabled me to attend an international scientific meeting at IIT Madras.

I would also like to thank our super-resolution microscopy support staff, Taseen, Ikram, and Bindiya, for their immense support in maintaining the facility in the best possible way.

I want to thank Vidya Bhaiya for all the work he does and for putting an unplanned autoclave on any day of the week.

I would also like to extend gratitude to our institute librarian, administrative staff, and housekeeping staff for their continuous support and for maintaining institute facilities in the best possible way.

I was fortunate enough to share the bench with the brightest and humble senior personalities in the lab. I will start with Priyanka Madhu, who mentored me during the start of my PhD. I learned many things from her, including temperament, a never-say-die attitude, patience, and critical assessment of ideas and data. She has been a fantastic mentor. She always kept a close eye on my progress. I thank Priyanka Dogra for her stimulating scientific discussions in the lab and during coffee breaks. I have always admired her for pushing her limits and having a fighting attitude. I am more than thankful to Aishwarya Agarwal, with whom I thoroughly

enjoy working with, she has been a fantastic collaborator cum mentor, and I will always cherish those periods. I am greatly thankful to Debapriya Das. She was my go-to person in any doubt in fluorescence. I got to learn various things from her, including professionalism. She always stood by my side whenever I stumbled. I overly enjoyed the company of Sayanta Mahapatra, who has always been a strong well-wisher of mine. His wittiness, "one more punch" in adverse conditions, and critical assessment of any data have always impressed me and helped me fight bad days in the lab. I will miss his "out-of-nowhere" jokes, which somehow ease the pressure in the lab. I also extend my thanks to Swapnil and especially Anupa Majumdar; they have been phenomenal colleagues. Anupa was the person who guided me in starting phase separation of tau full-length in the lab and consistently monitored my progress.

Now, I want to thank my batchmates Ashish Joshi, Lisha Arora, Ekta Shandilya, and so-called batchmate Anamika Avni for their contribution and support throughout this journey. They always provided extra cushioning and helped me come out of my comfort zone. Lisha has been a great colleague and friend who I know can go to any extent if I am in need. She always takes care of every minute thing that I am sure I would have forgotten to carry on any lab-outing. I always enjoyed annoying her randomly and discussing fluorescence. Thank you, Lisha, for always standing by my side.

I will always cherish the early bird fighting with Anamika Avni. She has been a fantastic colleague and cheerful friend who shared a witty bond with me and consistently pushed me to be a better version of myself. She has helped me learn AFM and Raman and has always been there for me whenever I was in need.

I want to thank Ashish for playing the "friend cum Elder Brother" role throughout my stay at IISER Mohali, outside campus stays during the COVID period, as well as in PhD journey. Both of us always feel that we have some background connection, which we have yet to discover fully. I always enjoy early morning discussions on Cricket, IPL, movies, and NEWS with him, as well as serious discussions on scientific matters and day-to-day life. I can safely say he was my eye/ear for the outside world, and we share a mutual respect, which I think is rare. He always takes care of my uncomfortable zone, and I always try to count on him blindly. To sum up, the one person with whom I can share my 2-storey apartment and academic space is Ashish where we will continue our scientific quest together on full-capability.

Now, I want to extend my thanks to Ekta Shandilya, "The Confident One." She has been a strong personality and the most independent individual I have ever met. She has always been

there for me through the ups and downs and has been a steadfast companion, offering unwavering support during my moments of vulnerability, both professionally and personally. I owe a special acknowledgment to her, who has consistently been a friend in need. From pointing out where I went wrong to guiding me on how to make things right, her counsel has been invaluable. I am truly grateful for her presence in my life.

I owe my sincere thanks to Roopali Khanna, who accidentally became my mentee and later major collaborator. I must say I was very lucky as she joined me in the midst of my PhD and I was going through a hard period. She has a little "annoying angry bird" kind of personality, which was complementary to my personality, so we vibe together very well on and off the bench. Roopali remained a very hard-working scientist who was ready to do any experiment anytime, face any deadlines, and was very supportive throughout our association. Her help during my thesis writing, the future application process, and critically reviewing it is unparalleled.

I can't thank enough Anusha, "the laughter girl," Anuja, "the hard-working one," Dhruba, "BBC," and Snehasis, "handsome like me," for making this journey cheerful and memorable. Your presence and contributions have made my journey truly extraordinary, filled with countless cherished moments. I am immensely grateful for the opportunity to learn so much from each of you. Special shout-out to Anusha; she has contributed enormously to my thesis, as well as to her nonchalant yet focused personality, which I would like to learn from her. Thank you for being an integral part of my journey and enriching it in ways I could have never imagined.

I want to thank Dr. Dipankar Bhowmik, "Bangali Bhaiya," for his constant encouragement and moral support throughout the journey. I always cherish random night outings with him on weekends and discussing exciting science happening in various interdisciplinary fields and techniques. He has been a phenomenal "criticque cum friend" in many ways.

I thank the master thesis students, Shalini "The Rebel Star," Sneha "Dhaakad," Jyoti "Star" and rotation students, Rakshana Balaji "The Sincere," Keshav and Aayush "Chintu & Pintu" for their lively attitude and raw innocency. They are the ones who kept the lab environment cheerful. I owe a special thanks to Shalini for her help during my thesis writing. "Keep shining, boss; you are more than what you think you are." I thank Deepti for being a warm junior in the lab. I want to thank Swastik, "the perfect one," for being such an amazing person and junior cum friend in the lab. I wish him all the achievements and wish I could win the IPL trophy for

him before RCB does. I extend my thanks to Neha, “the curious one,” and Harshita, “the stylist,” for being an amazing part of my journey. They all hold a special place in my story.

I take this opportunity to thank my friends in Dr. Rachna Lab, Dr. Mahak Lab, and Dr. Bachawat Lab, especially Deeptodeep and gang, Sankalita, Shri Harsha, Shradha, Nikita, and Pratiksha for sharing enzymes, and chemicals, for a moment of a laugh. It’s because of them I could plan my work without worrying about the availability of enzymes, autoclave machines, and incubators.

Finally, I want to express my heartfelt gratitude to my family, whose unwavering presence has been the cornerstone of my journey. Their sacrifice, blessings, support, and unconditional love have made every step of this path very easy. My mother has been my guiding light, teaching me resilience and self-reliance. My father has always taken immense pride in my achievements and has provided me with nothing but the best. From him, I learned so much, especially discipline and “losing is not an option.” My elder brothers, Rahul and Ajeet, have always stood by my side and protected me from outside noise, offering guidance and serving as a beacon of light. My sisters Rani and Soni have been my closest confidante, offering support and understanding. I want to sincerely thank them for their love, blessings, and the immense pride they always have in me. In every possible way, I want to acknowledge and thank my family for everything they have done for me. It is because of their unwavering support and sacrifices that I am who I am today. To my family and mentors, I dedicate this thesis as a testament to their love, support, and belief in me.

**Sandeep Kumar Rai**

*****

# Synopsis

# Delineating the Mechanism of Heterotypic Multicomponent Phase Separation of Tau using Multicolor Fluorescence Imaging and Single-Molecule FRET

## Chapter 1. Introduction

Biological systems exist as complex, interconnected networks of a multitude of intricate biochemical and signaling pathways, each working in perfect harmony with the other to carry out a range of functions essential for the survival and maintenance of the system as a whole. Very often, a distinct chemical environment becomes crucial in order for each such function to be carried out in isolation, even in the densely crowded surroundings of a cell. Compartmentalization, therefore, becomes an indispensable feature of the cellular milieu and is fundamental in maintaining the functional coherency of a cell. Emerging evidence now suggests that apart from various conventionally studied membrane-bound organelles, cells can selectively partition specific subsets of biomolecules into on-demand, membrane-less, dynamic, mesoscopic assemblies formed via the physical process of phase separation, which results in the spontaneous emergence of co-existing phases of different compositions, having minimum free energy, from a single homogeneous phase. The resulting membrane-less, non-canonical spherical structures, often termed biomolecular condensates, can effectively function as membrane-less organelles (MLOs) owing to their permeability and ability to selectively concentrate biomolecules and are emerging as central players at all levels of essential cellular activity: ranging from the expression and regulation of genes to the modulation of intricate signaling pathways. Well-studied membrane-less condensates include the nucleolus, which acts as the primary site for ribosome biogenesis, in addition to Cajal bodies and P bodies that regulate splicing and function as translation regulators, respectively. These dense membrane-less assemblies are mainly enriched with biological polymers such as proteins and nucleic acids, in addition to small molecules which often regulate their formation and dissolution with the cell, in addition to modulating their material properties, which are a direct consequence of the underlying interactions within the components of these condensates. Generally, a fuzzy network of weak, transient, and non-covalent interactions promotes phase separation. In the cellular context, proteins having low complexity domains (LCD), intrinsically disordered

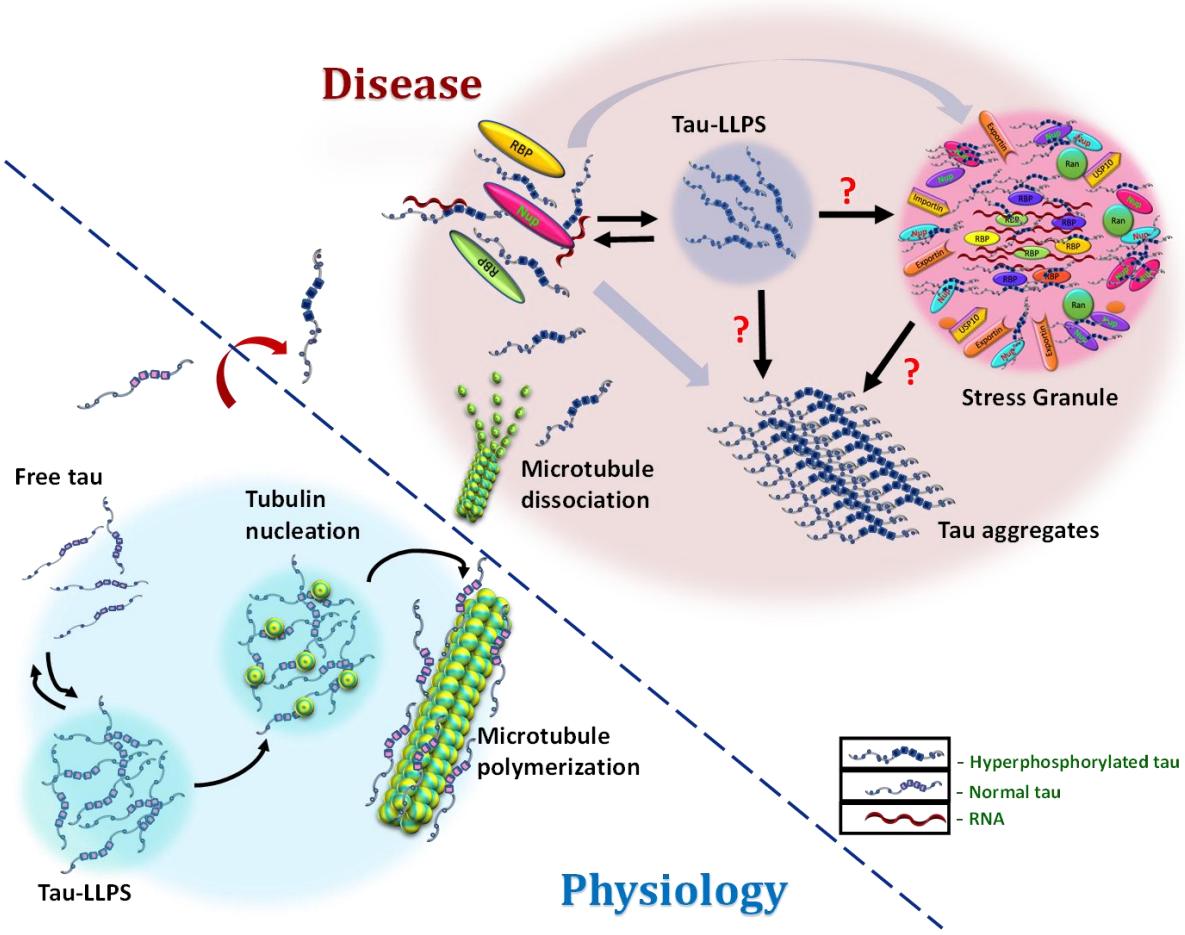


Rai, S. K., Savastano, A., Singh, P., Mukhopadhyay, S. & Zweckstetter, M., *Protein Sci.* (2021)

regions (IDRs), and globular domains can impart multivalency to the system and, together with charged elements like nucleic acids, drive the formation of spatiotemporally regulated, multicomponent biological condensates of different sizes and order. The interactions amongst the constituents of condensates are synchronized with the compositions and material properties of biological condensates in cells, which can, therefore, vary with the physiology of the cell. Over time or under stress conditions, such condensates can undergo liquid-to-solid aberrant phase transitions, which may disrupt the complex, interconnected network that is essential for a cell's operation in addition to accelerating the formation of toxic amyloid-like aggregates that are implicated in cellular dysfunction. Concurrent evidence now suggests that such transitions are involved in the development of some deadly neurodegenerative disorders, such as Alzheimer's Disease and amyotrophic lateral sclerosis (ALS), in addition to diseases such as cancer. In fact, neurofibrillary tangles composed of the human microtubule-associated protein tau (MAPT) are a characteristic hallmark of such progressive neuronal disorders, which are

collectively known as tauopathies. Although tau is a central player in maintaining the cytoskeletal network in cells, its physiological activities are overshadowed by its unregulated phase separation, accelerating its aggregation. Numerous studies have reported the co-deposition of other neuronal IDPs in such pathogenic aggregates in conjugation with tau, suggesting a complex interplay of molecular interactions in guiding the overlapping neuropathology of several such diseases. On the other side of the coin, tau also interacts with components of the cellular machinery that are particularly important in perturbing or halting protein misfolding and amyloid formation. These proteins, called molecular chaperones, form the cellular protein quality control machinery and are essential in disposing of any potentially misfolded species in the cell. Interestingly, the role of phase separation in these aspects remains elusive. Using a combination of biochemical and biophysical tools, this thesis delves into the heterotypic phase separation of tau, both in the context of the promotion and abrogation of its aggregation.

## Chapter 2. Materials and Methods

In this chapter, we outline the methodologies employed in this thesis to investigate the complex coacervation of tau. Employing a multidisciplinary approach, we examined different facets of tau phase behavior using a wide range of biophysical, molecular, and microscopic tools. These tools encompassed various techniques such as recombinant protein purification, site-directed mutagenesis, ensemble, single-molecule fluorescence-based microscopic tools for steady-state and time-resolved fluorescence anisotropy measurements, single-molecule förster energy transfer (smFRET), Airyscan confocal imaging, Raman spectroscopy, atomic force imaging, transmission electron microscopy imaging, and ultracentrifugation.

## Chapter 3. Heterotypic electrostatic interactions control complex phase separation of tau and prion into multiphasic condensates and co-aggregates

Oppositely charged polymeric chains can undergo associative phase separation driven by electrostatic interactions to give rise to an intricately connected viscoelastic network within condensates in a process known as complex coacervation. This phenomenon is typical in biological systems, where even a single amphiphilic polymeric chain can undergo homotypic phase separation via counter-ion release. An example of such a biopolymer is the tau protein, which is a natively unstructured, microtubule-associated neuronal protein that undergoes

electrostatically-fueled phase separation in the presence of low salt. Additionally, the highly concentrated environment of tau condensates is known to act as a reaction crucible for promoting aberrant phase transitions involved in disease progression. Interestingly, tau is known to colocalize in protein aggregates along with other neuronal IDPs. Tau protein deposits have also been observed in patients afflicted by diseases with a significant underlying pathological contribution by the human prion protein (PrP). Collectively, numerous findings indicate an intriguing interplay of molecular interactions between different IDPs that may present as intersecting pathological features in the etiology of various diseases. These findings are further strengthened by the ability of tau to interact with RNA-binding proteins, similar to PrP, which also contains a putative RNA-binding site. Therefore, we set out to elucidate the mechanistic basis underlying tau-PrP interactions. As a step towards elucidating the overlapping features of the two proteins in terms of pathology, we show the indispensable role of the human prion protein in regulating the phase separation of tau.

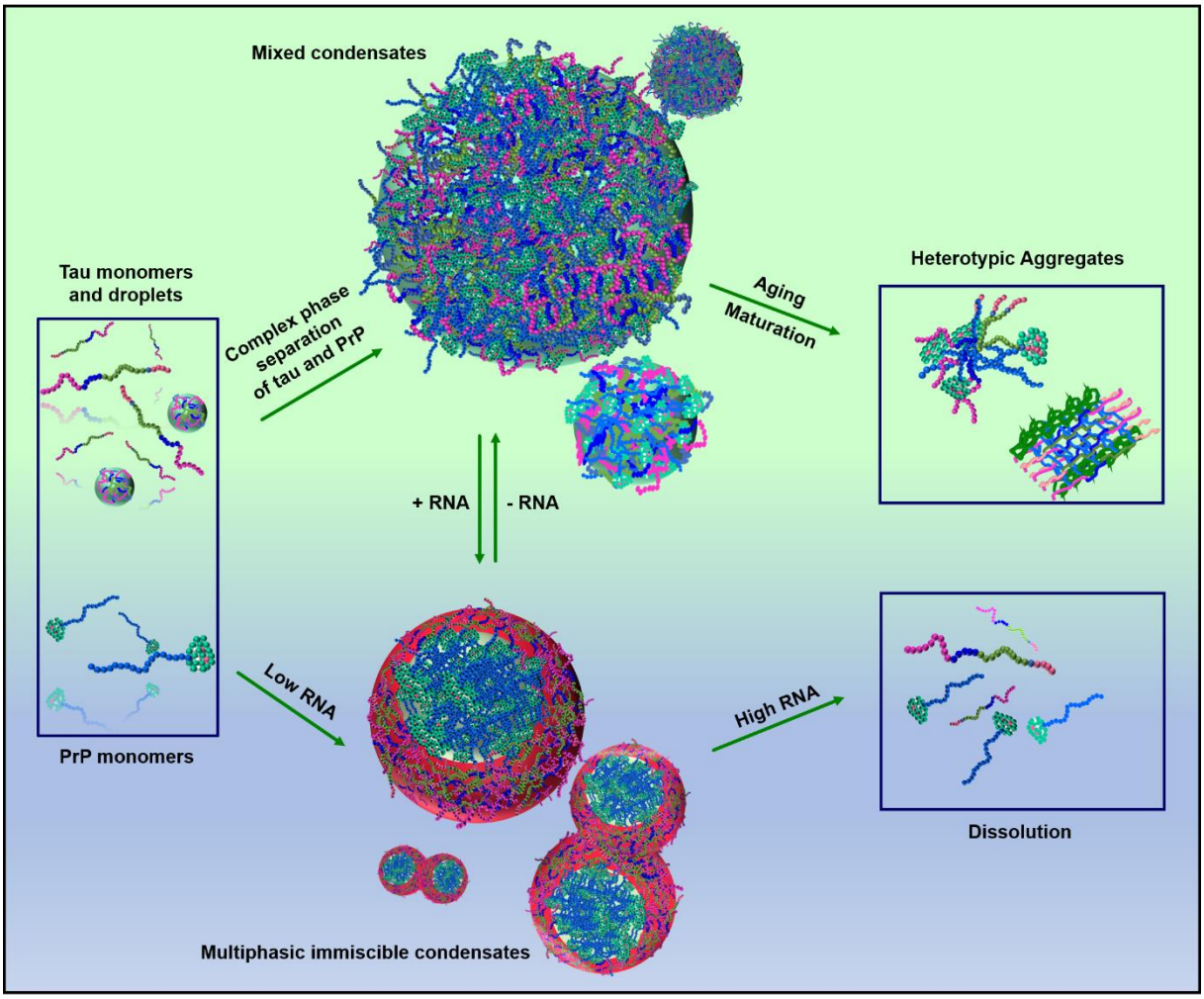


Rai, S. K., Khanna, R., Avni, A. & Mukhopadhyay, S., Proc. Natl. Acad. Sci. U.S.A. (2023)

Using a range of biophysical tools, we show that PrP potentiates tau phase separation under native, crowding-agent-free conditions and drives its multimerization by electrostatically interacting with tau in a domain-specific manner, subsequently forming tau-PrP heterotypic coacervates. Further, we show that in the presence of RNA, perfectly colocalized tau-PrP assemblies transition into immiscible yet mobile, multiphasic condensates. Moreover, this ternary system behaves in a typical three-regime fashion reminiscent of nucleolar condensates. Combining our findings with pico-second resolved fluorescence anisotropy, time-dependent FRAP, vibrational Raman spectroscopy, and AFM, we provide evidence of the liquid-to-solid transition of tau-PrP hetero-assemblies, which results in the formation of intermixed amyloid fibrils. These results corroborate previous findings underpinning the convergent role of prion in the overlapping pathophysiology of several neurodegenerative diseases.

**Chapter 4. Chaperone-Mediated Phase Separation Regulates Liquid-to-Solid Phase Transitions of Tau into Amyloid Fibrils**

Biomolecular condensates formed via phase separation of proteins and nucleic acids are thought to regulate a myriad of cellular processes in a highly spatiotemporally controlled manner. Such highly dynamic, viscoelastic, mesoscopic, intracellular membraneless bodies can undergo aberrant liquid-to-solid transitions into a range of pathological amyloid-like nanoscopic aggregates. The mechanism of the protein quality control machinery in regulating the protein phase behavior and the material property of biomolecular condensates remains elusive. Here, we present a unique case to demonstrate that a heat shock protein 40 (Hsp40), Ydj1, promotes heterotypic phase separation of intrinsically disordered tau via intermolecular electrostatic and hydrophobic interactions. Unlike tau droplets, these tau-Ydj1 droplets do not undergo maturation into amyloid fibrils. By sequentially deleting motifs, we show that the amyloidogenic hexapeptide motifs located in the central hydrophobic microtubule-binding region of tau interact with the peptide-binding regions of Ydj1 promoting heterotypic association leading to the formation of tau-Ydj1 condensates morphologies and material properties of which can be tuned by adding RNA. Our single-molecule FRET studies reveal Ydj1-induced conformational shapeshifting of tau that alters the tau phase behavior resulting in the abrogation of tau fibrillation. Our results underscore an intriguing interplay of molecular drivers that govern chaperone-mediated phase separation and will have broader implications for the chaperoning of a wide range of intrinsically disordered proteins involved in function and diseases.

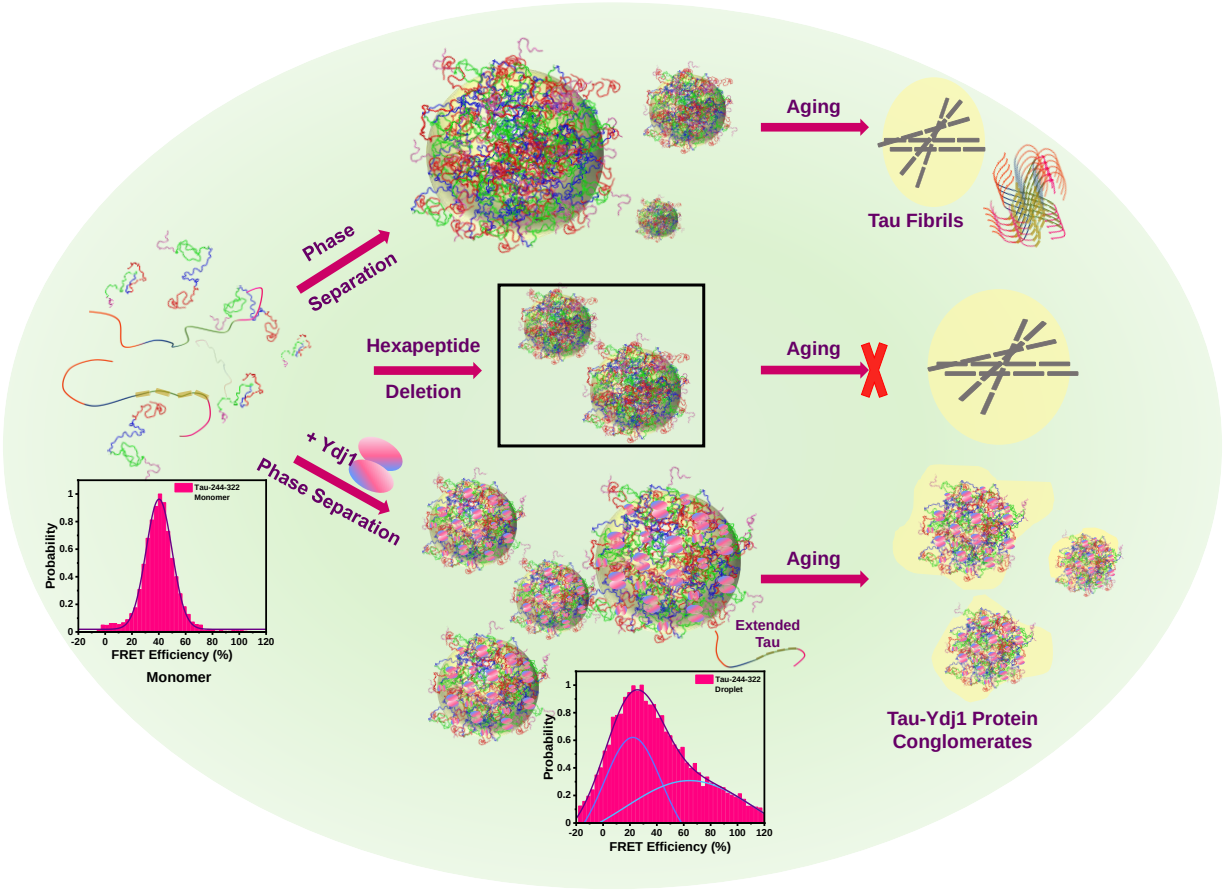


Rai, S. K., Khanna, R., Sarbahi, A., Joshi, A. & Mukhopadhyay, S. (Manuscript in preparation)

## Chapter 5. Conclusions

The experiments and studies carried out in this thesis were undertaken to explore and analyze the multifaceted nature of the heterotypic complex coacervation of the human microtubule-associated protein tau. This chapter aims to build a comprehensive understanding of associative phase transitions in a biological context, guided by the findings described in the previous sections of this thesis. Our work provides the mechanistic underpinnings of the (I) heterotypic, electrostatically controlled interactions in the control complex phase separation of tau and prion into multiphasic condensates and co-aggregates (chapter 3) and elucidates the (II) effect of molecular chaperones on tau phase separation and conformations (chapter 4). In summary, this chapter provides a broad overview of the significance of electrostatically fueled associative phase transitions in neuronal dysfunction.

## List of publications

- **S. K. Rai**, R. Khanna, A. Sarbahi, A. Joshi, & S. Mukhopadhyay* "Chaperone-Mediated Phase Separation Regulates Liquid-to-Solid Phase Transitions of Tau into Amyloid Fibrils " (manuscript in preparation).

○ Joshi, A. Avni,* A. Walimbe, **S. K. Rai**, S. Sarkar, & S. Mukhopadhyay* "The Hydrogen-Bonded Network of Water in Phase-Separated Biomolecular Condensates" (manuscript in preparation).

- **S. K. Rai**, R. Khanna, A. Avni & S. Mukhopadhyay* "Heterotypic Electrostatic Interactions Control Complex Phase Separation of Tau and Prion into Multiphasic Condensates and Co-aggregates" ***Proc. Natl. Acad. Sci. U. S. A.*** 2023, 120, e2216338120.

○ Joshi, A. Walimbe, A. Avni, **S. K. Rai**, L. Arora, S. Sarkar, & S. Mukhopadhyay* "Single-Molecule FRET Unmasks Structural Subpopulations and Crucial Molecular Events During FUS Low-Complexity Domain Phase Separation" ***Nat. Commun.*** 2023, 14, 7331.

○ **S. K. Rai** & S. Mukhopadhyay* "Small Molecules Playing Big Roles: Tuning Material Properties of Nucleolar Condensates" ***Biophys. J.*** 2022, 121, 3768-3770 (*New and Notable*).

○ Agarwal, L. Arora, **S. K. Rai**, A. Avni & S. Mukhopadhyay* "Spatiotemporal Modulations in Heterotypic Condensates of Prion and α-Synuclein Control Phase Transitions and Amyloid Conversion" ***Nature Commun.*** 2022, 13, 1154.

○ Agarwal§, **S. K. Rai**§, A. Avni & S. Mukhopadhyay* "An Intrinsically Disordered Pathological Prion Variant Y145Stop Converts into Self-Seeding Amyloids via Liquid-Liquid Phase Separation" ***Proc. Natl. Acad. Sci. U. S. A.*** 2021, 118, 45, e2100968118.

§ **Contributed equally**

- **S. K. Rai**, A. Savastano, P. Singh, S. Mukhopadhyay*, & M. Zweckstetter* "Liquid-Liquid Phase Separation of Tau: From Molecular Biophysics To Physiology And Disease" ***Protein Sci.*** 2021, 30, 7, 1294-1314.

○ Not part of this thesis work

## Presentations and Talks

- Sandeep K. Rai, Roopali Khanna, Anusha Sarbahi, Anamika Avni, Ekta Shandilya, Ashish Joshi & Samrat Mukhopadhyay: "Elucidating the Multifaceted Nature of Multiphasic Condensates in Neuronal Diseases" in FCSXIV, the 14th National Workshop on Fluorescence and Raman Spectroscopy meeting **2023**, Indian Institute of Science Education and Research Mohali (IISER Mohali) and Institute of Nanoscience (INST), India.
- Sandeep K. Rai, Roopali Khanna, Anusha Sarbahi, Anamika Avni, Ekta Shandilya, Ashish Joshi & Samrat Mukhopadhyay: "Elucidating the Multifaceted Nature of Multiphasic Condensates in Neuronal Diseases" in Complex Fluid International Conference (**CompFlu 2023**), Indian Institute of Technology (IIT) Madras, Chennai, India.

## Table of contents

# CHAPTER 1

## Complex Coacervation: Principles, Mechanisms, and Tools to Study its Behavior

## 1.1 Introduction

Even the simplest of prokaryotic cells manifest as intricate amalgamations of a myriad of components, each working harmoniously to execute essential biochemical reactions, which expand to form complex pathways. These pathways, each working in synchrony with the other, build a coherent biological system. This intricacy is reflected in the numerous different biological macromolecules that seamlessly interact together to create larger molecular machines that are synonymous with biological function. What becomes critical in this respect is the maintenance of distinct chemical environments within a cell and the regulation of the way different constituents and products of several pathways are interconnected together to achieve rationality. Compartmentalization, therefore, becomes critical in this respect.[1] Different regions of cells are enriched with specific cellular machines to carry out a set of assigned functions: for the mitochondria, ATP synthesis becomes important, while the Golgi apparatus is tasked with cargo modification, packaging, and delivery.

Since 1682, when Antonie van Leeuwenhoek first observed the nucleus, the spatial organization of the cellular milieu was thought to depend on the presence of the surrounding membrane. Evidence collected over the past decade or so now challenges this traditional perception.[2-11] Subsets of biomolecules in cells can spontaneously coalesce into mesoscopic, membrane-less assemblies known as membrane-less organelles (MLOs) that are demixed from the rest of the cytoplasm. Such transient MLOs allow the rapid and efficient exchange of molecules from the surrounding environment and are formed via the physical process of phase separation. The presence of phase-separated MLOs will enable cells to achieve spatiotemporal organization of the millions of molecules on their hosts while simultaneously ensuring functions are carried out in a regulated manner.

The concept of phase separation due to macromolecular crowding in the dense cytoplasm was first proposed as a mode for "micro compartmentalization" in 1995.[12, 13] This idea was again revisited in 2009, with the observation of the liquid-like nature of P granules in *Caenorhabditis elegans* due to liquid-liquid phase separation (LLPS), after they were first reported in the 1980s.[2, 14] Since then, numerous such assemblies with a diverse set of functions have now come to the forefront: the nucleoli[15] act as sites for ribosome biogenesis, Cajal bodies[16] are important for splicing, nucleocytoplasmic transport is regulated by the Nuclear-pore complexes (NPCs),[17, 18] centrosomes are centers for tubulin microtubule nucleation,[19] while gene expression is partially controlled via heterochromatin condensation.[20, 21] In addition to a large

number of MLOs that have been prescribed distinct functions, a significant class of biomolecular condensates formed aberrantly are also associated with disease.[22-28] Although a deluge of studies have reported phase separation as being implicated in both function and dysfunction, the molecular determinants and the physical principles underlying the formation of these condensates are only beginning to emerge (Figure 1.1).

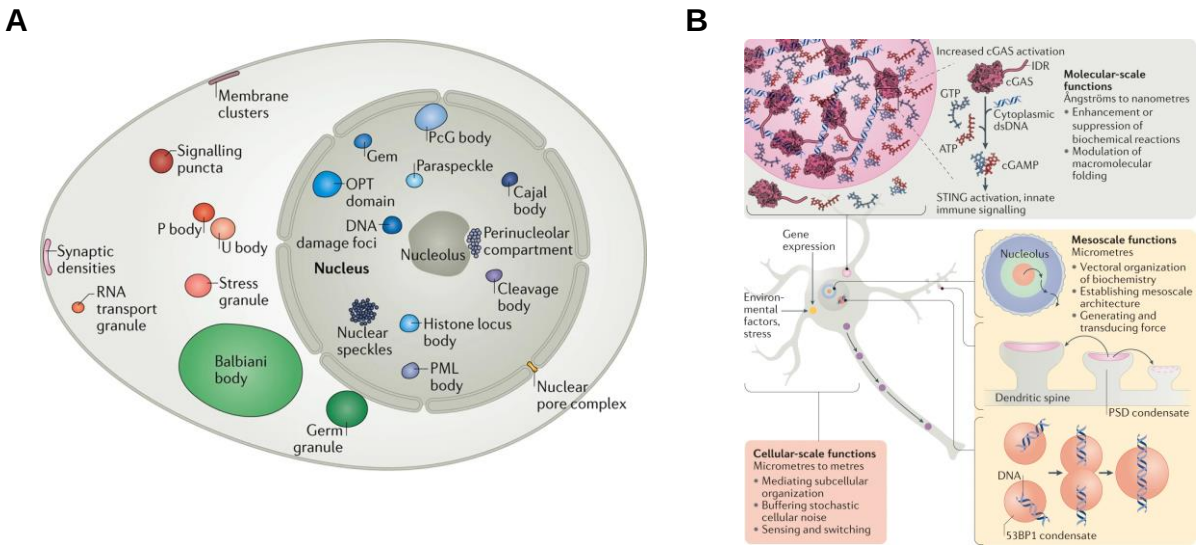


**Figure 1.1. A.** Membraneless organelles in a eukaryotic cell are formed via biomolecular phase separation. Some organelles, shown here for a complete picture, are specific to certain cell types. For example, synaptic densities are exclusive to neuronal cells, while Balbiani bodies and germ granules are only found in germ cells. **B.** Subsets of biological condensates can be clubbed together based on their contrivance and function across different length scales, ranging from a molecular to a cellular level, which can achieve lengths of up to a meter in mammalian neurons. Additionally, functions at different lengths may overlap with each other. [cGAS: cyclic guanosine monophosphate–adenosine monophosphate (cGAMP) synthase; dsDNA: double-stranded DNA; IDR: intrinsically disordered region; 53BP1: p53 binding protein 1; PSD: postsynaptic density; STING: stimulator of interferon genes]. Reproduced with permission from Ref (3),(8).

## 1.2 Molecular drivers of phase separation

Elucidating the molecular determinants that introduce the physical properties that promote phase separation in a system is an essential task since these physicochemical elements underscore the regulation of this complex phenomenon in the cellular environment. In this regard, the role of intrinsic disorder in the participating polypeptide is central. The proteome that shapes the biological membraneless assemblies is significantly more disordered than the

rest of the cellular proteome and classified under a class of Intrinsically disordered proteins, or IDPs.[1] These polypeptides do not assume conventional, properly folded, three-dimensional shapes. Because of their dynamic personality, IDPs can engage in more promiscuous, transient interactions, consequently introducing multivalency and higher dynamics within a system, potentiating its phase separation.[3-29] Additionally, the exposure of amino acids in IDPs is also associated with higher post-translational modifications in such sequences, another factor towards their greater phase-separation capacity. In combination with IDPs and IDRs, folded protein domains are also major contributors to biomolecular condensation, sometimes even overtaking the importance of IDPs in this process. Several categories of folded domains are usually involved in this phenomenon. These include oligomerization domains and RNA recognition motifs (RRMs) that can distinguish and bind certain RNA sequences, in addition to folded domains that are functionally important for any membraneless organelle in cells.[3-31] In some cases, an amalgamation of folded domains and flexible, disordered linkers can act together in order to phase separate, with the physical properties of the resulting condensate being highly dependent on the sequence characteristics of this protein. Notably, folded domains have a much higher probability of undergoing aggregation or even crystallization.[32-35] Consequently, the range in the phase diagram where folded domains can demix in a solution is much narrower than disordered proteins.

The interactions amongst IDPs, or between IDPs and folded proteins that are crucial for phase separation are underscored by a multitude of physical forces that govern the nature of the resulting membrane-less organelles (Figure 1.2 a). The diverse amino acid side chains in proteins, in addition to the wide variety of post-translational modifications they undergo, lead to the emergence of many non-covalent interaction modes underlying the association between protein chains. In this regard, electrostatic interactions between charged amino acids are widespread in the proteome of phase-separating proteins. These interactions can drive the phase separation of a single amphiphilic chain, such as for the tau protein or in the case of LAF-1, or it may drive the complex coacervation between two oppositely charged polypeptides or a mixture of polypeptides and nucleic acids. Additionally, PTMs on the protein residues heavily influence this interaction mode. Apart from electrostatic interactions, planar interactions such as π-π interactions can take place between the $sp^2$-hybridized side chains that are most commonly associated with aromatic amino acids and play an important role in mediating the phase separation of several proteins. Additionally, the partial-π nature of the amino acid backbones that compose all protein chains may also contribute to weak planar interactions throughout the whole sequence of the proteins and nucleic acids. The interactions between

cationic charged groups and sp2-hybridized side groups also act as predominant interaction motifs in driving phase separation, as exemplified by the interactions between aromatic residues and arginine and lysine side chains, or the interactions of proteins enriched in these amino acids with single-stranded nucleic acids such as RNA. In addition to these interactions, hydrophobic contacts between hydrophobic side groups, which are typically associated with intrinsic disorder, may also contribute towards the phase behavior of several proteins.[3-35] Sometimes, such interactions also extend to those between hydrophobic and aromatic side groups, as demonstrated in the hydrophobically driven interactions of FG-Nucleoporins such as Nup98 that form a central channel within nucleopore complexes to regulate the process of nucleocytoplasmic exchange. Finally, hydrogen bonding, which is normally associated with amino acid solvation, is also predominant in the dense environment of condensates owing to the presence of both hydrogen bond donors and acceptors in most amino acids. Such interactions are also essential when considering the sequestration of nucleic acids in protein condensates. In addition to these interaction motifs, how different classes of amino acids are distributed in a protein sequence may also heavily influence the physical basis for biological condensation. In addition to understanding the elements that govern phase separation, the physical principles governing this thermodynamic process are essential in understanding its significance in a more quantitative context in biological systems. The following section will discuss the physical process underlying the complex phase separation phenomena.

## 1.3 Physical principles

Phase separation, including LLPS, is an inherent property of polymeric solutions and refers to the formation of two or more co-existing homogenous phases, a “dense” and a “light” phase, via the demixing of a heterologous mixture of two or more components, akin to the demixing of oil in oil-water mixtures. However, intracellular phase transition differs from a chemical point of view of oil-water mixtures, as the large biological polymers, including proteins and nucleic acids, are hydrophilic, and the resulting condensate assemblies are enriched in water content (~60-70%). From a thermodynamical perspective, a balance between entropic contributions favoring a mixed state and the energetic interactions amongst the polymer chains controls the phase separation of macromolecules from a mixed solution.[9, 12, 29-37]

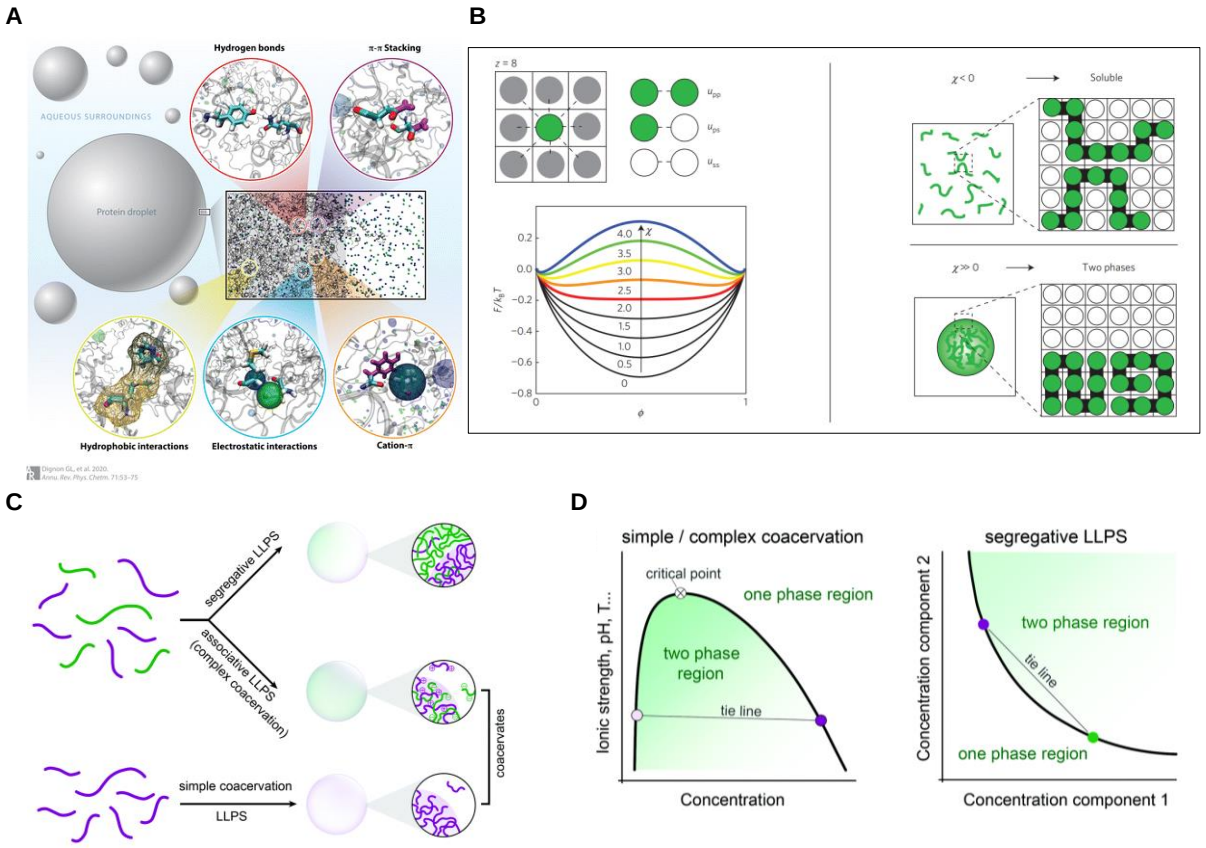


**Figure 2. A.** A variety of non-covalent interactions drives phase separation in biological systems. **B.** Two-dimensional lattice model to explain the physical basis for biological phase transitions. A polymeric mixture is modeled as an infinite lattice, where each site can be occupied either by a solvent molecule (grey) or a polymer bead (green) with a coordination number z. The Flory parameter $\chi$, determined by a balance of interaction energies between the polymer-polymer (up-p), solvent-solvent (us-s) interactions that favor demixing and polymer-solvent (up-s) interactions that favor mixing, decides the fate of the mixture. For $\chi > 0$, the polymer is in a 'poor solvent,' favoring phase separation. Above a critical value, a dominating energetic term results in higher values of the entropy of mixing per site, such that the free energy of mixing attains a region of negative curvature (colored curves in the phase diagram). The resulting destabilization in the heterogeneous mixture is resolved by phase separation. **C, D.** Phase separation can be of different types on the basis of the nature interactions of participating molecules. The schematic phase diagrams for simple/complex coacervation and segregative phase separation are also depicted. Reproduced with permission from Ref (32),(30), and (38).

The phase behavior of polymeric solutions is largely governed by Flory-Huggin's theory of polymer solutions, which is modeled on a lattice for deriving the Helmholtz free energy of mixing per site on the lattice, assuming that the volume of the solution remains constant (Figure 1.2 b). The volume associated with each site of the lattice is the volume of the smallest unit of

the system, whether it be the volume of a single solvent molecule or the excluded volume of one Kuhn unit of the monomeric unit of the polymer. For a lattice with *n* sites, the number of sites occupied by the solvent will be $n_s = \varphi_s n$, where $\varphi_s$ denotes the volume fraction of the solvent and describes the fraction of the total lattice volume occupied by the solvent. Similarly, the number of sites occupied by monomeric units of the polymer is given by $n_p = \frac{\varphi_p}{N_p} n$, where $N_p$ denotes the length of the polymer chain, and the subscripts s and p refer to the solvent and polymer, respectively. For a closed system, it is assumed that $\varphi_s + \varphi_p = 1$, which is equivalent to $\varphi_s = 1 - \varphi$, assuming $\varphi_P = \varphi$. Assuming a mean-field assumption, the Flory-Huggins free energy of mixing per lattice site can then be expressed in the units of thermal energy $k_BT$ as:

$$\frac{F}{k_B T} = \varphi N ln\varphi + (1-\varphi)\ln(1-\varphi) + \chi\varphi(1-\varphi) \qquad \text{------ (1.1)}$$

Here, the first two terms represent the entropic contributions to mixing. In contrast, the third term, which is dependent on the Flory interaction parameter $\chi$, is a measure of the energetic contributions towards the process. For a polymer solution, the entropy of mixing is always positive due to the higher number of possible conformations in the heterogenous mixed state. Whether a solution will, therefore, undergo any demixing will be based solely on the $\chi$-dependent energy term in the equation. The proportionality parameter $\chi$ is defined as:

$$\chi = \frac{z}{k_B T}\left[u_{p-s} - \frac{1}{2}\left(u_{p-p} - u_{s-s}\right)\right] \qquad \text{------ (1.2)}$$

It is a measure of the balance between the opposing energies of polymer-polymer ($u_{p\text{-}p}$), solvent-solvent ($u_{s\text{-}s}$) interactions that favor demixing, and polymer-solvent ($u_{p\text{-}s}$) interactions, which favor mixing. The interaction parameter essentially quantifies the energetic cost of a polymer unit being close to a solvent unit on the lattice. A higher energetic cost is, therefore, indicative of the polymer being in poor solvent conditions, which favors demixing. Above a critical value of $\chi$, the energetic term dominates the entropy of mixing, resulting in higher values of the entropy of mixing per site. The resulting destabilization in the heterogenous mixture is resolved by phase separation: the formation of a dense phase enriched in the polymer chains and a light phase that is depleted of it. Additionally, the values of $\chi$ are also modulated by the volume fractions of the components in the mixture. In addition to the composition of the resulting phases, the state of a system can be further modulated by physical parameters such as

temperature, pH, and ionic strength. These factors and the resulting phase changes are depicted as a phase diagram. The phase diagram is plotted as a range of concentrations (or parameters of interest) over which either a mixed or a demixed state is favorable for the system. A phase diagram, therefore, serves as a visual aid to represent a parameter-dependent-phase transition of a given system.

**Types of phase separation**

Depending on the nature of interactions amongst the components in a solution, phase separation can broadly be classified into three categories (Figure 1.2 c, d).[38-41] In the first class, two components, despite having a favorable mixing energy, undergo phase separation due to the repulsive interactions between them. This behavior is known as segregative phase separation and results in two phases, each enriched in one of the two components. These phase changes are commonly observed for non-ionic polymers, similarly charged species, or a mixture of non-ionic and charged polymers and are believed to occur due to the asymmetric interactions introduced into the system via the conformational reordering of one component. Such type of phase separation was previously observed for a mixture of gelatin/κ-carrageenan due to the differences in the ordering temperatures of the two components. Another classic example of such behavior is seen in the case of a mixture of poly (ethylene glycol) and dextran, which undergo demixing due to the repulsive forces between them.

The opposite is true for associative phase separation, where two components demix from the surrounding environment due to the attractive interactions between them. Such interactions, which are very frequently electrostatic in biological systems, lead to the formation of a complex coacervate that is enriched in both classes of polymers but still contains a significant amount of solvent. In the case of simple phase separation, a single component can form a condensed phase or a simple coacervate via a multitude of interactions amongst its different regions, which are, again, very frequently coulombic in nature, namely cation-pi, pi-pi, along with electrostatic interactions. An essential physical property shared by biomolecules, which is responsible for a significant subset of these precisely regulated interactions, is the charge that they carry. Charged biopolymers have emerged to be pervasive in all contexts, from biological to synthetic systems, owing to the versatility they introduce. In biological contexts, charge-mediated contacts exist as common interaction motifs, controlling a wide range of cellular processes, from DNA compaction to compartmentalization. In this regard, coacervates, especially those that are multicomponent, are an important class of complexes that exist in biological systems.

A modified form of Flory-Huggin's theory usually successfully explains the behavior of coacervates.[30] The Overbeek and Voorn model diversifies to take into account electrostatic interactions by introducing a term based on the Debye-Huckel formalism to consider the screening between the polyions in the solution. By considering the system as binary, where $\varphi_+ + \varphi_- = \varphi$, the Helmholtz free energy per lattice site of the system is expanded as:

$$\frac{F}{k_B T} = \varphi N ln \frac{\varphi}{2} + (1-\varphi)\varphi - \alpha(\sigma\varphi)^{\frac{3}{2}} \quad \text{------ (1.3)}$$

Where α is a measure of the strength of the electrostatic interactions, and σ describes the charge distribution on the polymer, which becomes extremely crucial when considering biological polymers such as polypeptide chains, where the distribution of charges becomes key in determining phase behavior, especially for a class of proteins that are intrinsically disordered (IDPs) or contain intrinsically disordered regions (IDRs). In this case, the Flory parameter χ becomes obsolete since even the long-range electrostatic interactions are much stronger than the short-range interactions amongst neutral groups. The third term is therefore replaced here with $\alpha(\sigma\varphi)^{\frac{3}{2}}$, to introduce the contribution of electrostatic interactions between a polycation of charge $Z^+$ and length N and an oppositely charged polyanion of the same length and magnitude of charge.

**Multiphasic condensation**

Complex coacervation of polyions driven by counterion release is a commonly employed phenomenon of biological significance. Very often, common polypeptides participating in this process assemble into multiphasic assemblies in a single solvent environment. In general, the formation of condensates is highly dependent on the physical parameters that directly control the molecular interactions governing condensates. A limiting value is usually applicable to most such systems, beyond which condensation takes place or is inhibited. In the case of charge-driven complex coacervation, the critical salt concentration is one such parameter. Typically, mixtures with different critical salt concentrations undergo multiphasic condensation, where one phase-separated mixture is engulfed by the other, resulting in immiscible, nested condensates with variable morphologies depending on the sequence composition of the polymers (Figure 1.3).[42-47]

Multiphasic condensates contain a core-inner condensed phase surrounded by one or more immiscible outer coacervates, which exist in a dilute phase. The viscosity of the innermost core-coacervate is usually the highest. At the same time, all phases have a liquid-like behavior,

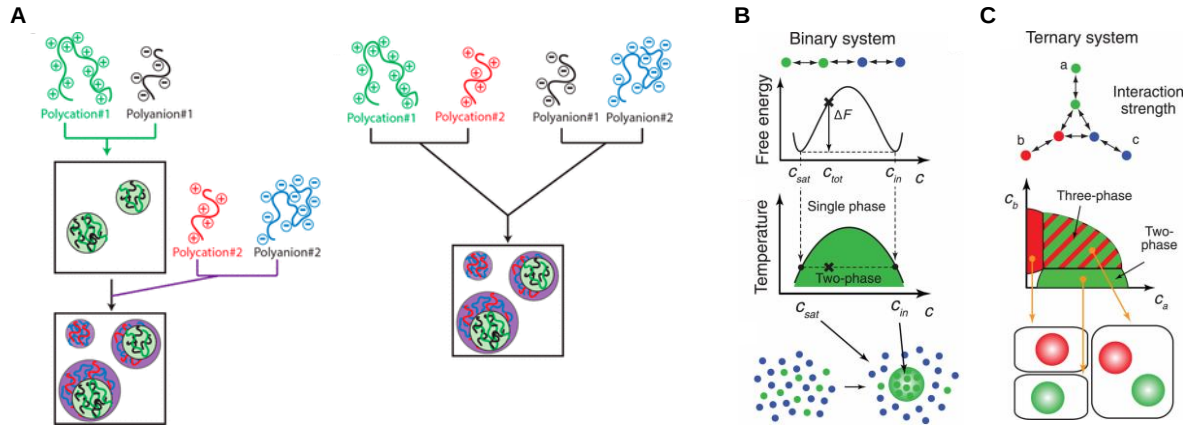


**Figure 1.3. A.** Complex coacervates form via the electrostatic association of two oppositely charged polymeric species and can adopt a range of morphologies. **B., C.** Thermodynamics underlying phase separation. For a binary system, the demixed state comprises a condensed phase with concentration $C_{in}$ and a dilute phase with concentration $C_{sat}$. The state of the system (mixed/demixed) can cover the entire phase space in a phase diagram with varying physical parameters such as temperature. The boundary separating the two states is the binodal. The left arm of this curve describes the $C_{sat,}$ and the right arm describes the $C_{in}$, which are connected by a tie-line. The polymeric mixture can, therefore, spontaneously demix under suitable physical conditions to form an enriched, dense phase and a surrounding dilute phase. Based on the interactions amongst the components, a ternary mixture can phase separate in different ways, giving rise to different phase diagrams. The mixture can exist in a three-phase region with varying droplet architecture as well as different two-phase regions. Reproduced with permission from Ref (51),(26).

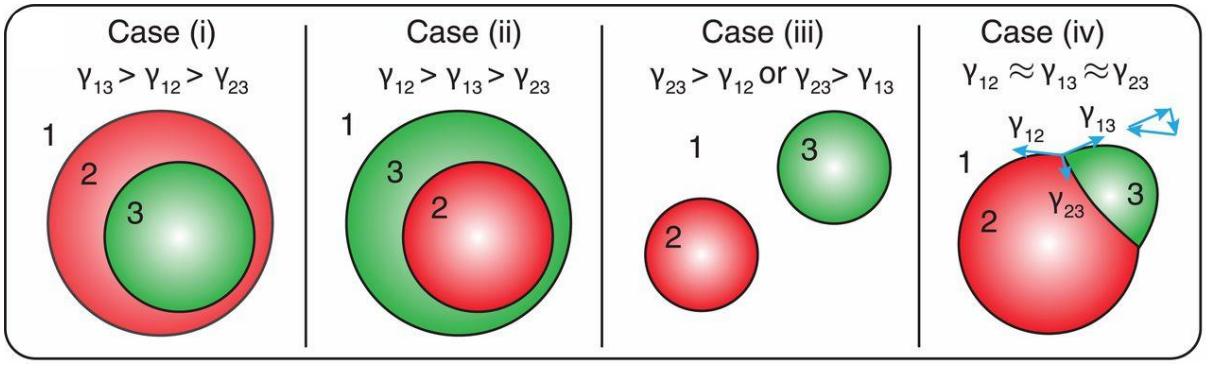


**Figure 1.4. A.** Different condensate architectures can result due to the interfacial tensions of the multiple condensates. Reproduced with permission from Ref (26).

as seen previously for synthetically reconstituted multiphasic systems as well as naturally occurring multiphasic condensates, the most prominent being the nucleolus (Figure 1.4). A mixture of coacervates can potentially acquire three equilibrium configurations: non-engulfing, where two coacervates are completely separated; engulfed, where one droplet is engulfed by the other; and partially engulfed, where the droplets exist as a doublet but do not completely coalesce. The morphology a system acquires will be determined by the resulting interfacial tensions amongst the droplet surfaces. As a general rule, a mixture of coacervates will be multiphasic if the combined interfacial energy of the resulting condensates is lesser than the energies of the individual droplets.[26, 48-53] The coacervate with the highest interfacial energy is usually the densest and has the highest critical salt concentration, making it the most likely to be engulfed. Additionally, this factor is also dependent on the size of the condensates formed, with the smallest most likely to be engulfed. Larger interfacial tensions for a mixture of condensates than for individual condensate components will cause complete non-wetting, leading to the condensates being isolated in space. This is characteristic in biological systems due to the highly crowded nature of the cytoplasm and nucleoplasm in cells and can explain why all membrane-less compartments do not coalesce into a single phase over time in biological systems.

Ubiquitous ionic polymers, most notably RNA, provide salient molecular features that decide the fate of biomolecular condensates, including their spatiotemporal localization, material state, and morphology within cells. The ability of RNA to act as a potent scaffold and engage in numerous multivalent interactions supports its role in the formation of extended networks within condensates. Numerous reports have now gathered enough evidence to ascertain the role of sequence composition as well as distribution, both for nucleic acids such as RNA and protein chains, in determining the nature of protein-protein, protein-RNA as well as RNA-RNA interactions in biological systems.[52, 53] The resultant sequence-encoded properties finally decide the complex architecture and dynamics of spontaneously formed multilayered condensates. In fact, any change in the nature of these interactions directly influences the architecture of these condensates, as suggested by the intrinsic transformation of perfectly miscible condensates into multiphasic condensates during the non-equilibrium process of aging.[43-45] The role of RNA is further demonstrated in the ability of nucleobases to engage in prominent cation-pi as well as pi-pi interactions with positively charged amino acids arginine and lysine (cation-pi), as well as aromatic amino acids such as tyrosine (pi-pi). This particular category of molecular interactions also features strongly in biological complex coacervation,

in addition to playing a critical role in the compositional demixing leading to the emergence of associative, multiphasic condensates.

Condensates with a complex sub-structure are increasingly coming to the forefront in terms of the diverse functions that they play.[3, 15, 17, 21, 25, 34, 54, 55] Perhaps the most well-studied organelle that displays this multiphasic architecture is the nucleolus, where a multilayered tripartite organization due to condensate immiscibility results in the innermost fibrillar component (FC), followed by a dense fibrillar component (DFC), which is finally surrounded by the granular component (GC). This multilayered architecture of this organelle is coupled to its function, where the formation of ribosomes proceeds from the innermost FC to the outermost GC, and the consequent structuring of the RNA contributes to the immiscibility and resultant interfacial tension. The structural heterogeneity in condensates at mesoscopic length scales may, therefore, be a general strategy used by cells to generate another level of spatial regulation in the processes that are being performed within them. Our basic understanding of phase separation has been facilitated by the increasing number of tools and techniques developed to study this process, both *in vitro* and in living systems. These tools have uncovered attributes ranging from the material properties of condensates to elucidating the conformational dynamics of the constituents that compose them. The following section describes various methods developed for studying biomolecular phase separation.

## 1.4 Tools

It is now becoming increasingly clear that phase separation, especially complex coacervation, is strongly coupled to both physiology and pathophysiology in biological systems.[3, 5-8, 25] In addition, it serves as an intriguing phenomenon to be exploited for various applications, which are of synthetic and biomedical interest. Understanding the underlying molecular processes governing biological phase separation is therefore requisite for gaining insights into the maintenance of cellular coherency via this process and requires the development of a robust set of tools for capturing the properties of biological condensates, both in vitro and in cells (Figure 1.5).[56, 57]

### 1.4.1 Sequence features and computational tools to identify common interaction motifs

Although generally, it may seem that phase separation acts as a generic property of many protein chains and nucleic acids such as RNA, there seem to be distinct motifs in biological polymers that support this process.[58] Classifying polymeric chains as scaffolds and clients has

proven to be a very constructive model in improving our understanding of biological phase separation. Polymers that drive phase separation act as scaffolds to recruit neighboring client molecules within a system. Together, the network formed by the scaffold and clients directly translates into the physical properties of the resulting condensates.[49, 59-60] Two dominating molecular signatures within proteins commonly act as drivers of phase separation. The first category includes a series of neighboring folded domains that can directly interact with short linear motifs or SLiMs in surrounding protein chains. A second sequence feature is the presence of intrinsic disorder with protein chains. Intrinsically disordered proteins or proteins with intrinsically disordered regions commonly act as drivers of phase separation in cells by engaging in a multitude of transient interactions. Due to a lack of singular lowest-energy structures, IDRs or IDPs can sample a wide range of conformations in space, allowing them to engage in contact at very short timescales. Both of these sequence features are essential in incorporating multivalency into any biological systems, which are important for establishing protein-RNA or protein-protein networks and guiding condensation. Additionally, an expansion of Flory-Huggin's formalism to explain phase separation includes the stickers and spacers model, where short interacting motifs that are essential for chain attractions typically act as stickers, which are interspersed by longer, more flexible spacers.[58, 59]

The phase behavior of protein chains is, therefore, a sequence-encoded property that is strongly affected by sequence determinants such as IDR length, charge patterning, the presence of hydrophobic stretches, which contributes to thermoresponsive behavior of polypeptides, and the nature of the intervening spacers. A very commonly occurring motif in numerous disordered proteins is prion-like low-complexity domains that are commonly enriched in polar residues and contribute to the phase separation of numerous archetypical proteins such as FUS, hnRNPA1, and TDP-43. A slightly different variant enriched in arginines includes RGG domains that can engage in coacervation by interacting with RNA chains. The correlation of primary sequence features with phase behavior has enabled the creation of algorithms that allow the prediction of phase behavior by comparative analysis. Disorder predictor tools, for example, have proven essential in locating regions in protein chains that might contribute to their phase behavior.[61-63] In this regard, computational analysis of charge patterning and mapping hydrophobic stretches on a protein chain are also useful tools in the functional repertoire of studying biological phase separation.

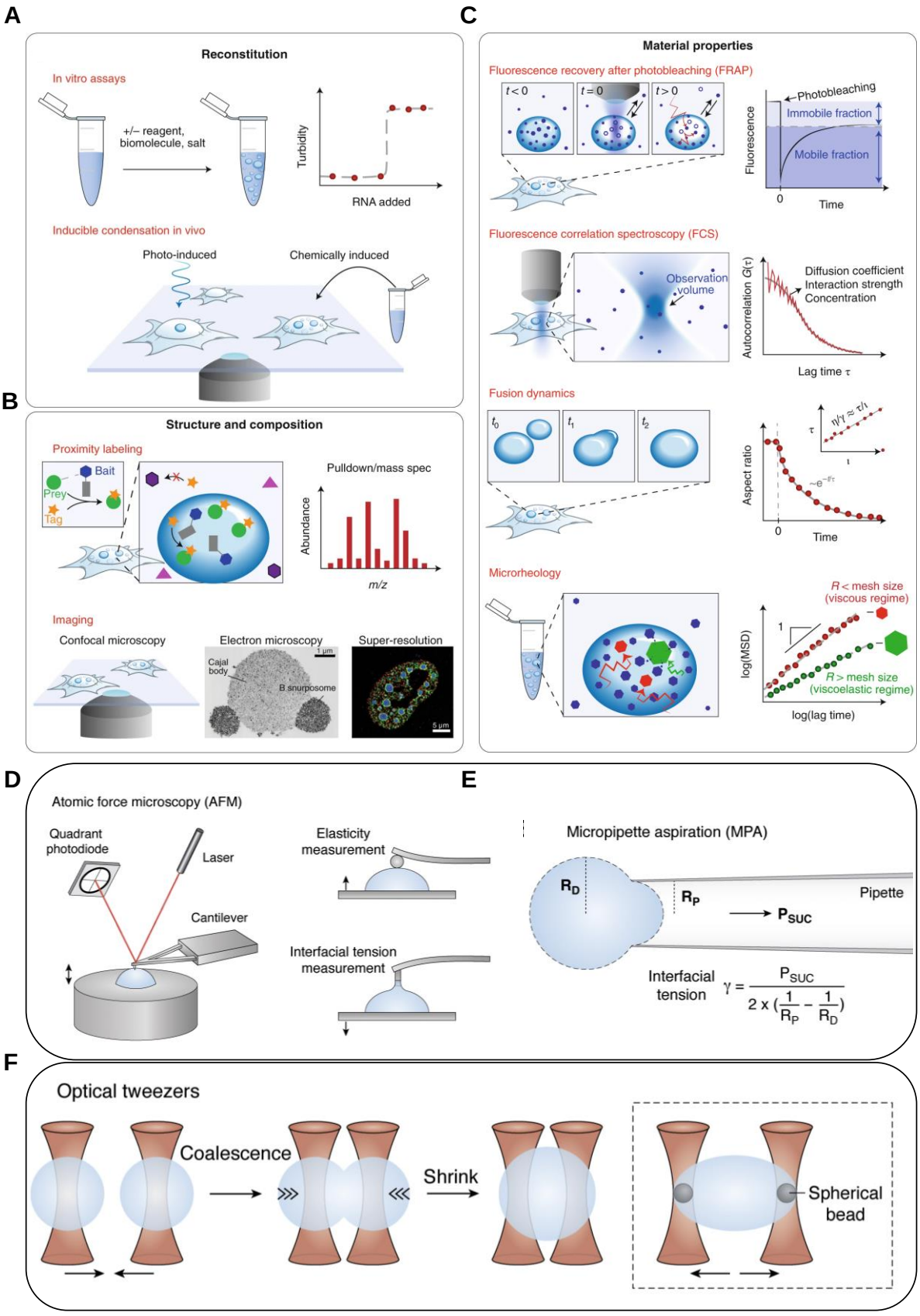


**Figure 1.5. Tools and technologies for the characterization of bimolecular condensates: A.** Multicomponent condensates can be constructed in vitro in controlled microenvironments

to study their properties, while their formation in vivo can be chemically or ontogenetically induced using a range of different technologies. **B.** Approaches such as proximity labeling in combination with proteomics-based tools can serve as a powerful means to study condensate composition. Additionally, the intricate structural features of condensates can be elucidated using advanced imaging approaches, as seen for Cajal bodies using electron microscopy and for nuclear speckles using super-resolution imaging. **C.** The material properties are an essential feature of biological condensates and can be probed using confocal fluorescence-imaging-based techniques such as FRAP and FCS. Further information about physical parameters related to the fluidity of condensates can be obtained by observing the fusion dynamics in combination with probe diffusion (passive microrheology). **D.** Schematic of the working principle of an Atomic Force Microscope, which can be used for characterizing the material nature of the condensate. Depending on the probe used, different quantities can be measured. **E.** In addition to other methods, a micropipette-based assay is an easily accessible tool to measure the interfacial tensions of condensates. **F.** Optical tweezers can be used to manipulate condensates in vitro in a non-contact fashion to obtain insights into the viscoelastic properties of condensates. Reproduced with permission from Ref (57),(67).

### 1.4.2 Reconstitution of membraneless organelles *in vitro*

Most membrane-less organelles in cells, especially those crucially dependent on IDRs/IDPs, form a fuzzy network of transient interactions amongst the numerous constituents that are essential for their formation. Consequently, discerning the absolute composition of condensate, as it exists in biological systems, becomes a challenging task. Therefore, an approach to identify the most crucial components of a naturally occurring condensate entails its carefully controlled reconstitution *in vitro*, with fully defined physical parameters.[56, 57] The use of purified components in this case perfectly allows the recapitulation of the driving forces resulting in the formation of any particular condensate and the quantitation of important physical properties pertaining to its components (Figure 1.5 A). Additionally, mimicking conditions that lead to the aberrant maturation of these condensates, for example, by using mutated proteins or changing solvent conditions, also allows the elucidation of factors associated with condensate pathophysiology and holds significance in the fields of pharmacology and drug design.

### 1.4.3 Light scattering

Light scattering is employed by numerous techniques and is an efficient preliminary mode for characterizing phase separation in a sample.[56, 64] The mesoscopic assemblies resulting from phase separation (with hydrodynamic radii ~ 0.2 nm – 3 μm) fall under the detectable limits of

techniques such as dynamic light scattering, multi-angle light scattering, and static light scattering. Additionally, phase-separated mixtures also scatter visible light in the range of 340-400 nm, where phase separation can be directly correlated to the solution turbidity. Although turbidity measurements cannot be relied upon to provide absolute quantitation of the extent of phase separation, they are a good starting point for determining the concentration ranges of different components over which phase separation does take place, i.e., in constructing phase diagrams. In fact, different parameters such as temperature and pH can be varied, and their effects are studied preliminarily using simple turbidity measurements.

More quantitative information, such as the particle shape and size (hydrodynamic radii), can be obtained from other light scattering methods, such as DLS, SLS, and MALS, which uses autocorrelation of particle motion as a result of the fluctuations in its Brownian motion to estimate particle size. It, therefore, serves as a useful tool to characterize the size of oligomeric species, which may form as a result of phase separation, in addition to building phase diagrams. Caution, however, must be exercised when using any of these techniques because of their inherently lower resolution in measuring particle size. In addition, care should be taken to ensure that the samples being used are homogenous and do not contain any aggregate-like species to prevent artefactual scattering. Additionally, the models used for calculations using light-scattering data should be carefully selected to take into account erroneous conclusions due to the actual shapes of particles and proteinaceous species deviating from the assumed spherical shape.

### 1.4.4 Microscopy

The first visualization of the internal organization of the cell started in the 1800s with the direct observation of the nucleolus. Since then, the major breakthroughs that microscopy has achieved, from simple light microscopy to super-resolution imaging, have revolutionized the study of complex biological systems. Imaging, whether it be using differential interference contrast microscopy or more sensitive fluorescence-based probes, offers the direct visualization of mesoscale assemblies formed via phase separation, both *in vitro* and in cells.[56, 57, 64-65] In vitro, fluorescence microscopy using a confocal setup is one of the strongest tools for assessing the phase behavior of a mixture with changing physical parameters. In cells, it offers a powerful method to observe the sub-cellular localization of various MLOs and to track their behavior spatiotemporally in response to a range of relevant conditions. Further, the development of sensitive yet efficient labeling strategies has enabled the elucidation of

complex cellular substructures and their composition in great detail. This is further circumvented by the development of super-resolution imaging techniques such as stimulated emission depletion (STED) microscopy, stochastic optical reconstruction microscopy (STORM), and photoactivation localization microscopy (PALM), which have broken the diffraction limit and have allowed the characterization of sub-cellular architecture in unprecedented details. Understanding the physical principles of condensate formation has been further supported by structure-based imaging tools such as cryo-EM, which allows the label-free visualization of cellular substructures in great detail. [56, 57, 64-65] In addition to providing information about the functional aspects of condensates in cells, the use of cryo-EM has been notable in describing the pathological structural changes associated with aberrant condensate formation and their transition into often toxic aggregates (Figure 1.5 B).

### 1.4.5 Techniques for studying the material properties of condensates

The material properties of a condensate directly result from the nature of interactions amongst its constituents. Studying the material properties of phase-separated condensates, therefore, offers a clear picture of the physical principles governing their formations and their functions or dysfunctions in biological systems.[56, 57, 64-67,] One of the most accessible and extensive tools for studying the dynamics of the components in condensates is fluorescence recovery after photobleaching (FRAP), which directly makes use of the intrinsic ability of fluorophores under light-induced photobleaching (Figure 1.5 C). Therefore, selectively bleaching a pre-defined area within condensates and monitoring the fluorescence recovery thereafter estimates the material state or liquidity within a condensate. FRAP is, therefore, a powerful tool to measure the mobility and diffusion of different components within droplets, in addition to measuring such values in different regions or for different components, thereby allowing the detailed spatiotemporal as well as the differential composition-dependent mobility of individual components within droplets, both in vitro and in vivo. Another complementary technique that is commonly used is FLIP, or fluorescence loss in photobleaching, which, contrary to FRAP, monitors the loss in fluorescence intensity next to a region of interest that is photobleached. Although each of these techniques is highly accessible, in terms of the resources required, they may not provide a very clear picture of the actual physical nature of the process because of their low resolution and inherent dependence on the models chosen for quantifying diffusion parameters. Fluorescence correlation spectroscopy (FCS) is a much stronger tool in this regard and offers a more accurate representation of the molecular diffusion of different components

within condensates. Using a pinhole-generated tightly focused laser beam within phase-separated assemblies, a confocal volume in the femtolitre regime can be generated, and the diffusion of fluorophores can be monitored selectively from within this volume. The resulting molecular fluctuations are autocorrelated to generate a correlation function, which can then be used to calculate the diffusion coefficient of the component of interest. This technique can be further extended to calculate the concentrations of individual components within condensates accurately. Although FCS measurements are extremely powerful for in vitro systems, the changes in refractive indices within cells can make considering the optical parameters for diffusion more challenging. Fluorescence correlation spectroscopy (FCS) offers a much stronger tool in this regard (Figure 1.5 C).

Due to the inherent liquid-like nature of condensates, the physical principles governing fluids can be approximated to condensate behavior to describe their bulk material properties precisely. For example, the interfacial tension of a condensate surface is responsible for its shape and the wetting behavior on glass surfaces.[56, 57] Additionally, the characteristic fusion or coalescence of multiple condensates is also an attempt to achieve minima in the total free energy of the system. The dynamics of such coalescence events that result in multiple condensate size distributions can be quantified to gain more information about the material properties of condensates. Further inferences on the surface tensions of droplets can be obtained by combining these measurements with passive microrheology-based approaches, which track the motion of inertly coated, spherical particles within condensates to gain information about the viscoelasticity of the surrounding condensate environment.[66-67] The development of an extension of such techniques, led by active rheology-based tools, holds the potential to further dissect the interplay of viscosity and elasticity within the component networks generated within condensates. Here, condensates can be deformed or fused under defined, mechanically controlled shear stress using microfluidics or optically trapping condensates using laser beams to quantify the physical parameters responsible for condensate behavior. This technique has the further benefit of being free from artefactual surface adhesion events on coverslips and glass surfaces and can extract information from non-equilibrium processes. Additionally, further information about the viscoelastic nature and the change in the material properties, especially for gel or solid-like condensates, can be inferred using conventional nanoscopic tools such as atomic force microscopy (AFM), or optical tweezers, which are particularly useful in characterizing the nature of nanoscopic assemblies that may form as a result of aberrant condensation (Figure 1.5 D, E).[57, 67]

### 1.4.6 Conformational dynamics in condensates

Although the measurement of condensate material properties is routinely undertaken by several studies, the inherent properties of the biopolymers that directly translate into the behavior of phase-separated assemblies, including influencing their function and, in some cases, their dysfunction, still remain elusive. Common motifs that potentiate phase separation behavior, such as the presence of intrinsic disorder and the ability to establish transient, highly multivalent contacts, are directly coupled with the physical and, consequently, biological states of condensates. Therefore, developing techniques that can efficiently capture the conformational dynamics of the protein and nucleic acid scaffold that builds them can offer a wealth of information about the implicit properties of condensates that shape their operations within biological systems.[69-84]

#### NMR Spectroscopy

The multivalency afforded by disordered protein regions contributes to their propensity to undergo phase separation. These low complexity regions in the protein sequence space are enriched with repeat elements that mediate weak, transient intra and intermolecular interaction networks, very often leading to the formation of fuzzy complexes, which exist on length scales ranging from a few angstroms to tens of nanometers. Although structured regions may also undergo phase separation due to the presence of several common structural motifs, the techniques and methods applicable to study the formation of stable secondary and tertiary protein structures and to gain insights into the conformational heterogeneity of folded proteins fail when it comes to conformationally disordered IDRs/IDPs.[69-73] In fact, the absence of stable structural elements and the extensive amount of conformational heterogeneity displayed by disordered proteins prevents their crystallization, and hence, the use of well-established crystallography or imaging techniques such as cryo-EM for studying their structure or the phase-separated bodies they are part of. Contrarily, NMR (nuclear magnetic resonance)-based tools have been heavily employed in the past to study intrinsically disordered proteins. Despite the set of challenges that this technique comes with, a notable number of studies have employed NMR spectroscopy and related tools to study the conformational dynamics of protein networks in their monomeric as well as phase-separated forms. These considerations and challenges will be discussed here.

NMR tools use atoms that exhibit non-zero nuclear spins (i.e., $I = 1/2$), which for biomolecules translates into atoms such as $^{1}$H, $^{13}$C, $^{15}$N, $^{19}$F, $^{\text{and }31}$P. While most of the isotopes

have a high abundance, atoms such as $^{13}C$ $^{15}N$ are much rarer.[69-73] This deficiency is usually resolved by supplying these isotopes in the media used during recombinant protein expression. The residue-specific chemical shift values (δ) of nuclei in the backbone of polypeptide chains act as a readout for the secondary structural elements (alpha helix and beta sheets) as well as random coils present in regions associated with these nuclei. Any changes in these values (chemical shift perturbations or CSPs) can, therefore, indicate the presence of conformational changes associated with specific regions, for example, due to inter-chain or intra-chain contacts established during phase separation. Therefore, changes in the chemical shifts can be used to map regions of proteins associated with structural changes upon phase separation. In this case, secondary chemical shift values (Δδ), which are deviations of the experimental chemical shifts from the theoretically assigned shifts for specific nuclei based on a "random coil" model, can report on the regio-specific conformational dynamics.

Although this technique is conceptually rather elementary, the poor dispersion of resonances across the protein chain, especially for disordered regions and multi-domain polypeptides, can interfere with the obtained resolution. This is addressed by the use of selective isotopic labeling using specialized protein ligation techniques or the direct detection of $^{13}C$ or $^{15}N$ nuclei. In this regard, much better spectral resolution is offered by using the Nuclear Overhauser Effect (NOE), where magnetization spins are transferred in a through-space manner via dipole coupling in a distance-dependent manner (proportional to $r^{-6}$; r: distance between two spin 1/2 nuclei). NOESY spectra based on $^{1}H$-$^{1}H$ coupling can show enhancements for distances up to 6 Å. An extension of this technique uses the dipolar interaction between backbone nuclei and the unpaired electrons of spin labels. These spin labels can be conjugated site-specifically throughout the protein chain and can, therefore, measure the resulting paramagnetic relaxation enhancements through a combination of NMR and EPR-based tools. An added advantage of using spin labels lies in the higher magnetic moment of unpaired electrons, thereby increasing the spatial reach of this technique. Additionally, the site-specific labeling of select residues offers greater control over the regions, which can be highly resolved.

In addition to providing information about the structural changes associated with phase separation, NMR has been previously used to elucidate the molecular dynamics of the underlying contacts. This is usually measured based on the width of the resonance line shape, which is proportional to the transverse relaxation rate $R_2$. In this case, the full width at half maxima of the Lorentzian line shape ($\Delta V_{FWHM}$) is given by:

$$\Delta V_{FWHM} = \frac{1}{\pi T_2} = \frac{R_2}{\pi} \quad \text{------ (1.4)}$$

Where T2 is the transverse relaxation time, and R2 is the transverse relaxation rate, which gives information on the motion of nuclei from picoseconds up to milliseconds. An extension of this technique can be used to measure diffusion coefficients in pulsed field gradient NMR (PFG-NMR), where attenuations in the resonance intensities can be correlated to protein diffusion and, therefore, measure the diffusion coefficient. This becomes particularly informative for complex mixtures such as phase-separated condensates that can potentially display a range of fluctuating structures, the motions of which can be temporally resolved.

Further, measurements of the relaxation rates along different axes, in addition to heteronuclear NOE (hnNOE) enhancements, can also be used in nuclear spin relaxation techniques to dissect the fundamental bond vibrations and fluctuations at the picosecond to nanosecond time scale and can capture ultra-fast events associated with biomolecular condensation. A further extension of NMR involves the chemical exchange-mediated transfer of magnetization from transient, NMR-invisible states, such as a ligand-bound state of a large protein, to a more detectable species, which could be a smaller, unbound state of a protein. Such dark-state exchange saturation transfer (DEST) experiments can achieve temporal resolutions from a few milliseconds to a second and can provide residue-specific information on the kinetics of a two-state system, such as a protein that undergoes condensation from a monomeric state.

Apart from capturing the dynamics in liquid-like condensates, NMR-based tools can also be used to probe the changes in structural heterogeneity coupled to phase transitions into more gel-like or solid-like states. Solid-state NMR (ss-NMR) based approaches become more useful in this case. Here, ultra-high field NMR setups and the use of ultrafast magic angle spinning (MAS) probes can provide a detailed description of the conformational dynamics of complex proteins that form condensates.

Even with the vast applications of NMR in the study of biomolecular condensates, this technique is inherently insensitive and requires very high concentrations of samples, even with the most advanced instruments.

**Small angle scattering**

Information about the size of molecules, albeit at lower resolutions, can be obtained from small-angle scattering (SAS) measurements, which is suitable for molecules of sizes ranging from 5kDa to 100 MDa.[69, 74-78] In such measurements, the isotropic deflection of collimated

beam radiation such as X-rays (electron scattering in small angle X-ray scattering (SAXS)) or neutron beams (neutron scattering in small angle neutron scattering (SANS)) at small angles in a polymer mixture, for example, a biological condensate is measured to construct a scattering curve, that represents the radially averaged scattering intensity I(q) in comparison to the measurement angle, q. Each of these is a contrast measurement, where differences in the scattering length arising from the solute in comparison to the solvent are measured. From small-angle scattering, the following is inferred:

$$I(q) = P(q)S(q) \qquad \text{------ (1.5)}$$

Where P(q) is the radiation-dependent form factor and measures the scattering amplitude by a single isolated atom, and S(q) is the structure factor that describes how a material scatters radiation. At high dilutions, the structure factor is assumed to be equal to 1; the Guinier approximation can be applied for very low scattering angles at the beginning of the curve ($q < \sim 1/R_g$) to calculate the radius of gyration ($R_g$), which is a measure of the overall size of the biomolecule. Upon Fourier transformation of the resulting scattering curve, yields the pairwise distance distribution function P(r):

$$P(r) = \frac{r^2}{2\pi^2}\int_0^\infty I(q)\frac{\sin qr}{qr}q^2 dq \qquad \text{------ (1.6)}$$

Where r is the interatomic distance, this function provides a distance distribution of all possible interatomic distances within the volume of a particle and can be used to infer the structural features of the particle under consideration, including its maximum dimension ($D_{max}$). Extending this analysis can provide information on the compactness of a biopolymer by constructing a Kratky plot ($q^2I(q)$ *vs*. q), which can be further normalized by the $R_g$ to compare the properties of biomolecules with different masses and conformations. Such analysis is particularly useful for dissecting the inherent conformational heterogeneity within condensates. In combination with an X-ray source, the information captured by SAXS can be used to gain insights into conformational changes, such as chain compaction and the formation of higher-order structures within condensates.[74-78] Supplementing SAXS with ultra-small or wide-angle scattering approaches (USAXS and WAXS) can allow the comprehensible length range to be expanded from less than 1 nanometer to almost a micrometer for the measurement of larger particles as well as more intricate details. Alternatively, the measurement of neutron scattering intensity in SANS is dependent on the presence of isotopes present in the polymeric mixtures. Owing to the well-established mathematical models as well as characterization parameters for

polymeric demixed mixtures, SANS measurements can be efficiently extrapolated to physically similar biological systems.

Each of these techniques provides an ensemble-averaged description of the state of a large number of labeled biomolecules (for example, isotopically for SANS and NMR) present in condensates. In contrast, fluorescence methods use efficient fluorophores as reporters, which are also very often intrinsically present within the protein and, owing to their versatility, can be extended to single-molecule measurements using correct optics for a range of different experiments.

**Fluorescence-based methods**

The richly heterogeneous microenvironment within densely crowded phase-separated assemblies contributes to several challenges when it comes to monitoring the conformational dynamics and diffusion of the participating components. In this regard, the high sensitivity afforded by fluorescence-based tools offers a unique perspective on the conformational gymnastics of IDPs within biomolecular condensates. In simplest terms, fluorescence refers to the radiative emission by molecules upon the absorption of electromagnetic radiation. The development of efficient, highly fluorescent molecular probes and their relative ease of incorporation within protein as well as nucleic acid molecules, in combination with the vast theoretical understanding of the physical principles of fluorescence in biological systems, makes fluorescence microscopy and spectroscopy attractive techniques to delineate the fundamental molecular mechanisms associated with biological function.[79-84] Several strategies that allow the use of such techniques in biological systems by incorporating fluorophores exist, including the routine use of thiol-based chemistry to modify native or artificially genetically encoded cysteine residues within proteins. Additional variations of the use of side-group chemistry involve the succinimide-based labeling of lysine residues or the genetic incorporation of unnatural amino acids for the site-specific *in vivo* labeling of proteins.

Different information can be extracted from a system with the use of different fluorescence techniques and, consequently, changes in the optical setup used depending on the nature of the measurement. It is, for example, possible to localize structures using a range of microscopy-based techniques, perform lifetime measurements, or even define the diffusion and correlation of molecules in specific environments. In conjunction with ensemble fluorescence measurements, the use of single-molecule fluorescence tools allows the elucidation of the heterogeneous sub-populations that exist within condensates.[79-84] Such resolution is usually

executed by the reduction of the observation volume to a few femtolitres and the reduction of the concentration of fluorescently labeled species sown to the picomolar to the nanomolar regime and is implemented either by the use of a confocal or a total internal reflection (TIRF)-based setup. The following sections discuss an amalgamation of fluorescence-based techniques suitable for capturing the complex conformational landscape of macromolecules within condensates, both in vitro and in vivo.

**Fluorescence Anisotropy**

Fluorescence anisotropy measures the changing orientation of the molecule in space due to the unequal emission of polarized light along different axes and provides an ultrasensitive, multiparametric technique that can provide essential insights into the structural features of biomolecules such as proteins and nucleic acids within condensates.[84] This technique can be employed in one of two formats: steady-state and time-resolved, achieving a time resolution from a few femtoseconds to seconds. Steady-state measurements can provide information on the intensity profile, in addition to the local information on the rotational mobility of the fluorophore on the polymer chain and the effect of quenchers. When performed in a local format, steady-state measurements can serve as a valuable reporter of the local ordering of biomacromolecules in single condensates. Upon excitation with linearly polarized light, a fluorophore conjugated to the biomolecule may undergo depolarization due to a range of processes inherent to the system during the lifetime of the fluorophore. In this case, the extent of polarization, or the steady-state anisotropy, is calculated as:

$$r_{ss} = \frac{I_{\parallel} - I_{\perp}}{I_{\parallel} + 2GI_{\perp}} \qquad \text{------ (1.7)}$$

$I_{\parallel}$ and $I_{\perp}$ are the parallel and perpendicular fluorescence intensities, and the G-factor is a proportionality constant that depends on the sensitivity of the detector to detect the parallel and perpendicular components. These measurements become particularly useful when capturing the liquid-to-solid transitions that typically occur in condensates primarily composed of amyloid-associated neuronal intrinsically disordered proteins. Exquisite information about the kinetics of this process is further afforded when measurements are acquired in the time-resolved format.

Time-resolved fluorescence anisotropy captures the depolarization kinetics and hence the rotational movement of the polymeric chain during the excited-state lifetime of the fluorophore,

allowing the elucidation of the fluorescence lifetimes, distance distributions as well as the distribution of rotational correlation times. In this case, the sample is excited with a vertically polarized, pulsed excitation source, and the emission is recorded in both parallel and perpendicular directions. In order to quantify the different rotational components, the global fitting of the decay curve is carried out with parameters that restrict the rotational motion of the fluorophore, as defined by the rotational correlation time, $\phi$. In this case, the time-dependent anisotropy, r(t) at time t, can be expressed in terms of the initial anisotropy at t=0 as:

$$r(t) = r_0 e^{\left(\frac{-t}{\Phi}\right)} \quad \text{------ (1.8)}$$

For a typical fluorophore attached to a protein, the expression can be extended to a bi-exponential fit, where the faster component is due to the local dynamics of the fluorophore ($\phi_1$), and the slower component($\phi_2$) derives from the segmental motion of the polymer backbone as:

$$r(t) = r_0[\beta_1 e^{\left(\frac{-t}{\Phi_1}\right)} + \beta_2 e^{\left(\frac{-t}{\Phi_2}\right)}] \quad \text{------ (1.9)}$$

Where $\beta_1$ and $\beta_2$are the amplitudes associated with each of the two components.
Alternatively, similar information can be obtained using the analogous, continuous wave electron paramagnetic resonance (EPR) spectroscopy, where the reporter used is a spin label, contrary to the fluorophore used in the case of fluorescence experiments.

**Fluorescence correlation spectroscopy**

Although this technique was originally conceptualized for measuring the translational diffusion of fluorophores through a small confocal volume, its use can be extended to access the different relaxation times-scales of the multi-component motion of disordered protein chains, especially in condensates. In combination with quenching effects, for example, those seen for aromatic residues within the protein chain, normal FCS measurements can be extended to PET-FCS (photoinduced energy transfer) when the fluorophore is in relatively close proximity to the molecular quencher. By measuring changes in the fluorescence correlation function in the presence of the quencher, the chain dynamics in the time scales of a few nanoseconds to milliseconds can be efficiently monitored. Additionally, by combining FCS with FRET measurements, the variations in the FRET efficiency due to the proximity of the donor and acceptor can be visualized using the autocorrelation for the individual fluorophores as well as

cross-correlation between the donor and acceptor fluorophores. Due to the ability of each of these methods to distinguish faster and slower time scales of the movement of a fluorophore, they can prove to be especially useful in gaining insights into the motion of molecules within condensates. Combining FCS measurements with polarization provides the added advantage of dissecting the faster rotational diffusion in addition to the slower backbone chain dynamics. FCS can be expanded to nanosecond measurements (nsFCS) for probing molecular events occurring at even shorter timescales.[82] Because of the innate dead time of the detectors commonly used, the resolution of normal FCS measurements is limited to a hundred microseconds, which is very often much higher than the timescales of the molecular processes occurring within condensates. In order to improve this resolution and capture events at the timescales of the lifetimes of the fluorophores, two or more detectors are usually employed in a variation of FCS. In the case of nanosecond FCS (nsFCS), by lowering the chances that any two photons end up at the same detector and by cross-correlating the signals from all the detectors used, timescale resolutions of up to 80 ps can be theoretically achieved. Using a combination of several of these techniques, information on the dynamism of protein chains with a resolution ranging from a few nanoseconds to seconds can be achieved. Additionally, the spatial resolution over which these measurements remain robust can vary depending on the technique used.

**Single-molecule FRET**

Förster resonance energy transfer (FRET) is a physical phenomenon associated with the non-radiative energy transfer between two fluorophores, a donor and an acceptor.[79-84] If a donor and acceptor fluorophore pair, with an overlapping emission and excitation spectrum, respectively, lie close enough in space, above a limiting Förster distance ($R_0$), the excited donor can transfer its energy via dipole-dipole coupling to the acceptor, which can subsequently emit this energy in the form of fluorescence (Figure 1.6).

In biological or reconstituted systems, labeling different positions on a polymer of interest with a donor and acceptor and measuring the efficiency of the fluorescence intensity from the acceptor upon donor excitation provides a readout of the distance-dependent efficiency of resonance energy transfer and serves as a proxy for extracting spatial information and therefore the conformations of a protein or nucleic acid chain. The emission intensity of the donor and acceptor can be used to get information on the energy transfer efficiency.
The efficiency of FRET is calculated as:

$$E_{FRET} \approx \frac{I_A(t)}{I_D(t)+I_A(t)} \quad \text{------ (1.10)}$$

Where $I_D$ and $I_A$ are the intensities of the donor and acceptor, respectively, since the FRET efficiency $E_{FRET}$ is inversely proportional to the distance between the donor and acceptor, R and the Forster distance $R_0$, R can be calculated as:

$$E_{FRET} = \frac{1}{1+\left(\frac{R}{R_0}\right)^6} \quad \text{------ (1.11)}$$

Since FRET is also essentially associated with the loss of energy from the excited electron in the donor, the resulting lifetime of the donor is consequently shortened. Therefore, alternatively, the transfer efficiency can also be calculated using the change in the lifetime of the donor in the presence of the acceptor, $\tau_{DA}$ lifetimes as:

$$E_{FRET} = 1 - \frac{\tau_{DA}}{\tau_D} \quad \text{------ (1.12)}$$

Where $\tau_D$ is the lifetime of the donor. FRET measurements, therefore, allow one to measure the mean ensemble-averaged FRET efficiency and the corresponding inter-residue distances for a given sample depending on the fluorophore pair used. In this case, information about single events is, however, lost.

Contrary to ensemble experiments, where molecular information may be skewed, single-molecule studies allow the measurements to be performed molecule-by-molecule to characterize structurally distinct states. Using a pinhole in the optical setup allows the laser beams to be focused into a tightly controlled confocal volume in the range of a few femtolitres. Further, reducing the fluorophore concentration down to the range of picomoles ensures the

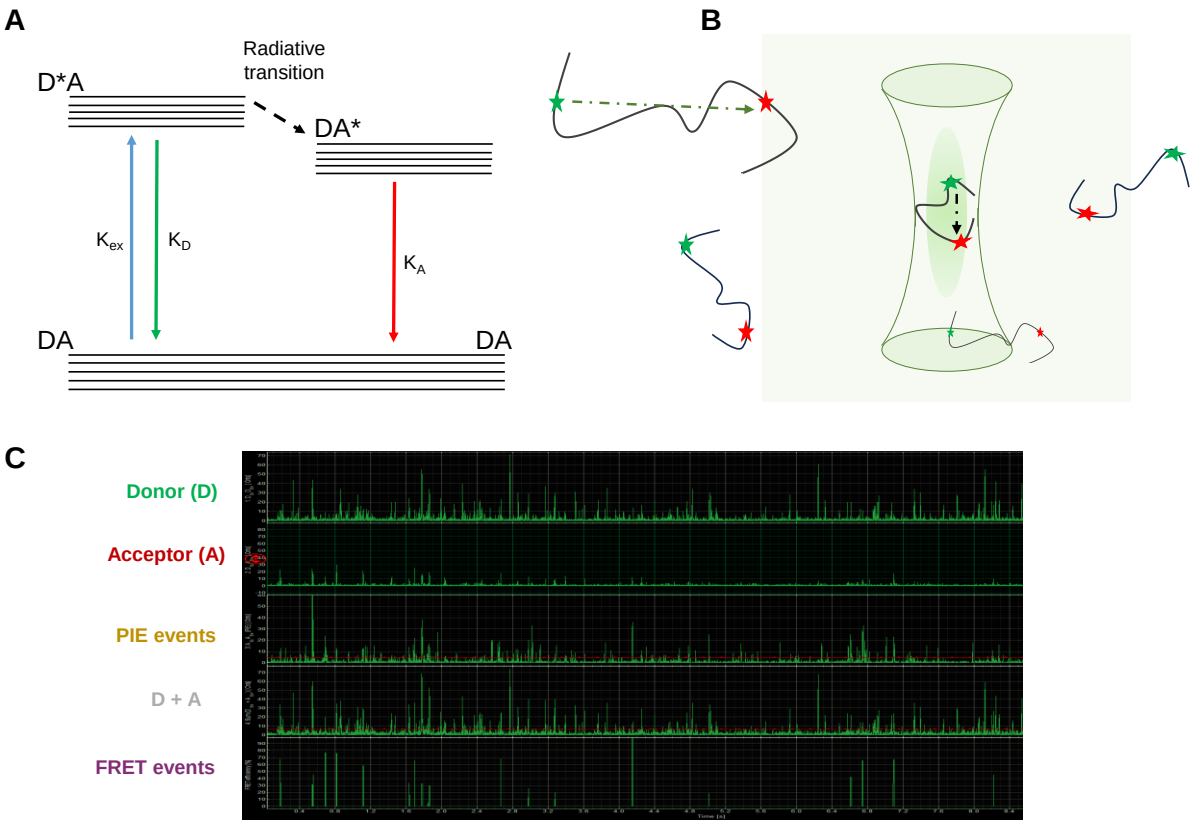


**Figure 1.6. A.** Jablonski diagram demonstrating the physical basis for Förster resonance energy transfer (FRET). **B.** Schematic depicting a dual fluorophore-labeled polymer in the confocal volume. **C.** Representative photons burst recorded during single-molecule FRET measurements (raw data).

presence of a single fluorescently labeled molecule of interest in the observation volume at any given time. Since the time spent by a single molecule in the confocal volume is longer than the timescale of fast conformational changes, information about the structural dynamics of molecules at short timescales can be efficiently captured.

Conventional FRET measurements are often complicated by the incomplete labeling or photobleaching of the molecule to be probed, which can frequently be devoid of a functional acceptor. Further, such measurements can also become convoluted due to the presence of multiple FRET processes. In such a scenario, FRET efficiencies can be incorrectly inferred to be very low, giving rise to a typical "zero FRET peak," which in many cases can shroud low FRET populations if they exist in the analyzed samples. An approach to solve this problem is based on PIE or pulsed interleaved excitation, where two lasers are used, one of which can excite the acceptor fluorophore independently of the FRET process, thereby confirming its

presence in a functional state. In a typical PIE FRET setup, two lasers that are delayed with respect to each other result in a series of interleaved laser pulses, ensuring that the emission from one fluorophore completely decays before the next laser pulse. By selectively using data acquired from molecules with both a functional acceptor and donor, PIE FRET enables the calculation of correction parameters that take into account incomplete labeling as well as spectral bleed-through to remove the zero-FRET peak and correctly resolve even low-FRET populations (Figure 1.7).

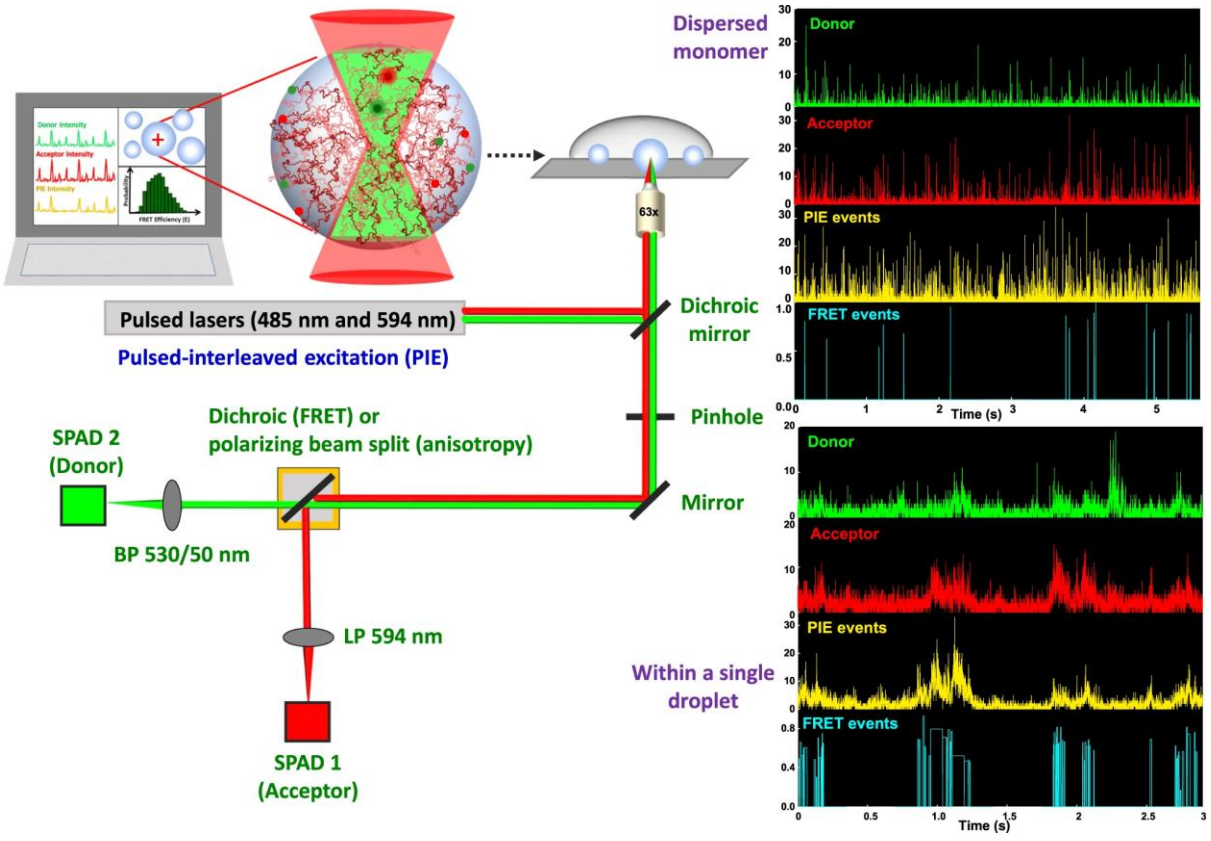


**Figure 1.7.** Schematic of a typical single-molecule microscopy setup with two picosecond pulsed excitation sources, an inverted microscope, and the confocal detection system with the additional required optical components. Representative fluorescence bursts in donor and acceptor channels and corresponding PIE and FRET events recorded in the monomeric dispersed (top) and droplet (bottom) phases are also depicted. Reproduced with permission from Ref (84).

Additionally, in order to minimize artifacts in the measurements due to scattering or autofluorescence, care must be taken when choosing suitable fluorophores and using correct optical filters for the fluorescence setup. Previously, smFRET measurements were successfully used to observe the conformational shapeshifting of the natively intrinsically disordered protein tau upon phase separation.[79-81]

In a recent study, smFRET was also utilized to detect and characterize structurally distinct conformation states within the structurally heterogeneous populations of the single-droplet condensed phase of the disordered low-complexity domain of FUS.[84] Additionally, an extension of this technique used acceptor photobleaching assays to measure FRET amongst the Nup98-FG domains of the nuclear pore complex within cells, where orthogonal labeling was achieved using unnatural amino acid labeling.[83] Characteristic of the slow diffusion of molecules within droplets, the emission bursts seen for the condensed phase in droplet measurements show a much more prolonged fluorescence signal as compared to the fluorescent bursts seen for monomeric solutions or molecular assemblies.

**Vibrational Raman Spectroscopy**

In addition to the above-mentioned tools, Raman spectroscopy is a powerful tool for elucidating the three-dimensional structure of proteins, as well as their dynamics and interaction networks within phase-separated biomolecular assemblies. Raman scattering refers to the inelastic scattering of photons upon the excitation of a molecule by electromagnetic radiation, which can have a wavelength either higher (Stokes Raman scattering) or lower (Anti-stokes Raman scattering) than the wavelength of light used for excitation. In proteins, the vibrational stretching and bending in the sequence backbone or side groups can be captured and assigned peak positions in the Raman spectrum. A Raman spectrum for a given protein, therefore, acts as a fingerprint for its three-dimensional structure and can elucidate the composition of various structural elements such as alpha helices, beta sheets, or various aromatic residues that are present in it. Due to the inherent insensitivity of Raman scattering, an extension of this technique that uses surface-active nanoparticles in surface-enhanced Raman spectroscopy (SERS) was developed. By performing this technique in a confocal microscopy format, information about the structural changes experienced by polypeptide chains upon condensation can be efficiently acquired in a label-free, droplet-by-droplet manner.

The recent surge in the development of methods dedicated to studying biomolecular phase separation has contributed immensely to the study of the same. As an essential phenomenon for maintaining complex systems, phase separation is crucial for cellular physiology. Conversely, any aberrancy in this process also contributes to the etiology of several diseases. This multidimensional role of phase separation is notably exemplified by several proteins that, although crucial for cellular biochemistry, are also majorly implicated in disease. One such archetypical protein is the neuronal tau, which is central to biological pathophysiology. The following sections describe, in detail, the crucial role of tau and the importance of its phase behavior, both in function and in disease.

## 1.5. A multifaceted protein Tau: Its involvement in physiology and pathology

Tau, a microtubule-associated protein, gained prominence in 1986 as a major component in Alzheimer 's-associated filaments.[85-99] Governed by the MAPT gene,[100] tau exhibits six isoforms through alternative splicing.[101, 102] The full-length tau (htau40) is a 45.9-kDa intrinsically disordered protein with distinct features (Figure 1.8). Isoforms, including the embryonal htau23, follow a developmental regulation, with htau23 up-regulated in fetal brains and down-regulated in mature stages in favor of the 4R isoform.[102-104] Mutations in tau are linked to frontotemporal dementia, categorizing it as a disease-causing agent. Neurodegenerative disorders with insoluble Tau deposits are collectively known as tauopathies.[99]

Initially, tau interaction with microtubule filaments in axons marked its primary biological role. Weingarten et al. in 1975 identified tau as a "protein factor" associated with microtubules, classifying it as a member of microtubule-associated proteins.[85-88] Studies have established its involvement in various aspects of microtubule dynamics, including promoting tubulin polymerization,[104, 105] elongating and stabilizing filaments, spacing microtubules,[85, 88, 106, 107,] and safeguarding them from severing enzymes.[108, 109] Tau interaction with tubulin and microtubule filaments is facilitated by distinct regions in its sequence, namely the proline-rich region and the adjacent imperfect repeat domain in the C-terminal half.[107, 110-113] It reduces tubulin dissociation and enhances filament stability by binding at the tubulin heterodimer interface.[103, 112-118] Recent studies indicate the formation of tau condensates, termed tau islands, on microtubule surfaces, protecting them from severing enzymes like katanin and spastin (Figure 1.9).[115, 119-122] This multifaceted role highlights its contribution to maintaining the structural integrity of microtubules in response to cellular needs.

Apart from this, tau, through its modulation of microtubule polymerization and dynamics, contributes to the cytoskeleton development and axonal growth process.[123, 124] The expression of tau isoforms varies during development, aligning with its role in neuronal development.[102-104] In vitro and in vivo studies have emphasized tau involvement in gene expression regulation, spine growth, and neuron maturation.[125-129] In terms of axonal transport regulation, tau shapes the interaction of motor proteins with microtubules, thereby regulating axonal transport.[130-132]

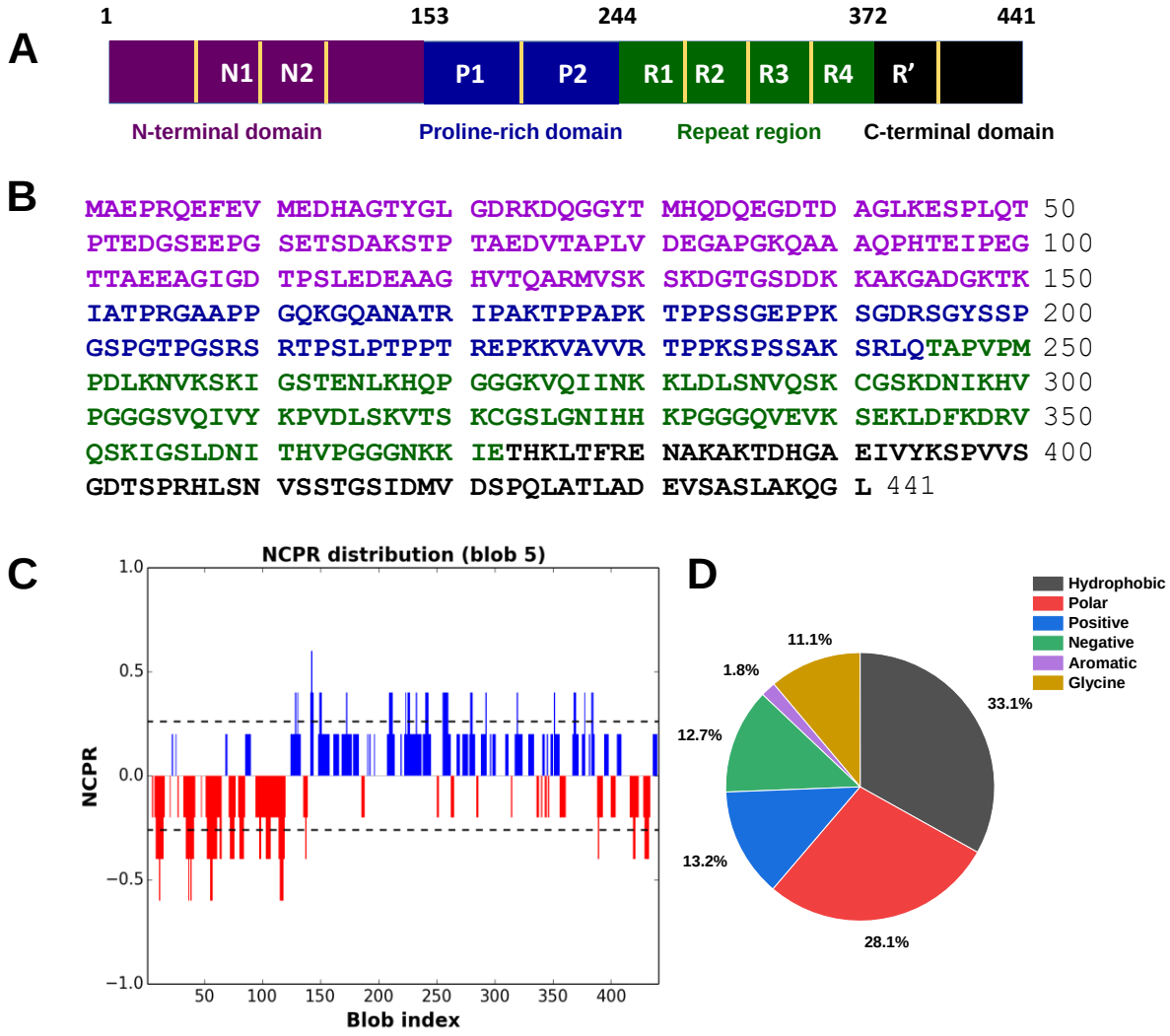


**Figure 1.8. A.** Sequence architecture and **B.** amino-acid sequence of the longest-isoform of the human full-length microtubule-associated protein tau. **C.** Charge distribution of tau depicted as the net charge per residue [NCPR; positive: blue, negative: red; generated using CIDER (Classification of Intrinsically Disordered Ensemble Regions)]. **D.** Amino acid distribution of tau described by a pie chart. Reproduced with permission from Ref (27).

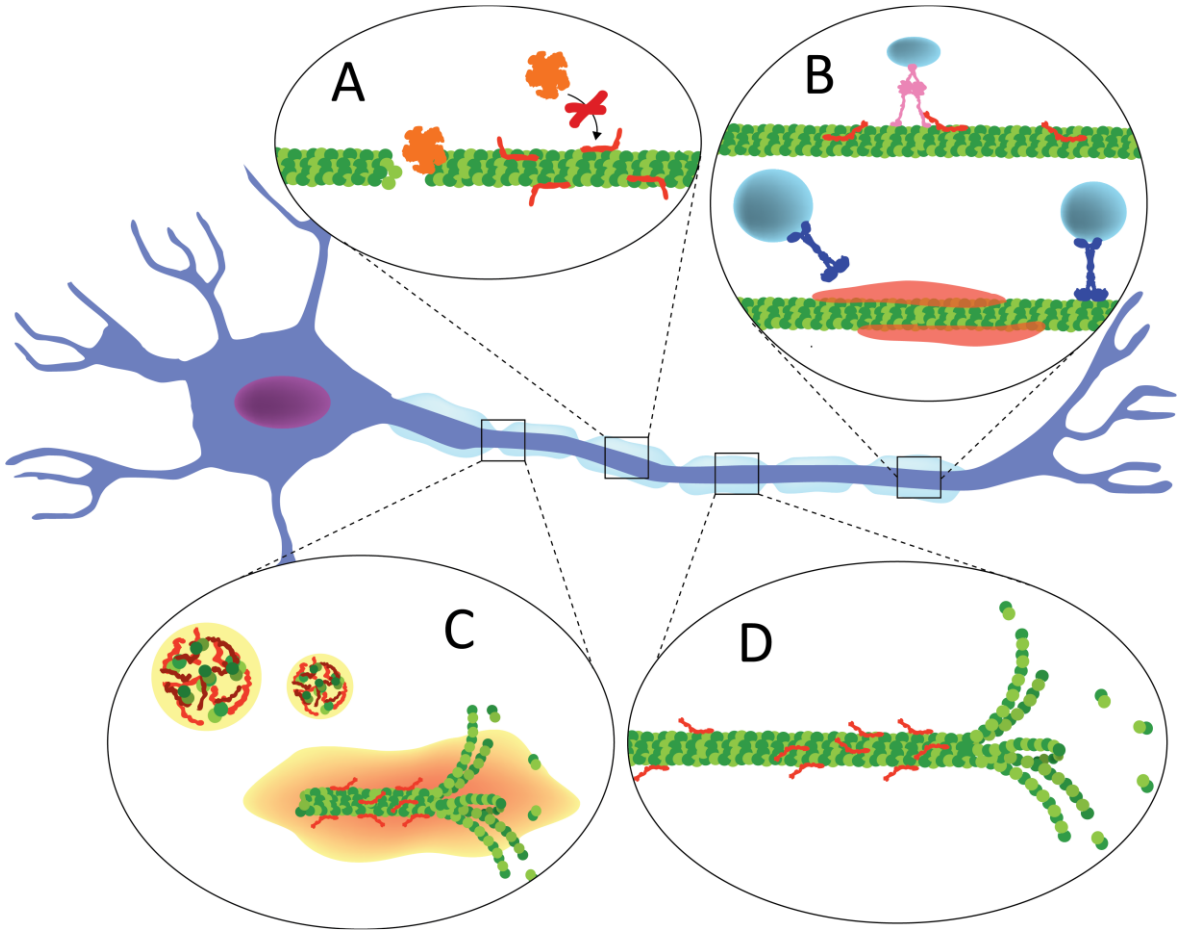


**Figure 1.9 Functional activities of the tau protein (red): A.** Tau protects microtubules against the action of severing enzymes such as Katanin. **B.** It can regulate both retrograde and anti-retrograde axonal transport in neurons. While it can regulate dynactin complexes (pink) on microtubules, its condensation can potentiate the dissociation of kinesin (blue). **C.** Tubulin recruitment in tau droplets promotes microtubule extension. **D.** Tau binding the labile ends of microtubules can stabilize these filaments, protecting them from catastrophe events and promoting their growth. Reproduced with permission from Ref (27).

Tau interacts with the dynactin complex via its N-terminal end, stabilizing its microtubule binding. The growth of tau islands on microtubule surfaces induces the detachment of kinesin-1 motor proteins, while other members of the kinesin-8 motor protein family and dynein-dynactin complexes display pausing on microtubule surfaces.[121-122] Additionally, tau, in the filamentous state, influences axonal transport by interacting with protein phosphatase 1, potentially activating GSK3-beta and impacting kinesin phosphorylation, inhibiting fast anterograde transport.[131, 133, 134] Beyond axonal transport, tau exhibits various activities,[103, 135,

[136] such as interactions with the tyrosine kinase Fyn in synapses. Fyn mediates tau phosphorylation upon interacting with it and regulates tau binding to neuronal membranes, filamentous actin, and synaptic vesicles, supporting its involvement in synapses and neuronal functions.[137, 138] The intrinsically disordered nature of tau allows for highly dynamic interactions regulated through post-translational modifications.[139, 140] Despite some challenges to certain tau activities, its diverse functions highlight its significance in shaping neuronal development and function.

Tau aggregation is a hallmark in various neurodegenerative diseases, collectively termed "tauopathies," including Alzheimer's disease (AD), Pick's disease (PiD), frontotemporal dementia, and others. These diseases are characterized by cognitive impairment linked to the buildup of aggregated tau in different brain regions.[99, 103] Tau can form distinct inclusions like neurofibrillary tangles (NFTs) and neuropil threads (NTs), with the morphological differences not fully understood.[99] In AD, NFTs, and NTs, composed of misfolded and hyperphosphorylated tau, accumulate in neuronal somata and dendrites.[94, 103] From the entorhinal cortex, tau fibrils spread to distinct regions of the brain during the disease progression, in distinct stages in AD brains.[141, 142]

Cryo-electron microscopy studies of *ex vivo* fibrils from the patient's brain have shown the three-dimensional structure of AD tau fibrils, with a cross-β-structure core composed of specific tau pseudo-repeats.[143] While AD analysis showed the enrichment of 4R and 3R isoforms of tau, in PiD, 3R isoforms are found in the majority.[144] In PiD, tau fibrils exhibit two conformations, wide and narrow filaments.[145] Tau fibrils are seen in oligodendrocytes as well as in astrocytes and accumulate in circular NFTs in neurons in Progressive Supranuclear Palsy.[99, 146] Different tauopathies correspond to specific fibril conformations or "strains," suggesting a link between structural properties and clinical/neuropathological hallmarks.[147-151]

Post-translational modifications (PTMs) of tau, for example, phosphorylation, acetylation, and ubiquitination impact the fibril structure.[152, 153] Cryo-EM combined with mass spectrometry revealed distinct PTM patterns in tau fibrils from AD and Corticobasal Degeneration, suggesting a connection between PTMs and disease-specific strains of tau. PTMs also influence the pathological behaviors of tau oligomers in AD, with phosphorylation correlating with higher seeding efficiency and oligomer-based seeding efficacy linked to clinical symptoms, indicating a potential influence on AD severity.[153]

## 1.6 Tau phase separation: Key regulating factors

LLPS, a physical process driven by a multitude of multivalent interactions, results in a protein-rich dense phase and a protein-depleted dilute phase. Electrostatic, cation-pi/pi-pi, and hydrophobic interactions contribute to the favorable interactions within and between constituting proteins/nucleic acids, overcoming entropic penalties during the phase separation process.[56-59, 68] Aromatic, non-polar, and charged amino acids, as well as crowding agents like polyethylene glycol (PEG), Ficoll, and cofactors, can promote LLPS.

NMR studies and bioinformatic analysis (PONDR-FIT[154] and IUpred2[155]) have shown that Tau is a natively unstructured protein, and bioinformatic tools such as CatGranule,[61] and FuzDrop,[63] predicted its phase separation propensity. Its dynamic conformation, characterized by a high proline content[156] (9.7%) and glycine (11%), along with polar and charged amino acids (Figure 1.8)[62] contributes to its liquid-liquid phase separation (LLPS) both in vitro and in cells.[53, 157-166] Lysine residues, the proline-rich domain (PRD), oppositely charged termini, the hexapeptide region, and KXGS motifs in the microtubule-binding region (MTBR) play crucial roles in tau LLPS.[162-168] Post-translational modifications, particularly on lysine residues, can regulate tau functions by tuning the overall charge of the polypeptide chain. Phosphorylation in the proline-rich domain and the presence of aggregation-prone hexapeptides influence the LLPS propensity. Different isoforms of tau exhibit varying phase separation abilities, correlating with their charge, isoelectric point (pI), presence of the N-terminal part, and the number of repeat regions. Notably, full-length tau (htau40) demonstrates a higher phase separation propensity than other isoforms under near-physiological conditions, compared to K18 (4R) and K19 (3R). Overall, an intricate interplay of electrostatic, hydrogen bonding, and hydrophobic interactions govern the homotypic and heterotypic LLPS of tau.[157, 164, 168]

## 1.7 Simple-coacervates and complex-coacervates of tau

Intrinsically disordered proteins (IDPs) exhibit a fascinating propensity for LLPS, driven by self-coacervation through intricate intra- and intermolecular interactions. This process finds assistance from diverse molecular factors, including crowding agents and small molecules. Moreover, IDPs are susceptible to electrostatically-fueled associative phase transitions with nucleic acids. Due to its negative charge, RNA emerges as a crucial regulator in coacervate assembly via such interactions. This intricate interplay between IDPs and RNA has been notably exemplified in the context of tau, where a rich interplay unfolds. Tau interaction with RNA molecules, both in vitro and in cells,[168, 170] underscores the multifaceted nature of this association (Figure 1.10). The strong electrostatic component arising from the positively

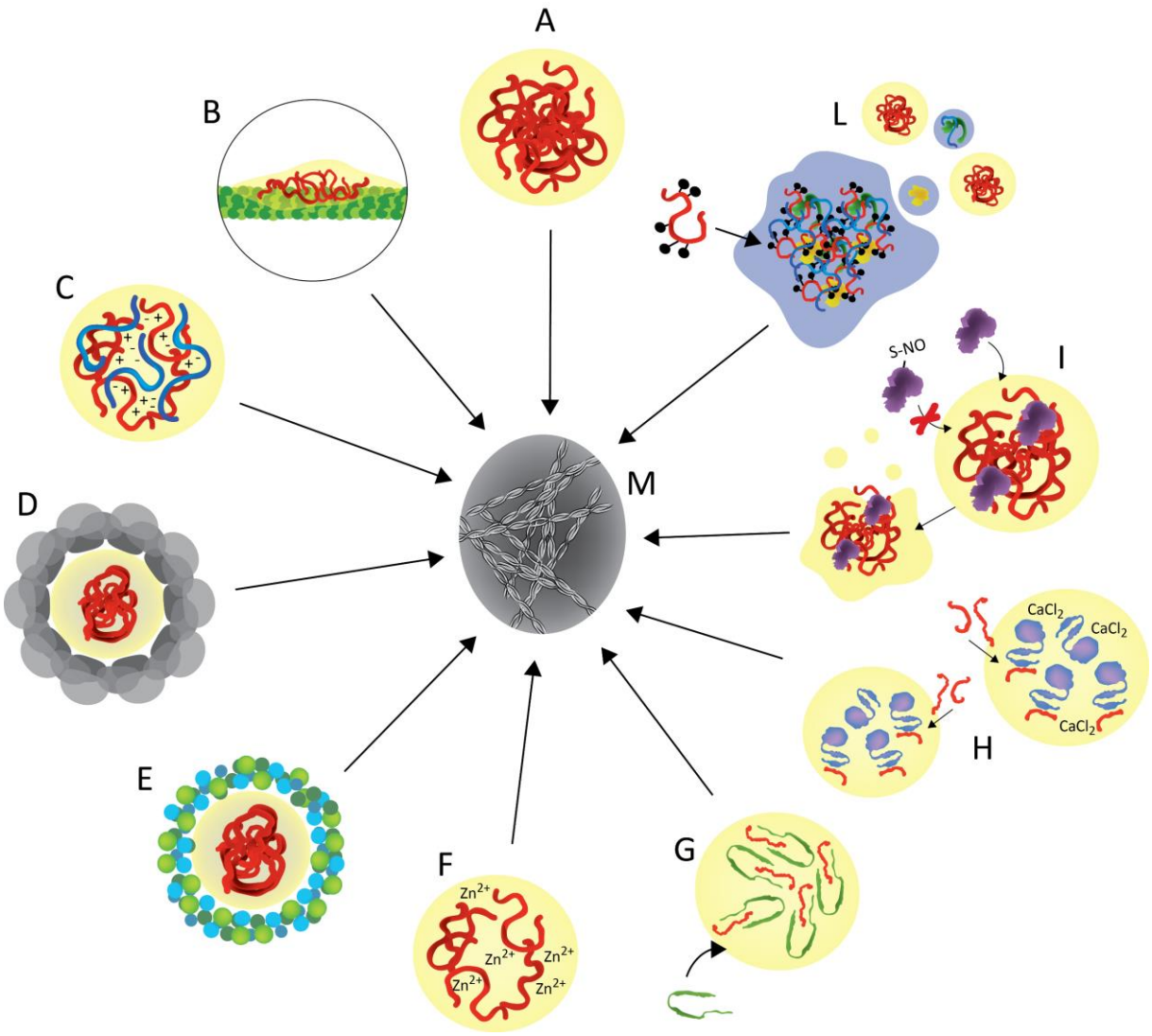


**Figure 10. Phase separation of tau in physiology and pathology**: **A.** Tau can phase separate in the absence of any co-factor by a domain-dependent, simple coacervation. **B.** Tau can form condensates termed microtubule islands on the surface of microtubules. **C.** Tau can interact with RNA electrostatically, leading to phase separation. **D** This process can be enhanced due to the excluded volume effects in the presence of molecular crowders. **E.** Tau phase separation can be induced by salting out at very high salt concentrations **F.** or in the presence of zinc. **G.** Tau can undergo heterotypic condensation with α-synuclein. **H.** Tau is sequestered into droplets formed by the calcium-binding protein Efhd2. These droplets are modulated by calcium and can transition into tau fibrils in the absence of $CaCl_2$. **I.** The chaperone PD11 can modulate tau droplets. Its recruitment leads to droplet dissolution. However, upon S-nitrosylation, the activity of the protein is lost, and tau fibrils are formed via phase separation. **J.** Excessive tau phase separation forms SGs, which leads to hyperphosphorylation and further recruitment into SGs, where RNA and proteins can interact with tau. **K.** Tau droplets can undergo aberrant liquid-to-solid changes. Reproduced with permission from Ref (27).

charged tau and negatively charged RNA establishes a foundation for LLPS induction and promotion by RNA. This phenomenon is robust, as evidenced by the insensitivity of tau-RNA complex coacervation to 1,6-hexanediol, which dissolves droplets based on the underlying hydrophobic interactions. Furthermore, the addition of polyanions like RNA and heparin has been instrumental in disturbing the electrostatic repulsion amongst tau molecules and inducing aggregation. The landscape of tau LLPS is further modulated by molecular crowding agents, metal ions, and salts.[171, 172] The presence of these factors influences the dynamics of tau phase separation both in the presence and absence of RNA.[162, 53]

Additionally, protein-protein interactions within membrane-less organelles offer intriguing insights into the modulation of protein LLPS. Various proteins, such as EFhd2 and protein disulfide isomerase (PDI), exhibit distinct effects on tau droplets, influencing their dissolution or promoting their aggregation (Figure 1.10).[173, 174] The recruitment of one protein into the condensates of another may contribute to the synergistic aggregation of proteins, as observed in α-synuclein and tau co-phase separation studies.[175, 176] Post-translational modifications (PTMs) are crucial in regulating liquid-liquid phase separation (LLPS) by modulating the net charge on the tau chain, conformation, and interaction abilities. Being intrinsically disordered, Tau is highly susceptible to PTMs like phosphorylation and acetylation. Phosphorylation, by introducing negative charges and lowering tau's overall positive charge, favors LLPS. Acetylation, conversely, neutralizes lysine residues' positive charges, increasing hydrophobicity and attenuating LLPS. These PTMs, particularly phosphorylation and acetylation, impact tau LLPS dynamics and may contribute to its pathological aggregation in neurodegenerative conditions.[166, 167, 177-180]

## 1.8 Association of tau condensates with microtubules and stress granules

Recent discoveries have linked tau phase separation to its role in tubulin binding and promoting the polymerization of microtubules.[119-122] In experiments by Hernández-Vega, tau phase separation, in the presence of tubulin and an energy source in the form of GTP, led to the nucleation of microtubules from the droplets.[119] Subsequent research by Savastano et al. revealed that disease-associated phosphorylation of T231 inhibits this nucleation by inducing salt bridges with R230, disrupting microtubule-promoting interactions with tubulin.[122] Contrary to earlier beliefs that tau-microtubule interaction induces aggregation,[181-183] recent findings indicate that microtubules act as platforms favoring phase transitions.[184] Fluorescence microscopy demonstrated tau forming condensate-like islands on the microtubule surface,

exhibiting liquid-like properties. These tau islands, formed at low concentrations, interact with motor proteins and recruit proteins like EB1, contributing to the establishment of microtubule architecture.[121, 122, 163] Stress granules (SGs) are membrane-less assemblies that exist in the cytosol and consist of non-coding mRNA molecules, in addition to specific translation factors, and various RNA-binding proteins (RBPs), including FUS, T-cell intracellular antigen 1 (TIA-1), and poly(A)-binding protein (PABP), which aggregate via the glycine-rich stretches present in their sequence.[185] The transient assembly of SGs in response to cellular stress contributes to cell survival.

Tau is implicated in the regulation of stress granule formation, and conversely, pathological changes in tau are stimulated by stress granule formation, proposing a potential pathway for tau aggregation. In this regard, the stress-induced hyperphosphorylation of tau leads to its mislocalization within neurons. Here, upon localizing to the somatic and dendritic regions in neurons, it interacts with the RNA and RBPs that are typically found in stress granules.[186-188] SGs comprise a concentrated core and a less-concentrated shell involving transport factors that are involved in nucleocytoplasmic shuttling, such as a range of karyopherins and various nucleoporins (Nups).[195, 196] Phosphorylated tau can colocalize and interacts with the FG-phase of Nup98 in the nuclear pore complex (NPC), multiple copies of which serve as gatekeepers for nucleocytoplasmic exchange, perturbing its function and impairing this process. Additionally, the highly negatively charged, C-terminal domain of Nup98, which is typically located within the NPC, can also promote the fibril assembly of tau in vitro, suggesting a potential role in the aggregation of tau in neurons.[197-199]Amongst the most notable tau interacting stress-granular components is the protein TIA-1, which is also implicated in several neurodegenerative diseases. The assembly of secondary RBPS, in response to TIA-1-associated nucleation, can form mature stress granules that further promote translational suppression. Due to its association with TIA-1, the condensation of tau is potentiated and is associated with neurodegeneration. [187, 188-192] Additionally, the documented localization of ubiquitin with neurofibrillary aggregates aligns with evidence highlighting the importance of Ubiquitin-specific protease 10 (USP10) as a modulator of stress-granule assembly in association with tau and TIA-1.[193, 194] Conversely, acetylation reduces tau's SG association, considering the increased neurotoxicity associated with acetylated tau, and consequently might play a protective role in this context.[162, 169]

## 1.9 Solidification of tau condensates

The transition of tau into amyloid-like aggregates that are implicated in the etiology of diseases such as AD from a soluble state follows typical sigmoidal kinetics. Soluble, monomeric tau can phase separate into condensates that may serve as reaction crucibles for the formation of pathological aggregates. However, how any modifications perturb the conformational dynamics of tau and lead to the formation of disease-associated aggregates still remains elusive. The transient formation of β-sheet structures during the phase separation of the tau K18 truncation, composed of the tau repeat region, may provide some answers in this direction[157, 165]. While the link between tau liquid-liquid phase separation (LLPS) and fibrillization is debated, factors like heparin, mutations, and hyperphosphorylation can promote tau condensation.[162, 166-168, 177-180] Moreover, protein disulfide isomerase suppresses tau droplet formation and aggregation, while EFhd2, a tau-associated protein, regulates LLPS.[173, 174, 200] Disease-related mutations can enhance tau phase separation, leading to varied outcomes. In this regard, hydrophobic interactions play an important role in interconnecting tau LLPS and fibrillization. [201] Although numerous such in vitro and in vivo studies have been undertaken, a direct connection between the liquid-to-solid transition of tau and the disease still remains an area of intense research.

## 1.10 Thesis motivation and perspective

Biomolecular condensation has emerged as a paradigm for modulating the spatiotemporal coherence of the crowded cellular milieu. The resulting membraneless organelles are an indispensable part of the cellular physiology. By creating a chemically distinct microenvironment, the phase separation of biologically relevant macromolecules allows millions of different metabolic processes and molecular events to function in chemical isolation, even in the absence of a delimiting membrane. Several crucial sequence motifs predispose specific biopolymers to engage in dynamic, multivalent interactions that promote their phase separation. The presence of intrinsic disorder is one such sequence feature that is also typical for numerous neuronal proteins, many of which are implicated in disease. The material properties of condensates are a direct readout of their function, and any aberrant changes associated with the same often prove to be pathological for biological systems. This is starkly observed for neuronal condensates, which transition into solid, amyloid-like aggregates linked to several neurodegenerative disorders due to aberrant phase changes. The liquid-to-solid transition of neuronal IDP condensates is exemplified by the tau protein, which is known to undergo associative phase transitions with a number of different interacting partners. The

work described in this thesis dissects the crucial molecular events that govern the complex coacervation of tau with known cellular interactors to recapitulate the events that contribute towards modulating its phase behavior. The interactions of tau with unrelated amyloidogenic proteins hint towards the contributions of neuronal protein networks in the pathophysiology of overlapping neurodegenerative diseases. Building on previous observations of the deposition of tau in solid aggregates in the brains of patients suffering from prion-related diseases, we investigated the role of the human prion protein on the phase behavior of tau. Here, we identified the heterotypic, complex coacervation as a pathway for the formation of tau-prion co-aggregates. Our results also demonstrated the modification of tau-PrP condensates in the presence of RNA to attain a multiphasic morphology. Additionally, using a combination of domain-specific variants in addition to steady-state and time-resolved fluorescence, we were able to dissect the molecular determinants of this associative interaction (Chapter 3).

Furthermore, in line with the importance of the material properties of condensates, we elucidate the role of the protein quality control machinery in influencing tau condensation and the conformational rationale behind the action of molecular chaperones in abrogating tau misfolding into amyloid-like species. Using super-resolution imaging and FRAP, we studied the co-phase separation of tau and Ydj1, a yeast analog of the human Hsp40, which is part of the initial defense mechanism against protein misfolding in higher-order species. Our results demonstrated the importance of an amalgamation of electrostatic and hydrophobic interactions in driving tau-Ydj1 complex formation. Further, to dissect the molecular events that lead to such interactions, we used ensemble fluorescence measurements in conjunction with sensitive single-molecule experiments to delineate the conformational landscape of phase-separated tau during its interaction with Ydj1. Here, we characterized the importance of two critical amyloid motifs in the tau polypeptide chain in not only regulating its interactions with chaperones like Ydj1 but also in crucially influencing its ability to undergo phase separation. Using electron tomography and Raman spectroscopy, we characterized the proteinaceous species formed upon the prolonged incubation of tau-Ydj1 mixtures and the structural basis for preventing amyloid formation (Chapter 4).

I believe that the work carried out in this thesis will contribute to our understanding of the role of biological phase separation in shaping molecular networks orchestrated by intrinsically disordered proteins such as tau. This thesis aimed to unravel the significance of complex coacervation in overlapping neuropathology and dissect the fundamental mechanisms that shape and influence the material properties of biomolecular condensates. The results described in the thesis promote the applicability and physiological relevance of the phase separation

phenomena, both in our basic understanding of the process and in identifying potentially paramount therapeutic targets.

(A part of this chapter is inspired by the reference: (27) Rai, S. K.; Savastano, A.; Singh, P.; Mukhopadhyay, S.; Zweckstetter, M. Liquid-liquid phase separation of tau: From molecular biophysics to physiology and disease. Protein Science **2021**, *30* (7), 1294-1314.)

## 1.11 References


1. Alberts, B.; Heald, R.; Johnson, A.; Morgan, D.; Raff, M.; Roberts, K.; Walter, P. Molecular Biology of The Cell. *Molecular Biology of The Cell* **2022**.

2. Brangwynne, C. P.; Eckmann, C. R.; Courson, D. S.; Rybarska, A.; Hoege, C.; Gharakhani, J.; Jülicher, F.; Hyman, A. A. Germline P Granules Are Liquid Droplets That Localize by Controlled Dissolution/Condensation. *Science* **2009**, *324* (5935), 1729–1732.

3. Banani, S. F.; Lee, H. O.; Hyman, A. A.; Rosen, M. K. Biomolecular Condensates: Organizers of Cellular Biochemistry. *Nature Reviews. Molecular Cell Biology* **2017**, *18* (5), 285–298.

4. Weber, S. C.; Brangwynne, C. P. Getting RNA and Protein in Phase. *Cell* **2012**, *149* (6), 1188–1191

5. Alberti, S. Phase Separation in Biology. *Current Biology: CB* **2017**, *27* (20), R1097–R1102.

6. Kilgore, H. R.; Young, R. A. Learning the Chemical Grammar of Biomolecular Condensates. *Nature Chemical Biology* **2022**, *18* (12), 1298–1306.

7. Alberti, S.; Hyman, A. A. Biomolecular Condensates at the Nexus of Cellular Stress, Protein Aggregation Disease and Ageing. *Nature Reviews. Molecular Cell Biology* **2021**, *22* (3), 196–213.

8. Lyon, A. S.; Peeples, W. B.; Rosen, M. K. A Framework for Understanding the Functions of Biomolecular Condensates across Scales. *Nature Reviews Molecular Cell Biology* **2021**, *22* (3), 215–235.

9. Mittag, T.; Pappu, R. V. A Conceptual Framework for Understanding Phase Separation and Addressing Open Questions and Challenges. *Molecular Cell* **2022**, *82* (12), 2201–2214.

10. Fuxreiter, M.; Vendruscolo, M. Generic Nature of the Condensed States of Proteins. *Nature Cell Biology* **2021**, *23* (6), 587–594.

11. Roden, C.; Gladfelter, A. S. RNA Contributions to the Form and Function of Biomolecular Condensates. *Nature Reviews. Molecular Cell Biology* **2021**, *22* (3), 183–195.

12. Choi, J.-M.; Holehouse, A. S.; Pappu, R. V. Physical Principles Underlying the Complex Biology of Intracellular Phase Transitions. *Annual Review of Biophysics* **2020**, *49* (1), 107–133.

13. Walter, H.; Brooks, D. E. Phase Separation in Cytoplasm, Due to Macromolecular Crowding, Is the Basis for Microcompartmentation. *FEBS Letters.* **1995**, *361* (2–3), 135–139.

14. Strome, S.; Wood, W. B. Generation of Asymmetry and Segregation of Germ-Line Granules in Early C. Elegans Embryos. *Cell* **1983**, *35* (1), 15–25.

15. Lafontaine, D. L. J.; Riback, J. A.; Bascetin, R.; Brangwynne, C. P. The Nucleolus as a Multiphase Liquid Condensate. *Nature Reviews Molecular Cell Biology* **2021**, *22* (3), 165–182.

16. Berry, J.; Weber, S. C.; Vaidya, N.; Haataja, M.; Brangwynne, C. P. RNA Transcription Modulates Phase Transition-Driven Nuclear Body Assembly. *Proceedings of the National Academy of Sciences U. S. A.* **2015**, *112* (38), E5237-45.

17. Schmidt, H. B.; Görlich, D. Transport Selectivity of Nuclear Pores, Phase Separation, and Membraneless Organelles. *Trends in Biochemical Sciences* **2016**, *41* (1), 46–61.

18. Hampoelz, B.; Andres-Pons, A.; Kastritis, P.; Beck, M. Structure and Assembly of the Nuclear Pore Complex. *Annual Review of Biophysics* **2019**, *48* (1), 515–536.

19. Woodruff, J. B.; Ferreira Gomes, B.; Widlund, P. O.; Mahamid, J.; Honigmann, A.; Hyman, A. A. The Centrosome Is a Selective Condensate That Nucleates Microtubules by Concentrating Tubulin. *Cell* **2017**, *169* (6), 1066-1077.e10.

20. Martin, R. M.; Cardoso, M. C. Chromatin Condensation Modulates Access and Binding of Nuclear Proteins. *FASEB J.* **2010**, *24* (4), 1066–1072.

21. Haws, S. A.; Simandi, Z.; Barnett, R. J.; Phillips-Cremins, J. E. 3D Genome, on Repeat: Higher-Order Folding Principles of the Heterochromatinized Repetitive Genome. *Cell* **2022**, *185* (15), 2690–2707.

22. Ray, S.; Singh, N.; Kumar, R.; Patel, K.; Pandey, S.; Datta, D.; Mahato, J.; Panigrahi, R.; Navalkar, A.; Mehra, S.; Gadhe, L.; Chatterjee, D.; Sawner, A. S.; Maiti, S.; Bhatia, S.; Gerez, J. A.; Chowdhury, A.; Kumar, A.; Padinhateeri, R.; Riek, R.; Krishnamoorthy, G.; Maji, S. K. α-Synuclein Aggregation Nucleates through Liquid-Liquid Phase Separation. *Nature Chemistry* **2020**, *12* (8), 705–716.

23. Wang, B.; Zhang, L.; Dai, T.; Qin, Z.; Lu, H.; Zhang, L.; Zhou, F. Liquid-Liquid Phase Separation in Human Health and Diseases. *Signal Transduction and Targeted Therapy* **2021**, *6* (1), 290.

24. Portz, B.; Lee, B. L.; Shorter, J. FUS and TDP-43 Phases in Health and Disease. *Trends in Biochemical Sciences* **2021**, *46* (7), 550–563.

25. Boeynaems, S.; Alberti, S.; Fawzi, N. L.; Mittag, T.; Polymenidou, M.; Rousseau, F.; Schymkowitz, J.; Shorter, J.; Wolozin, B.; Van Den Bosch, L.; Tompa, P.; Fuxreiter, M. Protein Phase Separation: A New Phase in Cell Biology. *Trends in Cell Biology* **2018**, *28* (6), 420–435.

26. Shin, Y.; Brangwynne, C. P. Liquid Phase Condensation in Cell Physiology and Disease. *Science* **2017**, *357* (6357), eaaf4382.

27. Rai, S. K.; Savastano, A.; Singh, P.; Mukhopadhyay, S.; Zweckstetter, M. Liquid-Liquid Phase Separation of Tau: From Molecular Biophysics to Physiology and Disease. *Protein Science: A Publication of the Protein Society* **2021**, *30* (7), 1294–1314.

28. Limorenko, G.; Lashuel, H. A. Revisiting the Grammar of Tau Aggregation and Pathology Formation: How New Insights from Brain Pathology Are Shaping How We Study and Target Tauopathies. *Chemical Society Reviews* **2022**, *51* (2), 513–565.

29. Flory, P. J.; Krigbaum, W. R. Thermodynamics of High Polymer Solutions. *Annual Review of Physical Chemistry* **1951**, *2* (1), 383–402.

30. Brangwynne, C. P.; Tompa, P.; Pappu, R. V. Polymer Physics of Intracellular Phase Transitions. *Nature Physics* **2015**, *11* (11), 899–904.

31. Vernon, R. M.; Chong, P. A.; Tsang, B.; Kim, T. H.; Bah, A.; Farber, P.; Lin, H.; Forman-Kay, J. D. Pi-Pi Contacts Are an Overlooked Protein Feature Relevant to Phase Separation. *Elife* **2018**, *7*.

32. Dignon, G. L.; Best, R. B.; Mittal, J. Biomolecular Phase Separation: From Molecular Driving Forces to Macroscopic Properties. *Annual Review of Physical Chemistry* **2020**, *71* (1), 53–75.

33. Mohanty, P.; Kapoor, U.; Sundaravadivelu Devarajan, D.; Phan, T. M.; Rizuan, A.; Mittal, J. Principles Governing the Phase Separation of Multidomain Proteins. *Biochemistry* **2022**, *61* (22), 2443–2455.

34. Shapiro, D. M.; Ney, M.; Eghtesadi, S. A.; Chilkoti, A. Protein Phase Separation Arising from Intrinsic Disorder: First-Principles to Bespoke Applications. *The Journal of Physical Chemistry. B* **2021**, *125* (25), 6740–6759.

35. Uversky, V. N. Intrinsically Disordered Proteins in Overcrowded Milieu: Membrane-Less Organelles, Phase Separation, and Intrinsic Disorder. *Current Opinion in Structural Biology* **2017**, *44*, 18–30.

36. Ruff, K. M.; Choi, Y. H.; Cox, D.; Ormsby, A. R.; Myung, Y.; Ascher, D. B.; Radford, S. E.; Pappu, R. V.; Hatters, D. M. Sequence Grammar Underlying the Unfolding and Phase Separation of Globular Proteins. *Molecular Cell* **2022**, *82* (17), 3193-3208.e8.

37. Ditlev, J. A.; Case, L. B.; Rosen, M. K. Who's in and Who's out-Compositional Control of Biomolecular Condensates. *Journal of Molecular Biology* **2018**, *430* (23), 4666–4684.

38. Abbas, M.; Lipiński, W. P.; Wang, J.; Spruijt, E. Peptide-Based Coacervates as Biomimetic Protocells. *Chemical Society Reviews* **2021**, *50* (6), 3690–3705.

39. Pak, C. W.; Kosno, M.; Holehouse, A. S.; Padrick, S. B.; Mittal, A.; Ali, R.; Yunus, A. A.; Liu, D. R.; Pappu, R. V.; Rosen, M. K. Sequence Determinants of Intracellular Phase

Separation by Complex Coacervation of a Disordered Protein. *Molecular Cell* **2016**, *63* (1), 72–85.

40. Yewdall, N. A.; André, A. A. M.; Lu, T.; Spruijt, E. Coacervates as Models of Membraneless Organelles. *Current Opinion in Colloid & Interface Science* **2021**, *52* (101416), 101416.

41. Fang, Y.; Li, L.; Inoue, C.; Lundin, L. Appelqvist, I. Associative and Segregative Phase Separations of Gelatin/κ-Carrageenan Aqueous Mixtures. *Langmuir* **2006**, *22* (23), 9532–9537.

42. Garaizar, A.; Espinosa, J. R.; Joseph, J. A.; Krainer, G.; Shen, Y.; Knowles, T. P. J.; Collepardo-Guevara, R. Aging Can Transform Single-Component Protein Condensates into Multiphase Architectures. *Proceedings of the National Academy of Sciences U. S. A.* **2022**, *119* (26), e2119800119.

43. Alshareedah, I.; Moosa, M. M.; Raju, M.; Potoyan, D. A.; Banerjee, P. R. Phase Transition of RNA−protein Complexes into Ordered Hollow Condensates. *Proceedings of the National Academy of Sciences* **2020** (27), 15650–15658.

44. Chew, P. Y.; Joseph, J. A.; Collepardo-Guevara, R.; Reinhardt, A. Aromatic and Arginine Content Drives Multiphasic Condensation of Protein-RNA Mixtures. *Biophysical Journal* **2023**, https://doi.org/10.1016/j.bpj.2023.06.024.

45. Chew, P. Y.; Joseph, J. A.; Collepardo-Guevara, R.; Reinhardt, A. Thermodynamic Origins of Two-Component Multiphase Condensates of Proteins. *Chemical Science* **2023**, *14* (7), 1820–1836.

46. Kelley, F. M.; Favetta, B.; Regy, R. M.; Mittal, J.; Schuster, B. S. Amphiphilic Proteins Coassemble into Multiphasic Condensates and Act as Biomolecular Surfactants. *Proceedings of the National Academy of Sciences U. S. A.* **2021**, *118* (51), e2109967118.

47. Lu, T.; Spruijt, E. Multiphase Complex Coacervate Droplets. *Journal of the American Chemical Society* **2020**, *142* (6), 2905–2914.

48. Lee, D. S. W.; Strom, A. R.; Brangwynne, C. P. The Mechanobiology of Nuclear Phase Separation. *APL Bioengineering* **2022**, *6* (2), 021503.

49. Fare, C. M.; Villani, A.; Drake, L. E.; Shorter, J. Higher-Order Organization of Biomolecular Condensates. *Open Biology* **2021**, *11* (6), 210137.

50. Riback, J. A.; Zhu, L.; Ferrolino, M. C.; Tolbert, M.; Mitrea, D. M.; Sanders, D. W.; Wei, M.-T.; Kriwacki, R. W.; Brangwynne, C. P. Composition-Dependent Thermodynamics of Intracellular Phase Separation. *Nature* **2020**, *581* (7807), 209–214.

51. Mountain, G. A.; Keating, C. D. Formation of Multiphase Complex Coacervates and Partitioning of Biomolecules within Them. *Biomacromolecules* **2020**, *21* (2), 630–640.

52. Kaur, T.; Raju, M.; Alshareedah, I.; Davis, R. B.; Potoyan, D. A.; Banerjee, P. R. Sequence-Encoded and Composition-Dependent Protein-RNA Interactions Control Multiphasic Condensate Morphologies. *Nature Communications* **2021**, *12* (1), 872.

53. Rai, S. K.; Khanna, R.; Avni, A.; Mukhopadhyay, S. Heterotypic Electrostatic Interactions Control Complex Phase Separation of Tau and Prion into Multiphasic Condensates and Co-Aggregates. *Proceedings of the National Academy of Sciences U. S. A.* **2023**, *120* (2), e2216338120.

54. Zbinden, A.; Pérez-Berlanga, M.; De Rossi, P.; Polymenidou, M. Phase Separation and Neurodegenerative Diseases: A Disturbance in the Force. *Developmental cell* **2020**, 55(1), 45–68.

55. Sabari, B. R.; Dall'Agnese, A.; Young, R. A. Biomolecular Condensates in the Nucleus. *Trends in Biochemical Sciences* **2020**, *45* (11), 961–977.

56. Alberti, S.; Gladfelter, A.; Mittag, T. Considerations and Challenges in Studying Liquid-Liquid Phase Separation and Biomolecular Condensates. *Cell* **2019**, *176* (3), 419–434.

57. Bracha, D.; Walls, M. T.; Brangwynne, C. P. Probing and Engineering Liquid-Phase Organelles. *Nature Biotechnology* **2019**, *37* (12), 1435–1445.

58. Wang, J.; Choi, J.-M.; Holehouse, A. S.; Lee, H. O.; Zhang, X.; Jahnel, M.; Maharana, S.; Lemaitre, R.; Pozniakovsky, A.; Drechsel, D.; Poser, I.; Pappu, R. V.; Alberti, S.; Hyman, A. A. A Molecular Grammar Governing the Driving Forces for Phase Separation of Prion-like RNA Binding Proteins. *Cell* **2018**, *174* (3), 688-699.e16.

59. Posey, A. E.; Holehouse, A. S.; Pappu, R. V. Phase Separation of Intrinsically Disordered Proteins. *Methods in Enzymology* **2018**, *611*, 1–30.

60. Banani, S. F.; Rice, A. M.; Peeples, W. B.; Lin, Y.; Jain, S.; Parker, R.; Rosen, M. K. Compositional Control of Phase-Separated Cellular Bodies. *Cell* **2016**, *166* (3), 651–663.

61. Bolognesi, B.; Lorenzo Gotor, N.; Dhar, R.; Cirillo, D.; Baldrighi, M.; Tartaglia, G. G.; Lehner, B. A Concentration-Dependent Liquid Phase Separation Can Cause Toxicity upon Increased Protein Expression. *Cell Reports* **2016**, *16* (1), 222–231.

62. Holehouse, A. S.; Das, R. K.; Ahad, J. N.; Richardson, M. O. G.; Pappu, R. V. CIDER: Resources to Analyze Sequence-Ensemble Relationships of Intrinsically Disordered Proteins. *Biophysical Journal* **2017**, *112* (1), 16–21.

63. Hardenberg, M.; Horvath, A.; Ambrus, V.; Fuxreiter, M.; Vendruscolo, M. Widespread Occurrence of the Droplet State of Proteins in the Human Proteome. *Proceedings of the National Academy of Sciences U. S. A.* **2020**, *117* (52), 33254–33262.

64. Mitrea, D. M.; Chandra, B.; Ferrolino, M. C.; Gibbs, E. B.; Tolbert, M.; White, M. R.; Kriwacki, R. W. Methods for Physical Characterization of Phase-Separated Bodies and Membrane-Less Organelles. *Journal of Molecular Biology* **2018**, *430* (23), 4773–4805.

65. Fei, J.; Jadaliha, M.; Harmon, T. S.; Li, I. T. S.; Hua, B.; Hao, Q.; Holehouse, A. S.; Reyer, M.; Sun, Q.; Freier, S. M.; Pappu, R. V.; Prasanth, K. V.; Ha, T. Quantitative Analysis of Multilayer Organization of Proteins and RNA in Nuclear Speckles at Super Resolution. *Journal of Cell Science* **2017**, *130* (24), 4180–4192.

66. Wang, Z.; Lou, J.; Zhang, H. Essence Determines Phenomenon: Assaying the Material Properties of Biological Condensates. *The Journal of Biological Chemistry* **2022**, *298* (4), 101782.

67. Alshareedah, I.; Kaur, T.; Banerjee, P. R. Methods for Characterizing the Material Properties of Biomolecular Condensates. *Methods in Enzymology* **2021**, *646*, 143–183.

68. Krainer, G.; Welsh, T. J.; Joseph, J. A.; Espinosa, J. R.; Wittmann, S.; de Csilléry, E.; Sridhar, A.; Toprakcioglu, Z.; Gudiškytė, G.; Czekalska, M. A.; Arter, W. E.; Guillén-Boixet, J.; Franzmann, T. M.; Qamar, S.; George-Hyslop, P. S.; Hyman, A. A.;

Collepardo-Guevara, R.; Alberti, S.; Knowles, T. P. J. Reentrant Liquid Condensate Phase of Proteins Is Stabilized by Hydrophobic and Non-Ionic Interactions. *Nature Communications* **2021**, *12* (1), 1085.

69. Mitrea, D. M.; Chandra, B.; Ferrolino, M. C.; Gibbs, E. B.; Tolbert, M.; White, M. R., Kriwacki, R. W. Methods for Physical Characterization of Phase-Separated Bodies and Membrane-less Organelles, *Journal of Molecular Biology* **2018**, *430* (23), 4773-4805.

70. Conicella, A. E.; Zerze, G. H.; Mittal, J.; Fawzi, N. L. ALS mutations disrupt phase separation mediated by α-helical structure in the TDP-43 low-complexity C-terminal domain. *Structure* **2016**, *24* (9), 1537-1549.

71. Burke, K. A.; Janke, A. M.; Rhine, C. L.; Fawzi, N. L. Residue-by-residue view of in vitro FUS granules that bind the C-terminal domain of RNA polymerase II. *Molecular Cell* **2015**, *60* (2), 231-241.

72. Mitrea, D. M.; Cika, J. A.; Guy, C. S.; Ban, D.; Banerjee, P. R.; Stanley, C. B.; Nourse, A.; Deniz, A. A.; Kriwacki, R.W. Nucleophosmin integrates within the nucleolus via multi-modal interactions with proteins displaying R-rich linear motifs and rRNA. *Elife* **2016**, 5, e13571.

73. Abyzov, A.; Blackledge, M; Zweckstetter, M. Conformational dynamics of intrinsically disordered proteins regulate biomolecular condensate chemistry. *Chemical Reviews* **2022**, *122* (6), 6719-6748.

74. Zaccai, N. R.; Serdyuk, I. N.; Zaccai, J.; Zaccai, G.; Methods in molecular biophysics. *Cambridge University Press* **2017.**

75. Chaudhuri, B. N. Emerging applications of small angle solution scattering in structural biology. *Protein Science* **2015**, *24* (3), 267-276.

76. Bernadó, P.; Shimizu, N.; Zaccai, G.; Kamikubo, H.; Sugiyama, M. Solution scattering approaches to dynamical ordering in biomolecular systems. *Biochimica et Biophysica Acta (BBA)-General Subjects* **2018**, *1862* (2), 253-274.

77. Bernadó, P., Mylonas, E., Petoukhov, M.V., Blackledge, M. and Svergun, D.I. Structural characterization of flexible proteins using small-angle X-ray scattering. *Journal of the American Chemical Society* **2007**, *129* (17), 5656-5664.

78. Blanchet, C. E.; Svergun, D. I. Small-angle X-ray scattering on biological macromolecules and nanocomposites in solution. *Annual review of physical chemistry* **2013**, 64, 37-54.

79. Lu, H. P. Probing single-molecule protein conformational dynamics. *Accounts of chemical research* **2005**, *38* (7), 557-565.

80. Roy, R.; Hohng, S.; Ha, T. A practical guide to single-molecule FRET. *Nature methods* **2008**, *5* (6), 507-516.

81. Ha, T. Single-molecule fluorescence resonance energy transfer. *Methods* **2001**, *25* (1), 78-86.

82. Galvanetto, N.; Ivanović, M. T.; Chowdhury, A.; Sottini, A.; Nüesch, M. F.; Nettels, D.; Best, R. B.; Schuler, B. Extreme dynamics in a biomolecular condensate. *Nature* **2023**, *619* (7971), 876–883.

83. Yu, M.; Heidari, M.; Mikhaleva, S.; Tan, P. S.; Mingu, S.; Ruan, H.; Reinkemeier, C. D.; Obarska-Kosinska, A.; Siggel, M.; Beck, M.; Hummer, G.; Lemke, E. A.; Visualizing the disordered nuclear transport machinery in situ. *Nature* **2023**, 1-8.

84. Joshi, A.; Walimbe, A.; Avni, A.; Rai, S. K.; Arora, L.; Sarkar, S.; Mukhopadhyay, S. Single-molecule FRET unmasks structural subpopulations and crucial molecular events during FUS low-complexity domain phase separation. *Nature Communications* **2023**, *14* (1), 7331.

85. Weingarten, M. D.; Lockwood, A. H.; Hwo, S. Y.; Kirschner, M. W. A Protein Factor Essential for Microtubule Assembly. *Proceedings of the National Academy of Sciences U. S. A.* **1975**, *72* (5), 1858–1862.

86. Witman, G. B.; Cleveland, D. W.; Weingarten, M. D.; Kirschner, M. W. Tubulin Requires Tau for Growth onto Microtubule Initiating Sites. *Proceedings of the National Academy of Sciences U. S. A.* **1976**, *73* (11), 4070–4074.

87. Cleveland, D. W.; Hwo, S. Y.; Kirschner, M. W. Physical and Chemical Properties of Purified Tau Factor and the Role of Tau in Microtubule Assembly. *Journal of Molecular Biology* **1977**, *116* (2), 227–247.

88. Cleveland, D.W.; Hwo, S.Y.; Kirschner, M.W., Purification of tau, a microtubule-associated protein that induces assembly of microtubules from purified tubulin. *Journal of Molecular Biology* **1977**, *116* (2), 207-225.

89. Grundke-Iqbal, I.; Iqbal, K.; Quinlan, M.; Tung, Y. C.; Zaidi, M. S.; Wisniewski, H. M. Microtubule-Associated Protein Tau. A Component of Alzheimer Paired Helical Filaments. *The Journal of Biological Chemistry* **1986**, *261* (13), 6084–6089.

90. Ihara, Y.; Nukina, N.; Miura, R.; Ogawara, M. Phosphorylated Tau Protein Is Integrated into Paired Helical Filaments in Alzheimer's Disease1. *The Journal of Biochemistry* **1986**, *99* (6), 1807–1810.

91. Nukina, N.; Ihara, Y. One of the Antigenic Determinants of Paired Helical Filaments Is Related to Tau Protein1. *The Journal of Biochemistry* **1986**, *99* (5), 1541–1544.

92. Wood, J. G.; Mirra, S. S.; Pollock, N. J.; Binder, L. I. Neurofibrillary Tangles of Alzheimer Disease Share Antigenic Determinants with the Axonal Microtubule-Associated Protein Tau (Tau). *Proceedings of the National Academy of Sciences U. S. A.* **1986**, *83* (11), 4040–4043.

93. Goedert, M.; Wischik, C. M.; Crowther, R. A.; Walker, J. E.; Klug, A. Cloning and Sequencing of the CDNA Encoding a Core Protein of the Paired Helical Filament of Alzheimer Disease: Identification as the Microtubule-Associated Protein Tau. *Proceedings of the National Academy of Sciences U. S. A.* **1988**, *85* (11), 4051–4055.

94. Wischik, C. M.; Novak, M.; Edwards, P. C.; Klug, A.; Tichelaar, W.; Crowther, R. A. Structural Characterization of the Core of the Paired Helical Filament of Alzheimer Disease. *Proceedings of the National Academy of Sciences U. S. A.* **1988**, *85* (13), 4884–4888.

95. Wischik, C. M.; Novak, M.; Thøgersen, H. C.; Edwards, P. C.; Runswick, M. J.; Jakes, R.; Walker, J. E.; Milstein, C.; Roth, M.; Klug, A. Isolation of a Fragment of Tau Derived

from the Core of the Paired Helical Filament of Alzheimer Disease. *Proceedings of the National Academy of Sciences U. S. A.* **1988**, *85* (12), 4506–4510.

96. Baker, M.; Kwok, J. B.; Kucera, S.; Crook, R.; Farrer, M.; Houlden, H.; Isaacs, A.; Lincoln, S.; Onstead, L.; Hardy, J.; Wittenberg, L.; Dodd, P.; Webb, S.; Hayward, N.; Tannenberg, T.; Andreadis, A.; Hallupp, M.; Schofield, P.; Dark, F.; Hutton, M. Localization of Frontotemporal Dementia with Parkinsonism in an Australian Kindred to Chromosome 17q21-22. *Annals of Neurology* **1997**, *42* (5), 794–798.

97. Froelich, S.; Basun, H.; Forsell, C.; Lilius, L.; Axelman, K.; Andreadis, A.; Lannfelt, L. Mapping of a Disease Locus for Familial Rapidly Progressive Frontotemporal Dementia to Chromosome 17q12-21. *American Journal of Medical Genetics* **1997**, *74* (4), 380–385.

98. Poorkaj, P.; Bird, T. D.; Wijsman, E.; Nemens, E.; Garruto, R. M.; Anderson, L.; Andreadis, A.; Wiederholt, W. C.; Raskind, M.; Schellenberg, G. D. Tau Is a Candidate Gene for Chromosome 17 Frontotemporal Dementia. *Annals of Neurology* **1998**, *43* (6), 815–825.

99. Arendt, T.; Stieler, J. T.; Holzer, M. Tau and Tauopathies. *Brain Research Bulletin* **2016**, *126*, 238–292.

100. Neve, R. L.; Harris, P.; Kosik, K. S.; Kurnit, D. M.; Donlon, T. A. Identification of CDNA Clones for the Human Microtubule-Associated Protein Tau and Chromosomal Localization of the Genes for Tau and Microtubule-Associated Protein 2. *Brain Research. Molecular Brain Research* **1986**, *1* (3), 271–280.

101. Goedert, M.; Spillantini, M. G.; Potier, M. C.; Ulrich, J.; Crowther, R. A. Cloning and Sequencing of the CDNA Encoding an Isoform of Microtubule-Associated Protein Tau Containing Four Tandem Repeats: Differential Expression of Tau Protein MRNAs in Human Brain. *The EMBO Journal* **1989**, *8* (2), 393–399.

102. Takuma, H.; Arawaka, S.; Mori, H. Isoforms Changes of Tau Protein during Development in Various Species. *Brain Research. Developmental Brain Research* **2003**, *142* (2), 121–127.

103. Mandelkow, E.-M.; Mandelkow, E. Biochemistry and Cell Biology of Tau Protein in Neurofibrillary Degeneration. *Cold Spring Harbor Perspectives in Medicine* **2012**, *2* (7), a006247.

104. Wang, J.-Z.; Liu, F. Microtubule-Associated Protein Tau in Development, Degeneration and Protection of Neurons. *Progress in Neurobiology* **2008**, *85* (2), 148–175.

105. Murphy, D. B.; Borisy, G. G. Association of High-Molecular-Weight Proteins with Microtubules and Their Role in Microtubule Assembly in Vitro. *Proceedings of the National Academy of Sciences U. S. A.* **1975**, *72* (7), 2696–2700.

106. Brandt, R.; Lee, G. The Balance between Tau Protein's Microtubule Growth and Nucleation Activities: Implications for the Formation of Axonal Microtubules. *Journal of Neurochemistry* **1993**, *61* (3), 997–1005.

107. Trinczek, B.; Biernat, J.; Baumann, K.; Mandelkow, E. M.; Mandelkow, E. Domains of Tau Protein, Differential Phosphorylation, and Dynamic Instability of Microtubules. *Molecular Biology of the Cell* **1995**, *6* (12), 1887–1902.

108. Qiang, L.; Yu, W.; Andreadis, A.; Luo, M.; Baas, P. W. Tau Protects Microtubules in the Axon from Severing by Katanin. *The Journal of Neuroscience* **2006**, *26* (12), 3120–3129.

109. Yu, W.; Qiang, L.; Solowska, J. M.; Karabay, A.; Korulu, S.; Baas, P. W. The Microtubule-Severing Proteins Spastin and Katanin Participate Differently in the Formation of Axonal Branches. *Molecular Biology of the Cell* **2008**, *19* (4), 1485–1498.

110. Goode, B. L.; Feinstein, S. C. Identification of a Novel Microtubule Binding and Assembly Domain in the Developmentally Regulated Inter-Repeat Region of Tau. *Molecular Biology of the Cell* **1994**, *124* (5), 769–782.

111. Goode, B. L.; Denis, P. E.; Panda, D.; Radeke, M. J.; Miller, H. P.; Wilson, L.; Feinstein, S. C. Functional Interactions between the Proline-Rich and Repeat Regions of Tau Enhance Microtubule Binding and Assembly. *Molecular Biology of the Cell* **1997**, *8* (2), 353–365.

112. Kadavath, H.; Hofele, R. V.; Biernat, J.; Kumar, S.; Tepper, K.; Urlaub, H.; Mandelkow, E.; Zweckstetter, M. Tau Stabilizes Microtubules by Binding at the Interface between

Tubulin Heterodimers. *Proceedings of the National Academy of Sciences U. S. A.* **2015**, *112* (24), 7501–7506.

113. Elbaum-Garfinkle, S.; Cobb, G.; Compton, J. T.; Li, X.-H.; Rhoades, E. Tau Mutants Bind Tubulin Heterodimers with Enhanced Affinity. *Proceedings of the National Academy of Sciences U. S. A.* **2014**, *111* (17), 6311–6316.

114. Fung, H. Y. J.; McKibben, K. M.; Ramirez, J.; Gupta, K.; Rhoades, E. Structural Characterization of Tau in Fuzzy Tau:Tubulin Complexes. *Structure* **2020**, *28* (3), 378-384.e4.

115. Mitchison, T.; Kirschner, M. Dynamic Instability of Microtubule Growth. *Nature* **1984**, *312* (5991), 237–242.

116. Brouhard, G. J.; Rice, L. M. Microtubule Dynamics: An Interplay of Biochemistry and Mechanics. *Nature Reviews. Molecular Cell Biology* **2018**, *19* (7), 451–463.

117. Qiang, L.; Sun, X.; Austin, T. O.; Muralidharan, H.; Jean, D. C.; Liu, M.; Yu, W.; Baas, P. W. Tau Does Not Stabilize Axonal Microtubules but Rather Enables Them to Have Long Labile Domains. *Current Biology: CB* **2018**, *28* (13), 2181-2189.e4.

118. Baas, P. W.; Qiang, L. Tau: It's Not What You Think. *Trends in Cell Biology* **2019**, *29* (6), 452–461.

119. Hernández-Vega, A.; Braun, M.; Scharrel, L.; Jahnel, M.; Wegmann, S.; Hyman, B. T.; Alberti, S.; Diez, S.; Hyman, A. A. Local Nucleation of Microtubule Bundles through Tubulin Concentration into a Condensed Tau Phase. *Cell Reports* **2017**, *20* (10), 2304–2312.

120. Savastano, A.; Flores, D.; Kadavath, H.; Biernat, J.; Mandelkow, E.; Zweckstetter, M. Disease-Associated Tau Phosphorylation Hinders Tubulin Assembly within Tau Condensates. *Angewandte Chemie (International Ed. in English)* **2021**, *60* (2), 726–730.

121. Siahaan, V.; Krattenmacher, J.; Hyman, A. A.; Diez, S.; Hernández-Vega, A.; Lansky, Z.; Braun, M. Kinetically Distinct Phases of Tau on Microtubules Regulate Kinesin Motors and Severing Enzymes. *Nature Cell Biology* **2019**, *21* (9), 1086–1092.

122. Tan, R.; Lam, A. J.; Tan, T.; Han, J.; Nowakowski, D. W.; Vershinin, M.; Simó, S.; Ori-McKenney, K. M.; McKenney, R. J. Microtubules Gate Tau Condensation to Spatially Regulate Microtubule Functions. *Nature Cell Biology* **2019**, *21* (9), 1078–1085.

123. Kapitein, L. C.; Hoogenraad, C. C. Building the Neuronal Microtubule Cytoskeleton. *Neuron* **2015**, *87* (3), 492–506.

124. Yamada, M.; Hayashi, K. Microtubule Nucleation in the Cytoplasm of Developing Cortical Neurons and Its Regulation by Brain-Derived Neurotrophic Factor. *Cytoskeleton (Hoboken)* **2019**, *76* (5), 339–345.

125. de Barreda, E. G.; Dawson, H. N.; Vitek, M. P.; Avila, J. Tau Deficiency Leads to the Upregulation of BAF-57, a Protein Involved in Neuron-Specific Gene Repression. *FEBS Letters.* **2010**, *584* (11), 2265–2270.

126. Chen, Q.; Zhou, Z.; Zhang, L.; Wang, Y.; Zhang, Y.-W.; Zhong, M.; Xu, S.-C.; Chen, C.-H.; Li, L.; Yu, Z.-P. Tau Protein Is Involved in Morphological Plasticity in Hippocampal Neurons in Response to BDNF. *Neurochemistry International* **2012**, *60* (3), 233–242.

127. Dawson, H. N.; Ferreira, A.; Eyster, M. V.; Ghoshal, N.; Binder, L. I.; Vitek, M. P. Inhibition of Neuronal Maturation in Primary Hippocampal Neurons from Tau Deficient Mice. *Journal of Cell Science* **2001**, *114* (Pt 6), 1179–1187.

128. Harada, A.; Oguchi, K.; Okabe, S.; Kuno, J.; Terada, S.; Ohshima, T.; Sato-Yoshitake, R.; Takei, Y.; Noda, T.; Hirokawa, N. Altered Microtubule Organization in Small-Calibre Axons of Mice Lacking Tau Protein. *Nature* **1994**, *369* (6480), 488–491.

129. Tint, I.; Slaughter, T.; Fischer, I.; Black, M. M. Acute Inactivation of Tau Has No Effect on Dynamics of Microtubules in Growing Axons of Cultured Sympathetic Neurons. *The Journal of Neuroscience* **1998**, *18* (21), 8660–8673.

130. Magnani, E.; Fan, J.; Gasparini, L.; Golding, M.; Williams, M.; Schiavo, G.; Goedert, M.; Amos, L. A.; Spillantini, M. G. Interaction of Tau Protein with the Dynactin Complex. *THE EMBO JOURNAL* **2007**, *26* (21), 4546–4554.

131. LaPointe, N. E.; Morfini, G.; Pigino, G.; Gaisina, I. N.; Kozikowski, A. P.; Binder, L. I.; Brady, S. T. The Amino Terminus of Tau Inhibits Kinesin-Dependent Axonal Transport:

Implications for Filament Toxicity. *The Journal of Neuroscience Res.* **2009**, *87* (2), 440–451.

132. Chaudhary, A. R.; Berger, F.; Berger, C. L.; Hendricks, A. G. Tau Directs Intracellular Trafficking by Regulating the Forces Exerted by Kinesin and Dynein Teams. *Traffic* **2018**, *19* (2), 111–121.

133. Kanaan, N. M.; Morfini, G.; Pigino, G.; LaPointe, N. E.; Andreadis, A.; Song, Y.; Leitman, E.; Binder, L. I.; Brady, S. T. Phosphorylation in the Amino Terminus of Tau Prevents Inhibition of Anterograde Axonal Transport. *Neurobiology of Aging* **2012**, *33* (4), 826.e15-30.

134. Stern, J. L.; Lessard, D. V.; Hoeprich, G. J.; Morfini, G. A.; Berger, C. L. Phosphoregulation of Tau Modulates Inhibition of Kinesin-1 Motility. *Molecular Biology of the Cell* **2017**, *28* (8), 1079–1087.

135. Wang, Y.; Mandelkow, E. Tau in Physiology and Pathology. *Nature Reviews. Neuroscience* **2016**, *17* (1), 5–21.

136. Kent, S. A.; Spires-Jones, T. L.; Durrant, C. S. The Physiological Roles of Tau and Abeta: Implications for Alzheimer's Disease Pathology and Therapeutics. *Acta Neuropathol* **2020**, *140*, 417–447.

137. Fontela, C.; Kadavath, Y.; Biernat, H.; Riedel, J.; Mandelkow, D.; Zweckstetter, E. Multivalent Cross-Linking of Actin Filaments and Microtubules through the Microtubule-Associated Protein Tau. *Nature Communications* **1981**, *8*.

138. Zhou, L.; McInnes, J.; Wierda, K.; Holt, M.; Herrmann, A. G.; Jackson, R. J.; Wang, Y.-C.; Swerts, J.; Beyens, J.; Miskiewicz, K.; Vilain, S.; Dewachter, I.; Moechars, D.; De Strooper, B.; Spires-Jones, T. L.; De Wit, J.; Verstreken, P. Tau Association with Synaptic Vesicles Causes Presynaptic Dysfunction. *Nature Communications* **2017**, *8* (1), 15295.

139. Mukrasch, M. D.; Bibow, S.; Korukottu, J.; Jeganathan, S.; Biernat, J.; Griesinger, C.; Mandelkow, E.; Zweckstetter, M. Structural Polymorphism of 441-Residue Tau at Single Residue Resolution. *PLoS Biology* **2009**, *7* (2), e34.

140. Martin, L.; Latypova, X.; Terro, F. Post-Translational Modifications of Tau Protein: Implications for Alzheimer's Disease. *Neurochemistry International* **2011**, *58* (4), 458–471.

141. Braak, H.; Braak, E.; Bohl, J. Staging of Alzheimer-Related Cortical Destruction. *Eur. Neurol.* **1993**, *33* (6), 403–408.

142. Braak, H.; Braak, E. Staging of Alzheimer's Disease-Related Neurofibrillary Changes. *Neurobiology of Aging* **1995**, *16* (3), 271–278; discussion 278-84.

143. Fitzpatrick, A. W. P.; Falcon, B.; He, S.; Murzin, A. G.; Murshudov, G.; Garringer, H. J.; Crowther, R. A.; Ghetti, B.; Goedert, M.; Scheres, S. H. W. Cryo-EM Structures of Tau Filaments from Alzheimer's Disease. *Nature* **2017**, *547* (7662), 185–190.

144. Zhukareva, V.; Mann, D.; Pickering-Brown, S.; Uryu, K.; Shuck, T.; Shah, K.; Grossman, M.; Miller, B. L.; Hulette, C. M.; Feinstein, S. C.; Trojanowski, J. Q.; Lee, V. M.-Y. Sporadic Pick's Disease: A Tauopathy Characterized by a Spectrum of Pathological Tau Isoforms in Gray and White Matter. *Annals of Neurology* **2002**, *51* (6), 730–739.

145. Falcon, B.; Zhang, W.; Murzin, A. G.; Murshudov, G.; Garringer, H. J.; Vidal, R.; Crowther, R. A.; Ghetti, B.; Scheres, S. H. W.; Goedert, M. Structures of Filaments from Pick's Disease Reveal a Novel Tau Protein Fold. *Nature* **2018**, *561* (7721), 137–140.

146. Pollock, N.; Mirra, S.; Binder, L.; Hansen, L.; Wood, J. Filamentous Aggregates in Pick's Disease, Progressive Supranuclear Palsy, and Alzheimer's Disease Share Antigenic Determinants with Microtubule-Associated Protein, Tau. *Lancet* **1986**, *328* (8517), 1211.

147. Goedert, M.; Falcon, B.; Zhang, W.; Ghetti, B.; Scheres, S. H. W. Distinct Conformers of Assembled Tau in Alzheimer's and Pick's Diseases. *Cold Spring Harbor Symposia on Quantitative Biology* **2018**, *83*, 163–171.

148. Lövestam, S.; Li, D.; Wagstaff, J. L.; Kotecha, A.; Kimanius, D.; McLaughlin, S. H.; Murzin, A. G.; Freund, S. M. V.; Goedert, M.; Scheres, S. H. W. Disease-Specific Tau Filaments Assemble via Polymorphic Intermediates. *Nature* **2024**, *625* (7993), 119–125.

149. Sanders, D. W.; Kaufman, S. K.; DeVos, S. L.; Sharma, A. M.; Mirbaha, H.; Li, A.; Barker, S. J.; Foley, A. C.; Thorpe, J. R.; Serpell, L. C.; Miller, T. M.; Grinberg, L. T.;

Seeley, W. W.; Diamond, M. I. Distinct Tau Prion Strains Propagate in Cells and Mice and Define Different Tauopathies. *Neuron* **2014**, *82* (6), 1271–1288.

150. Kaufman, S. K.; Sanders, D. W.; Thomas, T. L.; Ruchinskas, A. J.; Vaquer-Alicea, J.; Sharma, A. M.; Miller, T. M.; Diamond, M. I. Tau Prion Strains Dictate Patterns of Cell Pathology, Progression Rate, and Regional Vulnerability in Vivo. *Neuron* **2016**, *92* (4), 796–812.

151. Narasimhan, S.; Guo, J. L.; Changolkar, L.; Stieber, A.; McBride, J. D.; Silva, L. V.; He, Z.; Zhang, B.; Gathagan, R. J.; Trojanowski, J. Q.; Lee, V. M. Y. Pathological Tau Strains from Human Brains Recapitulate the Diversity of Tauopathies in Nontransgenic Mouse Brain. *The Journal of Neuroscience* **2017**, *37* (47), 11406–11423.

152. Arakhamia, T.; Lee, C. E.; Carlomagno, Y.; Duong, D. M.; Kundinger, S. R.; Wang, K.; Williams, D.; DeTure, M.; Dickson, D. W.; Cook, C. N.; Seyfried, N. T.; Petrucelli, L.; Fitzpatrick, A. W. P. Posttranslational Modifications Mediate the Structural Diversity of Tauopathy Strains. *Cell* **2020**, *180* (4), 633-644.e12.

153. Dujardin, S.; Commins, C.; Lathuiliere, A.; Beerepoot, P.; Fernandes, A. R.; Kamath, T. V.; De Los Santos, M. B.; Klickstein, N.; Corjuc, D. L.; Corjuc, B. T.; Dooley, P. M.; Viode, A.; Oakley, D. H.; Moore, B. D.; Mullin, K.; Jean-Gilles, D.; Clark, R.; Atchison, K.; Moore, R.; Chibnik, L. B.; Tanzi, R. E.; Frosch, M. P.; Serrano-Pozo, A.; Elwood, F.; Steen, J. A.; Kennedy, M. E.; Hyman, B. T. Tau Molecular Diversity Contributes to Clinical Heterogeneity in Alzheimer's Disease. *Nature Medicine* **2020**, *26* (8), 1256–1263.

154. Xue, B.; Dunbrack, R. L.; Williams, R. W.; Dunker, A. K.; Uversky, V. N. PONDR-FIT: A Meta-Predictor of Intrinsically Disordered Amino Acids. *Biochimica et Biophysica Acta* **2010**, *1804* (4), 996–1010.

155. Dosztányi, Z.; Csizmok, V.; Tompa, P.; Simon, I. IUPred: Web Server for the Prediction of Intrinsically Unstructured Regions of Proteins Based on Estimated Energy Content. *Bioinformatics* **2005**, *21* (16), 3433–3434.

156. Martin, E. W.; Holehouse, A. S.; Grace, C. R.; Hughes, A.; Pappu, R. V.; Mittag, T. Sequence Determinants of the Conformational Properties of an Intrinsically Disordered

Protein Prior to and upon Multisite Phosphorylation. *Journal of the American Chemical Society* **2016**, *138* (47), 15323–15335.

157. Ambadipudi, S.; Biernat, J.; Riedel, D.; Mandelkow, E.; Zweckstetter, M. Liquid-Liquid Phase Separation of the Microtubule-Binding Repeats of the Alzheimer-Related Protein Tau. *Nature Communications* **2017**, *8* (1), 275.

158. Zhang, X.; Lin, Y.; Eschmann, N. A.; Zhou, H.; Rauch, J. N.; Hernandez, I.; Guzman, E.; Kosik, K. S.; Han, S. RNA Stores Tau Reversibly in Complex Coacervates. *PLoS Biology* **2017**, *15* (7), e2002183.

159. Ferreon, J.; Jain, A.; Choi, K.-J.; Tsoi, P.; MacKenzie, K.; Jung, S.; Ferreon, A. Acetylation Disfavors Tau Phase Separation. *International Journal of Molecular Sciences* **2018**, *19* (5), 1360.

160. Wegmann, S.; Eftekharzadeh, B.; Tepper, K.; Zoltowska, K. M.; Bennett, R. E.; Dujardin, S.; Laskowski, P. R.; MacKenzie, D.; Kamath, T.; Commins, C.; Vanderburg, C.; Roe, A. D.; Fan, Z.; Molliex, A. M.; Hernandez-Vega, A.; Muller, D.; Hyman, A. A.; Mandelkow, E.; Taylor, J. P.; Hyman, B. T. Tau Protein Liquid-Liquid Phase Separation Can Initiate Tau Aggregation. *THE EMBO JOURNAL* **2018**, *37* (7).

161. Majumdar, A.; Dogra, P.; Maity, S.; Mukhopadhyay, S. Liquid-Liquid Phase Separation Is Driven by Large-Scale Conformational Unwinding and Fluctuations of Intrinsically Disordered Protein Molecules. *The Journal of Physical Chemistry Letters* **2019**, *10* (14), 3929–3936.

162. Ukmar-Godec, T.; Hutten, S.; Grieshop, M. P.; Rezaei-Ghaleh, N.; Cima-Omori, M.-S.; Biernat, J.; Mandelkow, E.; Söding, J.; Dormann, D.; Zweckstetter, M. Lysine/RNA-Interactions Drive and Regulate Biomolecular Condensation. *Nature Communications* **2019**, *10* (1), 2909.

163. Zhang, X.; Vigers, M.; McCarty, J.; Rauch, J. N.; Fredrickson, G. H.; Wilson, M. Z.; Shea, J.-E.; Han, S.; Kosik, K. S. The Proline-Rich Domain Promotes Tau Liquid-Liquid Phase Separation in Cells. *Molecular Biology of the Cell* **2020**, *219* (11).

164. Boyko, S.; Surewicz, K.; Surewicz, W. K. Regulatory Mechanisms of Tau Protein Fibrillation under the Conditions of Liquid-Liquid Phase Separation. *Proceedings of the National Academy of Sciences U. S. A.* **2020**, *117* (50), 31882–31890.

165. Ambadipudi, S.; Reddy, J. G.; Biernat, J.; Mandelkow, E.; Zweckstetter, M. Residue-Specific Identification of Phase Separation Hot Spots of Alzheimer's-Related Protein Tau. *Chemical Science* **2019**, *10* (26), 6503–6507.

166. Kanaan, N. M.; Hamel, C.; Grabinski, T.; Combs, B. Liquid-Liquid Phase Separation Induces Pathogenic Tau Conformations in Vitro. *Nature Communications* **2020**, *11* (1), 2809.

167. Hochmair, J.; Exner, C.; Franck, M.; Dominguez-Baquero, A.; Diez, L.; Brognaro, H.; Kraushar, M. L.; Mielke, T.; Radbruch, H.; Kaniyappan, S.; Falke, S.; Mandelkow, E.; Betzel, C.; Wegmann, S. Molecular Crowding and RNA Synergize to Promote Phase Separation, Microtubule Interaction, and Seeding of Tau Condensates. *THE EMBO JOURNAL* **2022**, *41* (11), e108882.

168. Freiman, R. N.; Tjian, R. Regulating the Regulators: Lysine Modifications Make Their Mark. *Cell* **2003**, *112* (1), 11–17. https://doi.org/10.1016/s0092-8674(02)01278-3.

169. Ukmar-Godec, T.; Wegmann, S.; Zweckstetter, M. Biomolecular Condensation of the Microtubule-Associated Protein Tau. *Seminars in Cell & Developmental Biology* **2020**, *99*, 202–214.

170. Ginsberg, S. D.; Crino, P. B.; Lee, V. M.; Eberwine, J. H.; Trojanowski, J. Q. Sequestration of RNA in Alzheimer's Disease Neurofibrillary Tangles and Senile Plaques. *Annals of Neurology* **1997**, *41* (2), 200–209.

171. Lin, Y.; Fichou, Y.; Longhini, A. P.; Llanes, L. C.; Yin, P.; Bazan, G. C.; Kosik, K. S.; Han, S. Liquid-Liquid Phase Separation of Tau Driven by Hydrophobic Interaction Facilitates Fibrillization of Tau. *Journal of Molecular Biology* **2021**, *433* (2), 166731.

172. Singh, V.; Xu, L.; Boyko, S.; Surewicz, K.; Surewicz, W. K. Zinc Promotes Liquid-Liquid Phase Separation of Tau Protein. *The Journal of Biological Chemistry* **2020**, *295* (18), 5850–5856.

173. Vega, I. E.; Umstead, A.; Kanaan, N. M. EFhd2 Affects Tau Liquid-Liquid Phase Separation. *Frontiers in Neuroscience* **2019**, *13*, 845.

174. Wang, K.; Liu, J.-Q.; Zhong, T.; Liu, X.-L.; Zeng, Y.; Qiao, X.; Xie, T.; Chen, Y.; Gao, Y.-Y.; Tang, B.; Li, J.; Zhou, J.; Pang, D.-W.; Chen, J.; Chen, C.; Liang, Y. Phase Separation and Cytotoxicity of Tau Are Modulated by Protein Disulfide Isomerase and S-Nitrosylation of This Molecular Chaperone. *Journal of Molecular Biology* **2020**, *432* (7), 2141–2163.

175. Siegert, A.; Rankovic, M.; Favretto, F.; Ukmar-Godec, T.; Strohäker, T.; Becker, S.; Zweckstetter, M. Interplay between Tau and A-synuclein Liquid–Liquid Phase Separation. *Protein Science: A Publication of the Protein Society* **2021**, *30* (7), 1326–1336.

176. Gracia, P.; Polanco, D.; Tarancón-Díez, J.; Serra, I.; Bracci, M.; Oroz, J.; Laurents, D. V.; García, I.; Cremades, N. Molecular Mechanism for the Synchronized Electrostatic Coacervation and Co-Aggregation of Alpha-Synuclein and Tau. *Nature Communications* **2022**, *13* (1), 4586.

177. Min, S.-W.; Cho, S.-H.; Zhou, Y.; Schroeder, S.; Haroutunian, V.; Seeley, W. W.; Huang, E. J.; Shen, Y.; Masliah, E.; Mukherjee, C.; Meyers, D.; Cole, P. A.; Ott, M.; Gan, L. Acetylation of Tau Inhibits Its Degradation and Contributes to Tauopathy. *Neuron* **2010**, *67* (6), 953–966.

178. Cohen, T. J.; Guo, J. L.; Hurtado, D. E.; Kwong, L. K.; Mills, I. P.; Trojanowski, J. Q.; Lee, V. M. Y. The Acetylation of Tau Inhibits Its Function and Promotes Pathological Tau Aggregation. *Nature Communications* **2011**, *2* (1), 252.

179. Kamah, A.; Huvent, I.; Cantrelle, F.-X.; Qi, H.; Lippens, G.; Landrieu, I.; Smet-Nocca, C. Nuclear Magnetic Resonance Analysis of the Acetylation Pattern of the Neuronal Tau Protein. *Biochemistry* **2014**, *53* (18), 3020–3032.

180. Saito, M.; Hess, D.; Eglinger, J.; Fritsch, A. W.; Kreysing, M.; Weinert, B. T.; Choudhary, C.; Matthias, P. Acetylation of Intrinsically Disordered Regions Regulates Phase Separation. *Nature Chemical Biology* **2019**, *15* (1), 51–61.

181. Ackmann, M.; Wiech, H.; Mandelkow, E. Nonsaturable Binding Indicates Clustering of Tau on the Microtubule Surface in a Paired Helical Filament-like Conformation. *The Journal of Biological Chemistry* **2000**, *275* (39), 30335–30343.

182. Makrides, V.; Shen, T. E.; Bhatia, R.; Smith, B. L.; Thimm, J.; Lal, R.; Feinstein, S. C. Microtubule-Dependent Oligomerization of Tau. Implications for Physiological Tau Function and Tauopathies. *The Journal of Biological Chemistry* **2003**, *278* (35), 33298–33304.

183. Gyparaki, M. T.; Arab, A.; Sorokina, E. M.; Santiago-Ruiz, A. N.; Bohrer, C. H.; Xiao, J.; Lakadamyali, M. Tau Forms Oligomeric Complexes on Microtubules That Are Distinct from Pathological Oligomers in Disease. *bioRxiv*, 2020.

184. Maucuer, A.; Desforges, B.; Joshi, V.; Boca, M.; Kretov, D. A.; Hamon, L.; Bouhss, A.; Curmi, P. A.; Pastré, D. Microtubules as Platforms for Probing Liquid-Liquid Phase Separation in Cells - Application to RNA-Binding Proteins. *Journal of Cell Science* **2018**, *131* (11).

185. Wolozin, B. Regulated Protein Aggregation: Stress Granules and Neurodegeneration. *Molecular Neurodegeneration* **2012**, *7* (1), 56.

186. Stamer, K.; Vogel, R.; Thies, E.; Mandelkow, E.; Mandelkow, E.-M. Tau Blocks Traffic of Organelles, Neurofilaments, and APP Vesicles in Neurons and Enhances Oxidative Stress. *Molecular Biology of the Cell* **2002**, *156* (6), 1051–1063.

187. Ash, P. E. A.; Lei, S.; Shattuck, J.; Boudeau, S.; Carlomagno, Y.; Medalla, M.; Mashimo, B. L.; Socorro, G.; Al-Mohanna, L. F. A.; Jiang, L.; Öztürk, M. M.; Knobel, M.; Ivanov, P.; Petrucelli, L.; Wegmann, S.; Kanaan, N. M.; Wolozin, B. TIA1 Potentiates Tau Phase Separation and Promotes Generation of Toxic Oligomeric Tau. *Proceedings of the National Academy of Sciences U. S. A.* **2021**, *118* (9), e2014188118.

188. Hoover, B. R.; Reed, M. N.; Su, J.; Penrod, R. D.; Kotilinek, L. A.; Grant, M. K.; Pitstick, R.; Carlson, G. A.; Lanier, L. M.; Yuan, L.-L.; Ashe, K. H.; Liao, D. Tau Mislocalization to Dendritic Spines Mediates Synaptic Dysfunction Independently of Neurodegeneration. *Neuron* **2010**, *68* (6), 1067–1081.

189. Vanderweyde, T.; Yu, H.; Varnum, M.; Liu-Yesucevitz, L.; Citro, A.; Ikezu, T.; Duff, K.; Wolozin, B. Contrasting Pathology of the Stress Granule Proteins TIA-1 and G3BP in Tauopathies. *The Journal of Neuroscience* **2012**, *32* (24), 8270–8283.

190. Vanderweyde, T.; Apicco, D. J.; Youmans-Kidder, K.; Ash, P. E. A.; Cook, C.; Lummertz da Rocha, E.; Jansen-West, K.; Frame, A. A.; Citro, A.; Leszyk, J. D.; Ivanov, P.; Abisambra, J. F.; Steffen, M.; Li, H.; Petrucelli, L.; Wolozin, B. Interaction of Tau with the RNA-Binding Protein TIA1 Regulates Tau Pathophysiology and Toxicity. *Cell Reports* **2016**, *15* (7), 1455–1466.

191. Apicco, D. J.; Ash, P. E. A.; Maziuk, B.; LeBlang, C.; Medalla, M.; Al Abdullatif, A.; Ferragud, A.; Botelho, E.; Ballance, H. I.; Dhawan, U.; Boudeau, S.; Cruz, A. L.; Kashy, D.; Wong, A.; Goldberg, L. R.; Yazdani, N.; Zhang, C.; Ung, C. Y.; Tripodis, Y.; Kanaan, N. M.; Ikezu, T.; Cottone, P.; Leszyk, J.; Li, H.; Luebke, J.; Bryant, C. D.; Wolozin, B. Reducing the RNA Binding Protein TIA1 Protects against Tau-Mediated Neurodegeneration in Vivo. *Nature Neuroscience* **2018**, *21* (1), 72–80.

192. Silva, J. M.; Rodrigues, S.; Sampaio-Marques, B.; Gomes, P.; Neves-Carvalho, A.; Dioli, C.; Soares-Cunha, C.; Mazuik, B. F.; Takashima, A.; Ludovico, P.; Wolozin, B.; Sousa, N.; Sotiropoulos, I. Dysregulation of Autophagy and Stress Granule-Related Proteins in Stress-Driven Tau Pathology. *Cell Death and Differentiation* **2019**, *26* (8), 1411–1427.

193. Zhang, Y.; Chen, X.; Zhao, Y.; Ponnusamy, M.; Liu, Y. The Role of Ubiquitin Proteasomal System and Autophagy-Lysosome Pathway in Alzheimer's Disease. *Reviews in the Neurosciences* **2017**, *28* (8), 861–868.

194. Piatnitskaia, S.; Takahashi, M.; Kitaura, H.; Katsuragi, Y.; Kakihana, T.; Zhang, L.; Kakita, A.; Iwakura, Y.; Nawa, H.; Miura, T.; Ikeuchi, T.; Hara, T.; Fujii, M. USP10 Is a Critical Factor for Tau-Positive Stress Granule Formation in Neuronal Cells. *Scientific Reports* **2019**, *9* (1), 10591.

195. Jain, S.; Wheeler, J. R.; Walters, R. W.; Agrawal, A.; Barsic, A.; Parker, R. ATPase-Modulated Stress Granules Contain a Diverse Proteome and Substructure. *Cell* **2016**, *164* (3), 487–498.

196. Zhang, K.; Daigle, J. G.; Cunningham, K. M.; Coyne, A. N.; Ruan, K.; Grima, J. C.; Bowen, K. E.; Wadhwa, H.; Yang, P.; Rigo, F.; Taylor, J. P.; Gitler, A. D.; Rothstein, J. D.; Lloyd, T. E. Stress Granule Assembly Disrupts Nucleocytoplasmic Transport. *Cell* **2018**, *173* (4), 958-971.e17.

197. Eftekharzadeh, B.; Daigle, J. G.; Kapinos, L. E.; Coyne, A.; Schiantarelli, J.; Carlomagno, Y.; Cook, C.; Miller, S. J.; Dujardin, S.; Amaral, A. S.; Grima, J. C.; Bennett, R. E.; Tepper, K.; DeTure, M.; Vanderburg, C. R.; Corjuc, B. T.; DeVos, S. L.; Gonzalez, J. A.; Chew, J.; Vidensky, S.; Gage, F. H.; Mertens, J.; Troncoso, J.; Mandelkow, E.; Salvatella, X.; Lim, R. Y. H.; Petrucelli, L.; Wegmann, S.; Rothstein, J. D.; Hyman, B. T. Tau Protein Disrupts Nucleocytoplasmic Transport in Alzheimer's Disease. *Neuron* **2018**, *99* (5), 925-940.e7.

198. Goedert, M.; Jakes, R.; Spillantini, M. G.; Hasegawa, M.; Smith, M. J.; Crowther, R. A. Assembly of Microtubule-Associated Protein Tau into Alzheimer-like Filaments Induced by Sulphated Glycosaminoglycans. *Nature* **1996**, *383* (6600), 550–553.

199. Kampers, T.; Friedhoff, P.; Biernat, J.; Mandelkow, E. M.; Mandelkow, E. RNA Stimulates Aggregation of Microtubule-Associated Protein Tau into Alzheimer-like Paired Helical Filaments. *FEBS Letters.* **1996**, *399* (3), 344–349.

200. Vega, I. E.; Sutter, A.; Parks, L.; Umstead, A.; Ivanova, M. I. Tau's Three-Repeat Domain and EFhd2 Co-Incubation Leads to Increased Thioflavin Signal. *Frontiers in Neuroscience* **2018**, *12*, 879.

201. Lin, Y.; Fichou, Y.; Zeng, Z.; Hu, N. Y.; Han, S. Electrostatically Driven Complex Coacervation and Amyloid Aggregation of Tau Are Independent Processes with Overlapping Conditions. *ACS Chemical Neuroscience* **2020**, *11* (4), 615–627.

202. Kovacs, G. G.; Rahimi, J.; Ströbel, T.; Lutz, M. I.; Regelsberger, G.; Streichenberger, N.; Perret-Liaudet, A.; Höftberger, R.; Liberski, P. P.; Budka, H.; Sikorska, B. Tau Pathology in Creutzfeldt-Jakob Disease Revisited: Tau Pathology in CJD. *Brain Pathology (Zurich, Switzerland)* **2017**, *27* (3), 332–344.

203. Hallinan, G. I.; Hoq, M. R.; Ghosh, M.; Vago, F. S.; Fernandez, A.; Garringer, H. J.; Vidal, R.; Jiang, W.; Ghetti, B. Structure of Tau Filaments in Prion Protein Amyloidoses. *Acta Neuropathologica*. **2021**, *142* (2), 227–241.

********

# CHAPTER 2

# Materials and Methods

## 2.1 Introduction

We utilized a multidisciplinary approach to study various aspects of complex coacervates of tau protein which includes a diverse array of biochemical and biophysical tools namely recombinant protein purification, site-directed mutagenesis, ensemble, and single-molecule fluorescence-based microscopic tools for steady-state, and time-resolved fluorescence anisotropy measurements both for the phase-separated mixture as well as single droplets, single-molecule förster energy transfer (smFRET), Airyscan confocal imaging, Raman spectroscopy, atomic force imaging, transmission electron microscopy imaging, and ultracentrifugation. In this chapter, I described the techniques, materials, and methodology used for the work performed in this thesis.

## 2.2 Materials

2-(N-morpholino)ethanesulfonic acid (MES), glacial acetic acid, ammonium sulfate, 2-[4-(2-hydroxyethyl)piperazin-1-yl]ethanesulfonic acid (HEPES), sodium phosphate monobasic dihydrate, sodium phosphate dibasic dihydrate, tris base, sodium hydroxide, sodium chloride, magnesium chloride, potassium chloride, imidazole, L-glutathione reduced, 2-mercaptoethanol, Thioflavin T, 1,4-dithiothreitol (DTT), Triton X-100, Thrombin from bovine plasma, Poly-U sodium salt, phenylmethylsulfonyl fluoride (PMSF), ethylenediaminetetraacetic acid (EDTA), nuclease-free water (NFW), were of highest purity grade, obtained from Sigma (St. Louis, MO, USA). Urea and guanidinium hydrochloride were purchased from Amresco. Ampicillin, chloramphenicol, streptomycin sulfate, and isopropyl-β-thiogalactopyranoside (IPTG) were purchased from Gold Biocom (USA). All the fluorescent probes used in this study mainly, fluorescein-5-maleimide (F-5-M), AlexaFluor488-C5-maleimide, AlexaFluor488-NHS Ester (Succinimidyl Ester), AlexaFluor594-C5-maleimide, AlexaFluor647-C5-maleimide, and IAEDANS (1,5-IAEDANS, 5-((((2-Iodoacetyl)amino)ethyl)amino)Naphthalene-1-Sulfonic Acid), were obtained from Molecular Probes, Invitrogen. SP-sepharose, Co-NTA, and Ni-NTA resin were purchased from Qiagen. HiLoadTM Superdex-G75 16/600 prep grade (pg), and NAP-10 columns were obtained from GE Healthcare Life Sciences (USA). Amicon membrane filters for concentrating protein were purchased from Merck Millipore. All the buffer solutions were freshly prepared in Milli-Q water and filtered before use. The pH of each buffer solution was adjusted (± 0.02) at 25 °C using a Metrohm 827 lab pH meter.

## 2.3 Methods

### 2.3.1 Bioinformatic Analysis

- **Chapter 3 & 4:** Phase separation propensities of tau, PrP, and Ydj1were analyzed using FuzDrop[1] (http://protdyn-fuzpred.org/) and catGRANULE[2] (http://s.tartaglialab.com/new_submission/catGRANULES). The distribution of charges throughout both protein chains was analyzed using the Classification of Intrinsically Disordered Ensemble Regions (http://pappulab.wustl.edu/CIDER/analysis) CIDER[3] tool. Origin 2020b was used to generate the plots.

### 2.3.2 Site-directed mutagenesis and construct details

- **Chapter 3:** All the single cysteine and other variants of full-length tau, Nh2htau (26-230), tau truncation (151-399), and tau triple phosphomimetic mutant (tau3P) were created using the tau 6x-Histag-2N4R-17C plasmid which was a kind gift from Prof. Elizabeth Rhoades (University of Pennsylvania, USA). Each variant was made using the QuickChange site-directed mutagenesis kit (Agilent). The primers used for the respective mutations are listed in Table 1. The 6X-Histidine tag was removed from all these constructs by cloning. The human PrP (23-231) plasmid was a kind gift from Prof. Witold Surewicz (Case Western Reserve University, USA). Single cysteine variants of full-length PrP (W31C, W99C, and A120C), its N & C-terminal truncations, and the cysteine mutants of PrPY145 were created as described before. All the mutations were verified by sequencing.
- **Chapter 4:** All the variants of tau used in this study, including the single and double cysteine variants, the PHF6 and PHF6* deletion mutants, and the domain-specific mutants of tau (Nh2htau (26-230) and tau truncation (151-399)) were created using this cloned construct via site-directed mutagenesis using a QuickChange kit (Stratagene). The primers used for the respective mutations are listed in Table 1. Additionally, unless mentioned otherwise, a null-cysteine variant of tau (C291S, C322S) was used for all our experiments. The phosphomimetic variants of tau (tau 17E and tau MARK) were synthesized using Genescript. The yeast Ydj1 plasmid was a kind gift from Prof. Deepak Sharma (Council of Scientific and Industrial Research, IMTECH, Mohali, India). The C-terminal truncation of Ydj1 was cloned in the same vector using wild-type as a template. All the mutations were verified using sequencing.

### 2.3.3 Recombinant protein expression and purification

- **Chapter 3:** All the variants of full-length tau protein, except Nh2htau (26-230), were purified in a native condition by using cation-exchange chromatography on an SP-Sepharose column followed by gel filtration on a HiPrep 16/60 Superdex-G-75 (GE) column. Briefly, proteins were expressed by growing bacterial cell cultures at 37 °C, 220 rpm. At O.D.600 = 0.6, expression was induced with 0.5 mM IPTG for 1 h at 37 °C. After harvesting bacterial cells by centrifugation at 4 °C, 4000 rpm for 30 minutes, the cell pellets were dissolved in lysis buffer (20 mM MES, 500 mM NaCl, 1 mM EDTA, 2 mM DTT, 1mM $MgCl_2$, 1mM PMSF, pH 6.5). Cells were lysed using a probe sonicator (5% amplitude, 15 seconds on and 10 seconds off pulses, for 25 minutes), following which the lysates were boiled for 10-15 minutes. Cell debris was removed by centrifugation at 11,000 rpm at 4 °C for 30 minutes. The supernatant was collected and treated with streptomycin sulfate (136 µL/mL) and glacial acetic acid (226 µL/mL) to remove any nucleic acid contamination. Again, the residue was removed using high-speed centrifugation. The supernatant was treated with 60% ammonium sulfate, and the precipitated tau protein was collected by high-speed centrifugation for 30 minutes at 4 °C. Protein pellets were dried and dissolved in buffer A (20 mM MES, 50 mM NaCl, 1 mM EDTA, 1mM $MgCl_2$, 2 mM DTT, 1mM PMSF, pH 6.5). The dissolved protein solution was loaded onto the cation exchange column, and the protein was eluted using a linear gradient of 100 % final concentration of buffer B (20 mM MES, 50 mM NaCl, 1 mM EDTA, 1 mM $MgCl_2$, 2 mM DTT, 1 mM PMSF, 1 M NaCl, pH 6.5). Fractions spanning only the peak's central region were pooled together and further polished by gel-filtration in buffer C (25 mM HEPES, 50 mM NaCl, pH 7.4). Purity was ascertained by SDS-PAGE. The purified protein was concentrated using a 10 kDa MWCO Amicon-membrane filter and stored in small aliquots at - 80 °C for future use.

  For the Nh2htau, the purification procedure was the same as above, except, in this case, anion-exchange chromatography with a Q-Sepharose column was performed. After precipitation by ammonium sulfate, pellets were dissolved in buffer C. The protein was eluted using a linear gradient of 100% final concentration of salt (25 mM HEPES, 1 M NaCl, pH 7.4).

  For PrP expression, PrP plasmids were transformed into *E. coli* BL21(DE3) pLysS, and cells were grown in the same conditions described above. Protein expression was induced with 1 mM IPTG at 30 °C for 8 hours. The cells were harvested by centrifugation as

described above. The purification for the thrombin cleavable His-tagged constructs of full-length PrP (23-231) and its variants was performed using Ni-NTA chromatography under denaturing conditions along with gradient oxidation. Protein was eluted using a buffer containing 500 mM imidazole as described previously.[4] The cysteine mutants of PrP (W31C, W99C, and A120C) were purified under a denaturing condition from inclusion bodies, as mentioned elsewhere.[5] Following purification, the proteins were dialyzed against a phosphate buffer (20 mM sodium phosphate, 50 mM NaCl, pH 6.4). The N-terminal 6xHis-tag was removed by setting up a cleavage reaction using thrombin protease (0.2U/mL) at 37 °C for 5 hours. After the cleavage, the protease was inactivated by 0.2 mM PMSF. Further, to separate the His-tag-cleaved and un-cleaved fractions, the sample was loaded onto a Ni-NTA column and eluted with a 20 mM imidazole buffer (8 M urea, 10 mM Tris-HCl, 100 mM sodium phosphate, pH 8.0). The protein was concentrated using a 3 kDa MWCO amicon membrane filter and refolded (14 mM HEPES, pH 6.8) using a PD10 column. The purity of the protein was confirmed by SDS-PAGE analysis. The concentrations of the proteins were estimated using $\varepsilon_{280}$ = 6400 $M^{-1}cm^{-1}$ for tau full-length, $\varepsilon_{280}$ = 2560 $M^{-1}cm^{-1}$ for both tau truncations, $\varepsilon_{280}$ = 56,590 $M^{-1}cm^{-1}$ for PrP (23- 231), $\varepsilon_{280}$= 43,670 $M^{-1}cm^{-1}$ for Y145 Stop, and $\varepsilon_{280}$ = 14,200 $M^{-1}cm^{-1}$ for PrP (112-231). To avoid freeze-thaw cycles, all the experiments were performed using freshly purified proteins.

- **Chapter 4:** All the variants of tau except tau 17E and tau 4E are expressed and purified as described in Chapter 3. In the case of tau 17E and tau 4E, slightly different ion exchange buffers were used. Tau 17E protein pellets were resuspended in 25 mM HEPES, 50 mM NaCl, 1 mM EDTA, 2 mM DTT, pH 7.4, and loaded onto a Q-Sepharose column. The protein was eluted in a linear gradient with a 100% final concentration of buffer B (25 mM HEPES, 50 mM NaCl, 1 mM EDTA, and 2 mM DTT, pH 7.4). For tau MARK, buffer A contained 20 mM MES, 50 mM NaCl, 1 mM EDTA, pH 6.5 and was bound to an SP-Sepharose column, while buffer B contained 20 mM MES, 1 M NaCl, 1 mM EDTA, pH 6.5. As described above, these mutants were further polished by size exclusion chromatography in the presence of 2 mM DTT. All double cysteine variants were directly eluted in 6M GdMCl, 10 mM HEPES, 50 mM NaCl, and pH 7.4 during size exclusion chromatography. The proteins were concentrated using 10kDa MWCO Amicon membrane filters and stored at -80 °C till further use.

  N-terminal 6X His-tagged recombinant pPROEX-Htb-Ydj1 from S. cerevisiae was overexpressed in Rosetta DE3 E. coli cells using 0.3 mM IPTG at 15 °C for 14 hours.

Harvested cells were resuspended in chilled lysis buffer (25 mM HEPES, 500 mM NaCl, 20 mM $MgCl_2$, 20 mM KCl, pH 7.4) and incubated with lysozyme (2 mg/ml) at 4 °C followed by sonication. The cell lysate was cleared using high-speed centrifugation, and purification was carried out using Co-NTA chromatography with an imidazole gradient. The 6X-His tag was removed overnight at 4 °C in 25 mM HEPES, 500 mM NaCl, 20 mM KCl,10 mM $MgCl_2$, 1 mM DTT, pH 7.4 using in-house purified recombinant Tobacco Etch virus (TEV) protease. His-tag removal was carried out by passing the cleaved Ydj1 through a Co-NTA column. The eluted protein was concentrated using a 10 kDa MWCO Amicon membrane filter and stored at -80 °C until further use. Before experiments, Ydj1 was freshly dialyzed into 20 mM HEPES, 2 mM DTT, pH 7.4 using 10kDa MWCO Amicon membrane filters. The purity of all the proteins was validated using SDS-PAGE, and freshly purified proteins were used for all experiments to avoid freeze-thaw cycles. The concentrations of the proteins were estimated using ε280 = 6400 M-1cm-1 for full-length tau and tau ΔPHF6*, ε280 = 2560 $M^{-1}cm^{-1}$ for Nh2tau and tau truncation, ε280 = 5120 $M^{-1}cm^{-1}$ for tau ΔPHF6, and ε280 = 23,475 $M^{-1}cm^{-1}$ for Ydj1.

### 2.3.4 Fluorescence labeling

- **Chapter 3:** Cysteine mutants of tau and PrP were labeled with fluorophores under denaturing conditions at pH 7.4. For fluorescein-5-maleimide (F-5-M) labeling, proteins were mixed in the molar ratio of 10:1 (dye: protein). For Alexa dyes (C5-maleimide), proteins were mixed in a 2:1 molar ratio (dye: protein). 1, 5 -IAEDANS labeling of tau was performed at a 20:1 molar ratio of dye: protein. The reaction mixtures were stirred for 2-3 hours in the dark at room temperature. After completion of the labeling reaction, the excess free dye was removed while buffer exchanging (Buffer C) using a 10 kDa MWCO Amicon membrane filter in the case of tau mutants. In contrast, in the case of PrP mutants, a PD10 column was used. The concentration of the labeled protein was estimated using $\varepsilon_{495}$ = 68,000 $M^{-1}cm^{-1}$, for F-5-M, $\varepsilon_{495}$ = 72,000 $M^{-1}cm^{-1}$, for AlexaFluor488 C5-maleimide, $\varepsilon_{590}$ = 92,000 $M^{-1}cm^{-1}$ for AlexaFluor594 C5-maleimide, and $\varepsilon_{337}$ = 5600 $M^{-1}cm^{-1}$ for 1,5 -IAEDANS.
- **Chapter 4:** All labeling reactions except polyU RNA labeling, were carried out using thiol-reactive maleimide labeling. Single cysteine variants of tau were site-specifically labeled under denaturing conditions (6M GdMCl, 10 mM HEPES, 50 mM NaCl, pH 7.4) using fluorescein-5-maleimide (F5M) and AlexaFluor C-5 (AlexaFluor 488 and

AlexaFluor 594) maleimide dyes for anisotropy, imaging, and single-molecule experiments, respectively. For F-5-M labeling, proteins were mixed in a 10:1 ratio (dye: protein); for AlexaFluor labeling, this ratio was 2:1 (dye: protein). The reactions were incubated in the dark for 2-3 hours while stirring and were dialyzed into 25 mM HEPES, 50 mM NaCl, pH 7.4 using 10 kDa MWCO centrifugal filters.

For dual labeling of the double cysteine variants of tau, the denatured protein was incubated on a stirrer with the donor (AlexaFluor 488) dye in a 1:0.5 ratio (protein:dye) for ~ 2 h at room temperature in the dark, then acceptor dyes (AlexaFluor 594) was added in a 0.5:5 ratio (donor:acceptor) for overnight at 4 °C with stirring. Next day, the free dye was removed by buffer exchange of the protein (6M GdMCl, 10 mM HEPES, 50 mM NaCl, pH 7.4) using 10kDa MWCO centrifugal filters. Finally, the dual-label protein was buffer-exchanged to 25 mM HEPES, 50 mM NaCl, and 2 mM DTT, pH 7.4. Ydj1 was labeled non-specifically under native conditions using AlexaFluor 647 C5 maleimide and AlexaFluor 488 C5 maleimide (1:1) for imaging and FRAP experiments. The concentrations of the labelled proteins were measured using ε495 = 68,000 $M^{-1}cm^{-1}$, for F-5-M, ε495= 72,000 $M^{-1}cm^{-1}$, for Alexa Fluor 488 C5-maleimide, ε590 = 92,000 $M^{-1}cm^{-1}$ for Alexa Fluor 594 C5-maleimide, and ε647 = 2,39,000 $M^{-1}cm^{-1}$ for AlexaFluor 647 C5 maleimide. For polyU RNA labeling, the 5'-end of RNA was activated using NHS-EDC coupling in pH 6.5 buffer followed by buffer exchange in MiliQ water using a 10 kDa MWCO Amicon membrane filter. The labeling of RNA was done by diluting the final reaction mixture in a buffer (20 mM Sodium phosphate, 50 mM NaCl, pH 7.4) prepared using MiliQ water. A two-fold molar excess of AlexaFluor488-NHS Ester (Succinimidyl Ester) was used for labeling at room temperature. Excess-free dye was removed using a membrane filter. Labeled RNA concentration was estimated by monitoring A260 and A495 (absorbance maxima of fluorophore).

### 2.3.5 Phase separation assays

- **Chapter 3:** Throughout experiments, the concentration of tau protein stock was kept constant at 360 μM. Tau phase separation was induced by diluting the protein (10 μM) in our reaction buffer without salt (droplet buffer: 14 mM HEPES, pH 6.8) at room temperature. Tau-PrP droplet formation was achieved by adding tau to PrP in the reaction buffer. The turbidity of the phase-separated samples (tau, tau-PrP, Nh2htau-PrP, tau-Y145Stop, tau-PrP (112-231), tau-RNA, PrP-RNA, tau-PrP-RNA) was monitored by

recording the absorbance at 350 nm, at 25 °C on a Multiskan Go (Thermo scientific) plate reader using 96-well NUNC optical bottom plates. A sample volume of 100 µL was used for these measurements, and raw turbidity data was plotted without background subtraction. The mean and the standard error were obtained from at least three independent sets of measurements performed on a single day. Unless otherwise indicated, tau and PrP concentrations were kept fixed, 10 µM and 20 µM, respectively.

- **Chapter 4:** The concentration of the stock of tau was kept constant at 360 µM throughout the experiments. Tau phase separation was induced in the reaction buffer (20 mM HEPES, 2 mM DTT, pH 7.4) by diluting the stock to 10µM. For tau-Ydj1 condensates, 10 µM tau was added to Ydj1 diluted to 10 µM in the same buffer. Phase separation was quantified by measuring the turbidity of the reactions at 350 nm, 25 °C on a MultiskanGo (Thermo scientific) plate reader using 96-well NUNC optical bottom plates. The sample volume was kept constant at 100 µL. For RNA-dependent turbidity measurement and with truncation variants nanodrop (Genova Life Science Spectrophotometer, ver 1.51.4) was used for the same. Data was plotted without any background subtractions. The mean and standard deviations were obtained from three independent sets of measurements recorded on the same day.

### 2.3.6 Confocal microscopy

- **Chapter 3:** Fluorescence imaging experiments were performed at room temperature on a ZEISS LSM 980 Elyra 7 super-resolution microscope equipped with a high-resolution monochrome cooled AxioCamMRm Rev. 3 FireWire(D) camera, using a ×63 oil-immersion objective (numerical aperture 1.4). Less than 1% of respective labeled proteins were doped for imaging droplets with the unlabeled proteins. The freshly prepared samples were incubated for 45 seconds at room temperature. A sample volume of 4-5 µL was placed onto the glass coverslips of a thickness of 1.5 mm. Alexa488-labeled proteins were imaged using a 488 nm laser diode (11.9 mW), and Alexa-594-labeled proteins were imaged using a 590 nm excitation source. The images were obtained at a resolution of 1840 × 1840 pixels at 16-bit depth. Images were processed and analyzed using the instrument's in-built Zen Blue 3.2 (3.2) software.
- **Chapter 4:** All the imaging was performed at room temperature using the same experimental setup as mentioned above in Chapter 3. For droplet reactions, the unlabeled proteins were doped with 1% labeled proteins in the reaction buffer and imaged using a

488 nm laser diode (11.9 mW) and a 590 nm excitation source for AlexaFluor 488 and AlexaFluor 594, respectively. For three-color imaging, a 632 nm excitation source for AlexaFluor 647, in addition to other two excitation sources was used. The images were acquired using an 1840 × 1840 pixels resolution at a 16-bit depth. The obtained images were processed and analyzed using the Zen Blue 3.2 (3.2) software.

### 2.3.7 Fluorescence recovery after photobleaching (FRAP)

- **Chapter 3 & 4:** FRAP experiments were performed on the same instrument used for confocal imaging. For all FRAP experiments, Alexa488-labeled (~1%) proteins were used. Measurements were performed for at least three independent samples. For comparison, the best 3-5 traces were used. A region of interest (ROI), having a diameter of 1 μm, was bleached using a 488 nm laser for all the coacervates. The recovery of the bleached spots was recorded using the in-built ZEN blue 3.2 (ZEISS) software provided with the instrument. Time-dependent FRAP was performed by taking aliquots from reaction mixtures (incubated at room temperature) at desired time points. The fluorescence recovery traces were background corrected, normalized, and plotted using Origin 2020b.

### 2.3.8 Estimation of saturation concentration ($C_{sat}$) using sedimentation assays

- **Chapter 3:** The light phase saturation concentration ($C_{sat}$) for reaction mixtures was estimated by ultra-centrifugation.[6] Tau-PrP droplet reactions doped with 10% F-5-M labeled tau were set up and incubated at 25 °C for 5 minutes. The reactions were then ultracentrifuged at ~ 180000 x g at 25 °C for 2 hours. The supernatant was collected and diluted in a salt buffer (14 mM HEPES, 50 mM NaCl) to avoid phase separation. For estimating protein concentration, absorbance at 495 nm was monitored. The resulting value was multiplied by a factor of 10 to obtain the light phase concentration.
- **Chapter 4:** The tau droplet and tau-Ydj1 reactions were set up and incubated at room temperature for 10 minutes, followed by high-speed centrifugation at 16,400 rpm at 25 °C for 35 minutes. The reactions were doped with 10% of F-5-M labeled tau. Following centrifugation, the supernatant was collected and diluted with a salt-containing buffer (25 mM HEPES, 50 mM NaCl, 2 mM DTT, pH 7.4) to prevent the induction of phase separation. Protein concentration was estimated in the light phase by monitoring

absorbance at 495 nm. The suitable dilution factor and a factor of 10 were incorporated into the calculations to obtain the Csat.

### 2.3.9 Steady-state fluorescence spectroscopy

- **Chapter 3:** Steady-state fluorescence experiments were performed on a FluoroMax-4 spectrofluorometer (Horiba Jobin Yvon, NJ, USA) using a 1-mm-pathlength quartz cuvette. In all fluorescence studies, the tau and PrP concentrations were kept constant at 10 μM and 20 μM, respectively. For recording the ThT fluorescence, a sample volume of 600 μL was used for all the reactions. Reactions were set up and, at desired time points, pelleted down at 16,400 rpm at 25 °C for 30 minutes. The supernatant was carefully removed, and the obtained pellet was resuspended in a 20 mM sodium phosphate, pH 7.5 buffer. This suspension was further incubated with 20 μM of ThT for 15 minutes before recording the spectrum. The samples were excited at 440 nm, and the emission spectra were collected in the range between 460 nm and 550 nm. For recording the F-5-M-labeled tau and PrP fluorescence (100 nM of labeled protein was mixed with the unlabeled protein), the samples were excited at 485 nm, and the emission spectra were recorded in the range of 510 nm and 600 nm. Steady-state fluorescence anisotropy of F-5-M-labeled tau and PrP were recorded at the emission maximum (~519 nm). The steady-state fluorescence anisotropy ($r_{ss}$) is estimated from the following relationship:

$$r_{ss} = \frac{I_{\parallel} - GI_{\perp}}{I_{\parallel} + 2GI_{\perp}} \qquad \text{------ (2.1)}$$

where $I_{\parallel}$ and $I_{\perp}$ are the parallel and perpendicular fluorescence intensities, respectively, in reference to the excitation polarizer. The G-factor is the geometry factor that was used for correcting the perpendicular components.

### 2.3.10 Single-droplet fluorescence anisotropy measurements

- **Chapter 3:** Single-droplet fluorescence anisotropy measurements experiments were performed on a PicoQuant MicroTime MT200 time-resolved fluorescence confocal microscope. A coverslip of 0.15 mm thickness (no. 1) was kept directly on a Super Apochromat 60x water immersion objective with 1.2 NA (Olympus). Laser beams of 488 nm were used for sample excitation and image acquisition. A bandpass emission filter (520/35) for the green dye (F5M and Alexa-488) was used before the pinhole. Out-of-

focus emission light was blocked by a 50 μm pinhole and the in-focus emission light was then split by a polarizer into 2 detection paths. Single Photon Avalanche Diodes (SPADs) were used as detectors. The correction factor G was estimated using a free dye solution by following manufacturer protocol. Data acquisition and analysis were performed on the commercially available SymphoTime64 software v2.7. For single droplet anisotropy measurements, a region of interest (ROI) selection tool was used for individual droplet anisotropy value extraction.

### 2.3.11 Single-droplet steady-state and time-resolved anisotropy measurements

- **Chapter 4:** Single-droplet anisotropy measurements were recorded using the PicoQuant MicroTime (MT200) microscope as described above. Monomeric tau and phase-separated tau-Ydj1 reactions were freshly prepared using F5M-labeled single cysteine variants of tau, which were excited using a 488 nm laser. The emitted fluorescence was selectively collected using a 520/35 bandpass filter, out-of-focus light was filtered out using a 50μM pinhole, and the collected light was divided by a polarizer into two detectors (SPADs). For steady-state measurements, anisotropy imaging was performed, while for time-resolved information, point time traces were collected. Correction factors required for data analysis were calculated using measurements with free dye solutions. In the case of tau-Ydj1 reactions, droplets were chosen as regions of interest (ROI) using the associated SymphoTime64 v2.7 software. Data acquisition and analysis were performed on the same software. Steady-state anisotropy is given by

$$r_{ss} = \frac{I_{\perp} - I_{\parallel}}{[1-3L2]I_{\parallel} + [2-3L1]I_{\perp}} \quad \text{------ (2.2)}$$

where $I_{\parallel}$ and $I_{\perp}$ are the background corrected parallel and perpendicular fluorescence intensities, and L1 and L2 are the correction factors for the used objective lens.

The time-resolved anisotropy decay profiles that were acquired, were fitted globally using the following relations:

$$I_{\parallel}(t) = 1/3I(t)[1 + 2r(t)] \quad \text{------ (2.3)}$$

$$I_{\perp}(t) = 1/3I(t)[1 - r(t)] \quad \text{------ (2.4)}$$

Here, $I_{\parallel}(t)$, $I_{\perp}(t)$, and I(t) denote the time-dependent fluorescence intensities collected at the parallel, perpendicular, and magic angle (54.7°) geometry, respectively.
The collected intensity decays could be approximated to a biexponential decay model[7] as follows:

$$r(t) = r_0[\beta_1 e^{\left(\frac{-t}{\phi_1}\right)} + \beta_2 e^{\left(\frac{-t}{\phi_2}\right)}] \quad \text{------ (2.5)}$$

where $\phi_1$ and $\phi_2$ denote the fast and the slow rotational correlation times associated with the local and global dynamics of the associated protein chain, respectively. $\beta_1$ and $\beta_2$ denote the respective amplitudes associated with these fast and slow rotational correlation times, while $r_0$ denotes the intrinsic time-zero fundamental anisotropy of the fluorophore. Reduced $\chi^2$ values were used to assess the goodness of fit.

### 2.3.12 Fluorescence correlation spectroscopy

- **Chapter 3 & 4:** FCS measurements were performed on the same instrument as mentioned above (MT200). The confocal volume ($V_{eff}$) and its structural parameter ($\kappa$) for our system were determined using a 1 nM solution of Alexa488 which gave us $V_{eff}$ > 1 fL and $\kappa = 4.7$. These parameters were used as calibration values while curve-fitting data for the monomers and droplets. Dispersed monomeric and droplet solutions (tau, tau-PrP, Ydj1, and tau-Ydj1) were prepared by mixing nanomolar concnetration of the Alexa488 labeled single cysteine variants of respective proteins with unlabeled proteins. The freshly prepared reaction mixtures (50 µL) were spotted onto the coverslip and measurements were performed. In the case of monomer, experiments were performed 50 µm inside the solution, whereas individual droplets were focused in the case of phase-separated solution. Correlation curves (G(t)) were fitted using the triplet model.

$$G(t) = \left[1 + T\left[e^{\left(\frac{-t}{\tau_{Trip}}\right)} - 1\right]\right] \sum_{i=0}^{n_{Diff}-1} \frac{\rho[i]}{\left[1+\frac{t}{\tau_{Diff}[i]}\right]\left[1+\frac{t}{\tau_{Diff}[i]\kappa^2}\right]^{0.5}} \quad \text{------ (2.6)}$$

where G(t) is the correlation amplitude, $\rho$ denotes the contribution of the $i^{th}$ diffusing species, T denotes the fraction of the triplet state, $\tau_{Trip}$ is the lifetime of the triplet state,

$\tau_{Diff}$ is the diffusion time of the $i^{th}$ diffusing species, and κ is the structure parameter of the corresponding focal volume.

### 2.3.13 Time-resolved fluorescence anisotropy measurements

- **Chapter 3:** All ensemble time-resolved florescence anisotropy decays were acquired at 25°C using a time-correlated single-photon counting (TCSPC) setup (Horiba Jobin Yvon, NJ). F5M and IAEDANS labeled proteins were excited using 485 and 375 nm picosecond NanoLED laser diodes. The instrument response function (IRF) was measured using a dilute solution of colloidal silica (Ludox) and the full width at half-maximum (FWHM) was found to be 55 ps. The decay profiles were recorded at the corresponding emission maxima. Using a bandpass of 8nm, the fluorescence intensities were collected at $0^o$ ($I_{\parallel}$) and $90^o$ ($I_{\perp}$) with respect to the geometric orientation of the excitation polarizer. The G-factor, calculated on the basis of free dyes in water, was taken into account to correct the perpendicular fluorescence intensity decays. All measurements were performed for 3 independent replicates, with 3 acquisitions from each sample. The anisotropy decays were analyzed by globally fitting the acquired data according to the following equations:

$$I_{\parallel}(t) = 1/3I(t)[1 + 2r(t)] \quad \text{------ (2.7)}$$

$$I_{\perp}(t) = 1/3I(t)[1 - r(t)] \quad \text{------ (2.8)}$$

where *I* denotes the time-dependent fluorescence intensity collected at the magic angle ($54.7^o$). The fast ($\phi_1$) and slow ($\phi_2$) rotational correlation times arising due to the local dynamics of the fluorophore and the segmental dynamics of the backbone, which determine the time-resolved fluorescence decay kinetics can be approximated to a biexponential decay model:

$$r(t) = r_0[\beta_1 e^{\left(\frac{-t}{\phi_1}\right)} + \beta_2 e^{\left(\frac{-t}{\phi_2}\right)}] \quad \text{------ (2.9)}$$

Here, $r_0$ represents the intrinsic time-zero fundamental anisotropy of the fluorophore. $\beta_1$ and $\beta_2$ denote the amplitudes associated with fast and slow rotational correlation time, respectively. Reduced $\chi^2$ values, randomness of residuals, and the autocorrelation function gave a measure of the goodness of fit. The residue-specific anisotropy decays

for the dispersed monomers (residue 56 of tau and 99 of PrP) could be approximated to a biexponential decay profile. In the case of droplets, a triexponential decay model[7] that also took into an additional slower correlation time ($\phi_3$) was required to describe the time-resolved anisotropy decays as follows:

$$r(t) = r_0[\beta_1 e^{\left(\frac{-t}{\phi_1}\right)} + \beta_2 e^{\left(\frac{-t}{\phi_2}\right)} + \beta_3 e^{\left(\frac{-t}{\phi_3}\right)}] \quad \text{------ (2.10)}$$

Where $\beta_3$ denotes the associated amplitude. A fluorescence probe with a longer lifetime (12 ns) was used to improve the estimation of $\phi_3$, which was estimated to be ~ 43 ns (Table S2). Using these values, the hydrodynamic radii ($R_h$) of the nano-clusters were approximated. The Stokes-Einstein relationship was used for this purpose:

$$\phi_3 = \frac{\eta V}{k_B T} \quad \text{------ (2.11)}$$

where η is the viscosity of the medium, V is the volume of the rotating unit ($V = \frac{4}{3}\pi {R_h}^3$), $k_B$ is the Boltzmann constant, and T is the temperature. The robustness of the recovered correlation time ($\phi_3$) was also assessed by using both free and forced fits.

### 2.3.14 Raman spectroscopy

- **Chapter 3 & 4:** For all Raman measurements, the dense phase from reaction mixtures was used. Reaction mixtures (of 600 µL volume) were pelleted down at specific time points, and the dense phase (pellet) was resuspended in 5 µL of 20 mM sodium phosphate buffer, pH 7.4. The resuspended dense phase was deposited onto a glass slide covered with an aluminum sheet and half-dried. An inVia laser Raman microscope (Renishaw, UK) was used for recording all the spectra. The sample was focused using a 100x objective lens (Nikon, Japan), and a 785-nm NIR laser was used for excitation, with an exposure time of 10 s and 100% laser power. Spectra were recorded for tau and tau:PrP droplets at different time points. An edge filter of 785 nm was used for filtering Rayleigh scattering. The Raman scattering was collected and dispersed using a 1200 lines/mm diffraction grating and detected using an air-cooled CCD detector. The instrument's in-built Wire 3.4 software was used for data acquisition. All the data were averaged over 10

scans. Acquired spectra were baseline corrected and smoothened using Wire 3.4. Spectra were plotted using Origin 2018b.

### 2.3.15 Atomic force microscopy (AFM) imaging

- **Chapter 3:** AFM images were acquired using an Innova atomic force microscope (Bruker) operating in tapping mode. For sample preparation, 10 µL aliquots were taken from reaction mixtures (incubated for 48 hr at room temperature) and deposited on freshly cleaved, Milli-Q water-washed muscovite mica (Grade V-4 mica from SPI, PA). The samples were incubated for 10-15 minutes at room temperature and were washed with 150 µL of filtered Milli-Q water. The samples were further air-dried using a gentle stream of nitrogen gas before AFM imaging. Data was acquired using NanoDrive (v8.03) software, and the WSxM 5.0D 8.1 software[8] was used for image processing. The height profiles were analyzed from WSxM and were plotted using Origin 2020b.

### 2.3.16 Aggregation kinetics

- **Chapter 4:** All Thioflavin T-based aggregation kinetics were recorded on a POLARstar Omega Plate Reader Spectrophotometer (BMG LABTECH, Germany) in NUNC-96 well plates. Each well was incubated with 150 µl of the reaction supplemented with a glass bead having 3 mm diameter. ThT was used at a final concentration of 20 µM for all reactions. The kinetics were recorded under continuous stirring conditions at 100 rpm. The ThT intensity was plotted using Origin 2020b.

### 2.3.17 Transmission electron microscopy

- **Chapter 4:** The end product of tau droplet and tau-Ydj1 droplet reactions were taken out from the plate reader and pelleted down by centrifugation at 16,400 rpm, 25 °C. After pelleting down, supernatant was discarded and pellets were dissolved in 30 µl of reaction buffer. A small volume (5 µl) of the reactions was drop cast on 300-mesh carbon-coated electron microscopy grids and incubated for 5 minutes. Negative staining with 5 µl of uranyl acetate (1% w/v) was performed, followed by overnight incubation at room temperature after excessive stain removal. Imaging was performed on Jeol JEM F-200.

### 2.3.18 Single-molecule FRET measurements and data analysis

- **Chapter 4:** Single-molecule FRET experiments were performed on the Picoquant Microtime 200 (MT200) inverted time-resolved fluorescence confocal microscope. All experiments were performed in the PIE (Pulsed Interleaved Excitation) mode using pulsed laser sources (488 and 594) with a frequency of 20 MHz. The reactions were drop cast on 0.15 mm thick coverslips (#1) placed on a Super Apochromat 60x water immersion objective with 1.2 NA. The emitted fluorescence was collected using the same objective, filtered using a 50µM pinhole, and subsequently separated into donor and acceptor channels using a dichroic mirror (zt594rdc). Optical filters were placed before the two SPADs (single avalanche photodiodes) that were used as detectors (530/50 BP for the donor and 645/75 BP for the acceptor). Dual-labeled tau was diluted to a final concentration of ~ 150 pM in 25 mM HEPES, 50 mM NaCl, pH 7.4 buffer, and doped with 50 nM of unlabeled protein for monomer measurement, to achieve surface passivation. For droplet reactions, 10-15 pM dual labeled protein concentration was doped in a protein mixture containing 10 µM of both unlabeled tau and Ydj1. Propyl Gallate was used at a concentration of 250 µM in the reaction buffer as an oxygen scavenger to improve the photostability of the dye pair. A binning time of 0.5 ms and a minimum of 35 counts was used as a threshold for the obtained bursts for further analysis. FRET was calculated as:

$$E = \frac{I_A - \alpha}{\gamma I_D + (I_A - \alpha)} \qquad \text{------ (2.12)}$$

Where $I_D$ and $I_A$ are the intensities in the donor and acceptor channels, respectively, and γ accounts for the difference in the quantum yields and detection efficiencies of the donor and acceptor. α signifies the donor fluorescence leakage into the acceptor channel.

**Table 2.1** Primers used for creating point mutations and truncations:

| | |
|---|---|
| C17T Forward | GGAAGATCACGCTGGGACTTACGGGTTGGGGG |
| C17T Reverse | CCCCCAACCCGTAAGTCCCAGCGTGATCTTCC |
| S56C Forward | CACTGAGGACGGATGTGAGGAACCGGGC |
| S56C Reverse | GCCCGGTTCCTCACATCCGTCCTCAGTG |
| A158C Forward | CACCGCGGGGAGCATGCCCTCCAGGCCAG |

| | |
|---|---|
| A158C Reverse | CTGGCCTGGAGGGCATGCTCCCCGCGGTG |
| S199C_S202E_T205E _S208E Forward | CAGCTGCCCCGGCGAGCCAGGCGAGCCCGGCGAGCGC TCCCGCACCCC |
| S199C_S202E_T205E _S208E Reverse | GGGGTGCGGGAGCGCTCGCCGGGCTCGCCTGGCTCGCC GGGGCAGCTG |
| Nh2htau Forward | ATATATCATATGCAGGGGGGCTACACCATGCACC |
| Nh2htau Reverse | ATATATCTCGAGTCAACGGACCACTGCCACCTTCTTGG |
| Tau (151-399) Forward | ATATATCATATGATCGCCACACCGCGGGG |
| Tau (151-399) Reverse | ATATATCTCGAGTCACTCCGCCCCGTGGTCTGTCTTGG |
| S291C Forward | GCAACGTCCAGTCCAAGTGCGGCTCAAAGG |
| S291C Reverse | CCTTTGAGCCGCACTTGGACTGGACGTTGC |
| S322C Forward | GAGCAAGGTGACCTCCAAGTGCGGCTCATTAGGC |
| S322C Reverse | GCCTAATGAGCCGCACTTGGAGGTCACCTTGCTC |
| S400C Forward | GTCGCCAGTGGTGTGTGGGGACACGTCTC |
| S400C Reverse | GGAGACGTGTCCCCACACACCACTGGCGAC |
| S433C Forward | GCTGACGAGGTGTGTGCCTCCCTGGCC |
| S433C Reverse | GGCCAGGGAGGCACACACCTCGTCAGC |
| S199C Forward | CAGCGGCTACAGCTGCCCCGGCTCCCC |
| S199C Reverse | GGGGAGCCGGGGCAGCTGTAGCCGCTG |
| Tau ΔPHF6* Forward | CCAGCCGGGAGGCGGGAAGAAGCTGGATCTTAGCAACG |
| Tau ΔPHF6* Reverse | CGTTGCTAAGATCCAGCTTCTTCCCGCCTCCCGGCTGG |
| Tau ΔPHF6 Forward | CGTCCCGGGAGGCGGCAGTCCAGTTGACCTGAGC |
| Tau ΔPHF6 Reverse | GCTCAGGTCAACTGGACTGCCGCCTCCCGGGACG |
| CTD Forward | ATATATCTCGAGTCATTGAGATGCACATTGAACACC |
| CTD Reverse | ATATATCATATGAAAGTTGAAAACGAAAGGAAGATCCT AGAAGTCCATG |

## 2.4 References

1. Hardenberg, M.; Horvath, A.; Ambrus, V.; Fuxreiter, M.; Vendruscolo, M. Widespread occurrence of the droplet state of proteins in the human proteome. *Proceedings of the National Academy of Sciences U.S.A.* **2020**, *117*, 33254-33262.

2. Bolognesi, B.; Lorenzo Gotor, N.; Dhar, R.; Cirillo, D.; Baldrighi, M.; Tartaglia, G. G.; Lehner, B. A Concentration-Dependent Liquid Phase Separation Can Cause Toxicity upon Increased Protein Expression. *Cell Reports* **2016**, *16* (1), 222-231.

3. Holehouse, A. S.; Das, R. K.; Ahad, J. N.; Richardson, M. O. G., Pappu, R. V. CIDER: Resources to Analyze Sequence-Ensemble Relationships of Intrinsically Disordered Proteins. *Biophysical Journal* **2017**, *112*, 16-21.

4. Madhu, P.; Mukhopadhyay, S. Preferential Recruitment of Conformationally Distinct Amyloid-β Oligomers by the Intrinsically Disordered Region of the Human Prion Protein. *ACS Chemical Neuroscience* **2020**, *11*, 86-98.

5. Zahn, R.; von Schroetter, C.; Wüthrich, K. Human Prion Proteins Expressed in Escherichia Coli and Purified by High-Affinity Column Refolding. *FEBS Letter* **1997**, *417*, 400-404.

6. Alberti, S.; Gladfelter, A.; Mittag, T. Considerations and Challenges in Studying Liquid-Liquid Phase Separation and Biomolecular Condensates. *Cell* **2019**, *176* (3), 419–434.

7. Das, D.; Arora, L.; Mukhopadhyay, S. Short-Range Backbone Dihedral Rotations Modulate Internal Friction in Intrinsically Disordered Proteins. *Journal of American Chemical Society* **2022**, *144*, 1739-1747.

8. Horcas, I.; Fernández, R.; Gómez-Rodríguez, J. M.; Colchero, J.; Gómez-Herrero, J.; Baro, A. M. WSXM: A Software for Scanning Probe Microscopy and a Tool for Nanotechnology. *Review of Scientific Instrument* **2007**, *78* (1).

*****

# CHAPTER 3

## Heterotypic electrostatic interactions control complex phase separation of tau and prion into multiphasic condensates and co-aggregates

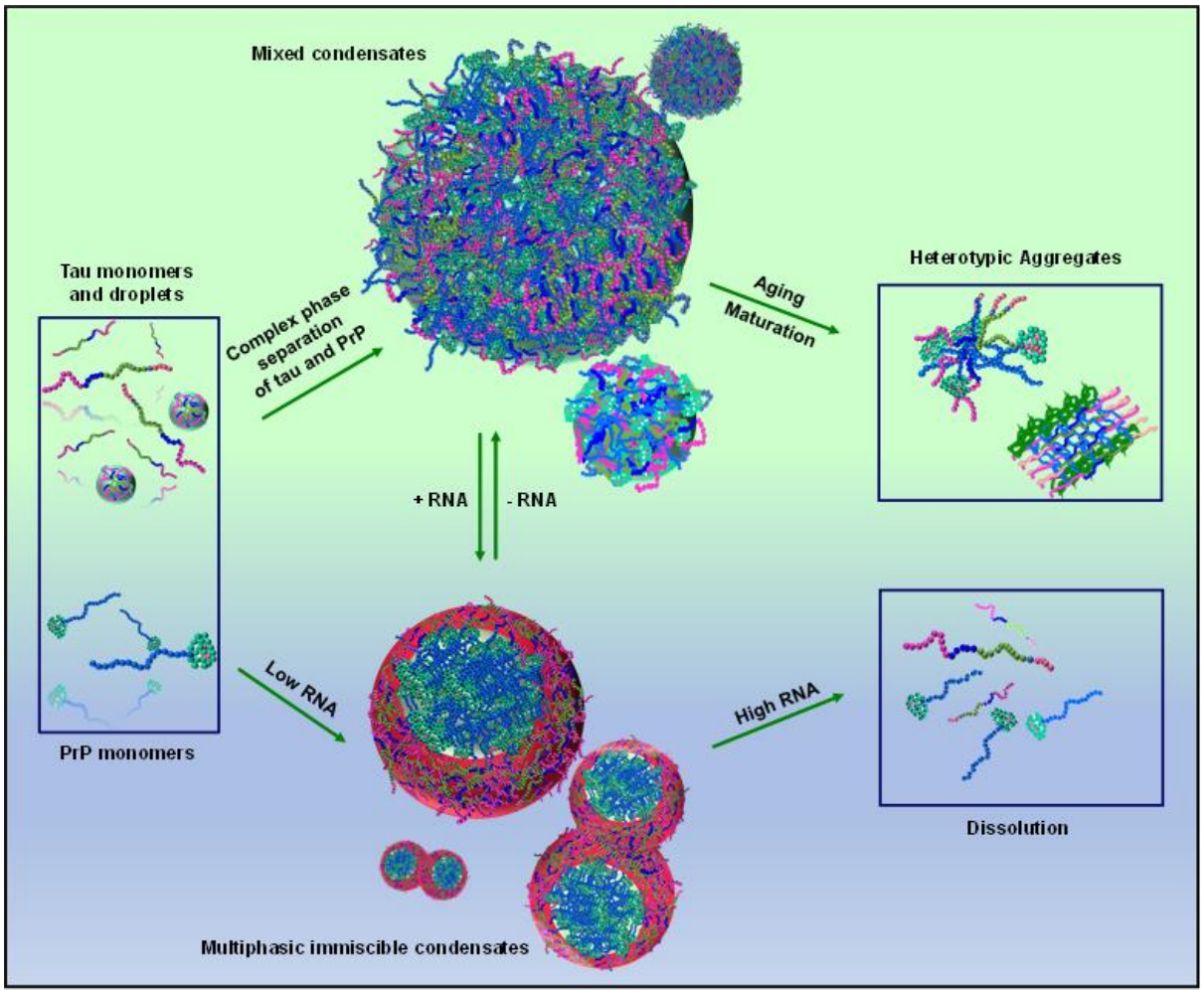


Rai, S. K., Khanna, R., Avni, A., Mukhopadhyay, S. *Proc. Natl. Acad. Sci. U.S.A.* (2023)

## 3.1 Introduction

Owing to their ability to form and dissipate in response to cellular cues, regulatability, permeability, and their ability to selectively concentrate the biomolecules, these noncanonical, liquid-like, membraneless compartments are emerging as central players at all levels of essential cellular activities ranging from gene expression and regulation to modulation of intricate signaling pathways.[1-11] An emerging body of work has revealed that intrinsically disordered proteins/regions (IDPs/IDRs) often comprising polypeptide repeat units, low sequence complexity, and prion-like domains are ideal candidates for biological phase separation. Such sequence features offer a fuzzy network of weak, multivalent, non-covalent, and transient contacts that govern the relay of making and breaking of weak interactions and promote phase separation into liquid-like condensates.[12-19] Material properties of these biomolecular condensates can be tuned by other proteins and nucleic acids such as RNA. Heterotypic interactions between the molecular entities involving a multitude of proteins and nucleic acids can often lead to the formation of multicomponent, multiphasic, and mutually immiscible compartments such as nucleolar condensates.[20-25] *In vitro*, many of the essential biophysical features of liquid-like intracellular membraneless organelles can be recapitulated by using purified proteins with or without nucleic acids that can spontaneously demix from a mixed homogeneous phase into two co-existing phases namely, the dense phase and the light phase.[11, 26, 27] Macromolecular phase separation is proposed to involve a density transition coupled to percolation that results in the dense phase comprising a viscoelastic network fluid.[4] Such physical microgels can undergo maturation into solid-like aggregates via time-dependent changes in the material properties. These protein aggregates formed via aberrant phase transitions are thought to be involved in a range of deadly neurodegenerative diseases such as Alzheimer's Disease, Amyotrophic Lateral Sclerosis (ALS), Frontotemporal Lobar Degeneration (FTLD), and so forth.[28-32] Therefore, the understanding of the precise molecular determinants of biological phase separation is of great importance in both physiology and pathology. Here, we describe an intriguing interplay of two neuronal proteins such as tau and prion proteins that undergo complex coacervation resulting in the formation of heterotypic condensates. These condensates transform into multiphasic condensates in the presence of RNA and exhibit a time-dependent maturation into solid-like aggregates.

Tau is a microtubule-associated neuronal IDP that is expressed in the human brain as six different spliced variants.[33, 34] The longest isoform, full-length tau, harbors two N- terminal

inserts and a proline-rich domain followed by four repeat regions, one pseudo repeat region, and a C-terminal domain (Figure 3.1 *A*). Under normal conditions, tau interacts with other microtubular proteins mediated by its proline-rich and repeat domains. These domains are prone to modifications in the form of post-translational hyperphosphorylation under disease conditions.[35, 36] Additionally, tau contains a heterogeneous cluster of charged residues, oppositely charged domains, and polar residues with a high proline and glycine content throughout the sequence making it a highly dynamic and amphipathic polypeptide. Recent reports have shown that under physiological conditions, tau can undergo a liquid-to-solid transition via phase separation driven by homotypic as well as heterotypic interactions in the absence or presence of a crowding agent.[37-40] Such condensates have been proposed to act as reaction crucibles that can promote aberrant phase transitions involved in disease progression. Besides, tau pathology extends to many other neuronal and RNA-binding proteins (RBPs). The interactions of tau and its hyperphosphorylated variants with several RBPs including Musashi and T-cell intracellular antigen 1 have been proposed to result in heterotypic inclusions that might be responsible for the exacerbation of overlapping neuropathological features and diseases.[41] Moreover, the accumulation of neurofibrillary tangles (NFTs) of tau with another IDP, α-synuclein (α-Syn), in Parkinson's disease hints toward the synergistic interactions between tau and α-Syn.[42] Tau protein deposits have also been found in the brains of patients affected by familial cerebral amyloid angiopathy associated with the misfolding and aggregation of the human prion protein (PrP). These patients displayed a nonsense stop codon mutation (Q160Stop) in PrP resulting in a highly unstructured truncated variant of PrP. Additionally, Gerstmann-Sträussler-Scheinker (GSS) syndrome associated with a missense mutation in PrP (F198S) is attributed partly to tau deposits.[43-45] These findings revealed a complex interplay of tau and PrP in a range of pathological manifestations. The cellular form of PrP ($PrP^C$) is a GPI-anchored protein consisting of an N-terminal signal peptide (residues 1-22), a highly positively charged, intrinsically disordered, N-terminal tail containing oligopeptide repeats (residues 23-120), a globular C-terminal domain (residues 121-230), and a GPI-anchor signal (residues 231-253)[46-48] (Figure 3.1 *B*). It also contains a putative RNA binding site and is often classified as an RBP. In order to elucidate the molecular basis of tau-PrP interactions associated with overlapping neuropathological features, we set out to investigate the role of PrP in regulating the phase behavior of tau and discovered an intriguing interplay of molecular drivers in modulating their complex phase transitions.

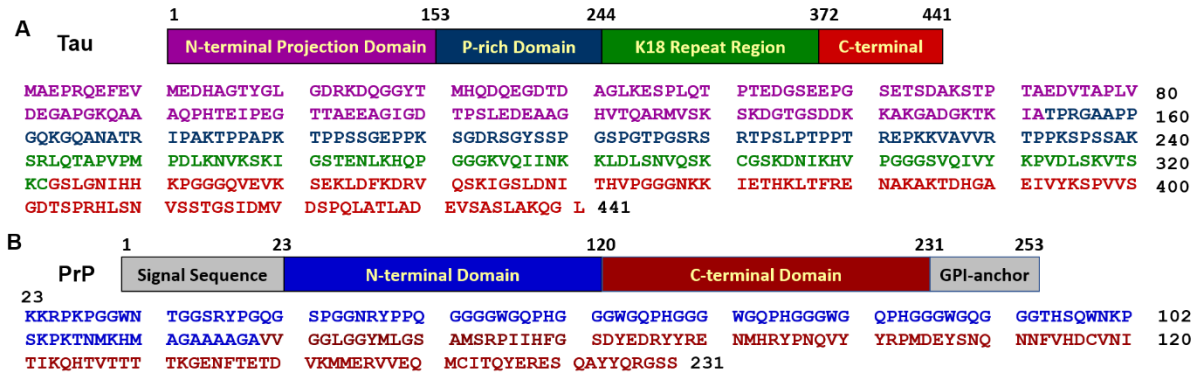


**Figure 3.1. Sequence composition and domain architecture: (A)** Domain architecture and amino acid sequence of full-length tau. A null-cysteine variant of full-length tau (C291S, C322S) was used for our studies. **(B)** Domain architecture and amino acid sequence of full-length PrP.

## 3.2 Results

### 3.2.1 PrP potentiates spontaneous phase separation of tau through heterotypic interactions

Sequence composition governs the phase behavior of a protein by tuning its multivalent interactions. Clustered negatively and positively charged residues, weakly hydrophobic segments, and cation-π modulators such as arginine and aromatic amino acids are important for regulating these interactions. First, we analyzed the amino acid sequence of full-length tau protein. It has a negatively charged N-terminal and positively charged Proline-rich domain, in addition to a hydrophobic repeat domain and a mildly negatively charged C-terminal end, making it a highly unstructured amphipathic polymer and hence an ideal candidate for phase separation (Figure 3.1 *A*). This was further supported by sequence-based phase separation predictors such as FuzDrop[49] and catGRANULE,[50] which predicted a high phase separation propensity for the tau protein (Figure 3.2 A and Figure 3.2 *B*). We began with turbidity measurements and confocal microscopy to complement our bioinformatic analyses with experimental proof and established the *in vitro* phase separation of tau at a near-physiological condition. We observed that under our condition (14 mM HEPES, pH 6.8) tau remains in a monomeric dispersed form even at very high concentrations (~ 1 mM) in the presence of 50 mM NaCl. Upon lowering the salt concentration (< 10 mM NaCl), the turbidity of the protein solution rose even at protein concentrations as low as ~ 6 μM, which is close to the

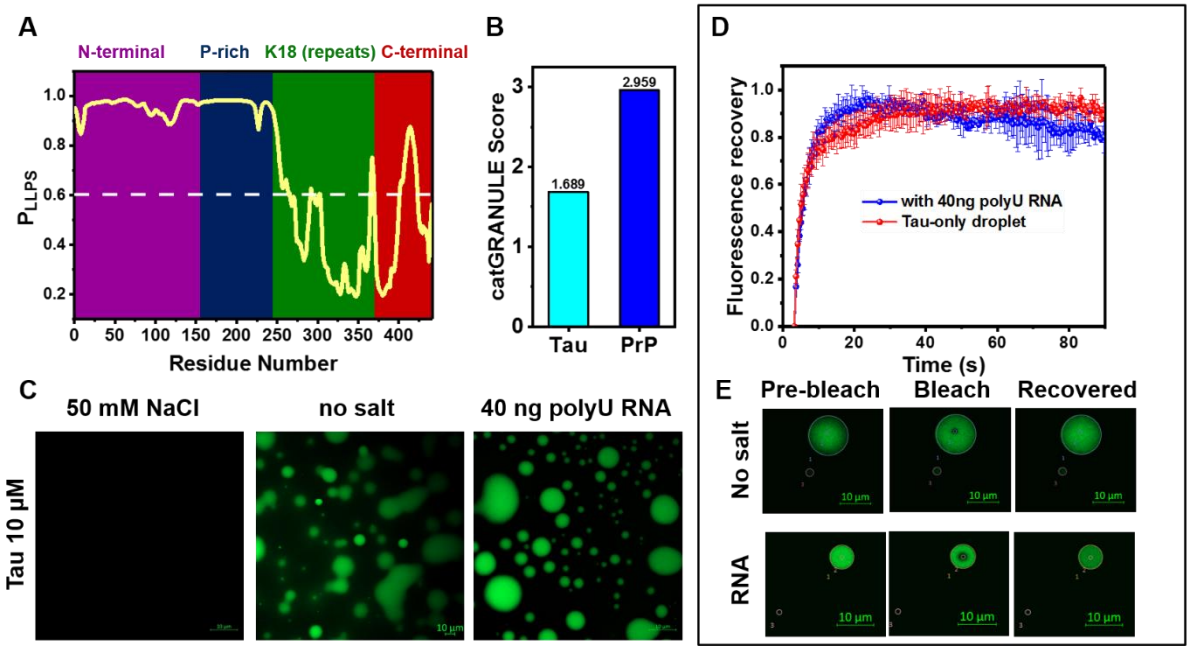


**Figure 3.2. Tau undergoes phase separation under physiological concentration. (A)** The propensity of phase separation predicted for tau using FuzDrop. **(B)** Tau and PrP phase separation propensity predicted using catGRANULE. **(C)** Confocal imaging of tau monomer (homogeneous phase) in 50 mM NaCl salt buffer (14 mM HEPES), tau-only droplets (10 µM), and tau:RNA droplets. Alexa Fluor 488-labeled (~ 1%) tau FL17C protein was doped with unlabeled protein for imaging. The imaging was performed at least thrice with similar observations (scale bar 10 µm). **(D)** FRAP kinetics of tau-only and tau:RNA droplets. Alexa Fluor 488-labeled protein (~ 1%) was used for FRAP. The data represent mean ± s.d. for n = 3 independent experiments. **(E)** Tau-only (upper) and tau:RNA (lower) droplets images in the time-course of FRAP.

physiological concentration of tau (2 µM). To further verify the increase in turbidity with observable evidence, we used an Alexa Fluor488-maleimide labeled single-Cys variant of the protein (tau-T17C) to perform confocal fluorescence imaging. Tau protein doped with the labeled variant (~ 1%) was used for imaging, which reveals the formation of tau protein droplets under this condition (Figure 3.2 *C*). These droplets underwent characteristic fusions and surface-wetting and displayed a rapid fluorescence recovery after photobleaching (FRAP) indicating their liquid-like behavior (Figure 3.2 *D* and *E*). These findings demonstrate the coacervation of tau via homotypic interactions and are in accordance with previous findings on the phase separation of tau.[37, 38] Previous results have indicated the ability of RNA to act as an inducer for protein phase separation by engaging in heterotypic interactions with polypeptide chains. Under our conditions, a low concentration of RNA (~ 5 ng/µL) was able to enhance the

phase-separation ability of tau as evidenced by increased turbidity and confocal imaging (Figure 3.2 *C*). These tau:RNA complex condensates behave similarly to tau-only droplets exhibiting liquid-like behavior and rapid FRAP (Figure 3.2 *D* and *E*).

We next investigated the effect of PrP on the phase behavior of tau. The N-terminal IDR of PrP has a high propensity to undergo phase separation (Figure 3.3 *A*), however, under our solution condition at pH 6.8, full-length PrP does not undergo spontaneous phase separation (Figure 3.3 *B*).

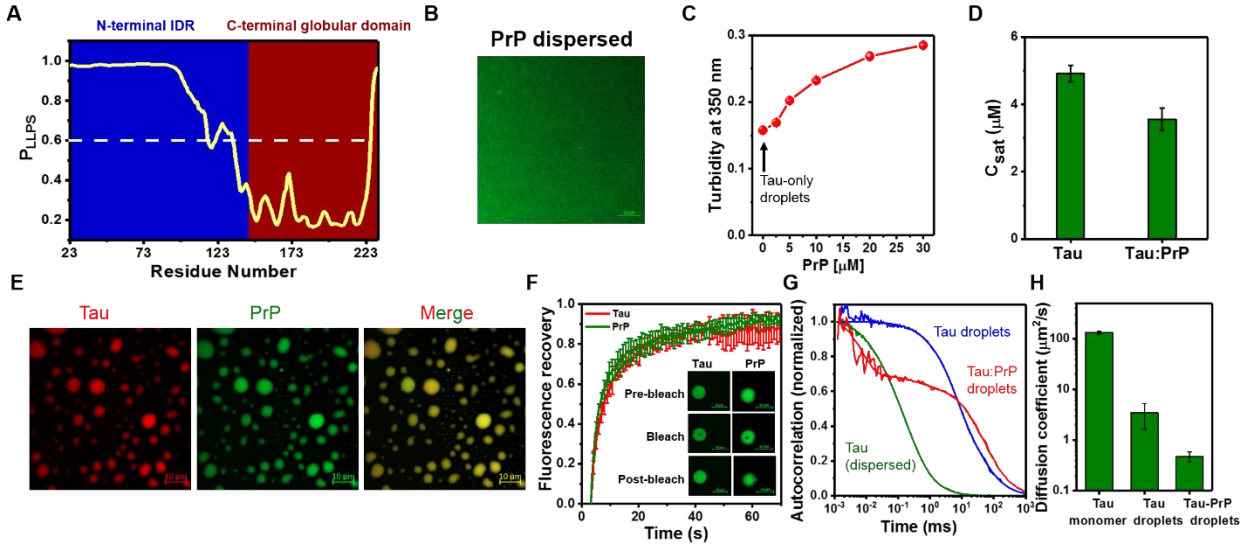


**Figure 3.3. PrP potentiate tau phase separation. (A)** The propensity of phase separation predicted for PrP using FuzDrop. **(B)** A mixed homogeneous phase of PrP (monomer). Alexa Fluor 488-labeled (~ 1%) W99C protein was doped with the unlabeled protein for imaging (scale bar 10 µm). **(C)** The turbidity at 350 nm is plotted for tau (10 µM) in the presence of an increasing concentration of PrP (14 mM HEPES, pH 6.8, 1.5 mM NaCl). **(D)** The saturation concentration ($C_{sat}$) of tau for tau-only and tau:PrP condensates estimated by ultracentrifugation. **(E)** A high-resolution two-color Airyscan confocal image of colocalized tau (tau-T17C-AlexaFluor594, red) and PrP (PrP-W99CAlexaFluor488, green) in tau:PrP coacervates (scale bar 10 µm). Tau and PrP concentrations were 10 and 20 µM, respectively. The imaging was performed at least thrice with similar observations. **(F)** FRAP kinetics of tau:PrP droplets. AlexaFluor488-labeled proteins were used for both tau and PrP for independent FRAP studies. The data represents mean ± s.d.; n = 5. **(G)** The normalized autocorrelation plot obtained from FCS measurements performed for 5 different droplets. **(H)** Diffusion coefficients (plotted on a log scale) of tau in monomeric dispersed form, tau-only droplets, and tau:PrP droplets obtained from FCS measurements (n = 5). For all FCS measurements, 5 nM of labeled protein (tau-T17C-AlexaFluor488) was used. Tau and PrP concentrations were 10 and 20 µM, respectively. See Methods for details.

We then measured the turbidity of tau solutions (10 μM) in the presence of an increasing concentration of PrP. Our data showed an increase in turbidity of the solution upon the addition of PrP suggesting an increase in the phase separation propensity of tau in the presence of PrP (Figure 3.3 *C*). To quantify this observation, we performed ultracentrifugation to estimate and compare the saturation concentration ($C_{sat}$) of tau for tau-only and tau:PrP condensates. These results indicated the lowering of $C_{sat}$ values of tau in the presence of PrP (Figure 3.3 *D*). Next, to check whether PrP is recruited inside the droplet and undergoing complex phase separation with tau, we performed two-color Airyscan confocal imaging to visualize the heterotypic coacervation of tau and PrP. We labeled single-Cys variants of tau (T17C) and PrP (W99C) using AlexaFluor594-maleimide and AlexaFluor488-maleimide, respectively. We carried out phase separation assays with tau and PrP in the presence of ~ 1% labeled proteins and imaged them under a confocal microscope. Two-color imaging revealed the colocalization of tau and PrP within these liquid condensates (Figure 3.3 *E*). Heterotypic coacervation of tau and PrP yielded a much larger number of droplets that were smaller and more spherical compared to tau-only droplets. Next, in order to study the internal material properties of these droplets, we performed FRAP experiments that revealed rapid near-complete recoveries for both proteins indicating their mobility inside the droplets (Figure 3.3 *F*).

Further, to probe the diffusional properties of the dense phase on a microsecond to sub-millisecond timescale, we monitored the diffusion time of Alexa488-labeled tau inside tau-only and tau:PrP droplets by performing fluorescence correlation spectroscopy (FCS) within individual droplets. The diffusion time extracted from our correlation measurements suggested the presence of slower diffusion of tau in tau:PrP droplets compared to tau-only droplets indicating heterotypic interactions of tau and PrP resulting in slower diffusion of tau (Figure 3.3 *G* and Figure 3.3 *H*). Taken together, our observations suggest that PrP potentiates the phase separation of tau and is recruited within the droplets resulting in stronger physical crosslinks comprising an intermolecular network of tau and PrP. Next, to further unmask the nature of intermolecular interactions driving tau:PrP complex coacervation, we investigated the sequence features of both proteins. Given the clustering of opposite charges in both proteins, we postulated that they could potentially interact electrostatically in a manner similar to what has been reported before for the complex coacervation of IDPs.[51, 52] To investigate the effect of electrostatic interactions, we set out to study the influence of salt on tau:PrP complex coacervation.

### 3.2.2 Electrostatic interactions are the principal driver of tau:PrP heterotypic coacervation

Tau and PrP possess similar net charges and have isoelectric points (pI) of 8.24 and 9.44, respectively. Although based on their overall charge, one would expect repulsion between these two polypeptide chains, a closer inspection of the amino acid sequence and charge distribution throughout both protein chains[53] revealed that tau and PrP are oppositely charged at the N-terminal ends which can drive their complex coacervation (Figure 3.4 *A* and *B*). To test our hypothesis, we performed salt-dependent turbidity assays and confocal imaging of the tau:PrP condensates (Figure 3.4 *C* and *D*). With an increasing salt concentration, the turbidity of the tau:PrP mixture dropped sharply with a dissolution of droplets at 50 mM NaCl highlighting the role of intermolecular electrostatic interactions in driving their complex coacervation. With

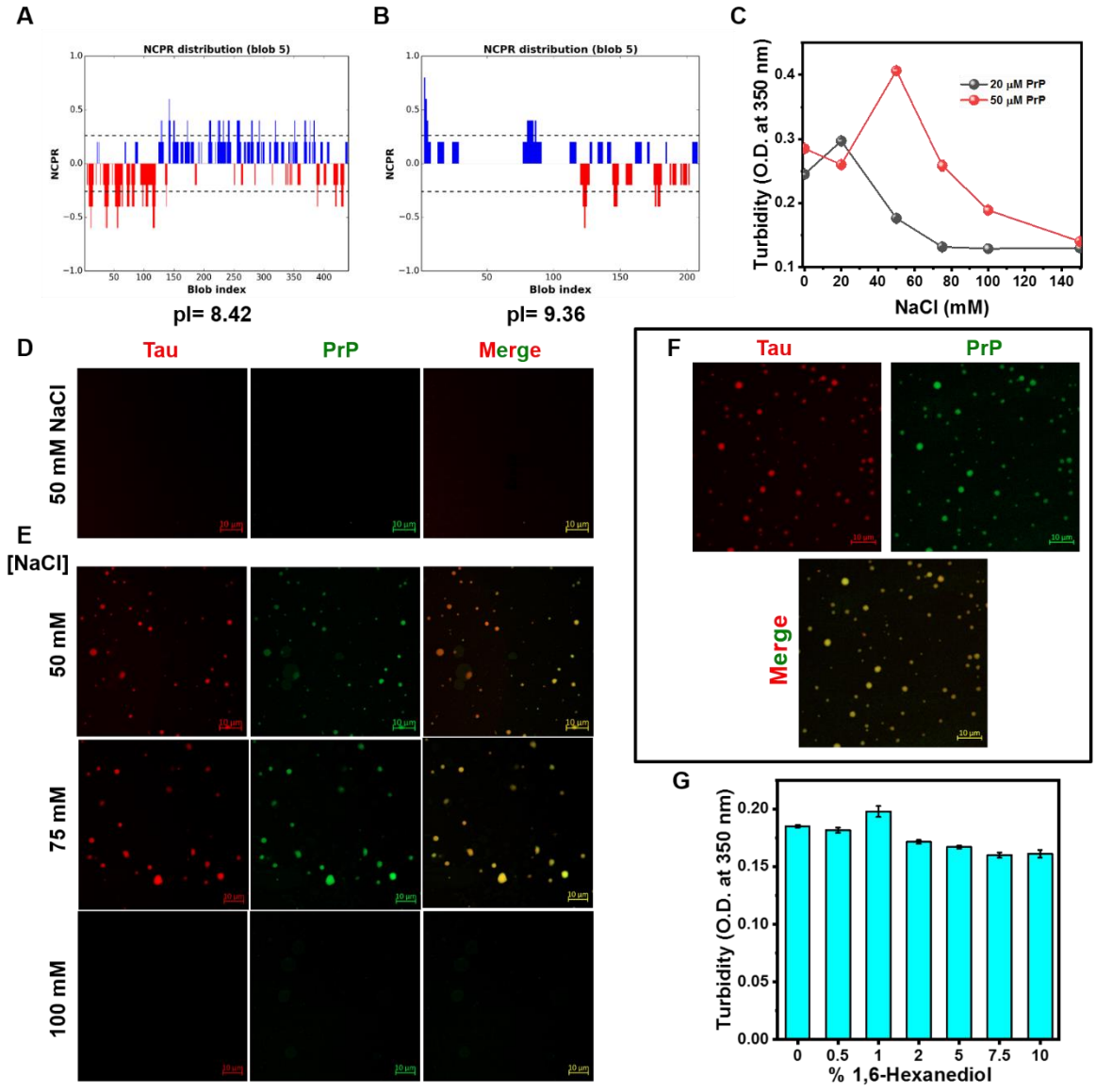

**Figure 3.4. Electrostatic interaction regulates tau:PrP coacervation. (A)** Charge distribution profile (NCPR: net charge per residue) of tau and **(B)** PrP using CIDER. Red and blue indicate negatively and positively charged residues, respectively. **(C)** Salt-dependent turbidity (at O.D. 350 nm) of tau:PrP reaction mixtures (Black curve: tau 10 µM, PrP 20 µM and Red curve: tau 30 µM, PrP 60 µM respectively). The data represent mean ± s.d. for n = 3 independent single-day measurements. **(D)** Salt-induced dissolution of tau:PrP droplets (tau 10 µM, PrP 20 µM) in the presence of NaCl (scale bar 10 µm). **(E)** Tau (10 µM, red) and PrP (50 µM, green) complex coacervates in the presence of an increasing concentration of salt (scale bar 10 µm). **(F)** At higher concentrations of tau and PrP (30 and 60 µM, respectively) tau and PrP undergo complex coacervation at physiological salt concentration (150 mM) of NaCl. **(G)** The turbidity plot of tau-PrP condensates (tau 10 µM, PrP 20 µM) in the presence of 1,6-hexanediol.

increasing PrP concentration, these heterotypic assemblies were able to sustain higher salt concentrations (Figure 3.4 *C* and Figure 3.4 *E*). At a physiological salt concentration (~ 150 mM NaCl), higher protein concentrations (tau 30 µM and PrP 60 µM) were needed to drive complex phase separation (Figure 3.4 *F*). We also observed no significant changes in the phase separation propensity upon the addition of increasing amounts of 1,6-hexanediol possibly indicating the presence of more pronounced electrostatic interactions within condensates compared to hydrophobic effects (Figure 3.4 *G*). Post-translational modifications (PTMs) of a protein often play a crucial role in modulating its phase separation ability and interactions with other proteins or biomolecules primarily by changing its charge distribution.[54, 55] We next probed whether the frequently occurring phosphorylation of tau, which adds negative charges to the protein, would increase the phase separation propensity of tau:PrP. To test this, we created a triple phosphomimetic variant of tau (tau 3P) by selectively mutating three residues to glutamate (S202E, S205E, T208E). This variant of tau (tau 3P) exhibited a higher propensity for phase separation with PrP as observed by our turbidity assays (Figure 3.5 *A*). Further, even a much lower concentration of PrP (~ 2 µM) promoted the phase separation of tau 3P compared to wild-type tau. Two-color imaging also corroborated our turbidity measurements (Figure 3.5 *B*). Imaging and FRAP experiments validated the liquid-like nature of tau 3P:PrP droplets (Figure 3.5 *C*). These tau 3P:PrP droplets were larger and more mobile compared to tau:PrP droplets (Figure 3.5 *D*). These results together suggested that electrostatic interactions modulate the complex coacervation of tau and PrP. We next set out to elucidate the roles of specific protein domains in driving the complex coacervation of tau and PrP.

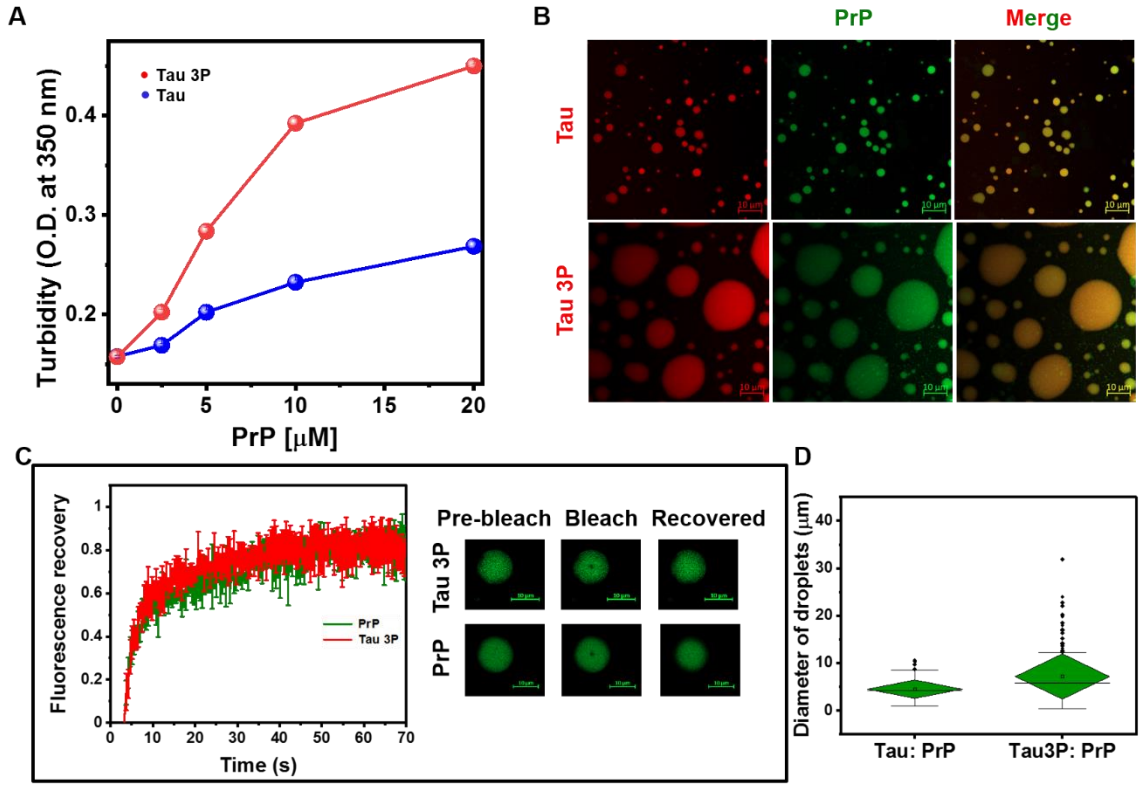


**Figure 3.5 Phosphorylation of tau increases tau:PrP phase-separation. (A)** Turbidity plot of tau (10 μM) and triple phosphomimetic mutant of tau (tau 3P, 10 μM) as a function of the PrP concentration. The data represent mean ± s.d.; n= 3. **(B)** Two-color Airyscan confocal images of tau 3P (10 μM, red) and PrP (10 μM, green) droplets (lower panel) compared with tau (upper panel) (scale bar 10 μm). **(C)** FRAP kinetics of tau and PrP components in tau 3P:PrP droplets. The data represent mean ± s.d. for n = 3 independent singleday experiments. The adjacent panel shows the images of droplets during FRAP experiments. The imaging was performed at least thrice for all experiments with similar observations. Alexa488-labeled proteins were used for FRAP studies with both tau and PrP. **(D)** Comparison of the size distribution of tau:PrP and tau 3P:PrP droplets.

### 3.2.3 Domain-specific interactions drive the co-condensation of tau and PrP.

In order to obtain domain-specific insights into the electrostatic interactions between tau and PrP, we created several truncated variants of both proteins (Figure 3.6 *A* and *B*). First, we aimed to characterize the role of the negatively charged N-terminal fragment and positively charged P-rich region of tau and created two naturally occurring truncations namely, Nh2-tau (aa 26-230, pI = 5.32) and tau 0N4R (aa 151-391, pI = 10.23). These variants of tau are found in tau

deposits in the Alzheimer's disease brain and are thought to play a vital role in tau pathogenesis.[56, 57]

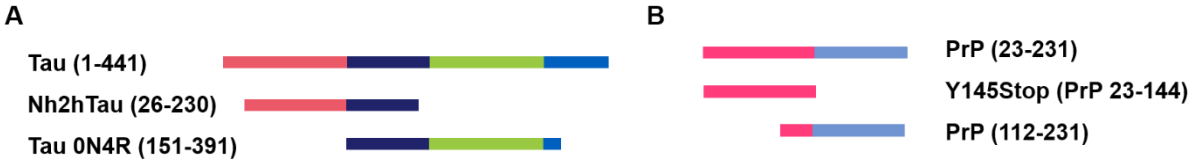


**Figure 3.6. (A-B)** The depiction of tau and PrP truncations used.

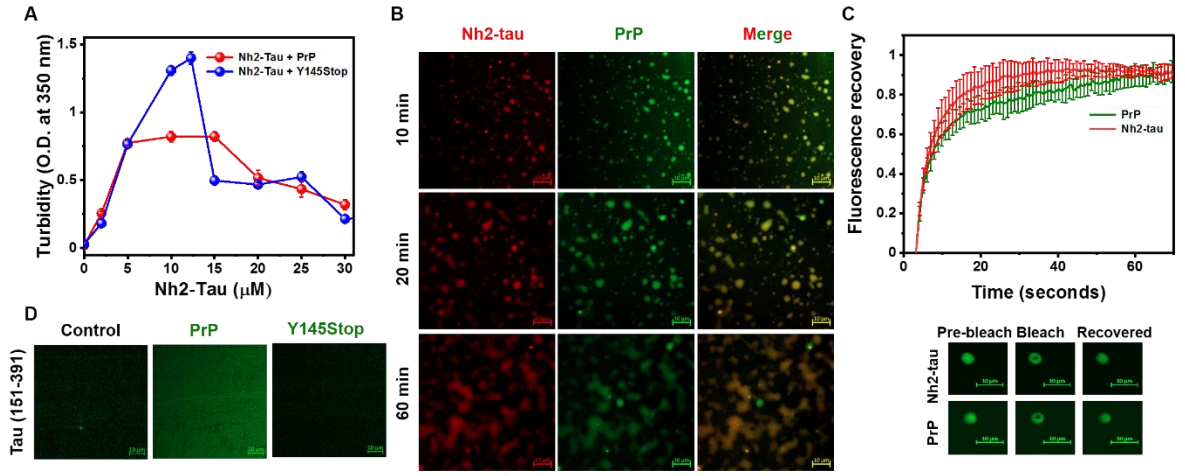


**Figure 3.7. (A)** Turbidity plots of Nh2-tau:PrP (PrP, 10 μM) and Nh2-tau:Y145Stop (Y145Stop, 10 μM). The data represent mean ± s.d.; n = 3. **(B)** Two-color Airyscan confocal images of Nh2-tau:PrP over time (Nh2-tau 20 μM, PrP 10 μM) (scale bar 10 μm). **(C)** FRAP profiles of Nh2-tau and PrP components inside Nh2-tau:PrP droplets. The adjacent lower panel shows the droplet profile during FRAP. The data represent mean ± s.d. for n = 3 independent experiments. **(D)** Images of the mixed homogeneous phase of 0N4R tau (right most panel, green), 0N4R with PrP (second panel, green), and 0N4R with Y145Stop (third panel, green), (scale bar 10 μm). Same concentration of each protein (20 μM) was used.

Based on the high net negative charge, we posited that Nh2-tau (predicted net charge ~ - 5) could undergo phase separation with PrP (predicted net charge ~ + 10) by a charge-neutralization mechanism that is reminiscent of RNA-driven reentrant phase transitions. Indeed, our turbidity measurements showed a bell-shaped profile for Nh2-tau:PrP at a fixed concentration of PrP (10 μM) (Figure 3.7 *A*). The turbidity value peaked at a 2:1 stochiometric ratio of Nh2-tau:PrP where the charge neutralization was expected. Our two-color fluorescence microscopy also corroborated this observation (Figure 3.7 *B*). These Nh2-tau:PrP droplets showed liquid-like characteristics, grew with time, and after 1 h these droplets appeared to

completely coalesce (Figure 3.7 *B* & *C*). Further, as expected, the other positively charged fragment of tau, tau 0N4R, did not phase separate either alone or in the presence of PrP (Figure 3.7 *D*). These results indicated that the negatively charged N-terminal domain of tau is important for the heterotypic condensation of tau and PrP.

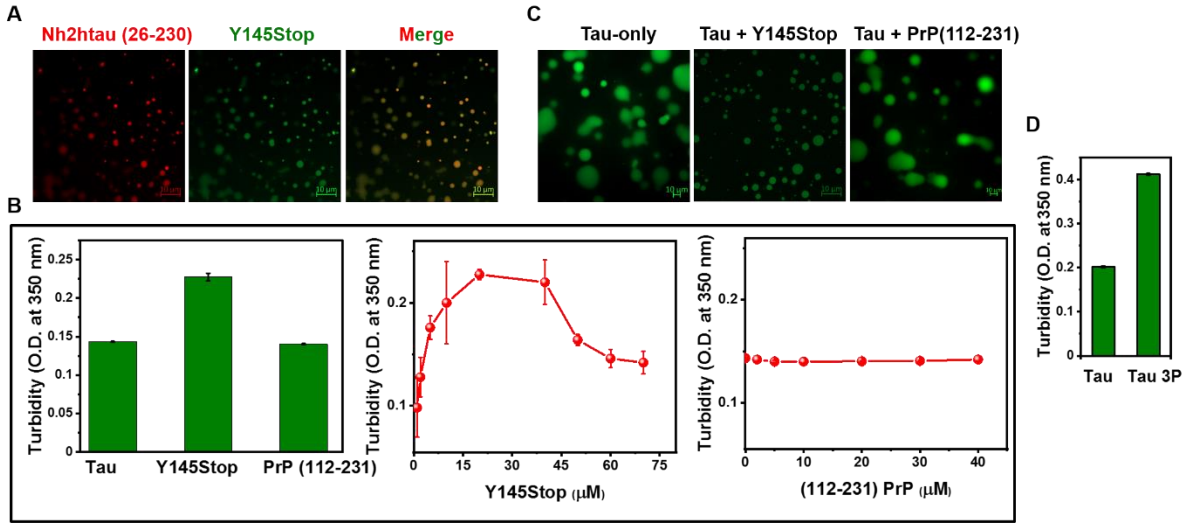


**Figure 3.8. (A)** Nh2-tau:Y145Stop (Nh2-tau 20 µM, Y145Stop 10 µM) droplets. **(B)** Effect of PrP truncations (20 µM) on tau (10 µM) turbidity. The data represent mean ± s.d.; n = 3. **(C)** Confocal images of droplets of tau (10 µM with 1% tau-T17C-AlexaFluor488) in the presence of N- and C-terminal truncations of PrP (20 µM each, scale bar 10 µm). **(D)** Comparison of tau and tau 3P turbidity in the presence of Y145Stop.

In order to investigate the role of different regions of PrP in tau:PrP co-condensation, we used a naturally occurring, pathological C-terminally truncated variant of PrP, namely, Y145Stop (PrP 23-144) (Figure 3.6 *B*).[58] Y145Stop exhibited a phase separation behavior with tau similar to full-length PrP, as evident from the turbidity measurements and imaging (Figure 3.7 *A* and 3.8 *B, C*). Moreover, the turbidity and droplet profiles of Nh2-tau:Y145Stop were similar to that obtained with full-length PrP (Figure 3.7 *A*). Similarly, as in the case of full-length PrP, with the tau3P variant, Y145Stop showed an increase in turbidity in comparison to the unmodified tau, highlighting the role of electrostatic interactions (Figure 3.8 *D*). However, the C-terminal globular domain of PrP (PrP 112-231) neither enhanced the phase separation propensity nor changed the morphological appearance of tau droplets (Figure 3.8 *B, C*). These findings highlight that the N-terminal intrinsically disordered segment of PrP is the key modulator for complex coacervation of tau and PrP primarily via electrostatic interactions between oppositely charged disordered domains. Previous studies have shown that such domain-specific electrostatic interactions yield nanocomplexes that can serve as primary units

for such heterotypic complex coacervates.[52] These primary units can offer a dynamic network of physical crosslinks resulting in a dense phase that exhibits liquid-like properties at the mesoscopic length scale but contains short-range ordering and dynamic heterogeneity at the nanoscopic level. We thus hypothesized that region-specific electrostatic interactions could potentially induce temporal molecular ordering within the condensed phase. Next, we used site-specific picosecond time-resolved fluorescence anisotropy measurements to discern short-range dynamic heterogeneity.

### 3.2.4 Electrostatic nanoclusters in heterotypic condensates.

In order to investigate the region-specific structural ordering in tau:PrP condensates, we performed fluorescence anisotropy measurements that report the local rotational flexibility. To record the site-specific anisotropy, we used a thiol-active fluorescent dye, Fluorescein-5-maleimide (F-5-M) to label single-Cys variants of tau at residue locations 17, 56, 158, 291, 322, 400, and 433 spanning the entire protein chain. Any rise in the steady-state anisotropy is interpreted as the loss of conformational flexibility. The steady-state fluorescence anisotropy exhibited an increase at all positions compared to monomeric dispersed tau (Figure 3.9 *A*). Upon the formation of tau:PrP complex condensates, we observed a rise in the anisotropy at locations 56, 158, 400, and 433 indicating these regions of tau possessing negatively charged residues are involved in heterotypic interactions with the positively charged N-terminal domain of PrP (Figure 3.9 *A*). In contrast, residues 291 and 322 located near the basic region of tau did not exhibit an increase in the anisotropy presumably due to electrostatic repulsions with the positively charged N-terminal domain of PrP. Notably, the anisotropy value at residue 56 located at the negatively charged N-terminal domain of tau showed the most significant increase followed by residue positions 158 and 400 (C-terminal end). Additionally, we measured the changes in the anisotropy at various residue positions in PrP by using respective cysteine variants (Figure 3.9 *C*). A significant increase in the anisotropy at residue position 99 located at the positively charged intrinsically disordered N-terminal domain of PrP indicated the role of this segment in promoting the electrostatically driven complex coacervation of tau and PrP. Moreover, our single-droplet anisotropy measurements for tau and PrP also corroborated our ensemble measurements (Figure 3.9 *B* and *D*). These observations are in line

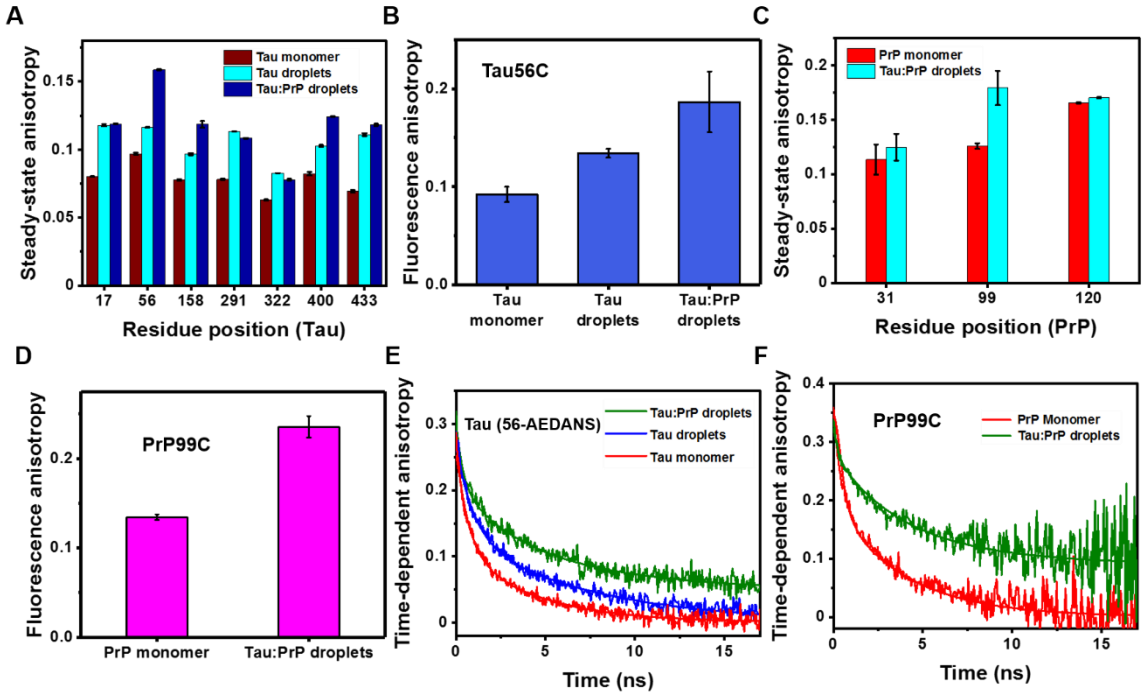


**Figure 3.9. Steady-state and Time-resolved anisotropy measurement**. **(A)** Steady-state fluorescence anisotropy measurements of F-5-M labeled single-Cys mutants of tau spanning the sequence; in the dispersed monomeric (wine), tau-only droplets (cyan), and tau:PrP droplets (blue). The data represent mean ± s.d.; n = 3. **(B)** Steady-state fluorescence anisotropy measurements using a confocal microscope for F-5- M-labeled tau at residue 56, in monomer, tau-only, and tau:PrP droplets. For droplets, single-droplet anisotropy measurements were performed in the confocal microscopy mode for 10 individual droplets. **(C)** Steady-state fluorescence anisotropy measurements of F-5-M labeled single-Cys mutants of PrP in the dispersed monomeric (red) and tau:PrP droplets (cyan). The data represent mean ± s.d.; n = 3. **(D)** Single droplet anisotropy measurements were performed for F-5-M-labeled PrP at residue 99. An increase in the anisotropy values suggested the domain-specific interaction between tau and PrP. The data represent mean ± s.d. for n = 3 independent experiments. Region-specific anisotropy value was extracted from at least 10 different droplets in the case of phase-separated solution. **(E)** Time-resolved fluorescence anisotropy decays of IAEDANS labeled at S56C of tau in monomer (red), tau-only droplets (blue), and tau:PrP droplets (olive). The solid lines are fits obtained using decay analysis. Similar anisotropy decay profiles were obtained for the N-terminal segment of PrP. **(F)** Time-resolved fluorescence anisotropy decays of F-5-M labeled PrP W99C in monomer (red) and tau:PrP (olive) droplets. The solid lines are fits obtained using the biexponential and triexponential decay analysis for monomers and droplets, respectively. Tau and PrP concentrations were 10 and 20 μM, respectively. See *Chapter 2: Methods*, for details of measurements and analysis and Table 1 for recovered parameters.

**Table 3.1. Recovered parameters from time-resolved fluorescence anisotropy decay analyses.**

| **Tau-S56C-AEDANS** | **$\phi_1$ ($\beta_1$)** | **$\phi_2$ ($\beta_2$)** | **$\phi_3$ ($\beta_3$)** |
|---|---|---|---|
| Tau monomer | 0.72 ± 0.11 ns (0.59 ± 0.025) | 4.85 ± 0.61 ns (0.41± 0.025) | - |
| Tau droplets | 1.07 ± 0.08 (0.56 ± 0.011) | 8.09 ± 0.11 (0.44 ± 0.011) | - |
| Tau:PrP droplets | 0.45 ± 0.058 (0.39 ± 0.031) | 3.99 ± 0.26 (0.36 ± 0.027) | 43.29 ± 3.63 (0.25 ± 0.021) |

with our results on domain-specific interactions described in the previous section. Together our steady-state fluorescence anisotropy measurements highlighted the central role of the acidic N-terminal segment of tau and the basic N-terminal domain of PrP in forming heterotypic tau:PrP condensates.

Steady-state fluorescence measurements provide time-averaged information and thus cannot distinguish between the different modes of rotational dynamics experienced by polypeptide chains. In order to discern the different modes of chain dynamics as well as to estimate the hydrodynamic sizes of the primary units formed via electrostatic interactions, we performed picosecond time-resolved fluorescence anisotropy measurements using fluorescently-labeled tau at the 56$^{th}$ position which showed the most significant increase in the steady-state anisotropy upon complex phase separation of tau and PrP. Monomeric dispersed tau exhibited fast depolarization kinetics that is typical for an expanded polypeptide chain (Figure 3.9 *E*). A bi-exponential decay model resolved a fast (sub-nanosecond) rotational correlation time corresponding to the local motion of the fluorophore and a characteristic slower (nanosecond) rotational correlation time that is attributed to collective backbone dihedral rotations and long-range conformational fluctuations. Similar de-polarization kinetics were also observed for the F-5-M labeled W99C- PrP (Figure 3.9 *F*). Upon homotypic phase separation of tau, the depolarization kinetics became slower indicating the chain-chain interactions within condensates. Upon heterotypic phase separation of tau and PrP, the depolarization kinetics exhibited an additional slower rotational correlation time (~ 43 ns) suggesting the formation of heterotypic clusters. Assuming these clusters are spherical and there is no significant change in the viscosity within droplets, the estimated hydrodynamic

radius of these tau:PrP heterotypic electrostatic clusters is ~ 3.6 nm. We would like to point out that this is an approximate estimate of the dimensions of the nanoclusters within tau:PrP condensates. Such nanoclusters were detected in other electrostatically driven complex coacervates.[32, 52] Taken together, these findings show that domain-specific electrostatic interactions between the acidic N-terminal domain of tau and the basic N-terminal domain of PrP drive the complex phase separation of tau and PrP. Additionally, since nucleic acids are known to alter the protein phase behavior, we next set out to examine the effect of RNA on the complex phase separation of tau and PrP.

### 3.2.5 RNA drives tau:PrP heterotypic assemblies into multiphasic condensates.

The interior of biomolecular condensates is thought to be a dense, yet dynamic, tangled-mesh-like organization of proteins and nucleic acids. RNA, because of its shape, charge, sequence, and conformational plasticity acts as a scaffold for the proteins and introduces multivalency into a multicomponent system.[59, 60] Because of these properties, RNA can modulate the phase behavior and tune the partitioning and material properties of condensates. Typically, RNA-controlled electrostatically driven condensates exhibit a distinct three-regime phase behavior.[61, 62]

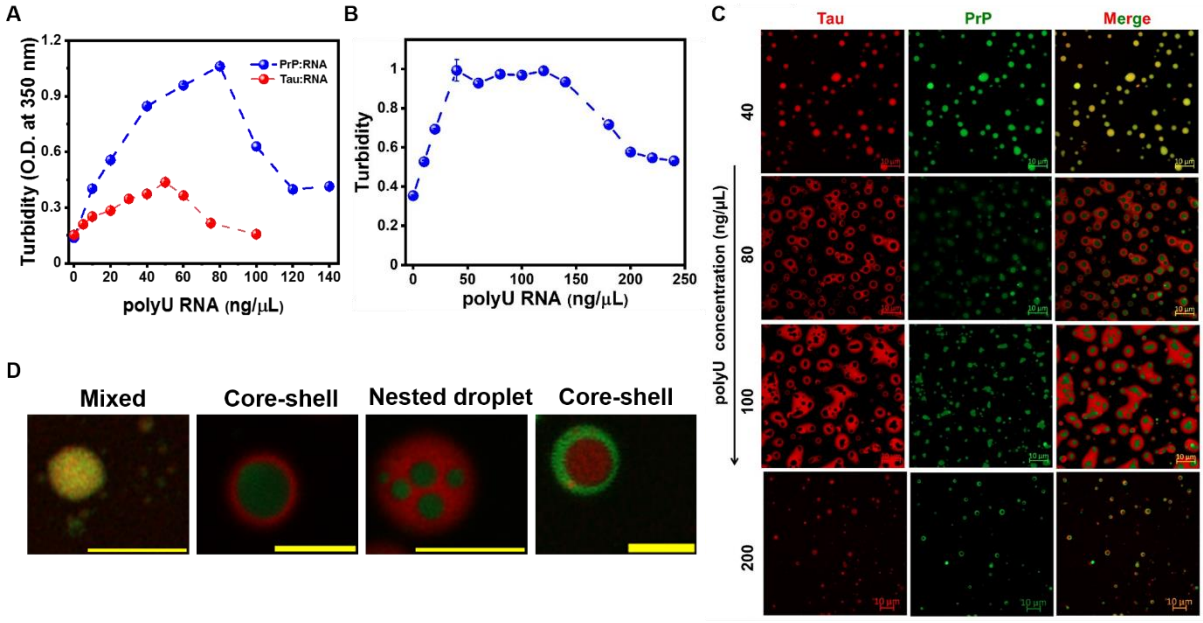


**Figure 3.10. Tau:PrP coacervates form multiphasic condensates in the presence of RNA.** **(A)** Turbidity (at O.D. 350 nm) profile of PrP and tau against an increasing concentration of PolyU RNA. **(B)** The tau:PrP binary system shows a reentrant phase behavior in the presence of polyU RNA. **(C)** Two-color Airyscan confocal imaging of tau:PrP:RNA (tau-red; PrP-green) ternary system as the function of increasing RNA concentration. With increasing

concentration of RNA, tau:PrP coacervates form immiscible multiphasic condensates that transition into a core-shell structure followed by nested droplets. In these multiphasic condensates, PrP is concentrated in the core, and tau is in the periphery. A further increase in RNA results in an inverse core-shell structure (tau and PrP form the core and the shell, respectively) and subsequently leads to droplet dissolution (scale bar 10 μm). **(D)** Select single condensates to clearly show mixed, core-shell, nested, and inverse core-shell morphologies obtained in the presence of an increasing concentration of RNA (scale bar of 5 μm is shown in yellow).

To recapitulate this behavior in the tau:PrP system, we started with individual tau and PrP droplet formation. Tau and PrP demonstrate a reentrant phase behavior, with PrP phase separating over a wider regime than tau for approximately the same protein mass (Figure 3.10 *A*). This difference in the profile can be attributed to the sequence composition of both proteins; tau is K/G-rich, whereas the N-terminal disordered domain of PrP is enriched with R/G/Y residues. Compared to a K-rich polypeptide, an R-rich polypeptide interacts more strongly with RNA because of its potential to engage with RNA via cation-π interactions in addition to the electrostatic interactions.[63, 64] Next, we set out to study the effect of polyU RNA on pre-formed tau:PrP heterotypic condensates. For this ternary system (tau:PrP:RNA) the phase separation regime gets further broadened and taller in comparison to the individual protein-RNA systems (Figure 3.10 *A* and *B*). At low RNA concentrations, tau:PrP droplets remain miscible and colocalize within the droplets (type I) (Figure 3.10 *C*, first panel, and *D*). With increasing concentrations of RNA, however, these assemblies acquire a wide range of immiscible multiphasic morphologies from a core-shell structure to a nested-droplet organization and then an inverse core-shell structure (Figure 3.10 *C*). This type of architecture is a result of differing interfacial tension, viscosity, and density amongst the interacting coacervates.[65-68] In our system, this behavior might be a result of the preferential binding of PrP with RNA through a distinct RNA binding site at the N-terminal domain of PrP, that is absent in tau. In the core-shell morphology (type II) (Figure 3.10 *C*, second panel, and *D*), towards the left side of the RNA-dependent phase diagram, PrP forms the core of the droplet (green) whereas tau distributes itself around the core. With increasing RNA concentrations, a higher amount of PrP gets recruited inside tau droplets resulting in nested droplets (type III) (Figure 3.10 *C*, third panel, and *D*). Interestingly, tau and PrP remain immiscible at this stoichiometric ratio and retain their individual droplet identity as depicted by the FRAP profile for the tau:PrP:RNA ternary mixture (Figure 3.11 *A*). The formation of these multiphasic nested condensates remained relatively unaffected by changing the order in which the components were added to

the reaction mixture suggesting its preference for the tau:PrP:RNA ternary-phase system (Figure 3.11 *B*). On moving towards the right side of the turbidity curve, we again observed a core-shell morphology (type IV), however, with an inverse distribution profile for tau and PrP (Figure 3.10 *C*, bottom panel, and *D*). This observation is further corroborated by our steady-state anisotropy measurements performed for tau:PrP with varying amounts of RNA in the ternary mixture (Figure 3.11 *C* and *D*). This organization can be attributed to the different dissolution concentrations of RNA required for each component because of their net charge

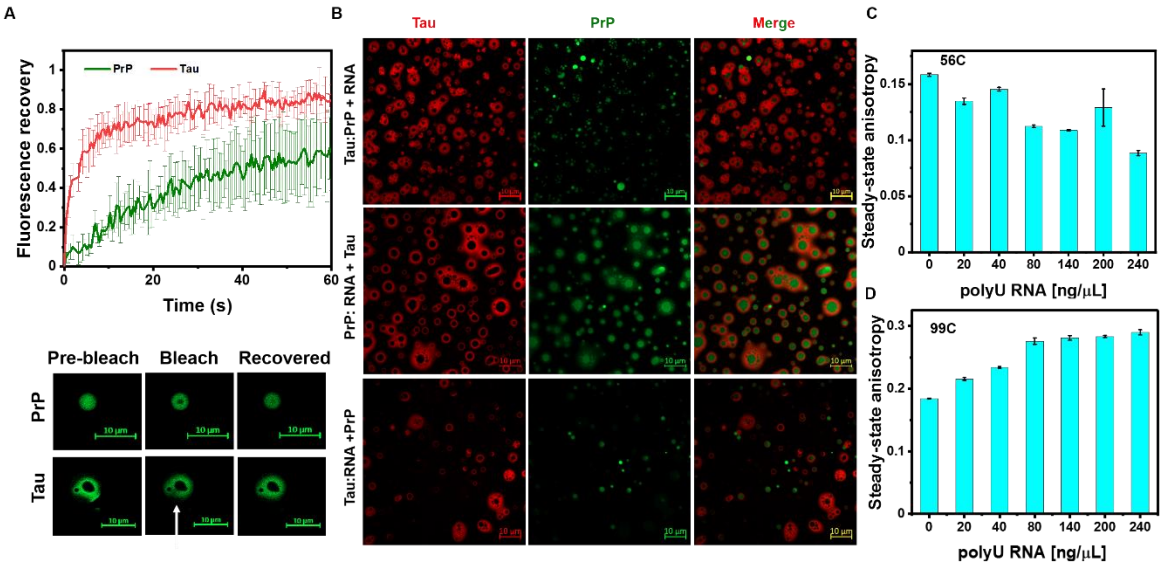


**Figure 3.11.** FRAP kinetics of tau (red) and PrP (olive) in the tau:PrP:RNA ternary system. Alexa488-labled proteins were used for both tau and PrP in independent FRAP experiments. The data represent mean ± s.d. for n = 3 independent experiments. The white arrows in the tau FRAP images show the bleaching spot. **(B)** Two-color imaging of tau:PrP:RNA droplets by changing the order of component addition. Tau was labeled with Alexa Fluor 594 (red) whereas green labeled (Alexa Fluor 488) PrP was used (scale bar 10 μm). The imaging was performed at least thrice with similar observations. **(C)** Steady-state fluorescence anisotropy for F-5-M-labeled tau at residue 56 indicates its redistribution within the condensates with increasing RNA concentrations. The data represent mean ± s.d. for n = 3 independent experiments. **(D)** Steadystate fluorescence anisotropy for F-5-M-labeled PrP at residue 99 indicates an increase in the order within multiphasic condensates with the increase in the RNA concentration. The data represent mean ± s.d. for n = 3 independent experiments.

difference.[63] Inverting the charge on tau:RNA complexes enables them to interact non-specifically with PrP:RNA complexes. The addition of RNA to the pre-formed tau:PrP heterotypic droplets, therefore, results in the switching of coacervate morphology and composition. A further increase in RNA concentration results in the complete dissolution of

assemblies. The morphological transitions of these multicomponent condensates appear to be reversible as indicated by the RNA hydrolysis using ribonuclease A (RNase A) (Figure 3.12 *A*, and *B*). We observed the reappearance of tau:PrP mixed droplets upon the addition of RNase A after an RNA-mediated complete dissolution of tau:PrP condensates. Taken together, our results indicate an RNA-induced tuning of these multicomponent condensates in a context-dependent manner (Figure 3.12 *C*). Such an interplay can potentially introduce an additional level of spatiotemporal regulation in molecular enrichment in condensates. However, the increased enrichment of biomolecules within these condensates makes them vulnerable to aberrant phase transitions into pathological aggregates. Therefore, we next set out to elucidate the effect of tau:PrP complex coacervation on the aggregation propensity of these heterotypic condensates.

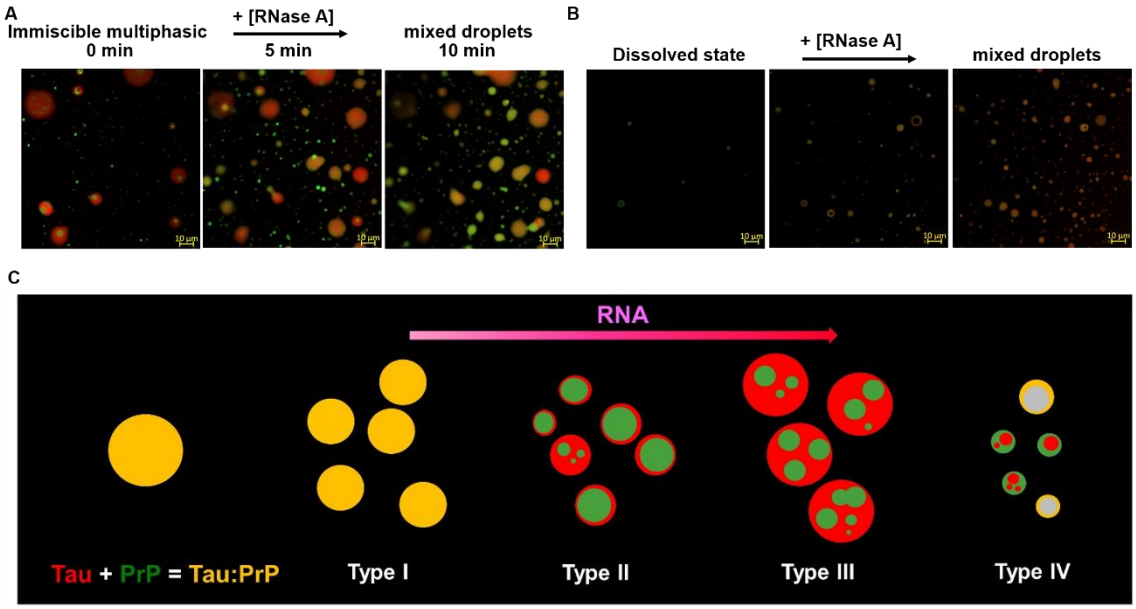


**Figure 3.12. (A)** The transition of multiphasic condensates to colocalized mixed droplets upon RNA hydrolysis using RNase A (1.5 µM) showing the reversibility in morphologies (scale bar 10 µm). **(B)** The reappearance of tau:PrP mixed droplets upon the addition of RNase A after an RNA-mediated (400 ng/µL) complete dissolution of condensates (scale bar 10 µm). Tau and PrP concentrations were 10 and 20 µM, respectively. See Methods for details. **(C)** Schematic illustration of morphological transformations during complex phase separation of tau, PrP, and RNA.

### 3.2.6 Complex coacervates of tau and PrP convert into solid-like co-aggregates

We observed that upon longer incubation, heterotypic condensates of tau and PrP, in the absence of RNA, undergo maturation into gel-like and solid-like aggregates as evident by the

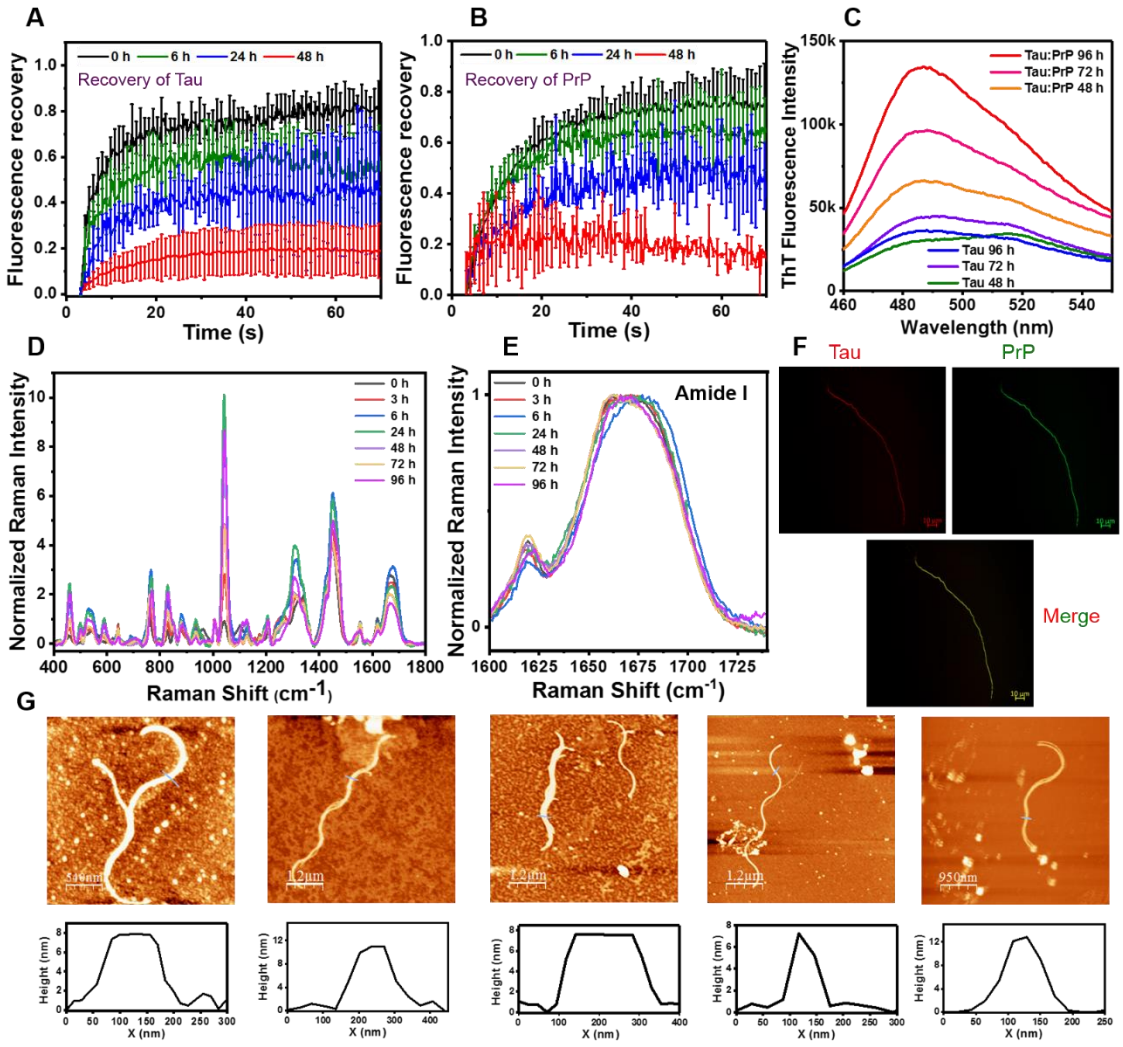


**Figure 3.13. Maturation of tau:PrP droplets into solid-like aggregates. (A)** Time-dependent FRAP kinetics of tau and **(B)** PrP inside tau:PrP condensates. Alexa488-labeled proteins (~ 1%) were used for FRAP in both cases. The data represent mean ± s.d.; n = 3. **(C)** Time-dependent ThT fluorescence spectra of the dense phase of tau-only and tau:PrP reaction mixtures. **(D)** Vibrational Raman spectra of tau:PrP dense phase over time. **(E)** Amide I vibrational Raman band of the dense phase of tau:PrP reaction mixture recorded over time. **(F)** Two-color high-resolution Airyscan confocal image of ~ 48 h old tau:PrP reaction mixture showing the heterotypic association of tau (red) and PrP (green) in fibrils (scale bar 10 µm). **(G)** AFM images with height profiles of 48 h tau:PrP reaction mixture showing the presence of amyloid fibrils along with amorphous species. Tau and PrP concentrations were 10 and 20 µM, respectively. See Methods for details.

time-dependent FRAP kinetics over a period of 48 h (Figure 3.13 *A* and *B*). Next, we asked if these aggregates were amyloid-like. We monitored the conversion kinetics of tau:PrP condensates using a well-known amyloid marker namely, thioflavin-T (ThT) that exhibits a characteristic emission band at ~ 483 nm. When compared to tau-only droplets, tau:PrP

condensates exhibited a significant increase in the ThT fluorescence after 48 h indicating the formation of ThT-positive aggregates upon the liquid-to-solid phase transition of these heterotypic condensates (Figure 3.13 *C* ). However, the emission maxima at ~ 487 nm indicated the presence of amorphous aggregates along with amyloid-like aggregates. We next structurally characterized these phase separation-mediated heterotypic aggregates using vibrational Raman spectroscopy, which allowed us to identify the secondary structural components that were present in these aggregates. For Raman experiments, we used the dense phase of the tau:PrP reaction mixture and monitored the time-dependent changes in the amide I peak (1630 - 1720 $cm^{-1}$) that primarily arise due to the C=O stretching of the backbone. A broad peak spanning from 1660 $cm^{-1}$ to 1675 $cm^{-1}$ indicated the presence of the hydrogen-bonded cross-β amyloid organization as well as amorphous aggregates supporting our ThT-binding results (Figure 3.13 *D* and *E*). Additionally, we used atomic force microscopy (AFM) to visualize these heterotypic aggregates. AFM images of 48-h-old mixtures revealed the presence of amyloid-like fibrillar morphologies together with amorphous aggregates (Figure 3.13 *F*). Further, our two-color high-resolution Airyscan imaging of incubated samples indicated the presence of colocalized tau:PrP into rod-like fibrillar structures (Figure 3.13 *G*) indicating heterotypic fibrillation as observed for other neuronal proteins.[52, 69] Taken together, our findings showed that tau and PrP together undergo phase separation into complex coacervates that gradually transition into intermixed aggregates comprising both amorphous and amyloid-like species.

## 3.3 Discussion

In this work, we showed that tau and PrP undergo spontaneous complex phase separation that is primarily driven by domain-specific electrostatic interactions. Such a complex coacervation gives rise to highly dynamic, two-component, liquid-like droplets. The slower fusion, smaller size, slower internal diffusion, and increased robustness of these droplets formed by the complex phase separation of the two proteins suggested that tau forms condensates comprising a highly networked viscoelastic fluid in the presence of PrP. Moreover, as suggested by our estimated $C_{sat}$ values, the phase separation propensity of tau increases in the presence of PrP. Tau and PrP interact electrostatically in a domain-specific manner and these heterotypic interactions are further strengthened in the case of the phosphomimetic mutant of tau since glutamic acid residues increase the net negative charge of tau. By using naturally occurring truncated variants of tau and PrP, we elucidate the importance of their N-terminal domains in

driving tau:PrP complex coacervation. Our results provide mechanistic support for such a heterotypic interaction between tau and PrP.[70, 71] Our site-specific picosecond time-resolved fluorescence anisotropy data revealed the formation of relatively ordered, short-range, electrostatic nanoclusters of tau and PrP. Such electrostatic nanoclusters have been shown to act as the primary units of heterotypic condensates.[52] These clusters are stable on the nanosecond timescale but can potentially undergo making and breaking on a slower timescale. Such a relay of making-and-breaking of interactions can make the assembly highly dynamic, mobile, and liquid-like as indicated by our FRAP studies. On a slower timescale of FCS and FRAP (milliseconds-to-seconds), this complex coacervate possessing a mobile interior can exhibit a typical liquid-like behavior. In such a liquid-like two-component assembly, a protein can also undergo oligomerization. Our work is in line with the RBP-induced phase separation and vitrification of tau.[41] Additionally, our findings also indicate the buffering capacity of RNA[72] in the context of tau:PrP interactions. Tau:PrP heterotypic condensates that remain colocalized and miscible at lower concentrations of RNA assume multiphasic morphologies upon the increase in the RNA concentration. The resulting immiscible multiphasic condensates of differing architecture comprise core-shell and nested droplets reminiscent of nucleolar condensates. These co-existing, immiscible, nested condensates in which the core of the large droplets is constituted by smaller PrP-rich droplets with tau occupying the peripheral regions, arise as a result of differing interfacial tensions between individual condensates formed by the two proteins in the presence of RNA. This morphology undergoes a transformation into an inverse core-shell and mixed hollow droplets upon the addition of higher amounts of RNA. These morphological transitions of tau:PrP condensates are reversible as evident by RNA hydrolysis by the addition of RNase A. Further, our aging experiments demonstrated that liquid-like tau:PrP condensates gradually mature into solid-like aggregates comprising both amorphous and amyloid-like species. Taken together, our study unveils an intriguing interplay of molecular determinants that promote and regulate the heterotypic phase transition, multiphasic coacervation, and maturation into intermixed ordered aggregates highlighting the molecular basis of overlapping neurodegenerative diseases involving tau and PrP (Figure 3.14). The inherent sequence attributes of tau, which are also typical of many other phase-separating proteins, regulate its ability to undergo phase separation. Tau, therefore, assembles into membraneless compartments, which sequester tubulin dimer units into well-defined foci,

where it is proposed to regulate microtubule polymerization.[73] Moreover, tau is also known to localize in other membraneless bodies, including the nucleolus[74] and stress granules,[75] where

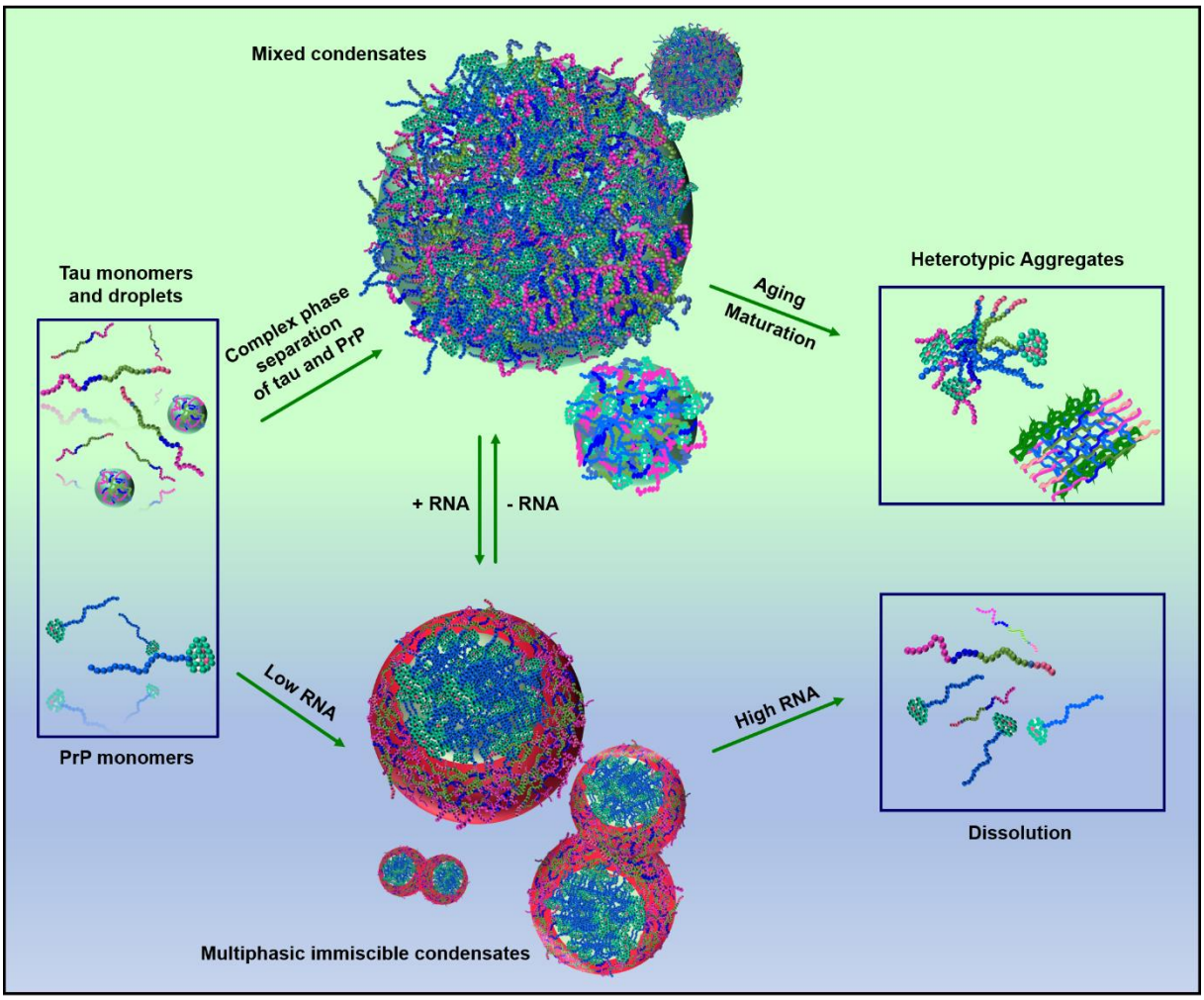


**Figure 3.14. Schematic illustration of complex phase separation of tau and PrP.** The N-terminal segments of tau and PrP interact electrostatically to potentiate tau phase separation into heterotypic condensates that mature into intermixed aggregates. Upon the addition of RNA, tau:PrP mixed droplets convert into immiscible, multiphasic condensates and are dissolved at a much higher concentration of RNA.

it may contribute to various physiological and pathological roles. Such liquid-like biomolecular condensates of tau can mature into an aggregated form that is a hallmark of neurodegenerative diseases like Alzheimer's disease and FTLD-associated tauopathies.[76, 77] The pathology of tau is not only limited to Alzheimer's disease and tauopathies but also extends to various forms of prion diseases and synucleinopathies.[42-44, 78] The colocalization of tau and PrP as cytoplasmic inclusion bodies and the accumulation of tau NFTs in the brain of prion disease patients have

been observed.[71, 79] Interestingly, like Aβ oligomers and α-Syn, various forms of tau have been thought to interact with PrP resulting in dysfunction of the synaptic plasticity.[78, 80] Although PrP is a GPI-anchored protein, a sparse level of neurotoxic intracellular PrP exists during ER stress. Additionally, in some instances, PrP may only partially cross the ER membrane and adopt one of two transmembrane topologies because of its core hydrophobic region and ineffective translocation.[46, 47, 81] In healthy brains of different species, these forms make up no more than 10% of the total PrP molecules, while in transmissible spongiform encephalopathies, they can comprise up to 30%. Two different mechanisms have been proposed for the $PrP^C$-mediated neurotoxicity caused by several protein aggregates. In one case, $PrP^C$ acts as a receptor and facilitates the internalization of specific extracellular proteins. In another, it activates metabotropic glutamate receptors (mGluRs) by functioning as a transducer to elicit the detrimental effects of certain protein deposits.[80, 82, 83] Moreover, $PrP^C$-Aβ-oligomer-mediated Fyn kinase activation results in tau hyperphosphorylation.[81] Inclusions of hyperphosphorylated tau have also been observed in various acquired and familial forms of prion diseases. Thus, tau and prion show a spectrum of overlapping pathologies following the heterogeneity of these tau:PrP co-deposits. Our results emphasize the phase separation-mediated heterotypic clustering of tau and PrP that can potentially mature into mixed inclusions found in the pathophysiology of several neurodegenerative diseases. Given that variants of tau and PrP are also known to localize in the stress granules[75, 84, 85] as well as in the nucleus,[86-89] more precisely in the nucleolar region in the case of tau, our current findings can potentially explain the role of multicomponent tau:PrP assemblies, especially considering the pertinent role of tau, in rRNA-coding, DNA transcription, stabilization, and rRNA processing.[90] These types of multicomponent, multiphasic, and anisotropic condensates may be common for many other intracellular nucleoprotein bodies.[20, 21, 25] We propose that such interactions might be present in the cellular milieu depending on the subcellular locations. In addition to the direct secretion and absorption of soluble tau isoforms from the membrane-bound receptors, tau, similar to Aβ oligomers and α-syn, is also transmitted amongst neuronal bodies via extracellular vesicles and exosomes.[90] These compartments are rich in RNA[91-93] and can therefore provide sites for the formation of tau:PrP:RNA ternary complexes.

In summary, our study relates to both the functional and pathological aspects of complex phase separation of tau and PrP with or without nucleic acids. Heterotypic phase separation of α-Syn and PrP has been shown to drive the formation of intermixed α-Syn:PrP amyloids.[52] Therefore, PrP can potentially play a central role in recruiting other neuronal IDPs

into multicomponent condensates via electrostatic coacervation. Aberrant phase transitions mediated by complex phase separation can potentially serve as a common mechanism for the development and progression of late-life neurodegenerative diseases having overlapping neuropathological features. Targeting such complex phase-separated condensates using small molecules might serve as a potent therapeutic strategy against these debilitating human diseases.

## 3.4 References

1. Kilgore, H. R.; Young, R. A., Learning the chemical grammar of biomolecular condensates. *Nature Chemical Biology* **2022,** *18* (12), 1298-1306.

2. Alberti, S.; Hyman, A. A., Biomolecular condensates at the nexus of cellular stress, protein aggregation disease and ageing. *Nature Reviews Molecular Cell Biology* **2021**, *22* (3), 196-213.

3. Lyon, A. S.; Peeples, W. B.; Rosen, M. K., A framework for understanding the functions of biomolecular condensates across scales. *Nature Reviews Molecular Cell Biology* **2021**, *22* (3), 215-235.

4. Mittag, T.; Pappu, R. V., A conceptual framework for understanding phase separation and addressing open questions and challenges. *Molecular Cell* **2022**, *82* (12), 2201-2214.

5. Fuxreiter, M.; Vendruscolo, M., Generic nature of the condensed states of proteins. *Nature Cell Biology* **2021**, *23* (6), 587-594.

6. Roden, C.; Gladfelter, A. S., RNA contributions to the form and function of biomolecular condensates. *Nature Reviews Molecular Cell Biology* **2021**, *22* (3), 183-195.

7. Choi, J. M.; Holehouse, A. S.; Pappu, R. V., Physical Principles Underlying the Complex Biology of Intracellular Phase Transitions. *Annual Review of Biophysics* **2020**, *49* (1), 107-133.

8. Dignon, G. L.; Best, R. B.; Mittal, J., Biomolecular Phase Separation: From Molecular Driving Forces to Macroscopic Properties. *Annual Review of Physical Chemistry* **2020**, *71* (1), 53-75.

9. Mohanty, P.; Kapoor, U.; Sundaravadivelu Devarajan, D.; Phan, T. M.; Rizuan, A.; Mittal, J., Principles Governing the Phase Separation of Multidomain Proteins. *Biochemistry* **2022**.

10. Lee, D. S. W.; Strom, A. R.; Brangwynne, C. P., The mechanobiology of nuclear phase separation. *APL Bioengineering* **2022**, *6* (2), 021503.

11. Shapiro, D. M.; Ney, M.; Eghtesadi, S. A.; Chilkoti, A., Protein Phase Separation Arising from Intrinsic Disorder: First-Principles to Bespoke Applications. *The Journal of Physical Chemistry B* **2021**, *125* (25), 6740-6759.

12. Banani, S. F.; Lee, H. O.; Hyman, A. A.; Rosen, M. K., Biomolecular condensates: organizers of cellular biochemistry. *Nature Reviews Molecular Cell Biology* **2017**, *18* (5), 285-298.

13. Brangwynne, C. P.; Tompa, P.; Pappu, R. V., Polymer physics of intracellular phase transitions. *Nature Physics* **2015**, *11* (11), 899-904.

14. Vernon, R. M.; Chong, P. A.; Tsang, B.; Kim, T. H.; Bah, A.; Farber, P.; Lin, H.; Forman-Kay, J. D., Pi-Pi contacts are an overlooked protein feature relevant to phase separation. *eLife* **2018**, *7*, e31486.

15. Ruff, K. M.; Choi, Y. H.; Cox, D.; Ormsby, A. R.; Myung, Y.; Ascher, D. B.; Radford, S. E.; Pappu, R. V.; Hatters, D. M., Sequence grammar underlying the unfolding and phase separation of globular proteins. *Molecular Cell* **2022**, *82* (17), 3193-3208.

16. Ditlev, J. A.; Case, L. B.; Rosen, M. K., Who's In and Who's Out—Compositional Control of Biomolecular Condensates. *Journal of Molecular Biology* **2018**, *430* (23), 4666-4684.

17. Sabari, B. R.; Dall'Agnese, A.; Young, R. A., Biomolecular Condensates in the Nucleus. *Trends in Biochemical Sciences* **2020**, *45* (11), 961-977.

18. Boeynaems, S.; Deniz, S.; Fawzi, N. L.; Mittag, T.; Polymenidou, M.; Rousseau, F.; Schymkowitz, J.; Shorter, J.; Wolozin, B.; Van Den Bosch, L.; Tompa, P.; Fuxreiter, M., Protein Phase Separation: A New Phase in Cell Biology. *Trends in Cell Biology* **2018**, *28* (6), 420-435.

19. Uversky, V. N., Intrinsically disordered proteins in overcrowded milieu: Membrane-less organelles, phase separation, and intrinsic disorder. *Current Opinion in Structural Biology* **2017**, *44*, 18-30.

20. Fare, C. M.; Villani, A.; Drake, L. E.; Shorter, J., Higher-order organization of biomolecular condensates. *Open Biology* **2021**, *11* (6), 210137.

21. Riback, J. A.; Zhu, L.; Ferrolino, M. C.; Tolbert, M.; Mitrea, D. M.; Sanders, D. W.; Wei, M.T.; Kriwacki, R. W.; Brangwynne, C. P., Composition-dependent thermodynamics of intracellular phase separation. *Nature* **2020**, *581* (7807), 209-214.

22. Mountain, G. A.; Keating, C. D., Formation of Multiphase Complex Coacervates and Partitioning of Biomolecules within them. *Biomacromolecules* **2020**, *21* (2), 630-640.

23. Abbas, M.; Lipiński, W. P.; Wang, J.; Spruijt, E., Peptide-based coacervates as biomimetic protocells. *Chemical Society Reviews* **2021**, *50* (6), 3690-3705.

24. Kaur, T.; Raju, M.; Alshareedah, I.; Davis, R. B.; Potoyan, D. A.; Banerjee, P. R., Sequence-encoded and composition-dependent protein-RNA interactions control multiphasic condensate morphologies. *Nature Communications* **2021**, *12* (1), 872.

25. Lafontaine, D. L. J.; Riback, J. A.; Bascetin, R.; Brangwynne, C. P., The nucleolus as a multiphase liquid condensate. *Nature Reviews Molecular Cell Biology* **2021**, *22* (3), 165-182.

26. Wang, J.; Choi, J. M.; Holehouse, A. S.; Lee, H. O.; Zhang, X.; Jahnel, M.; Maharana, S.; Lemaitre, R.; Pozniakovsky, A.; Drechsel, D.; Poser, I.; Pappu, R. V.; Alberti, S.; Hyman, A. A., A Molecular Grammar Governing the Driving Forces for Phase Separation of Prion-like RNA Binding Proteins. *Cell* **2018**, *174* (3), 688-699.e16.

27. Krainer, G.; Welsh, T. J.; Joseph, J. A.; Espinosa, J. R.; Wittmann, S.; de Csilléry, E.; Sridhar, A.; Toprakcioglu, Z.; Gudiškytė, G.; Czekalska, M. A.; Arter, W. E.; Guillén-Boixet, J.; Franzmann, T.M.; Qamar, S.; George-Hyslop, P. S.; Hyman, A. A.; Collepardo-Guevara, R.; Alberti, S.; Knowles, T. P. J., Reentrant liquid condensate phase of proteins is stabilized by hydrophobic and non-ionic interactions. *Nature Communications* **2021,** *12*, 1085.

28. Ray, S.; Singh, N.; Kumar, R.; Patel, K.; Pandey, S.; Datta, D.; Mahato, J.; Panigrahi, R.; Navalkar, A.; Mehra, S.; Gadhe, L.; Chatterjee, D.; Sawner, A. S.; Maiti, S.; Bhatia, S.; Gerez, J. A.; Chowdhury, A.; Kumar, A.; Padinhateeri, R.; Riek, R.; Krishnamoorthy, G.; Maji, S. K., α-Synuclein aggregation nucleates through liquid-liquid phase separation. *Nature Chemistry* **2020**, *12* (8), 705-716.

29. Wang, B.; Zhang, L.; Dai, T.; Qin, Z.; Lu, H.; Zhang, L.; Zhou, F., Liquid-liquid phase separation in human health and diseases. *Signal Transduction and Targeted Therapy* **2021**, *6* (1), 290.

30. Portz, B.; Lee, B. L.; Shorter, J., FUS and TDP-43 Phases in Health and Disease. *Trends in Biochemical Sciences* **2021**, *46* (7), 550-563.

31. Shin, Y.; Brangwynne, C. P., Liquid phase condensation in cell physiology and disease. *Science* **2017**, *357* (6357), eaaf4382.

32. Dhakal, S.; Wyant, C. E.; George, H. E.; Morgan, S. E.; Rangachari, V., Prion-like C-Terminal Domain of TDP-43 and α-Synuclein Interact Synergistically to Generate Neurotoxic Hybrid Fibrils. *Journal of Molecular Biology* **2021**, *433* (10), 166953.

33. Rai, S. K.; Savastano, A.; Singh, P.; Mukhopadhyay, S.; Zweckstetter, M., Liquid-liquid phase separation of tau: From molecular biophysics to physiology and disease. *Protein Science* **2021**, *30* (7), 1294-1314.

34. Limorenko, G.; Lashuel, H. A., Revisiting the grammar of Tau aggregation and pathology formation: how new insights from brain pathology are shaping how we study and target Tauopathies. *Chemical Society Reviews* **2022**, *51* (2), 513-565.

35. Guo, T.; Noble, W.; Hanger, D. P., Roles of tau protein in health and disease. *Acta Neuropathologica* **2017**, *133* (5), 665-704.

36. Mandelkow, E. M.; Mandelkow, E., Biochemistry and cell biology of tau protein in neurofibrillary degeneration. *Cold Spring Harbor Perspectives in Medicine* **2012**, *2* (7), a006247.

37. Wen, J.; Hong, L.; Krainer, G.; Yao, Q. Q.; Knowles, T. P. J.; Wu, S.; Perrett, S., Conformational Expansion of Tau in Condensates Promotes Irreversible Aggregation. *Journal of the American Chemical Society* **2021**, *143* (33), 13056-13064.

38. Kanaan, N. M.; Hamel, C.; Grabinski, T.; Combs, B., Liquid-liquid phase separation induces pathogenic tau conformations in vitro. *Nature Communications* **2020**, *11* (1), 2809.

39. Ambadipudi, S.; Biernat, J.; Riedel, D.; Mandelkow, E.; Zweckstetter, M., Liquid-liquid phase separation of the microtubule-binding repeats of the Alzheimer-related protein Tau. *Nature Communications* **2017**, *8* (1), 275.

40. Majumdar, A.; Dogra, P.; Maity, S.; Mukhopadhyay, S., Liquid–Liquid Phase Separation Is Driven by Large-Scale Conformational Unwinding and Fluctuations of Intrinsically Disordered Protein Molecules. *The Journal of Physical Chemistry Letters* **2019**, *10* (14), 3929-3936.

41. Ash, P. E. A.; Lei, S.; Shattuck, J.; Boudeau, S.; Carlomagno, Y.; Medalla, M.; Mashimo, B. L.; Socorro, G.; Al-Mohanna, L. F. A.; Jiang, L.; Öztürk, M. M.; Knobel, M.; Ivanov, P.; Petrucelli, L.; Wegmann, S.; Kanaan, N. M.; Wolozin, B., TIA1 potentiates tau phase separation and promotes generation of toxic oligomeric tau. *Proceedings of the National Academy of Sciences U.S.A* **2021**, *118* (9), e2014188118.

42. Gracia, P.; Polanco, D.; Tarancón-Díez, J.; Serra, I.; Bracci, M.; Oroz, J.; Laurents, D. V.; García, I.; Cremades, N., Molecular mechanism for the synchronized electrostatic coacervation and co-aggregation of alpha-synuclein and tau. *Nature Communications* **2022**, *13* (1), 4586.

43. Kovacs, G. G.; Rahimi, J.; Ströbel, T.; Lutz, M. I.; Regelsberger, G.; Streichenberger, N.; Perret-Liaudet, A.; Höftberger, R.; Liberski, P. P.; Budka, H.; Sikorska, B., Tau pathology in Creutzfeldt-Jakob disease revisited. *Brain Pathology* **2017**, *27* (3), 332-344.

44. Hallinan, G. I.; Hoq, M. R.; Ghosh, M.; Vago, F. S.; Fernandez, A.; Garringer, H. J.; Vidal, R.; Jiang, W.; Ghetti, B., Structure of Tau filaments in Prion protein amyloidoses. *Acta Neuropathologica* **2021**, *142* (2), 227-241.

45. Zhao, J.; Wu, H.; Tang, X. Q., Tau internalization: A complex step in tau propagation. *Ageing Research Reviews* **2021**, *67*, 101272.

46. Aguzzi, A.; Calella, A. M., Prions: Protein Aggregation and Infectious Diseases. *Physiological Reviews* **2009**, *89* (4), 1105-1152.

47. Condello, C.; DeGrado, W. F.; Prusiner, S. B., Prion biology: implications for Alzheimer's disease therapeutics. *The Lancet Neurology* **2020**, *19* (10), 802-803.

48. Viles, J. H.; Cohen, F. E.; Prusiner, S. B.; Goodin, D. B.; Wright, P. E.; Dyson, H. J., Copper binding to the prion protein: Structural implications of four identical cooperative binding sites. *Proceedings of the National Academy of Sciences U.S.A* **1999**, *96* (5), 2042-2047.

49. Hardenberg, M.; Horvath, A.; Ambrus, V.; Fuxreiter, M.; Vendruscolo, M., Widespread occurrence of the droplet state of proteins in the human proteome. *Proceedings of the National Academy of Sciences U.S.A* **2020**, *117* (52), 33254-33262.

50. Bolognesi, B.; Lorenzo Gotor, N.; Dhar, R.; Cirillo, D.; Baldrighi, M.; Tartaglia, G. G.; Lehner, B., A Concentration-Dependent Liquid Phase Separation Can Cause Toxicity upon Increased Protein Expression. *Cell Reports* **2016**, *16* (1), 222-231.

51. Pak, C. W.; Kosno, M.; Holehouse, A. S.; Padrick, S. B.; Mittal, A.; Ali, R.; Yunus, A. A.; Liu, D. R.; Pappu, R. V.; Rosen, M. K., Sequence Determinants of Intracellular Phase Separation by Complex Coacervation of a Disordered Protein. *Molecular Cell* **2016**, *63* (1), 72-85.

52. Agarwal, A.; Arora, L.; Rai, S. K.; Avni, A.; Mukhopadhyay, S., Spatiotemporal modulations in heterotypic condensates of prion and α-synuclein control phase transitions and amyloid conversion. *Nature Communications* **2022**, *13* (1), 1154.

53. Holehouse, A.S.; Das, R. K.; Ahad, J. N.; Richardson, M. O.; Pappu, R. V., CIDER: Resources to Analyze Sequence-Ensemble Relationships of Intrinsically Disordered Proteins. *Biophysical Journal* **2017**, *112* (1), 16-21.

54. Gruijs da Silva, L. A.; Simonetti, F.; Hutten, S.; Riemenschneider, H.; Sternburg, E. L.; Pietrek, L. M.; Gebel, J.; Dötsch, V.; Edbauer, D.; Hummer, G.; Stelzl, L. S.; Dormann,

D., Disease-linked TDP-43 hyperphosphorylation suppresses TDP-43 condensation and aggregation. *The EMBO Journal* **2022**, *41* (8), e108443.

55. Li, J.; Zhang, M.; Ma, W.; Yang, B.; Lu, H.; Zhou, F.; Zhang, L., Post-translational modifications in liquid-liquid phase separation: a comprehensive review. *Molecular Biomedicine* **2022**, *3* (1):13.

56. Amadoro, G.; Corsetti, V.; Stringaro, A.; Colone, M.; D'Aguanno, S.; Meli, G.; Ciotti, M.; Sancesario, G.; Cattaneo, A.; Bussani, R.; Mercanti, D.; Calissano, P., A NH2 tau fragment targets neuronal mitochondria at AD synapses: possible implications for neurodegeneration. *Journal of Alzheimer's Disease.* **2010**, *21* (2), 445-70.

57. Gu, J.; Xu, W.; Jin, N.; Li, L.; Zhou, Y.; Chu, D.; Gong, C. X.; Iqbal, K.; Liu, F., Truncation of Tau selectively facilitates its pathological activities. *Journal of Biological Chemistry* **2020,** *295* (40), 13812-13828.

58. Agarwal, A.; Rai, S. K.; Avni, A.; Mukhopadhyay, S., An intrinsically disordered pathological prion variant Y145Stop converts into self-seeding amyloids via liquid-liquid phase separation. *Proceedings of the National Academy of Sciences U.S.A* **2021**, *118* (45), e2100968118.

59. Sanders, D. W.; Kedersha, N.; Lee, D. S. W.; Strom, A. R.; Drake, V.; Riback, J. A.; Bracha, D.; Eeftens, J. M.; Iwanicki, A.; Wang, A.; Wei, M. T.; Whitney, G.; Lyons, S. M.; Anderson, P.; Jacobs, W. M.; Ivanov, P.; Brangwynne, C. P., Competing Protein-RNA Interaction Networks Control Multiphase Intracellular Organization. *Cell* **2020**, *181* (2), 306-324.e28.

60. Rhine, K.; Vidaurre, V.; Myong, S., RNA Droplets. *Annual Review of Biophysics* **2020**, *49* (1), 247-265.

61. Banerjee, P. R.; Milin, A. N.; Moosa, M. M.; Onuchic, P. L.; Deniz, A. A., Reentrant Phase Transition Drives Dynamic Substructure Formation in Ribonucleoprotein Droplets. *Angewandte Chemie International Edition in English* **2017**, *56* (38), 11354-11359.

62. Alshareedah, I.; Moosa, M. M.; Raju, M.; Potoyan, D. A.; Banerjee, P. R., Phase transition of RNA−protein complexes into ordered hollow condensates. *Proceedings of the National Academy of Sciences U.S.A* **2020**, *117* (27), 15650-15658.

63. Alshareedah, I.; Kaur, T.; Ngo, J.; Seppala, H.; Kounatse, L. A. D.; Wang, W.; Moosa, M. M.; Banerjee, P. R., Interplay between Short-Range Attraction and Long-Range Repulsion Controls Reentrant Liquid Condensation of Ribonucleoprotein–RNA Complexes. *Journal of the American Chemical Society* **2019**, *141* (37), 14593-14602.

64. Ukmar-Godec, T.; Hutten, S.; Grieshop, M. P.; Rezaei-Ghaleh, N.; Cima-Omori, M. S.; Biernat, J.; Mandelkow, E.; Söding, J.; Dormann, D.; Zweckstetter, M., Lysine/RNA-interactions drive and regulate biomolecular condensation. *Nature Communications* **2019**, *10* (1), 2909.

65. Feric, M.; Vaidya, N.; Harmon, T. S.; Mitrea, D. M.; Zhu, L.; Richardson, T. M.; Kriwacki, R. W.; Pappu, R. V.; Brangwynne, C. P., Coexisting Liquid Phases Underlie Nucleolar Subcompartments. *Cell* **2016**, *165* (7), 1686-1697.

66. Sanchez-Burgos, I.; Espinosa, J. R.; Joseph, J. A.; Collepardo-Guevara, R., Valency and Binding Affinity Variations Can Regulate the Multilayered Organization of Protein Condensates with Many Components. *Biomolecules* **2021**, *11* (2), 278.

67. Lu, T.; Spruijt, E., Multiphase Complex Coacervate Droplets. *Journal of the American Chemical Society* **2020**, *142* (6), 2905-2914.

68. Bhopatkar, A. A.; Dhakal, S.; Abernathy, H. G.; Morgan, S. E.; Rangachari, V., Charge and redox states modulate granulin-TDP-43 coacervation toward phase separation or aggregation. *Biophysical Journal* **2022**, *121* (11), 2107-2126.

69. Dhakal S.; Robang A. S.; Bhatt N.; Puangmalai N.; Fung L.; Kayed R.; Paravastu A. K.; Rangachari V., Distinct neurotoxic TDP-43 fibril polymorphs are generated by heterotypic interactions with α-Synuclein. *Journal of Biological Chemistry*, 2022, 298 (11), 102498.

70. Han, J.; Zhang, J.; Yao, H.; Wang, X.; Li, F.; Chen, L.; Gao, C.; Gao, J.; Nie, K.; Zhou, W.; Dong, X., Study on interaction between microtubule associated protein tau and prion protein. *Science in China Series C: Life Sciences* **2006**, *49* (5), 473-479.

71. Wang, X. F.; Dong, C. F.; Zhang, J.; Wan, Y. Z.; Li, F.; Huang, Y. X.; Han, L.; Shan, B.; Gao, C.; Han, J.; Dong, X. P., Human tau protein forms complex with PrP and some GSS- and fCJD-related PrP mutants possess stronger binding activities with tau in vitro. *Molecular and Cellular Biochemistry* **2008**, *310* (1), 49-55.

72. Maharana, S.; Wang, J.; Papadopoulos, D. K.; Richter, D.; Pozniakovsky, A.; Poser, I.; Bickle, M.; Rizk, S.; Guillén-Boixet, J.; Franzmann, T. M.; Jahnel, M.; Marrone, L.; Chang, Y. T.; Sterneckert, J.; Tomancak, P.; Hyman, A. A.; Alberti, S., RNA buffers the phase separation behavior of prion-like RNA binding proteins. *Science* **2018**, *360* (6391), 918-921.

73. Hernández-Vega, A.; Braun, M.; Scharrel, L.; Jahnel, M.; Wegmann, S.; Hyman, B. T.; Alberti, S.; Diez, S.; Hyman, A. A., Local Nucleation of Microtubule Bundles through Tubulin Concentration into a Condensed Tau Phase. *Cell Reports* **2017**, *20* (10), 2304-2312.

74. Thurston, V. C.; Zinkowski, R. P.; Binder, L. I., Tau as a nucleolar protein in human nonneural cells in vitro and in vivo. *Chromosoma* **1996**, *105* (1), 20-30.

75. Maina, M. B.; Bailey, L. J.; Wagih, S.; Biasetti, L.; Pollack, S. J.; Quinn, J. P.; Thorpe, J. R.; Doherty, A. J.; Serpell, L. C., The involvement of tau in nucleolar transcription and the stress response. *Acta Neuropathologica Communications* **2018**, *6* (1), 70.

76. Boyko, S.; Surewicz, K.; Surewicz, W. K., Regulatory mechanisms of tau protein fibrillation under the conditions of liquid-liquid phase separation. *Proceedings of the National Academy of Sciences U.S.A* **2020**, *117* (50), 31882-31890.

77. Wegmann, S.; Eftekharzadeh, B.; Tepper, K.; Zoltowska, K. M.; Bennett, R. E.; Dujardin, S.; Laskowski, P. R.; MacKenzie, D.; Kamath, T.; Commins, C.; Vanderburg, C.; Roe, A. D.; Fan, Z.; Molliex, A. M.; Hernandez-Vega, A.; Muller, D.; Hyman, A. A.; Mandelkow, E.; Taylor, J. P.; Hyman, B. T., Tau protein liquid-liquid phase separation can initiate tau aggregation. *The EMBO Journal* **2018**, *37* (7), e98049.

78. Nieznanski, K., Interactions of Prion Protein With Intracellular Proteins: So Many Partners and no Consequences? *Cellular and Molecular Neurobiology* **2010**, *30* (5), 653-666.

79. Ishizawa, K.; Komori, T.; Shimazu, T.; Yamamoto, T.; Kitamoto, T.; Shimazu, K.; Hirose, T., Hyperphosphorylated tau deposition parallels prion protein burden in a case of Gerstmann-Sträussler-Scheinker syndrome P102L mutation complicated with dementia. *Acta Neuropathologica* **2002**, *104* (4), 342-350.

80. Castle, A. R.; Gill, A. C., Physiological Functions of the Cellular Prion Protein. *Frontiers in Molecular Biosciences* **2017**, *4*, (19).

81. Stewart, R. S.; Drisaldi, B.; Harris, D. A., A transmembrane form of the prion protein contains an uncleaved signal peptide and is retained in the endoplasmic reticulum. *Molecular Biology of the Cell* **2001**, *12* (4), 881-889.

82. Larson, M.; Sherman, M. A.; Amar, F.; Nuvolone, M.; Schneider, J. A.; Bennett, D. A.; Aguzzi, A.; Lesné, S. E., The complex PrP(c)-Fyn couples human oligomeric Aβ with pathological tau changes in Alzheimer's disease. *The Journal of Neuroscience* **2012**, *32* (47), 16857-71a.

83. Corbett, G. T.; Wang, Z.; Hong, W.; Colom-Cadena, M.; Rose, J.; Liao, M.; Asfaw, A.; Hall, T. C.; Ding, L.; DeSousa, A.; Frosch, M. P.; Collinge, J.; Harris, D. A.; Perkinton, M. S.; Spires-Jones, T. L.; Young-Pearse, T. L.; Billinton, A.; Walsh, D. M., PrP is a central player in toxicity mediated by soluble aggregates of neurodegeneration-causing proteins. *Acta neuropathologica* **2020**, *139* (3), 503-526.

84. Goggin, K.; Beaudoin, S.; Grenier, C.; Brown, A. A.; Roucou, X., Prion protein aggresomes are poly(A)+ ribonucleoprotein complexes that induce a PKR-mediated deficient cell stress response. *Biochimica et biophysica acta* **2008**, *1783* (3), 479-491.

85. Vanderweyde, T.; Youmans, K.; Liu-Yesucevitz, L.; Wolozin, B., Role of stress granules and RNA-binding proteins in neurodegeneration: a mini-review. *Gerontology* **2013**, *59* (6), 524-533.

86. Bou Samra, E.; Buhagiar-Labarchède, G.; Machon, C.; Guitton, J.; Onclercq-Delic, R.; Green, M. R.; Alibert, O.; Gazin, C.; Veaute, X.; Amor-Guéret, M., A role for Tau protein in maintaining ribosomal DNA stability and cytidine deaminase-deficient cell survival. *Nature communications* **2017**, *8* (1), 693.

87. Bravard, A.; Auvré, F.; Fantini, D.; Bernardino-Sgherri, J.; Sissoëff, L.; Daynac, M.; Xu, Z.; Etienne, O.; Dehen, C.; Comoy, E.; Boussin, F. D.; Tell, G.; Deslys, J. P.; Radicella, J. P., The prion protein is critical for DNA repair and cell survival after genotoxic stress. *Nucleic Acids Research* **2014**, *43* (2), 904-916.

88. Silva, J. L. & Cordeiro, Y. The "Jekyll and Hyde" actions of nucleic acids on the prion-like aggregation of proteins. *Journal of Biological Chemistry* **2016**, *291*, 15482–15490.

89. Montalbano, M.; Jaworski, E.; Garcia, S.; Ellsworth, A.; McAllen, S.; Routh, A.; Kayed, R., Tau Modulates mRNA Transcription, Alternative Polyadenylation Profiles of hnRNPs, Chromatin Remodeling and Spliceosome Complexes. *Frontiers in Molecular Neuroscience* **2021**, *14*, 742790.

90. Brunello, C. A.; Merezhko, M.; Uronen, R. L.; Huttunen, H. J., Mechanisms of secretion and spreading of pathological tau protein. *Cellular and Molecular Life Sciences* **2020**, *77* (9), 1721-1744.

91. Li, M.; Zeringer, E.; Barta, T.; Schageman, J.; Cheng, A.; Vlassov, A. V., Analysis of the RNA content of the exosomes derived from blood serum and urine and its potential as biomarkers. *Philosophical Transactions of the Royal Society London B: Biological Sciences* **2014**, *369* (1652), 20130502.

92. Hartmann, A.; Muth, C.; Dabrowski, O.; Krasemann, S.; Glatzel, M., Exosomes and the prion protein: more than one truth. *Frontiers in Neurosciences* **2017**, *11*, 194.

93. Zomer, A.; Vendrig, T.; Hopmans, E. S.; van Eijndhoven, M.; Middeldorp, J. M.; Pegtel, D. M., Exosomes. *Communicative & Integrative Biology* **2010**, *3* (5), 447-450.

# CHAPTER 4

## Chaperone-Mediated Phase Separation Regulates Liquid-to-Solid Phase Transitions of Tau into Amyloid Fibrils

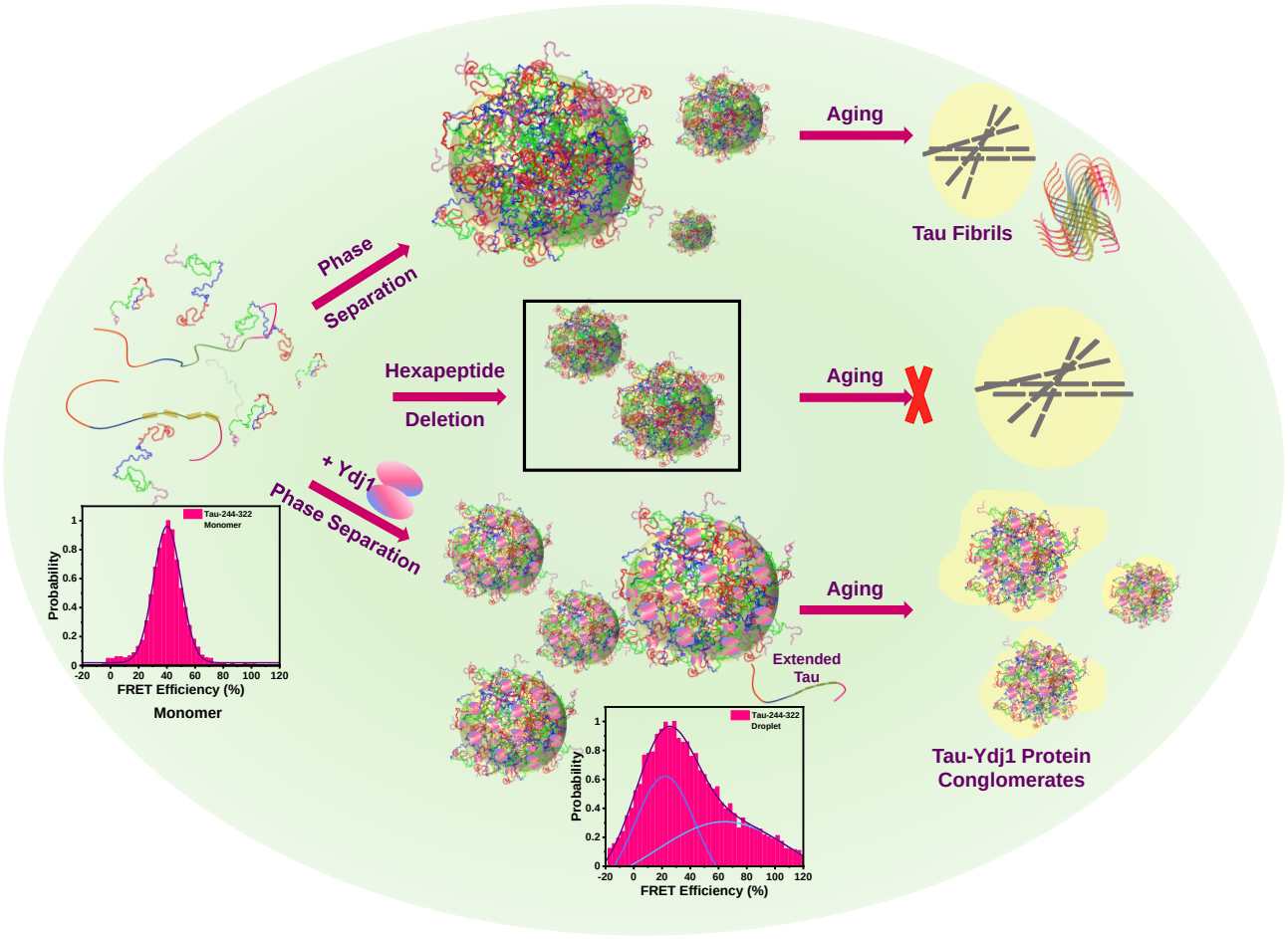


Rai, S. K., Khanna, R., Sarbahi, A., Joshi, A., Mukhopadhyay, S. (Manuscript in preparation)

## 4.1 Introduction

Biomolecular condensation is an efficient means to spatiotemporally regulate biomolecules and orchestrate coherency in a plethora of biological activities, ranging from enzymatic regulation, cellular transport, and signaling to genome processing and nuclear organization. Research over half a decade has proven that these non-canonical assemblies form via homotypic and heterotypic interactions between constituting polymeric biomolecules, the principle of which is regulated by the processes of phase separation.[1-15] Macromolecular phase-separation and, hence, the formation of these cellular bodies is governed by a multitude of physiochemical elements, exemplified by intrinsically disordered regions (IDRs) in addition to globular and oligomerization domains primarily because of their ability to introduce multivalency into a system due to the formation of non-covalent contacts via electrostatic, hydrophobic, cation-pi and pi-pi interactions.[4-9, 12, 14-18] Furthermore, this percolation-coupled density transition[4, 5] resulting in a condensed viscoelastic network is highly tunable under various external and internal stimuli such as small molecules, nucleic acids, and post-translational modifications (PTMs), which combined with the underlying nature of the interactions amongst the components of these assemblies, regulates their size and lifetime.[19-26] Any perturbations in these tightly regulated bodies in intracellular space translate into a change in their material properties, consequently disrupting their function, as implicated in a plethora of neurodegenerative diseases, including amyotrophic lateral sclerosis, frontotemporal lobar dementia, Alzheimer's, and Parkinson's disease.[26-31] While our perception of these architectures has substantially improved, the underlying cellular networks that directly influence their regulation remain elusive. In this regard, recent reports have suggested that the formation and lifetime of biological condensates can also be governed by protein quality control (PQC) units.[2] However, the exact molecular mechanisms of this process remain enigmatic. Here, we present a unique case of the abrogation of tau phase-separation mediated aggregation by a self-sufficient unit of a multi-chaperone complex.

Microtubule-associated tau is a natively unstructured, 441 amino acid-long protein that plays an essential role in maintaining the cytoskeletal network of cells and mediating transport in neurons.[32-35] As a result of its inherent sequence attributes, tau undergoes biomolecular condensation.[36-41] Functional tau-rich condensates can, however, undergo stress-mediated aberrant phase transitions associated with a change in their material state to form pathological amyloid-like aggregates, which are the characteristic hallmarks of neurodegeneration involved

in an array of tauopathies.[42] A growing body of research has revealed the broad role of molecular chaperones that form the cellular PQC in modulating several pathological tau aggregates.[43-49] Molecular chaperones, including heat shock proteins (Hsps), encompass a group of highly-conserved, related families of proteins that are crucial for maintaining cellular stability via protein homeostasis, with Hsp40 being an essential member of such multi-chaperone complex-controlled pathways.[50-53] The ATP-independent Hsp40 family of proteins is typified by a characteristic Hsp70-binding J-domain and acts as the first line of defense against misfolded proteinaceous species in cells. These J-domain proteins (JDPs) are associated with a highly-conserved domain architecture across species that includes an N-terminal J-domain, a glycine-phenylalanine (G/F) linker, a zinc-finger-like region (ZFLR), and peptide binding C-terminal domains (CTD I/II), followed by a dimerization-domain (DD).[50, 51] Despite the emphasis placed on the importance of the Hsp40-mediated chaperoning of tau and its significance, both in terms of tau pathology and function in existing reports, the molecular mechanisms underpinning this intricate network have not been well-elucidated. In our work, we have used an assortment of ensemble and single-molecule approaches in conjunction with vibrational Raman spectroscopy and transmission electron microscopy (TEM) imaging to characterize the importance of the tau sequence space in governing its interaction with Ydj1, a yeast homolog of the human class-I Hsp40, DnaJA1. Additionally, we provide a description of the dynamic events associated with the conformational shape-shifting of tau in its presence. Using a synergistic approach combining ensemble and single-molecule techniques in addition to super-resolution microscopy, we have elucidated the diverse structural configurations of tau present within phase-separated condensates that are otherwise predisposed to aggregation.

## 4.2 Results

### 4.2.1 Ydj1 drives tau toward condensation

Tau is a polyampholytic protein comprising clustered oppositely charged residues in its distinct domains, enabling it to undergo phase separation mediated by interdomain electrostatic interactions. We started by verifying tau phase separation under our conditions, at a physiological pH, and under low salt, as demonstrated previously by us and others (Figure 4.1 A).[36-41, 54] In order to establish the structural homology between Ydj1 and Human Hsp40s, we compared the sequence and structure of Ydj1 with those of its conventionally used analog DnaJA1. On analyzing the structure superimposition and sequence alignment, we observed a

striking similarity in terms of both their sequence compositions and domain architectures (Figure 4.1 B). Their similarity is also supported by previous studies that have reported on the mechanistic basis of their action and robustness through the species.[55-57] Our sequence analysis

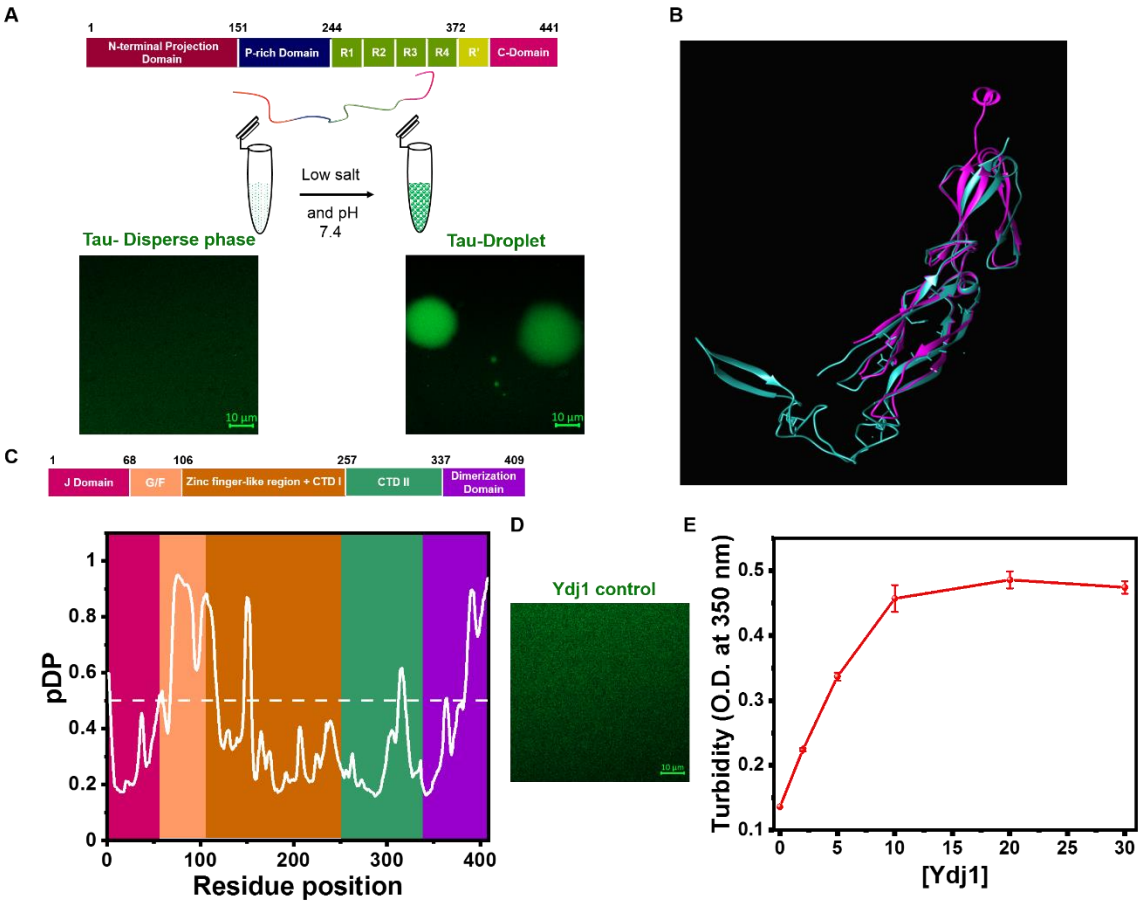


**Figure 4.1. Tau phase separation is modulated by Ydj1 (A)** Sequence architecture of the full-length human tau protein. We used a null cysteine variant (C291S, C322S) for our studies. Tau condensates were reconstituted using purified protein in the absence of salt at physiological pH (20 mM HEPES, 2 mM DTT, pH 7.4). **(B)** Domain architecture of Ydj1, a yeast analog of human DnaJA1, which is a member of the Hsp40 family of molecular chaperones. The yeast and human variants are similar and share high sequence and structure homology, as seen by the structural alignment of Ydj1 with another J-domain containing Hsp40 (Cyan: DnajB1; PDB: 2QLD; Magenta: Ydj1; PDB: 1NLT; RMSD between atom pairs = 1.030 Å). **(C)** Domain architecture of Ydj1, a yeast analog of human DnaJA1, which is a member of the Hsp40 family of molecular chaperones, and its phase separation propensity, predicted using FuzDrop. **(D)** Ydj1 (10 µM, Alexa Fluor 488, green) does not phase separate alone under our conditions (Scale bar, 10 µm). **(E)** Turbidity (O.D. at 350 nm) measurement of tau-Ydj1 reaction mixture (tau, 10 µM) as a function of Ydj1 concentration. The data represent mean ± SD; n = 3.

using FuzDrop[58] and turbidity measurements for Ydj1 suggest that it does not undergo phase separation under our condition. We visually confirmed this by performing confocal microscopy imaging for Ydj1 (10 µM) in the presence of ~ 1% of its sparsely labeled Alexa Fluor488-C5-maleimide equivalent (Figure 4.1 C, D). After establishing the absence of Ydj1 condensation, we set out to elucidate its effect on the phase behavior of tau, starting with turbidity measurements in the presence of Ydj1. The turbidity of the phase-separated tau-Ydj1 reaction mixture immediately rose, showing a strong concentration dependence on Ydj1, and plateaued after 30 µM of Ydj1 (Figure 4.1 E). Next, we measured the saturation concentration ($C_{sat}$) of tau in the absence and presence of Ydj1 and found it to be lower in the latter case (Figure 4.2 A).

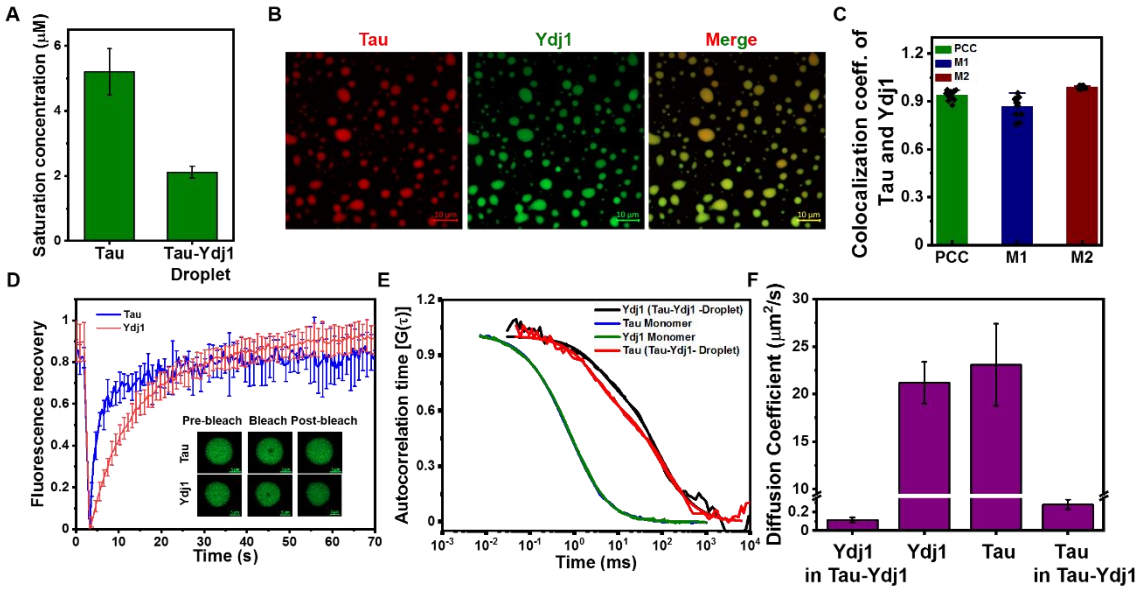


**Figure 4.2. Tau phase separation is modulated by Ydj1 (A)** The saturation concentration ($C_{sat}$) of tau for tau-only and tau-Ydj1 condensates was estimated by high-speed centrifugation. **(B)** A high-resolution two-color Airyscan confocal image of colocalized tau (tau-S244C-Alexa Fluor 594, red) and Ydj1 (sparsely labeled with Alexa Fluor 488, green) in tau-Ydj1 coacervates (Scale bar, 10 µm). Both tau and Ydj1 concentrations were 10 µM, respectively. **(C)** Plots of Pearson's and Mander's colocalization coefficients quantifying the presence of tau in the droplets of Ydj1 and vice-versa (n = 15 high-resolution confocal images were analyzed). **(D)** FRAP kinetics of tau-Ydj1 droplets. Alexa Fluor 488-labeled proteins were used for both tau and Ydj1 for independent FRAP studies. The data represent mean ± SD; n = 5. **(E)** The normalized autocorrelation plot was obtained from FCS measurements performed for monomeric dispersed tau and Ydj1, as well as tau and Ydj1 in tau-Ydj1 droplets. **(F)** Diffusion coefficients of Ydj1 in tau-Ydj1 condensates, Ydj1 in monomeric dispersed form, and tau in monomeric dispersed form and tau-Ydj1 droplets obtained from FCS measurements for five different droplets. For all FCS measurements of monomers, 5 nM of labeled proteins were used

(tau-S244C-Alexa Fluor 488, Ydj1 sparsely labeled with the same dye). For droplets, 0.5 nM of labeled proteins were used in both cases. Tau and Ydj1 concentrations were both 10 μM.

To observe and verify the co-phase separation of tau and Ydj1, we introduced a single cysteine at the 244$^{th}$ position (tau S244C) of a null-cysteine variant of full-length tau (C291S, C322S) via site-directed mutagenesis and labeled it using the Alexa Fluor594-C5-maleimide reporter. To visualize the tau-Ydj1 droplets, we doped 1% of each labeled protein with their corresponding unlabeled counterparts, i.e., tau (10 μM) and Ydj1 (10 μM) in the reaction mixture (in 20 mM HEPES, pH 7.4), and performed two-color Airyscan imaging. Our imaging results showed a perfect colocalization of tau and Ydj1 in droplets, which we further corroborated by the Pearsons' coefficient colocalization and Manders' overlap analysis (Figure 4.2 B, C). These droplets underwent rapid fusion, acquired a spherical shape, and showed full fluorescence recovery after photobleaching (FRAP), indicating their liquid-like nature (Figure 4.2 D). In addition, our FRAP measurements for Ydj1 in tau-Ydj1 condensates showed a slower recovery compared to tau, suggesting the formation of a densely interconnected network in the resulting heterotypic condensates. Our fluorescence correlation spectroscopy experiments further supported this observation, showing a higher diffusion time for Ydj1 compared to tau in the heterotypic mixture (Figure 4.2 E, F). Overall, our results demonstrated the Ydj1-mediated potentiation of tau phase separation, resulting in the heterotypic phase separation of tau-Ydj1 into viscoelastic droplets, with a densely interconnected network constituted by the two proteins. Next, to discern the underlying molecular principles governing tau-Ydj1 co-phase separation, we aimed to probe the effect of ionic strength and temperature on these heterotypic condensates.

### 4.2.2 An interplay of transient electrostatic and hydrophobic interactions regulates tau-Ydj1 coacervation

Heterotypic, complex coacervation is typically a result of electrostatic interactions between oppositely charged constituents, assisted by surrounding counter-ion release upon their association, resulting in an entropically favored demixing of the solution.[39, 59-61] At physiological pH, Ydj1 exists as a negatively charged polypeptide (pI = 6.30), while tau exhibits a positive charge under the same condition (pI = 8.24) (Figure 4.3 A, B).[62] The oppositely charged nature of these two proteins, therefore, suggests an important role of electrostatic interactions in this system. To test the same, we performed two-color confocal

imaging at increasing salt concentrations. In agreement with our hypothesis, droplet formation was completely inhibited above ~ 50 mM NaCl (Figure 4.3 C). Next, since many complex coacervations are entropically-favored processes,[61, 63] we set out to discern the role of increasing temperature on tau-Ydj1 coacervation. Our turbidity and microscopy experiments suggested that our system exhibited a typical lower critical solution transition (LCST) behavior, where an increase in temperature beyond a critical value favors phase separation (Figure 4.3 D, E). This increase in temperature promotes dehydration by breaking the surrounding water

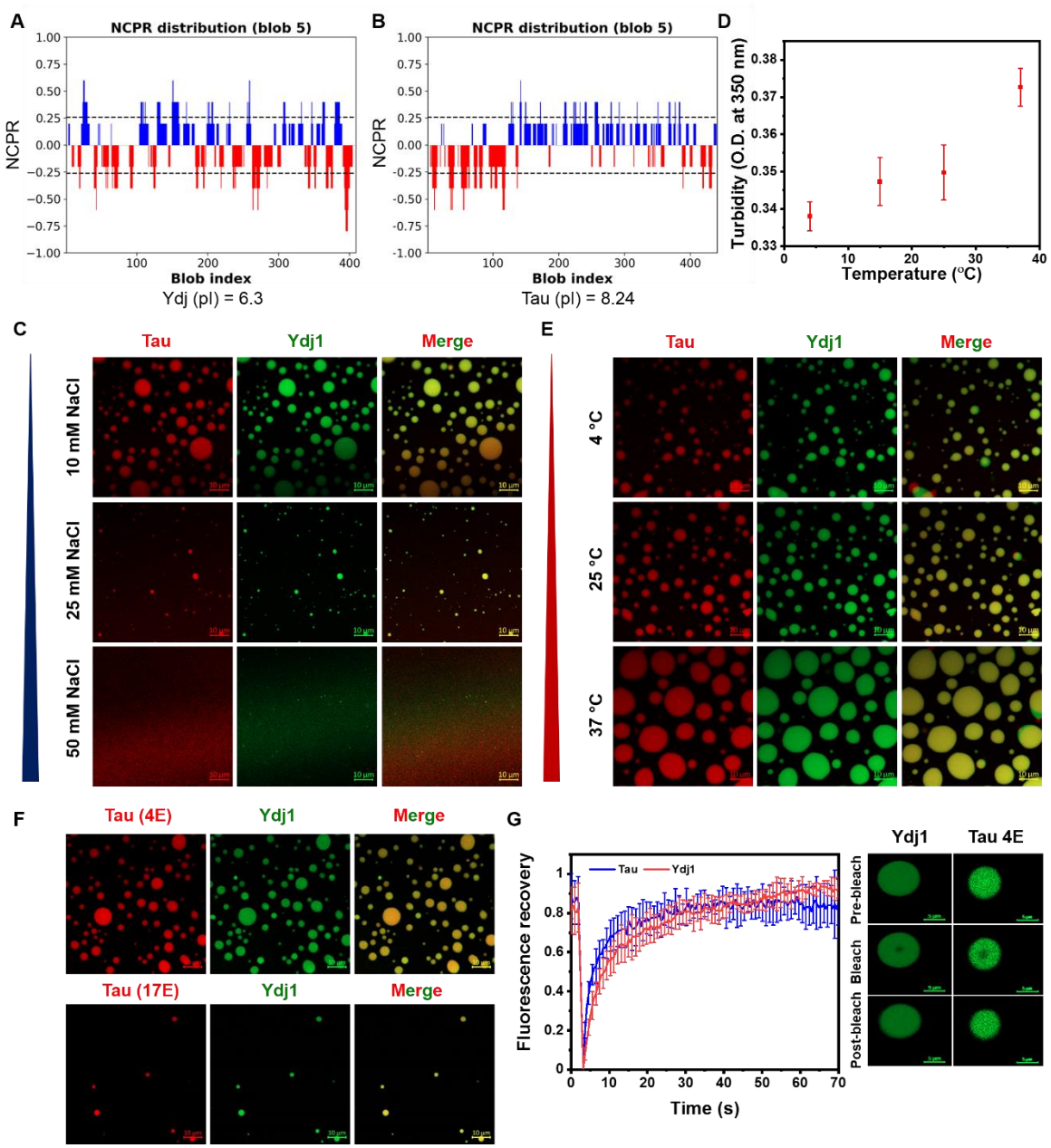


**Figure 4.3. An interplay of electrostatic and hydrophobic interactions drives tau-Ydj1 condensation. (A)** Net charge per residue profile of Ydj1 and **(B)** tau. **(C)** Two-color Airyscan

confocal images of tau (10 μM, red) and Ydj1 (10 μM, green) complex coacervates in the presence of an increasing concentration of salt (Scale bar, 10 μm). **(D)** Turbidity (O.D. at 350 nm) measurements of the tau-Ydj1 reaction mixture as a function of increasing temperature (tau and Ydj1 concentrations were both kept fixed at 10 μM). The data represent mean ± SD; n = 3. **(E)** Tau (10 μM, red) and Ydj1 (10 μM, green) condensate at increasing temperatures. (Scale bar, 10 μm). **(F)** Tau 4E (10 μM, red) and Ydj1 (10 μM, green) droplets (*Upper*) compared with droplets formed by tau 17E (*Lower*) (Scale bar, 10 μm). **(G)** FRAP kinetics of tau 4E-Ydj1 droplets. Alexa Fluor 488-labeled proteins were used for both tau and Ydj1 for independent FRAP studies (Both tau and Ydj1 concentrations were 10 μM). The data represent mean ± SD; n = 5.

shell, elevating protein-protein associations, hence favoring coacervation. Moreover, since both proteins have hydrophobic pockets clustered in their sequence, the microtubule-binding region (MTBR) region for tau,[33] and the peptide binding region (PBR) of Ydj1,[64] an increase in their association can also be attributed to the elevated hydrophobic interactions between them upon increasing temperatures. In cells, the post-translation modifications of tau by the introduction of phosphates throughout the protein chain by specific kinases are pathophysiologically significant. They are also associated with changes in its charge profile, leading to differences in the tau intra- and interdomain interactions. Moreover, previous reports have highlighted the phosphorylation-associated changes in the phase separation of tau. [33-36, 65] To recapitulate the same in our system, we used phosphomimetic tau mutants with similar phosphorylation patterns achieved by cellular kinases. One of these mutants (tau 4E; pI=7.16), where four residues were mutated to glutamate, recapitulated the phosphorylation usually attained by microtubule affinity-regulating kinases (MARKs).[36] The second mutant (tau 17E; pI= 5.60) was created by selectively replacing serine, threonine, and tyrosine residues throughout the tau chain to glutamate, as achieved by the PKA kinase that phosphorylates tau to a significantly greater extent.[66] Upon performing our imaging experiments with these mutants in the presence of Ydj1, we observed that although tau 4E phase separated with Ydj1, the greater negative charge on tau 17E abolished this interaction, probably due to the repulsion between the two protein chains under our conditions (Figure 4.3 F, G). This was also corroborated by our turbidity measurements and reiterated the importance of electrostatic interactions in modulating tau-Ydj1 co-phase separation. To summarize our observations, our salt- and temperature-dependent data, coupled with experiments using phosphomimetic tau mutants, suggested an intricate interplay of both electrostatic and hydrophobic interactions in tau-Ydj1 coacervation. Next, to further elucidate the mechanistic underpinnings of this

heterotypic complex coacervation, we performed our experiments with truncated variants of tau.

### 4.2.3 The central and hydrophobic regions of tau are responsible for tau-Ydj1 condensation

After establishing the change in the phase behavior of tau in the presence of Ydj1, we next set out to define the domains of tau that are crucial for this interaction. Towards the same, we

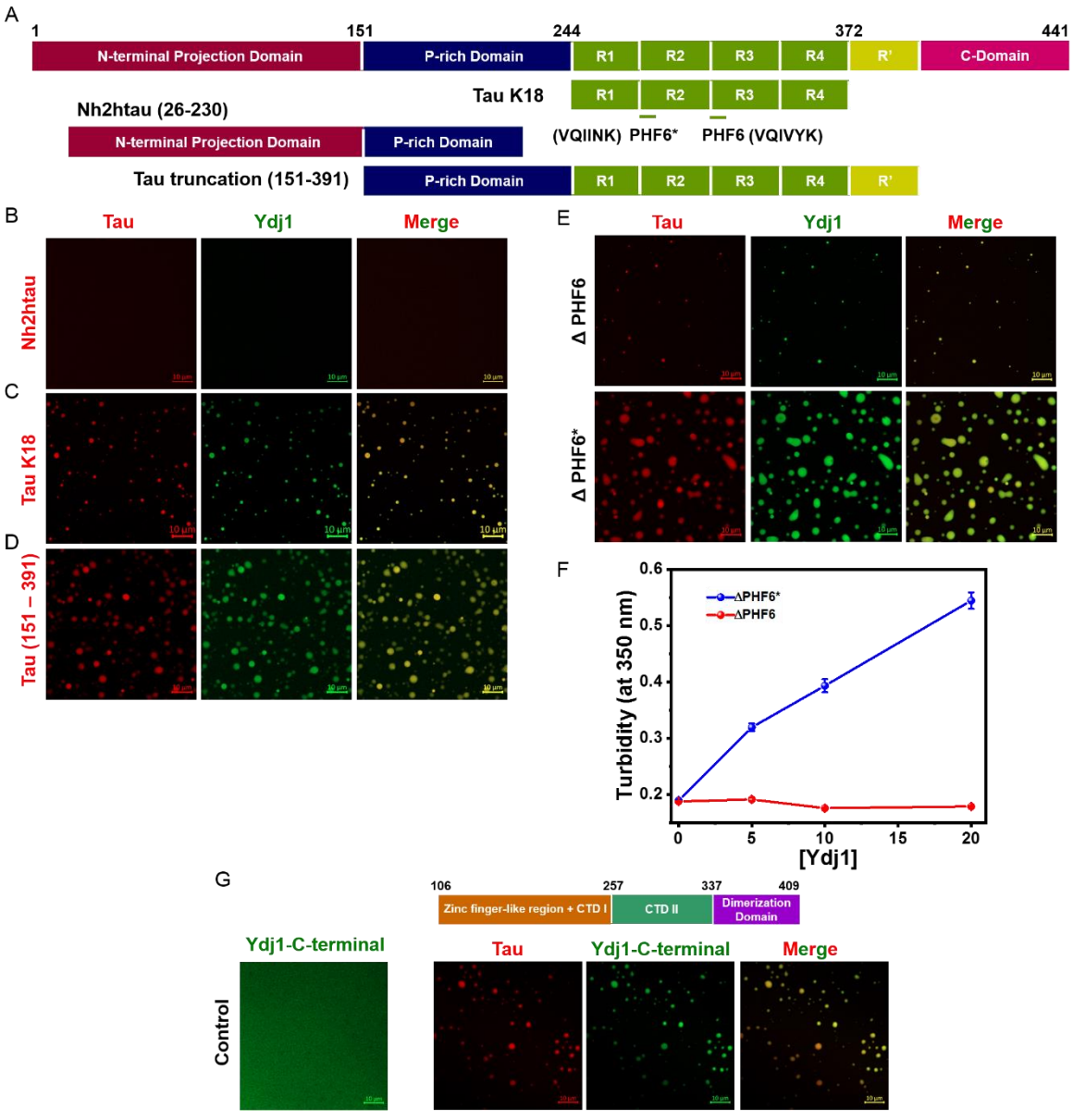


**Figure 4.4. Domain-specific interactions are fundamental to tau-Ydj1 phase separation:** (**A)** Depiction of the tau constructs used. Two-color Airyscan confocal images of **(B)** Nh2htau (10 μM, red) and Ydj1 (10 μM, green) (Scale bar, 10 μm), **(C)** tau K18 (10 μM, red) and Ydj1

(10 μM, green) (Scale bar, 10 μm), **(D)** tau truncation (10 μM, red) and Ydj1 (10 μM, green) (Scale bar, 10 μm) and, **(E)** tau ΔPHF6 (10 μM, red) and Ydj1 (10 μM, green) droplets (*Upper*) compared to tau ΔPHF6* (*Lower*) (Scale bar, 10 μm). **(F)** Turbidity plots of tau ΔPHF6 (10 μM) and tau ΔPHF6* (10 μM) as a function of the Ydj1 concentration. The data represent mean ± SD; n = 3. **(G)** Depiction of the Ydj1 C-terminal domain (CTD) construct. Two-color Airyscan confocal images of tau (10 μM, red) and Ydj1-CTD (10 μM, green) (Scale bar, 10 μm).

performed our experiments with biologically relevant truncations of tau. We began by using an N-terminal, negatively charged fragment of tau (Nh2-tau; 26-230, pI = 5.32) comprising the projection and the proline-rich domains (Figure 4.4 A). This truncation is involved in the pathology of several tauopathies and is also found in amyloid-like deposits in the brains of diseased patients.[67] As expected, we observed no droplet formation by this mutant in the presence of the similarly-charged Ydj1 (Figure 4.4 B). Inspired by studies that have previously reported the importance of the tau-repeat region in its interaction with various members of distinct chaperone families, we next used the well-studied tau K18 truncation, which only comprises repeats R1-R4 of the tau chain (Figure 4.4 A).[33, 46] In the presence of Ydj1, we observed droplet formation by tau K18, as suggested by our turbidity measurements and imaging, albeit at much higher protein concentrations. Moreover, the droplets formed were much smaller than those formed in the presence of full-length tau, even at higher protein concentrations (Figure 4.4 C). We further performed our experiments with a positively-charged C-terminal truncation of tau (tau truncation; 151-391, pI = 10.23) that comprises the proline-rich region repeats P1 and P2 in addition to the central (R1-R4) and pseudo repeat region (R') (Figure 4.4 A).[68] In contrast to the N-terminal truncation, our confocal imaging and turbidity measurements with this tau truncation showed the formation of mesoscopic, liquid-like droplets, much like full-length tau, even at much lower concentrations (Figure 4.4 D). Our data, therefore, suggests the importance of the repeat region as well as the neighboring positively charged proline-rich region of tau in driving tau-Ydj1 coacervation. This further corroborates our salt and temperature-dependent measurements in unveiling the importance of an interplay of electrostatic and hydrophobic interactions in the formation of tau-Ydj1 condensates. In addition to being essential for microtubule binding, the central repeat containing MTBR of tau also contains two-hexapeptide motifs, PHF6* ($^{275}$VQIINK$^{280}$) and PHF6 ($^{306}$VQIVYK$^{311}$) at the beginning of the second and the third repeats, respectively, which are crucial for tau aggregation (Figure 4.4 A).[33] To test the importance of these aggregation-promoting hexapeptide motifs in tau-Ydj1 phase separation, we created two deletion mutants, namely tau

ΔPHF6* and tau ΔPHF6, where we selectively deleted one hexapeptide while keeping the other. Under our conditions, while tau ΔPHF6* showed a phase behavior similar to full-length tau, the propensity of tau ΔPHF6 to undergo phase separation was considerably lower in the presence of Ydj1, as suggested by low solution turbidity and sparse droplet formation in our imaging experiments (Figure 4.4 E, F). This observation further highlighted the importance of the highly hydrophobic hexapeptide stretch, PHF6, in tau-Ydj1 coacervation. Moreover, by using the C-terminal truncation variant of Ydj1, incorporating hydrophobic CTDs I and II, we showed that this region of Ydj1, which is also known as the peptide binding region, is essential for its interaction and phase-separation with tau (Figure 4.4 G).

Next, to demonstrate the regio-specific structuring of tau upon tau-Ydj1 condensation, we performed residue-specific single droplet steady-state fluorescence anisotropy measurements using fluorescein-5-maleimide labeled single cysteine variants of tau

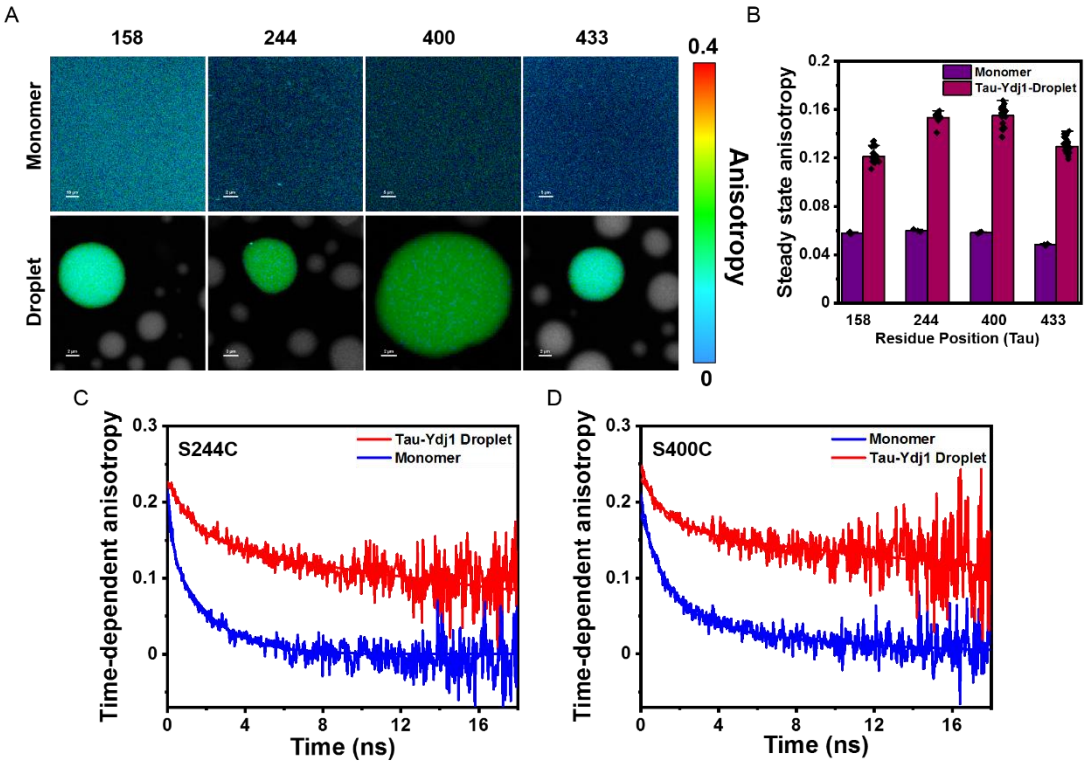


**Figure 4.5. Domain-specific interactions are fundamental to tau-Ydj1 phase separation** **(A)** Representative single-droplet steady-state fluorescence anisotropy images showing anisotropy heatmap of F-5-M labeled single-Cys mutants of tau spanning the sequence; in the dispersed monomeric (*Upper*), and tau-Ydj1 droplets (*Lower*). **(B)** Single-droplet **s**teady-state fluorescence anisotropy measurements of F-5-M labeled single-Cys mutants of tau spanning the sequence in the dispersed, monomeric state (purple) and in tau-Ydj1 droplets (wine). Data for more than n = 30 different droplets were considered for droplet anisotropy. **(C)** Time-resolved fluorescence anisotropy decays of F-5-M labeled tau-S244C and **(D)** tau S400C of tau

in monomeric state (red) and tau-Ydj1 droplets (blue). The solid lines are fits obtained using decay analysis.

**Table 4.1 Recovered parameters from time-resolved fluorescence anisotropy decay analyses.**

| **Tau-S244C-F-5-M** | **$\phi_1$ ($\beta_1$)** | **$\phi_2$ ($\beta_2$)** |
|---|---|---|
| Tau monomer | 0.89 ± 0.05 ns<br>(0.59 ± 0.011) | 4.93 ± 0.39 ns<br>(0.41± 0.015) |
| Tau-Ydj1 droplets | 0.99 ± 0.05<br>(0.32 ± 0.012) | 41.17 ± 1.24<br>(0.68 ± 0.013) |
| **Tau-S400C-F-5-M** | **$\phi_1$ ($\beta_1$)** | **$\phi_2$ ($\beta_2$)** |
| Tau monomer | 0.93 ± 0.03 ns<br>(0.59 ± 0.011) | 5.03 ± 0.29 ns<br>(0.41± 0.011) |
| Tau-Ydj1 droplets | 1.05 ± 0.04<br>(0.33 ± 0.011) | 39.87 ± 1.64<br>(0.67 ± 0.011) |

encompassing the entire tau polypeptide chain. Fluorescein-5-maleimide has a shorter lifetime (~ 4 ns) and linker, making it a suitable probe for capturing the rotational tumbling of a polypeptide chain. Our single droplet steady-state anisotropy measurements reported a sharp increase in the anisotropy values compared to the monomeric dispersed phase upon condensation, suggesting an increase in ordering and the presence of a dense environment within tau-Ydj1 condensates. Further, we observed the highest anisotropy values for the residues lying in the MTBR, indicating its greater structural ordering and the formation of preferable contacts with Ydj1 facilitated by this region (Figure 4.5 A, B). Since steady-state anisotropy provides only time-averaged information, we performed single-droplet picosecond time-resolved fluorescence anisotropy measurements to temporally discern the different rotational dynamics exhibited by the tau protein chain within tau-Ydj1 condensates. Here, we chose residues lying in the repeat region of tau, i.e., the 244th and 400th positions in the tau sequence. Our individual droplet measurements showed that tau exhibited slower depolarization kinetics (global rotational correlation time ~ 40 ns) compared to monomeric tau, which obeys faster biexponential decay kinetics typical for any archetypical IDP (Figure 4.5 C, D, Table 4.1). Such an increase in the rotational correlation time indicates the formation of a dense network within the coacervates, which can consequently hamper the reorientation

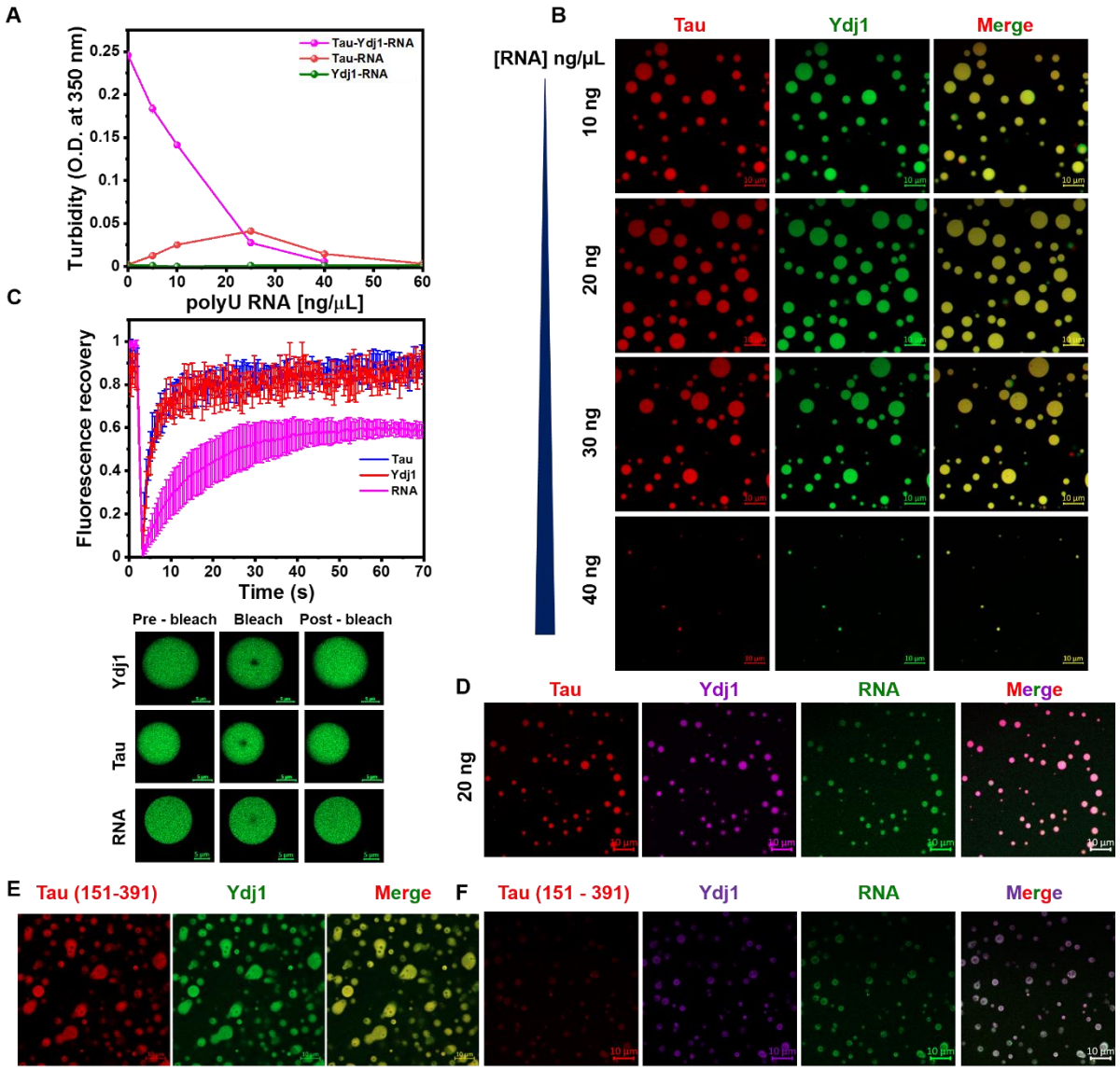


**Figure 4.6. RNA-mediated Tau-Ydj1 reentrant phase behavior (A)** Turbidity plots of tau-Ydj1-RNA, tau-RNA, and Ydj1-RNA as a function of RNA concentration (Both tau and Ydj1 concentrations were 10 μM). The data represent mean ± SD; n = 3. **(B)** Two-color Airyscan confocal image of the tau-Ydj1-RNA (tau-red; Ydj1-green) ternary system as a function of increasing RNA concentrations (Scale bar, 10 μm). **(C)** FRAP kinetics of tau-Ydj1-RNA droplets. Alexa Fluor 488-labeled proteins and RNA were used for tau, Ydj1, and RNA for independent FRAP studies (tau = Ydj1, 10 μM; RNA, 20 ng/μL). The data represent mean ± SD; n = 5. **(D)** Three-color Airyscan confocal image of colocalized tau (tau-244C-Alexa Fluor 594, red); Ydj1 (Alexa Fluor 647, pink) and RNA (5'Phosphate-Alexa Fluor 488, green) in tau-Ydj1-RNA coacervates (Scale bar, 10 μm). Both tau and Ydj1 concentrations were 10 μM, while RNA concentration was 20 ng/μL. **(E)** Two-color Airyscan confocal image of the tautruncation-Ydj1-RNA (tau truncation-red; Ydj1-green) ternary system (Scale bar, 10 μm). **(F)** Three-color Airyscan confocal image of co-localized tau-truncation, Ydj1, and RNA (tau truncation-red; Ydj1-pink; RNA-green) ) in tau-Ydj1-RNA coacervates (Scale bar, 10 μm).

Both tau truncation and Ydj1 concentrations were 10 μM, while RNA concentration was 20 ng/μL.

dynamics of the polypeptide chain. Having established the domains and regio-specific factors governing tau-Ydj1 droplet formation, we next established the RNA-mediated modulation of these coacervates. Because of its ability to act as a significant co-factor modulating tau liquid-to-solid transitions, RNA can have a strong impact on tau-Ydj1 phase behavior.

### 4.2.4 Competing interactions in the tau-Ydj1-RNA ternary system govern the properties of the three-component condensates

In cells, phase-separated condensates exist as complex assemblies of biomacromolecules such as proteins and nucleic acids. The polymeric nature of the constituents of these condensates affords multivalency to the system, allowing the creation of a functional, multi-component network.[21-24] In biological systems, the physical properties of nucleic acids such as RNA also contribute to the nature of compartmentalization achieved in addition to serving other more traditionally well-studied roles. The charge on any given RNA chain, in addition to its ability to recruit multiple protein partners and introduce multivalency into a system, makes RNA a potent scaffold in numerous biological condensates (70). To test the effects of RNA on our system, we performed our experiments in the presence of increasing concentrations of polyU RNA (Fig. 4A, B, S4A). Within a concentration range from 5-40 ng/μL, we observed no change in the morphology of the droplets compared to those formed in the absence of RNA (Fig. 4B). Our FRAP experiments also showed high recovery in the presence of RNA, indicative of the liquid-like nature of these condensates. Interestingly, although both tau and Ydj1 achieved complete recovery, the recovery of Ydj1 was faster than what we observed for droplets formed with just the addition of the protein components (Fig. 4C, D). The faster diffusion of Ydj1 in the presence of RNA suggested an overall relaxation of Ydj1 in the condensed phase via RNA-mediated multivalency and competing interactions between the negatively charged Ydj1 and RNA for tau in the tau-Ydj1-RNA ternary system. At higher concentrations of RNA, we observed the complete dissolution of condensates as expected for typical RNA-associated reentrant phase behavior (Fig. 4A, B) (71-73). Moreover, to visualize and monitor the RNA dynamics within coacervates, we labeled the 5' end of RNA with the NHS-AlexaFluor-488 (succinimidyl ester) dye via the EDC-NHS-coupling mediated activation of its 5' phosphate.[73] Our three-color Airyscan imaging experiments confirmed the localization of RNA with the protein components in tau-Ydj1 condensates (Figure 4.6 D). Next, in order to assess the nature

of the translational diffusion of RNA within these condensates, we performed FRAP experiments using labeled RNA. These results revealed a slower fluorescence recovery in comparison to tau and Ydj1, suggesting the formation of a dense RNA network in the interior of the heterotypic condensates (Figure 4.6 C). Moreover, our data is in line with previous, similar reports on the dynamics of RNA in droplets.[74] Since the central region of tau establishes contacts with Ydj1 and also acts as the primary site for RNA interaction owing to the presence of lysine clusters,[75] we set out to delineate the role of RNA in modulating tau truncation-Ydj1 coacervates. Our multi-color imaging experiments captured a change in the morphology of the condensates formed by this ternary system, unlike the previously observed completely mixed condensates observed for tau truncation-Ydj1 (Figure 4.6 E, F). In the presence of RNA, these condensates adopted a vacuolar morphology, as reported previously for non-stoichiometric multi-component mixtures, which undergo dissolution at high concentrations of RNA (77). Additionally, in the three-color imaging performed for this system, we observed the colocalization of all three components of the mixture in the rims of the resulting vacuolar condensates (Fig. S3*C*). The emergence of such a biopolymer-poor architecture within anisotropic condensates is typically attributed to a deviation from thermodynamic equilibrium. Although the sub-structure afforded by biomolecules such as RNA within condensates improves spatiotemporal synchronization, previous reports on the potent effects of RNA in the maturation of tau condensates further add to the notion of condensates as reaction crucibles for the exacerbation of their maturation into pathological species. Therefore, we next set out to delineate the consequence of the Ydj-1-mediated modulation of tau condensates on its aggregation propensity.

### 4.2.5 Ydj1 halts phase separation-mediated aggregation of tau

The highly enriched environment within biomolecular condensates makes them particularly susceptible to aberrant phase transitions. This is especially true for several neuronally-associated intrinsically disordered proteins because of their ability to engage in multivalent interactions within such condensates, as previously observed for polypeptides such as FUS, TDP-43 as well, and tau.[26-31] Prior evidence has confirmed the conversion of monomeric tau into amyloid-like aggregates, both in the presence as well as in the absence of cofactors, which is accelerated several folds upon phase-separation in the presence of cofactors or crowding. In cells, several such potentially pathogenic events are promptly halted or counteracted by the

cellular chaperone machinery comprising several Hsps.[43-48, 77] To recapitulate this biological phenomenon in our system, in a crowder or cofactor-free environment, we incubated the tau-

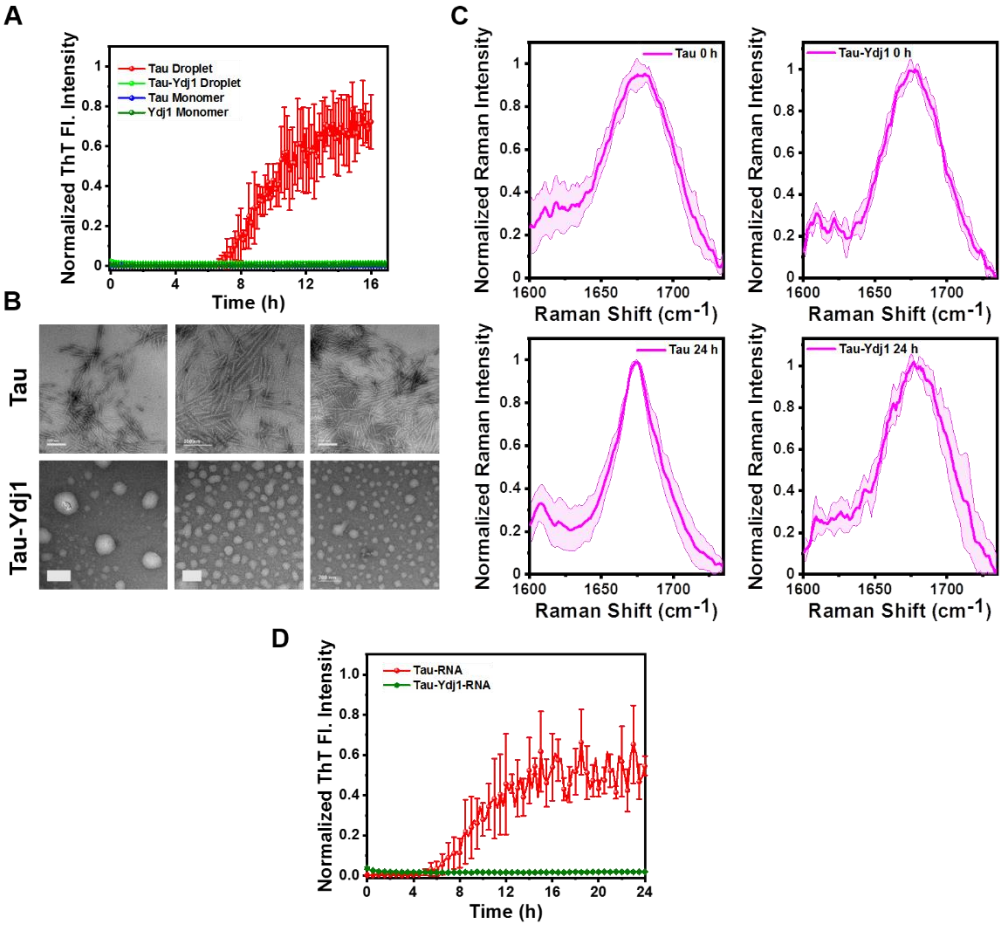


**Figure 4.7 Ydj1 halts tau fibril formation** (**A)** ThT kinetics of phase separation-mediated aggregation of tau via a liquid-to-solid transition; and separately, tau-Ydj1 droplets, monomeric Ydj1, and monomeric tau. Wherever used, tau and Ydj1 concentrations were equal to 10 μM. The data represent mean ± SD for n = 3 independent experiments. **(B)** TEM image of final species formed at the end of the aggregation kinetics of tau (*Upper*) and tau-Ydj1 condensates (*Lower*), indicating the presence of amyloid-like fibrils and proteinaceous oligomeric species in the absence and presence of Ydj1, respectively. The experiment was performed twice with similar observations. **(C)** Amide I vibrational Raman band of the dense phase of tau (*Left*) or tau-Ydj1 (*Right*) reaction mixture recorded over time, after 5 minutes of incubation (*Upper*), in comparison to 24 hours of incubation (*Lower*). **(D)** ThT kinetics of phase separation-mediated aggregation of tau-RNA via a liquid-to-solid transition and, separately, tau-Ydj1-RNA droplets. Wherever used, tau and Ydj1 concentrations were equal to 10 μM, and 20 ng/μL RNA concentration was used. The data represent mean ± SD for n = 3 independent experiments.

Ydj1 reactions mixtures with agitation. Simultaneously, we monitored the aggregation kinetics of our reaction mixture in the presence of thioflavin T (ThT), a well-known amyloid marker. As expected, over time, phase-separated tau formed amyloid-like aggregates in a nucleation-dependent manner, as suggested by the sigmoidal kinetics and positive ThT intensity (Figure 4.7 A). This was further corroborated by the TEM imaging of the end products, where we observed the formation of fibrillar species (Figure 4.7 B). Monomeric tau, on the other hand, did not aggregate under the monitored conditions. In the presence of Ydj1, however, we saw almost no rise in the ThT intensity, which is indicative of the Ydj1-mediated abrogation of tau aggregation. Upon imaging the final species of tau-Ydj1 reaction mixtures using TEM, we observed the formation of small cluster-like protein conglomerates (Figure 4.7 A, B). This is in line with previous reports where tau was shown to form oligomeric species in the presence of a complex of two major molecular chaperones, Hsp70-Hsp90.[46, 78] Hence, instead of halting tau in its monomeric state, tau-Ydj1 coacervation leads to the formation of nanoscopic hetero-clusters of tau in complex with Ydj1. To further characterize the nature of these species, we used vibrational Raman spectroscopy and monitored the amide I (1620-1720 $cm^{-1}$) vibrational band, which arises due to -CONH bending, assigned to the secondary structure of the protein. Our Raman experiments suggested the conformational trapping of the tau-Ydj1 condensates as indicated by the consistent full width at half maxima (FWHM) of the amide I band following incubation. In contrast, we observed a much sharper Amide I band having maxima around ~ 1675 $cm^{-1}$ for tau condensates upon aging, which is characteristic of the emergence of beta-rich structures (Figure 4.7 C). Moreover, our ThT-dependent aging experiments with the tau-Ydj1-RNA ternary system also showed similar aggregation kinetics as the binary system in the absence of RNA, signifying the importance of Ydj1 in modulating the liquid-to-solid transition of tau even in the presence of potent cofactors like RNA, which are typically associated with aggregation (Figure 4.7 D). Next, to discern the mechanistic basis of the Ydj1-mediated interruption of tau aggregation and the underlying conformational changes experienced by the tau polypeptide chain in this process, we set out to perform a single-molecule, single-droplet experiment.

### 4.2.6 Ydj1 mediated conformational expansion of tau in tau-Ydj1 heterotypic condensates

Monomeric tau is highly soluble and exists as a natively unstructured polypeptide. Previous reports on the molecular configurations of tau have shown that it naturally acquires a globally compact "S-shaped" or "paper-clip"-like structure, where both of its termini project onto the

central MTBR region.[79-81] In the presence of external stimuli, such as cofactors including heparin, polyphosphate, or tubulin, mutations, and phase separation, it goes through a conformational transition into a more "open" conformation where long-range intra-molecular contacts diminish, and preponderant inter-molecular contacts are established resulting in higher-order association and hence aggregation.[80, 82, 83] This is primarily a result of the exposure of the typically buried central hydrophobic region, which is enriched in several amyloid-triggering motifs. Single-molecule Förster resonance energy transfer (smFRET) has previously proven to be instrumental in capturing the conformational gymnastics of IDPs, including tau. Inspired by these findings and based on our results on the Ydj1-mediated abrogation of tau aggregation, we performed single-droplet, single-molecule fluorescence experiments for this heterotypic assembly to gain a better molecular description of the mechanistic action of Ydj1 on the tau polypeptide chain. In line with our hypothesis, we engineered two cysteines in the tau MTBR region to construct two FRET-pairs encompassing the R1-R3 (tau S244C-S322C) region and the R1-R' region (tau S244C-S400C) (Figure 4.8 A). For our experiments, we stochastically labeled these double cysteine variants of tau with the well-studied FRET positive fluorophore pair, Alexa Fluor 488 (donor)-Alexa Fluor 594 (acceptor). We performed smFRET experiments in the two-color pulsed-interleaved excitation (PIE) mode on a time-resolved confocal microscope set-up.[85] We started our measurements by acquiring smFRET data for monomeric tau. Very low concentrations (<150 pM) of labeled protein were used for our study to ensure the movement of a single labeled protein molecule through the observation volume (0.53 fl) during the measurement. To confirm surface passivation and rule out any surface-induced conformational changes, we doped our labeled protein with ~ 50 nM of unlabeled tau protein. Our smFRET results for the monomer suggested that while the FRET pair residing in the R1-R3 region conformed to the standard polymer random coiled model (40 % E as opposed to <E> = 37 %), the second pair, encompassing the tau pseudo repeat in the R1-R' region (29 % E as opposed to <E> = 4.5 %) deviated from it, indicative of significant compactness in the polypeptide structure (Figure 4.8 B, C). This observation aligns with the constructed charge-hydrophobicity plot for the same construct, suggesting that the C-terminal region of tau is collapsed (Figure 4.8 D). Having established the monomeric structure of tau, we next set out to capture the phase separation-induced conformational changes of tau using single-droplet single-molecule experiments. For droplet experiments, we considered the partitioning coefficient and used 5-15 pM of labeled protein concentration to ensure that the concentration of the labeled protein within droplets remained in the single-molecule regime. We induced tau-

Ydj1 phase separation by doping the dual-labeled protein with a mixture of unlabeled tau (10 µM) and Ydj1 (10 µM). After drop-casting the phase-separated solution on the coverslip, followed by a short incubation to allow the droplets to settle and reach equilibrium, we focused the laser spot in the center of large immobilized single droplets (5 – 10 µm diameter) to acquire data. Our measurements revealed that the tau polypeptide chain in R1-R3 and the pseudo-repeat region underwent conformational expansion inside tau-Ydj1 droplets. While the conformational shift was significant for the R1-R3 region (244-322 pair, 22 % E from 40 % E), a very marginal shift was observed for the 244-400 pair (19 % E from 27 % E) (Figure 4.8 E, F). Both of these regions showed a second smaller high-fret population suggesting local structuring in the presence of Ydj1 (64 % and 53 % E corresponding to 244-322 and 244-400, respectively). This stretching in the R1-R3 region further supports our observation of the tau hexapeptide deletion (tau ΔPHF6), which is essential for tau-Ydj1 interactions by accommodating Ydj1. Additionally, this region seems to have a higher conformational

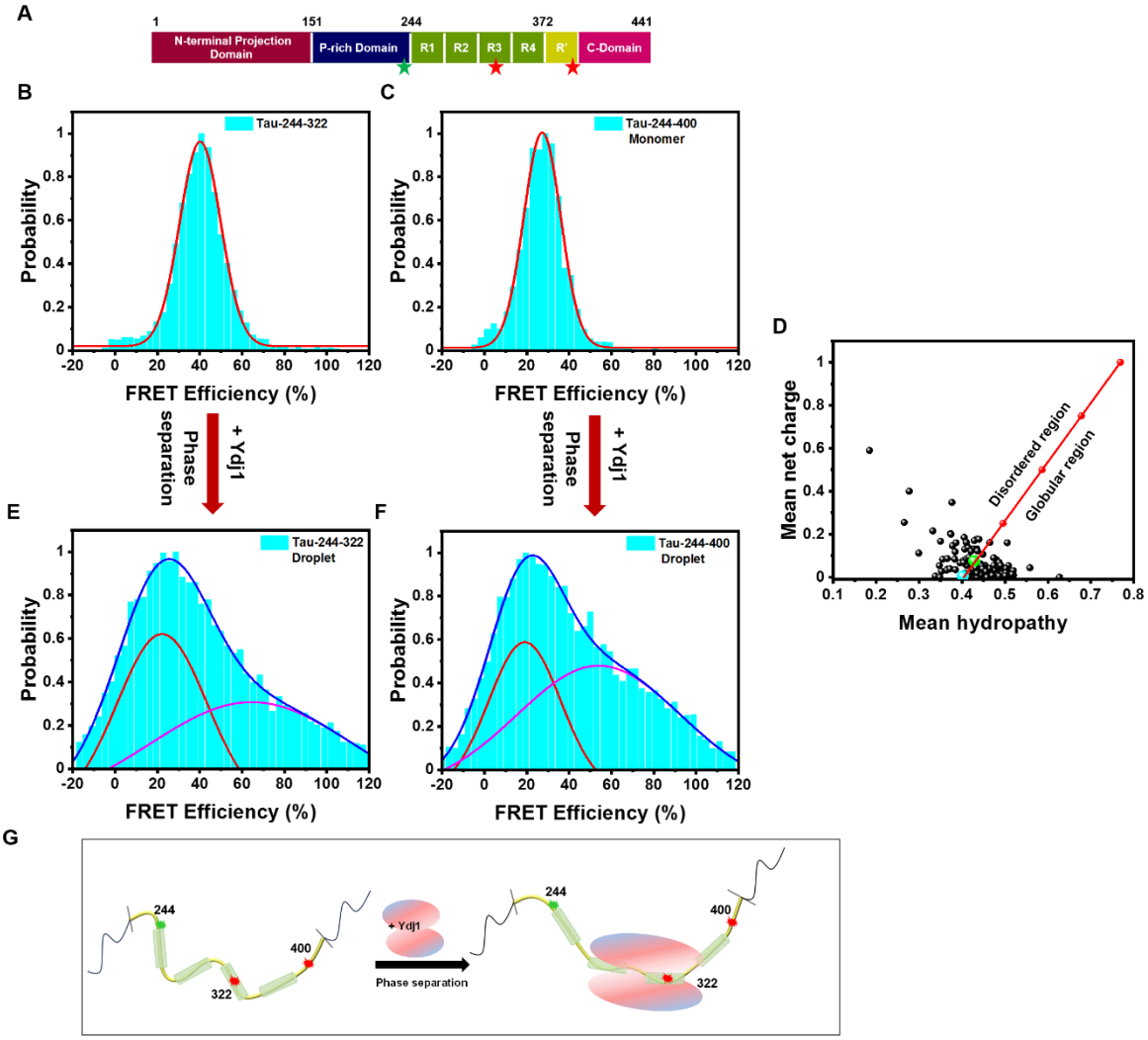

**Figure 4.8 Single-molecule FRET dissects the conformational shape-shifting of tau in tau-Ydj1 condensates (A)** A schematic of the construct used for single molecule study. **(B)** Single-molecule FRET histograms of monomeric tau in the monomeric dispersed phase for dual-labeled constructs 244-322 and **(C)** 244C-S400. **(D)** Mean net charge as a function of mean hydrophobicity for a range of natively ordered and disordered proteins. Tau null cysteine, 244-322, and 244-400 are represented in cyan, purple, and green, respectively. Upon phase separation, tau undergoes expansion, as seen from the broader histograms of tau in the tau-Ydj1 condensed phase for dual-label constructs **(E)** 244-322 and **(F)** 244-400. The total number of events for all measurements was > 20,000, and the number of events at maxima was more than 700 in all cases. **(G)** Schematic summarizing Ydj1 mediated conformational expansion in tau polypeptide chain.

flexibility, as the 244-400 pair did not show any significant alteration in the FRET efficiency in the presence of Ydj1. A similar structural remodeling of tau has also been observed following its binding to tubulin and other components of the chaperone machinery, where although the overall dimension of the tau repeat region remained unchanged, the lengths between individual repeats widened.[78, 82, 84] Moreover, the polypeptide chain experienced more conformational freedom upon condensation, as indicated by a broader histogram, compared to the monomeric dispersed phase, which displayed a sharper peak for both constructs. Of note here is that this broadness in the histogram is also coupled to the photon shot noise, in conjunction with the contribution from the orientation factor, $\kappa^2$. Overall, these findings revealed that upon co-phase separation with Ydj1, tau undergoes conformational unwinding, enabling it to make greater inter-molecular contacts and recruit more proteins into the droplet (Figure 4.8 G). Typically, upon tau phase separation, the enrichment of intermolecular interactions upon phase separation may lead to aggregation, whereas upon the addition of Ydj1, the aggregation-prone hot spots of tau localized in the repeat region are masked by Ydj1, resulting in diminished aggregation. Further, the broadness in the histogram in the presence of Ydj1 can also be attributed to the fuzzy/dynamic nature of the tau-Ydj1 complex, similar to other tau-chaperone complexes.[77, 78] The environment of this complex may also foster the creation of transient interchain contacts amongst the expanded tau chains, promoting the formation of nanoscopic protein "conglomerates" in conjunction with neighboring free tau molecules.

## 4.3 Discussion

In this work, we showed the Hsp40-mediated regulation of phase separation and aggregation of tau. In the presence of tau, Ydj1 undergoes co-phase separation, leading to the emergence

of highly dynamic, liquid-like condensates. The sequestration of Ydj1 within these condensates is associated with slower diffusion suggesting the formation of a densely crosslinked two-component protein network associated with partitioning this molecular chaperone. As indicated by our data, this tau-Ydj1 complex coacervation encompasses contributions both from electrostatic and hydrophobic interactions. The modulation of this heterotypic phase behavior via phosphorylation, as implied by our experiments using physiologically relevant phosphomimetic tau variants, further emphasizes this observation. Expanding on the importance of charged as well as hydrophobic regions in driving this process, our results with the central-C terminal hydrophobic stretch of tau, in addition to its charged proline-rich domain and hexapeptide deletion mutants, provide a structural basis for this conclusion. These results

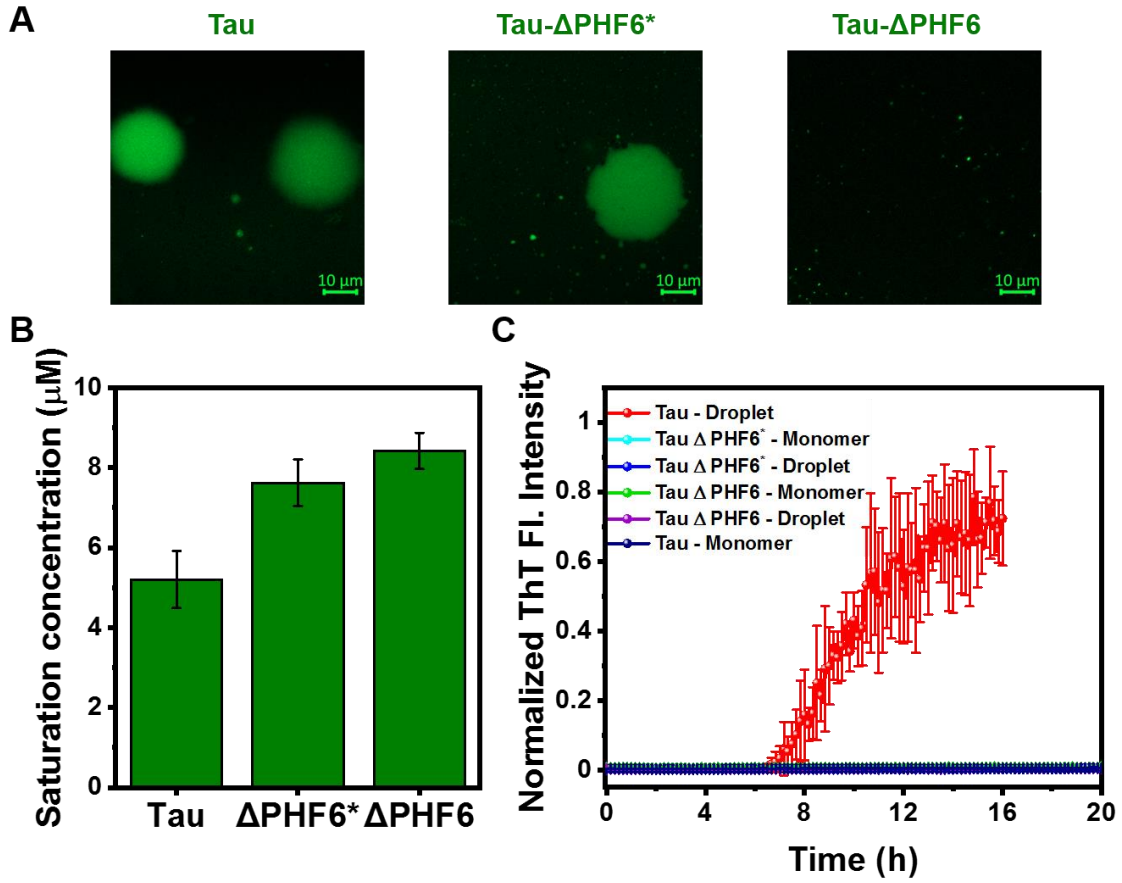


**Figure 4.9. Significance of tau PHF6 in governing its phase behavior: (A)** Airyscan confocal images of droplets of tau, tau ΔPHF6, and tau ΔPHF6* (10 μM unlabelled protein with 1% tau-T244C-Alexa Fluor 488; Scale bar, 10 μm). **(B)** The saturation concentration ($C_{sat}$) of tau for tau, tau ΔPHF6, and tau ΔPHF6* condensates is estimated by high-speed centrifugation. Data represent mean ± SD for n =3 independent reactions. **(C)** ThT kinetics of phase separation-mediated aggregation of tau via a liquid-to-solid transition; and separately, monomeric tau ΔPHF6 and droplet, monomeric tau ΔPHF6* and droplet, and monomeric tau.

Wherever used, wild-type and tau deletion variant concentrations were equal to 10 μM. The data represent mean ± SD for n = 3 independent experiments.

are further corroborated by our steady-state and picosecond time-resolved anisotropy measurements, which capture the local ordering in the central MTBR of tau, as indicated by lower anisotropy values for the N- and C-terminal ends of the tau chain in comparison to the central region. Furthermore, the heightened dynamics displayed by the ternary system upon the addition of RNA indicates the introduction of multivalency to the system. Additionally, our maturation and aggregation kinetic experiments demonstrated the Ydj1-mediated abrogation of tau aggregation and the transition of tau-Ydj1 liquid-like condensates into microscopic protein heterocomplexes. In conclusion, our study reveals the fundamental mechanistic origins of the chaperone-associated interactions that modulate the phase behavior of a neuronal disease-related IDP and govern its fate upon heterotypic coacervation.

The tau protein sequence incorporates well-characterized locally shielded and structured hexapeptide motifs, important for its phase separation and aggregation, out of which two lie at the interface of the R1/R2 and separately, the R2/R3 regions of the MTBR.[33, 81, 86] Any external stimuli, including mutations in the protein sequence, the presence of cofactors, or phase separation, are coupled to local structural re-ordering, promoting tau to adopt a pro-aggregation conformation. Separately, in our study, using selective hexapeptide deletion variants of tau, i.e., ΔPHF6* and ΔPHF6, we define the significance of these motifs for tau phase separation, both in the absence and presence of Ydj1, including the regulation of its phase transition into solid aggregates. We showed that under our conditions, while ΔPHF6* had a phase behavior similar to full-length tau, the propensity of ΔPHF6 to undergo phase separation was lower, with droplet formation seen only at higher protein concentrations. Our saturation concentration measurement further validated this observation. We observed a higher $C_{sat}$ for ΔPHF6 phase separation, underscoring the importance of the PHF6 region in driving tau condensation. Interestingly, while monitoring the thioflavin-T intensity during our aging experiments using these mutants, we noted the inhibition of aggregation for both tau ΔPHF6* and ΔPHF6, with both variants showing similarly low ThT intensities in comparison to full-length phase-separated tau (Figure 4.9). These results indicate the importance of the cooperativity between the aggregation-promoting hexapeptides, with either deletion inhibiting aggregation. This observation, however, does not hold true for the initiation of tau phase separation. As inferred from our results, the PHF6 region of tau, which usually makes up the N-terminal region of tau amyloid cores, is critical for tau condensation. We hypothesize that

the PHF6 sequence serves as a hotspot not only for governing tau aggregation as conventionally established but also on account of its significance in potentiating tau phase separation. This region has the highest propensity to form transient, beta-rich structured elements in the tau chain, potentially serving as sites for nucleating tau phase separation. On the contrary, for tau aggregation, the modular nature of these motifs in structuring tau warrants their cooperativity. This suggests that both amyloid-prone motifs must conjointly undergo a structural reconfiguration that is inhibited upon the deletion of either hexapeptide, allowing tau to retain its shielded anti-aggregation conformation. Moreover, in the context of the molecular chaperone-mediated shape-shifting of tau and its heterotypic phase separation with chaperones, including Hsps, the PHF6 region acts as a focal point of contact, as suggested by the diminution of tau ΔPHF6 phase separation even in the presence of Ydj1.

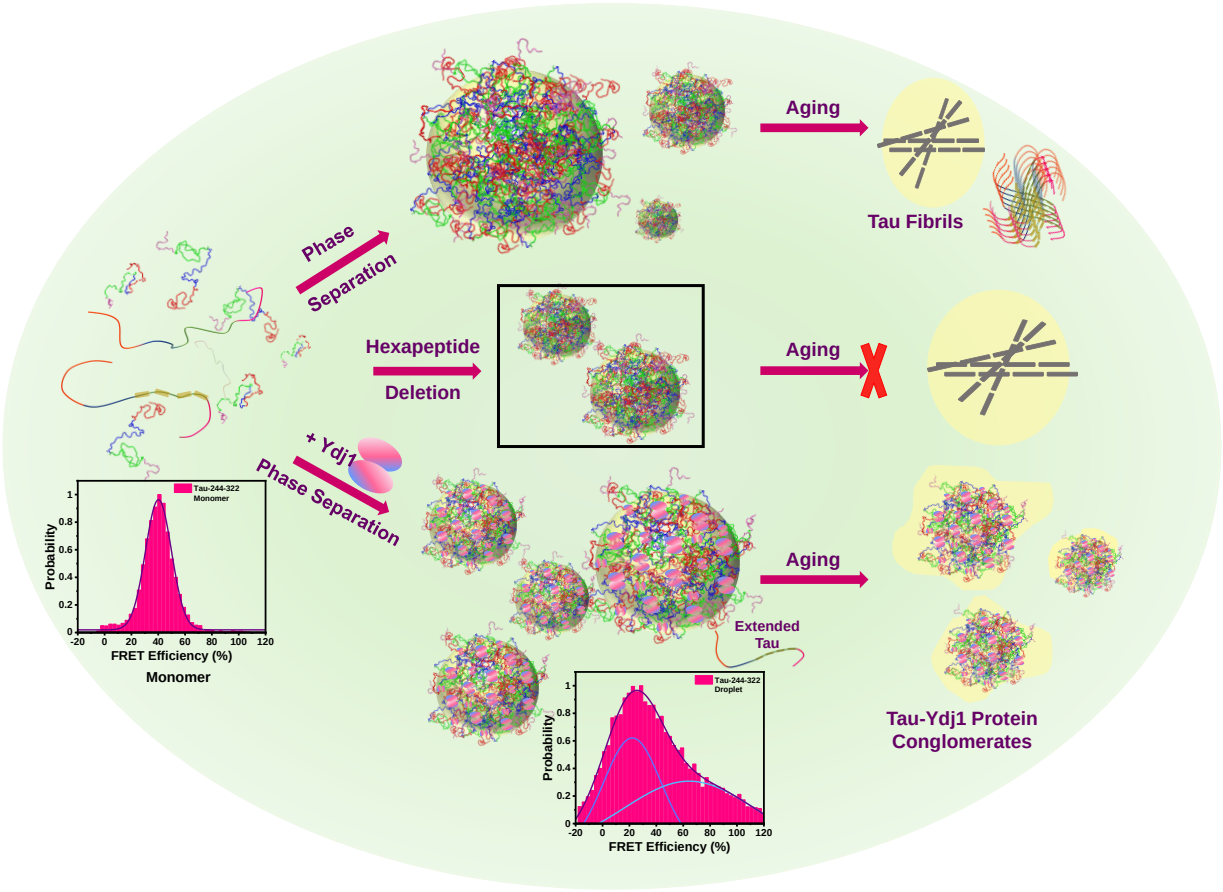


**Figure 4.10 Schematic illustration of the regulation of tau phase transitions in the presence of Ydj1:** Liquid-like phase-separated tau condensates can mature into solid amyloid-like aggregates implicated in neurodegeneration. This phase separation is associated with chain expansion and the exposure of the central MTBR region, containing hexapeptide amyloid motifs, which, in addition to regulation of aggregation, are also crucial for phase separation.

Ydj1 modulates tau phase behavior by binding the exposed tau MTBR via its CTD and halting condensate maturation at an oligomeric stage.

Next, using single-molecule studies, we captured the conformational shapeshifting experienced by the tau chain as it undergoes condensation in the presence of Ydj1. In solution, tau typically exists in a collapsed paperclip/S-shaped conformation, where the N and C-terminals of tau fold back upon the central MTBR region, consequently shielding it.[79, 80] Previously reported single-molecule studies on biomolecular condensates have reported the phase separation-associated conformational expansion of polypeptides, including tau.[83, 85, 87] Based on our observations using the PHF deletion mutants of tau, we hypothesize that phase separation leads to the exposure of its central, highly hydrophobic, aggregation-prone repeat region. The resulting long-range inter-chain contacts now established, allow the creation of a dense viscoelastic network within the condensed phase. Over time, this network, with dominating contributions from the contacts promoted within the repeat region, can mature into a gel and, finally, a solid-like state, potentially generating beta-rich amyloid-like fibrils. Conversely, upon tau-Ydj1 coacervation, Ydj1 competes for the already-exposed hexapeptide region of tau lying in the MTBR with neighboring tau molecules. The sequestration of this region by Ydj1 makes it inaccessible for inter-chain interactions with neighboring tau, subsequently halting tau fibrilization. We propose that the highly dynamic and fuzzy nature of the tau-Ydj1 complex results in frequent association and dissociation events within the condensate, allowing tau molecules to establish prolonged contacts, leading to the formation of heterotypic proteinaceous "conglomerates" (Figure 4.10). In line with our results, similar observations have also been previously noted.[78]

Although relatively unexplored, the role of the protein quality machinery in regulating the nature of biomolecular condensates is starting to emerge.[2] While complexes of major chaperone proteins, such as the Hsp70/Hsp90 complex, have been proven to be central in regulating tau aggregation and stability,[46, 47] the role of the ATP-independent class of co-chaperone, such as Hsp40, in regulating the tau maturation via phase separation remained less understood. Our results highlight the self-sufficiency of the Hsp40 family of chaperones in abrogating tau maturation into fibrils. However, cellular chaperoning is a complex process where multiple closely associated chaperones work in a feedback fashion leading to potentially more potent biological machinery that can successfully clear toxic species and pathological aggregates.[44-53] More detailed studies on chaperone-mediated regulation of the phase behavior

of a wide range of proteins will be of importance to understanding the critical balance between cellular physiology and pathology.

## 4.4 References

1. Kilgore, H. R.; Young, R. A. Learning the Chemical Grammar of Biomolecular Condensates. *Nature Chemical Biology* **2022**, *18* (12), 1298–1306.

2. Alberti, S.; Hyman, A. A. Biomolecular Condensates at the Nexus of Cellular Stress, Protein Aggregation Disease and Ageing. *Nature Reviews Molecular Cell Biology* **2021**, *22* (3), 196–213.

3. Lyon, A. S.; Peeples, W. B.; Rosen, M. K. A Framework for Understanding the Functions of Biomolecular Condensates across Scales. *Nature Reviews Molecular Cell Biology* **2021**, *22* (3), 215–235.

4. Pappu, R. V.; Cohen, S. R.; Dar, F.; Farag, M.; Kar, M. Phase Transitions of Associative Biomacromolecules. *Chemical Reviews* **2023**, *123* (14), 8945–8987.

5. Mittag, T.; Pappu, R. V. A Conceptual Framework for Understanding Phase Separation and Addressing Open Questions and Challenges. *Molecular Cell* **2022**, *82* (12), 2201–2214.

6. Fuxreiter, M.; Vendruscolo, M. Generic Nature of the Condensed States of Proteins. *Nature Cell Biology* **2021**, *23* (6), 587–594.

7. Roden, C.; Gladfelter, A. S. RNA Contributions to the Form and Function of Biomolecular Condensates. *Nature Reviews Molecular Cell Biology* **2021**, *22* (3), 183–195.

8. Choi, J.-M.; Holehouse, A. S.; Pappu, R. V. Physical Principles Underlying the Complex Biology of Intracellular Phase Transitions. *Annual Review of Biophysics* **2020**, *49*, 107–133.

9. Dignon, G. L.; Best, R. B.; Mittal, J. Biomolecular Phase Separation: From Molecular Driving Forces to Macroscopic Properties. *Annual Review of Physical Chemistry* **2020**, *71* (1), 53–75.

10. Fu, L.; Weiskopf, E. N.; Akkermans, O.; Swanson, N. A.; Cheng, S.; Schwartz, T. U.; Görlich, D. HIV-1 Capsids Enter the FG Phase of Nuclear Pores like a Transport Receptor. *Nature* **2024**.

11. Boeynaems, S.; Chong, S.; Gsponer, J.; Holt, L.; Milovanovic, D.; Mitrea, D. M.; Mueller-Cajar, O.; Portz, B.; Reilly, J. F.; Reinkemeier, C. D.; Sabari, B. R.; Sanulli, S.; Shorter, J.; Sontag, E.; Strader, L.; Stachowiak, J.; Weber, S. C.; White, M.; Zhang, H.; Zweckstetter, M.; Elbaum-Garfinkle, S.; Kriwacki, R. Phase Separation in Biology and Disease; Current Perspectives and Open Questions. *Journal of Molecular Biology* **2023**, *435* (5), 167971.

12. Mohanty, P.; Kapoor, U.; Sundaravadivelu Devarajan, D.; Phan, T. M.; Rizuan, A.; Mittal, J. Principles Governing the Phase Separation of Multidomain Proteins. *Biochemistry* **2022**, *61* (22), 2443–2455.

13. Lee, D. S. W.; Strom, A. R.; Brangwynne, C. P. The Mechanobiology of Nuclear Phase Separation. *APL Bioengineering* **2022**, *6* (2), 021503.

14. Shapiro, D. M.; Ney, M.; Eghtesadi, S. A.; Chilkoti, A. Protein Phase Separation Arising from Intrinsic Disorder: First-Principles to Bespoke Applications. *The Journal of Physical Chemistry. B* **2021**, *125* (25), 6740–6759.

15. Banani, S. F.; Lee, H. O.; Hyman, A. A.; Rosen, M. K. Biomolecular Condensates: Organizers of Cellular Biochemistry. *Nature Reviews Molecular Cell Biology* **2017**, *18* (5), 285–298.

16. Brangwynne, C. P.; Tompa, P.; Pappu, R. V. Polymer Physics of Intracellular Phase Transitions. *Nature Physics* **2015**, *11* (11), 899–904.

17. Vernon, R. M.; Chong, P. A.; Tsang, B.; Kim, T. H.; Bah, A.; Farber, P.; Lin, H.; Forman-Kay, J. D. Pi-Pi Contacts Are an Overlooked Protein Feature Relevant to Phase Separation. *Elife* **2018**, *7*.

18. Ruff, K. M.; Choi, Y. H.; Cox, D.; Ormsby, A. R.; Myung, Y.; Ascher, D. B.; Radford, S. E.; Pappu, R. V.; Hatters, D. M. Sequence Grammar Underlying the Unfolding and Phase Separation of Globular Proteins. *Molecular Cell* **2022**, *82* (17), 3193-3208.e8.

19. Ditlev, J. A.; Case, L. B.; Rosen, M. K. Who's in and Who's out-Compositional Control of Biomolecular Condensates. *Journal of Molecular Biology* **2018**, *430* (23), 4666–4684.

20. Romero-Perez, P. S.; Dorone, Y.; Flores, E.; Sukenik, S.; Boeynaems, S. When Phased without Water: Biophysics of Cellular Desiccation, from Biomolecules to Condensates. *Chemical Reviews* **2023**, *123* (14), 9010–9035.

21. Sabari, B. R.; Dall'Agnese, A.; Young, R. A. Biomolecular Condensates in the Nucleus. *Trends in Biochemical Sciences* **2020**, *45* (11), 961–977.

22. Boeynaems, S.; Alberti, S.; Fawzi, N. L.; Mittag, T.; Polymenidou, M.; Rousseau, F.; Schymkowitz, J.; Shorter, J.; Wolozin, B.; Van Den Bosch, L.; Tompa, P.; Fuxreiter, M. Protein Phase Separation: A New Phase in Cell Biology. *Trends in Cell Biology* **2018**, *28* (6), 420–435. 1

23. Uversky, V. N. Intrinsically Disordered Proteins in Overcrowded Milieu: Membrane-Less Organelles, Phase Separation, and Intrinsic Disorder. *Current Opinion in Structural Biology* **2017**, *44*, 18–30.

24. Fare, C. M.; Villani, A.; Drake, L. E.; Shorter, J. Higher-Order Organization of Biomolecular Condensates. *Open Biology* **2021**, *11* (6), 210137.

25. Watson, J. L.; Seinkmane, E.; Styles, C. T.; Mihut, A.; Krüger, L. K.; McNally, K. E.; Planelles-Herrero, V. J.; Dudek, M.; McCall, P. M.; Barbiero, S.; Vanden Oever, M.; Peak-Chew, S. Y.; Porebski, B. T.; Zeng, A.; Rzechorzek, N. M.; Wong, D. C. S.; Beale, A. D.; Stangherlin, A.; Riggi, M.; Iwasa, J.; Morf, J.; Miliotis, C.; Guna, A.; Inglis, A. J.; Brugués, J.; Voorhees, R. M.; Chambers, J. E.; Meng, Q.-J.; O'Neill, J. S.; Edgar, R. S.; Derivery, E. Macromolecular Condensation Buffers Intracellular Water Potential. *Nature* **2023**, *623* (7988), 842–852.

26. Silva, J. L.; Foguel, D.; Ferreira, V. F.; Vieira, T. C. R. G.; Marques, M. A.; Ferretti, G. D. S.; Outeiro, T. F.; Cordeiro, Y.; de Oliveira, G. A. P. Targeting Biomolecular Condensation and Protein Aggregation against Cancer. *Chemical Reviews* **2023**, *123* (14), 9094–9138.

27. Ray, S.; Singh, N.; Kumar, R.; Patel, K.; Pandey, S.; Datta, D.; Mahato, J.; Panigrahi, R.; Navalkar, A.; Mehra, S.; Gadhe, L.; Chatterjee, D.; Sawner, A. S.; Maiti, S.; Bhatia, S.; Gerez, J. A.; Chowdhury, A.; Kumar, A.; Padinhateeri, R.; Riek, R.; Krishnamoorthy, G.;

Maji, S. K. α-Synuclein Aggregation Nucleates through Liquid-Liquid Phase Separation. *Nature Chemistry* **2020**, *12* (8), 705–716.

28. Wang, B.; Zhang, L.; Dai, T.; Qin, Z.; Lu, H.; Zhang, L.; Zhou, F. Liquid-Liquid Phase Separation in Human Health and Diseases. *Signal Transduction and Targeted Therapy* **2021**, *6* (1), 290.

29. Portz, B.; Lee, B. L.; Shorter, J. FUS and TDP-43 Phases in Health and Disease. *Trends in Biochemical Sciences* **2021**, *46* (7), 550–563.

30. Shin, Y.; Brangwynne, C. P. Liquid Phase Condensation in Cell Physiology and Disease. *Science* **2017**, *357* (6357), eaaf4382.

31. Dhakal, S.; Wyant, C. E.; George, H. E.; Morgan, S. E.; Rangachari, V. Prion-like CTerminal Domain of TDP-43 and α-Synuclein Interact Synergistically to Generate Neurotoxic Hybrid Fibrils. *Journal of Molecular Biology 2021* (10).

32. Guo, T.; Noble, W.; Hanger, D. P. Roles of Tau Protein in Health and Disease. *Acta Neuropathologica* **2017**, *133* (5), 665–704.

33. Mandelkow, E.-M.; Mandelkow, E. Biochemistry and Cell Biology of Tau Protein in Neurofibrillary Degeneration. *Cold Spring Harbor Perspectives in Medicine* **2012**, *2* (7), a006247.

34. Limorenko, G.; Lashuel, H. A. Revisiting the Grammar of Tau Aggregation and Pathology Formation: How New Insights from Brain Pathology Are Shaping How We Study and Target Tauopathies. *Chemical Society Reviews* **2022**, *51* (2), 513–565.

35. Rai, S. K.; Savastano, A.; Singh, P.; Mukhopadhyay, S.; Zweckstetter, M. Liquid-Liquid Phase Separation of Tau: From Molecular Biophysics to Physiology and Disease. *Protein Science* **2021**, *30* (7), 1294–1314.

36. Ambadipudi, S.; Biernat, J.; Riedel, D.; Mandelkow, E.; Zweckstetter, M. Liquid–Liquid Phase Separation of the Microtubule-Binding Repeats of the Alzheimer-Related Protein Tau. *Nature Communications* **2017**, *8* (1).

37. Majumdar, A.; Dogra, P.; Maity, S.; Mukhopadhyay, S. Liquid-Liquid Phase Separation Is Driven by Large-Scale Conformational Unwinding and Fluctuations of Intrinsically

Disordered Protein Molecules. *The Journal of Physical Chemistry Letters* **2019**, *10* (14), 3929–3936.

38. Kanaan, N. M.; Hamel, C.; Grabinski, T.; Combs, B. Liquid-Liquid Phase Separation Induces Pathogenic Tau Conformations in Vitro. *Nature Communications* **2020**, *11* (1), 2809.

39. Rai, S. K.; Khanna, R.; Avni, A.; Mukhopadhyay, S. Heterotypic Electrostatic Interactions Control Complex Phase Separation of Tau and Prion into Multiphasic Condensates and Co-Aggregates. *Proceedings of the National Academy of Sciences U.S.A.* **2023**, *120* (2).

40. Najafi, S.; Lin, Y.; Longhini, A. P.; Zhang, X.; Delaney, K. T.; Kosik, K. S.; Fredrickson, G. H.; Shea, J.-E.; Han, S. Liquid–Liquid Phase Separation of Tau by Self and Complex Coacervation. *Protein Science* **2021**, *30* (7), 1393–1407.

41. Boyko, S.; Surewicz, K.; Surewicz, W. K. Regulatory Mechanisms of Tau Protein Fibrillation under the Conditions of Liquid-Liquid Phase Separation. *Proceedings of the National Academy of Sciences U.S.A.* **2020**, *117* (50), 31882–31890.

42. Hernández-Vega, A.; Braun, M.; Scharrel, L.; Jahnel, M.; Wegmann, S.; Hyman, B. T.; Alberti, S.; Diez, S.; Hyman, A. A. Local Nucleation of Microtubule Bundles through Tubulin Concentration into a Condensed Tau Phase. *Cell Reports* **2017**, *20* (10), 2304–2312.

43. Chang, Y.-L.; Yang, C.-C.; Huang, Y.-Y.; Chen, Y.-A.; Yang, C.-W.; Liao, C.-Y.; Li, H.; Wu, C.-S.; Lin, C.-H.; Teng, S.-C. The HSP40 Family Chaperone Isoform DNAJB6b Prevents Neuronal Cells from Tau Aggregation. *BMC Biol.* **2023**, *21* (1).

44. Ryder, B. D.; Wydorski, P. M.; Hou, Z.; Joachimiak, L. A. Chaperoning Shape-Shifting Tau in Disease. *Trends in Biochemical Sciences* **2022**, *47* (4), 301–313.

45. Irwin, R.; Faust, O.; Petrovic, I.; Wolf, S. G.; Hofmann, H.; Rosenzweig, R. Hsp40s Play Complementary Roles in the Prevention of Tau Amyloid Formation. *Elife* **2021**, *10*.

46. Moll, A.; Ramirez, L. M.; Ninov, M.; Schwarz, J.; Urlaub, H.; Zweckstetter, M. Hsp Multichaperone Complex Buffers Pathologically Modified Tau. *Nature Communications* **2022**, *13* (1).

47. Kundel, F.; De, S.; Flagmeier, P.; Horrocks, M. H.; Kjaergaard, M.; Shammas, S. L.; Jackson, S. E.; Dobson, C. M.; Klenerman, D. Hsp70 Inhibits the Nucleation and Elongation of Tau and Sequesters Tau Aggregates with High Affinity. *ACS Chemical Biology* **2018**, *13* (3), 636–646.

48. Chakraborty, P.; Zweckstetter, M. P23-FKBP51 Chaperone Complex Regulates Tau Aggregation. *bioRxiv*, 2023.

49. Dou, F.; Netzer, W. J.; Tanemura, K.; Li, F.; Hartl, F. U.; Takashima, A.; Gouras, G. K.; Greengard, P.; Xu, H. Chaperones Increase Association of Tau Protein with Microtubules. *Proceedings of the National Academy of Sciences U.S.A.* **2003**, *100* (2), 721–726.

50. Li, J.; Qian, X.; Sha, B. Heat Shock Protein 40: Structural Studies and Their Functional Implications. *Protein and Peptide Letters* **2009**, *16* (6), 606–612.

51. Rosser, M. F. N.; Cyr, D. M. Do Hsp40s Act as Chaperones or Co-Chaperones? In *Networking of Chaperones by Co-Chaperones*; Springer New York: New York, NY, 2007; pp 38–51.

52. Muchowski, P. J.; Schaffar, G.; Sittler, A.; Wanker, E. E.; Hayer-Hartl, M. K.; Hartl, F. U. Hsp70 and Hsp40 Chaperones Can Inhibit Self-Assembly of Polyglutamine Proteins into Amyloid-like Fibrils. *Proceedings of the National Academy of Sciences U.S.A.* **2000**, *97* (14), 7841–7846.

53. Summers, D. W.; Douglas, P. M.; Ramos, C. H. I.; Cyr, D. M. Polypeptide Transfer from Hsp40 to Hsp70 Molecular Chaperones. *Trends in Biochemical Sciences* **2009**, *34* (5), 230–233.

54. Hochmair, J.; Exner, C.; Franck, M.; Dominguez-Baquero, A.; Diez, L.; Brognaro, H.; Kraushar, M. L.; Mielke, T.; Radbruch, H.; Kaniyappan, S.; Falke, S.; Mandelkow, E.; Betzel, C.; Wegmann, S. Molecular Crowding and RNA Synergize to Promote Phase Separation, Microtubule Interaction, and Seeding of Tau Condensates. *The EMBO Journal* **2022**, *41* (11).

55. Mok, S.-A.; Condello, C.; Freilich, R.; Gillies, A.; Arhar, T.; Oroz, J.; Kadavath, H.; Julien, O.; Assimon, V. A.; Rauch, J. N.; Dunyak, B. M.; Lee, J.; Tsai, F. T. F.; Wilson, M. R.; Zweckstetter, M.; Dickey, C. A.; Gestwicki, J. E. Mapping Interactions with the Chaperone

Network Reveals Factors That Protect against Tau Aggregation. *Nature Structural & Molecular Biology* **2018**, *25* (5), 384–393.

56. Zhang, X.; Zhang, S.; Zhang, L.; Lu, J.; Zhao, C.; Luo, F.; Li, D.; Li, X.; Liu, C. Heat Shock Protein 104 (HSP104) Chaperones Soluble Tau via a Mechanism Distinct from Its Disaggregase Activity. *The Journal of Biological Chemistry* **2019**, *294* (13), 4956–4965.

57. Ring, J.; Tadic, J.; Ristic, S.; Poglitsch, M.; Bergmann, M.; Radic, N.; Mossmann, D.; Liang, Y.; Maglione, M.; Jerkovic, A.; Hajiraissi, R.; Hanke, M.; Küttner, V.; Wolinski, H.; Zimmermann, A.; Domuz Trifunović, L.; Mikolasch, L.; Moretti, D. N.; Broeskamp, F.; Westermayer, J.; Abraham, C.; Schauer, S.; Dammbrueck, C.; Hofer, S. J.; Abdellatif, M.; Grundmeier, G.; Kroemer, G.; Braun, R. J.; Hansen, N.; Sommer, C.; Ninkovic, M.; Seba, S.; Rockenfeller, P.; Vögtle, F.-N.; Dengjel, J.; Meisinger, C.; Keller, A.; Sigrist, S. J.; Eisenberg, T.; Madeo, F. The HSP40 Chaperone Ydj1 Drives Amyloid Beta 42 Toxicity. *EMBO Molecular Medicine* **2022**, *14* (5).

58. Hardenberg, M.; Horvath, A.; Ambrus, V.; Fuxreiter, M.; Vendruscolo, M., Widespread occurrence of the droplet state of proteins in the human proteome. *Proceedings of the National Academy of Sciences U.S.A.* **2020**, *117* (52), 33254-33262.

59. Abbas, M.; Lipiński, W. P.; Wang, J.; Spruijt, E. Peptide-Based Coacervates as Biomimetic Protocells. *Chemical Society Reviews* **2021**, *50* (6), 3690–3705.

60. Pak, C. W.; Kosno, M.; Holehouse, A. S.; Padrick, S. B.; Mittal, A.; Ali, R.; Yunus, A. A.; Liu, D. R.; Pappu, R. V.; Rosen, M. K. Sequence Determinants of Intracellular Phase Separation by Complex Coacervation of a Disordered Protein. *Molecular Cell* **2016**, *63* (1), 72–85.

61. Chang, L.-W.; Lytle, T. K.; Radhakrishna, M.; Madinya, J. J.; Vélez, J.; Sing, C. E.; Perry, S. L. Sequence and Entropy-Based Control of Complex Coacervates. *Nature Communications* **2017**, *8* (1).

62. Holehouse, A.S.; Das, R. K.; Ahad, J. N.; Richardson, M. O.; Pappu, R. V., CIDER: Resources to Analyze Sequence-Ensemble Relationships of Intrinsically Disordered Proteins. *Biophysical Journal* **2017**, *112* (1), 16-21.

63. Ou, Z.; Muthukumar, M. Entropy and Enthalpy of Polyelectrolyte Complexation: Langevin Dynamics Simulations. *The Journal of Chemical Physics* **2006**, *124* (15).

64. Li, J.; Qian, X.; Sha, B. The Crystal Structure of the Yeast Hsp40 Ydj1 Complexed with Its Peptide Substrate. *Structure* **2003**, *11* (12), 1475–1483.

65. Chakraborty, P.; Ibáñez de Opakua, A.; Purslow, J. A.; Fromm, S. A.; Chatterjee, D.; Zachrdla, M.; Puri, S.; Wolozin, B.; Zweckstetter, M. GSK3β Phosphorylation Catalyzes the Aggregation of Tau into Alzheimer's Disease-like Amyloid Strain. *bioRxiv*, 2023.

66. Wegmann, S.; Eftekharzadeh, B.; Tepper, K.; Zoltowska, K. M.; Bennett, R. E.; Dujardin, S.; Laskowski, P. R.; MacKenzie, D.; Kamath, T.; Commins, C.; Vanderburg, C.; Roe, A. D.; Fan, Z.; Molliex, A. M.; Hernandez-Vega, A.; Muller, D.; Hyman, A. A.; Mandelkow, E.; Taylor, J. P.; Hyman, B. T. Tau Protein Liquid-Liquid Phase Separation Can Initiate Tau Aggregation. *The EMBO Journal* **2018**, *37* (7).

67. Amadoro, G.; Corsetti, V.; Stringaro, A.; Colone, M.; D'Aguanno, S.; Meli, G.; Ciotti, M.; Sancesario, G.; Cattaneo, A.; Bussani, R.; Mercanti, D.; Calissano, P. A NH2 Tau Fragment Targets Neuronal Mitochondria at AD Synapses: Possible Implications for Neurodegeneration. *Journal of Alzheimer's Disease* **2010**, *21* (2), 445–470.

68. Gu, J.; Xu, W.; Jin, N.; Li, L.; Zhou, Y.; Chu, D.; Gong, C.-X.; Iqbal, K.; Liu, F. Truncation of Tau Selectively Facilitates Its Pathological Activities. *The Journal of Biological Chemistry* **2020**, *295* (40), 13812–13828.

69. Rhine, K.; Vidaurre, V.; Myong, S. RNA Droplets. *Annual Review of Biophysics* **2020**, *49* (1), 247–265.

70. Sanders, D. W.; Kedersha, N.; Lee, D. S. W.; Strom, A. R.; Drake, V.; Riback, J. A.; Bracha, D.; Eeftens, J. M.; Iwanicki, A.; Wang, A.; Wei, M.-T.; Whitney, G.; Lyons, S. M.; Anderson, P.; Jacobs, W. M.; Ivanov, P.; Brangwynne, C. P. Competing Protein-RNA Interaction Networks Control Multiphase Intracellular Organization. *Cell* **2020**, *181* (2), 306-324.e28.

71. Banerjee, P. R.; Milin, A. N.; Moosa, M. M.; Onuchic, P. L.; Deniz, A. A. Reentrant Phase Transition Drives Dynamic Substructure Formation in Ribonucleoprotein Droplets. *Angewandte Chemie (International Ed. in English)* **2017**, *56* (38), 11354–1135.

72. Alshareedah, I.; Moosa, M. M.; Raju, M.; Potoyan, D. A.; Banerjee, P. R. Phase Transition of RNA−protein Complexes into Ordered Hollow Condensates. *Proceedings of the National Academy of Sciences U.S.A 2020* (27), 15650–15658.

73. Rinaldi, A. J.; Suddala, K. C.; Walter, N. G. Native Purification and Labeling of RNA for Single Molecule Fluorescence Studies. In *RNA-RNA Interactions*; Springer New York: New York, NY, 2015; pp 63–95.

74. Yewdall, N. A.; André, A. A. M.; van Haren, M. H. I.; Nelissen, F. H. T.; Jonker, A.; Spruijt, E. ATP:Mg2+ Shapes Material Properties of Protein-RNA Condensates and Their Partitioning of Clients. *Biophysical Journal* **2022**, *121* (20), 3962–3974.

75. Ukmar-Godec, T.; Hutten, S.; Grieshop, M. P.; Rezaei-Ghaleh, N.; Cima-Omori, M. S.; Biernat, J.; Mandelkow, E.; Söding, J.; Dormann, D.; Zweckstetter, M. Lysine/RNAinteractions Drive and Regulate Biomolecular Condensation. *Nature Communications* **2019**, *10* (1).

76. Erkamp, N. A.; Sneideris, T.; Ausserwöger, H.; Qian, D.; Qamar, S.; Nixon-Abell, J.; St George-Hyslop, P.; Schmit, J. D.; Weitz, D. A.; Knowles, T. P. J. Spatially Non-Uniform Condensates Emerge from Dynamically Arrested Phase Separation. *Nature Communications* **2023**, *14* (1).

77. Karagöz, G. E.; Duarte, A. M. S.; Akoury, E.; Ippel, H.; Biernat, J.; Morán Luengo, T.; Radli, M.; Didenko, T.; Nordhues, B. A.; Veprintsev, D. B.; Dickey, C. A.; Mandelkow, E.; Zweckstetter, M.; Boelens, R.; Madl, T.; Rüdiger, S. G. D. Hsp90-Tau Complex Reveals Molecular Basis for Specificity in Chaperone Action. *Cell* **2014**, *156* (5), 963–974.

78. Weickert, S.; Wawrzyniuk, M.; John, L. H.; Rüdiger, S. G. D.; Drescher, M. The Mechanism of Hsp90-Induced Oligomerizaton of Tau. *Science Advances* **2020**, *6* (11).

79. Mukrasch, M. D.; Bibow, S.; Korukottu, J.; Jeganathan, S.; Biernat, J.; Griesinger, C.; Mandelkow, E.; Zweckstetter, M. Structural Polymorphism of 441-Residue Tau at Single Residue Resolution. *PLoS Biology* **2009**, *7* (2), e1000034.

80. Elbaum-Garfinkle, S.; Rhoades, E. Identification of an Aggregation-Prone Structure of Tau. *Journal of the American Chemical Society* **2012**, *134* (40), 16607–16613.

81. Chen, D.; Drombosky, K. W.; Hou, Z.; Sari, L.; Kashmer, O. M.; Ryder, B. D.; Perez, V. A.; Woodard, D. R.; Lin, M. M.; Diamond, M. I.; Joachimiak, L. A. Tau Local Structure Shields an Amyloid-Forming Motif and Controls Aggregation Propensity. *Nature Communications* **2019**, *10* (1).

82. Melo, A. M.; Coraor, J.; Alpha-Cobb, G.; Elbaum-Garfinkle, S.; Nath, A.; Rhoades, E. A Functional Role for Intrinsic Disorder in the Tau-Tubulin Complex. *Proceedings of the National Academy of Sciences U.S.A.* **2016**, *113* (50), 14336–14341.

83. Wen, J.; Hong, L.; Krainer, G.; Yao, Q.-Q.; Knowles, T. P. J.; Wu, S.; Perrett, S. Conformational Expansion of Tau in Condensates Promotes Irreversible Aggregation. *Journal of the American Chemical Society* **2021**, *143* (33), 13056–13064.

84. Elbaum-Garfinkle, S.; Cobb, G.; Compton, J. T.; Li, X.-H.; Rhoades, E. Tau Mutants Bind Tubulin Heterodimers with Enhanced Affinity. *Proceedings of the National Academy of Sciences U.S.A.* **2014**, *111* (17), 6311–6316.

85. Joshi, A.; Walimbe, A.; Avni, A.; Rai, S. K.; Arora, L.; Sarkar, S.; Mukhopadhyay, S. Single-Molecule FRET Unmasks Structural Subpopulations and Crucial Molecular Events during FUS Low-Complexity Domain Phase Separation. *Nature Communications* **2023**, *14* (1).

86. Mullapudi, V.; Vaquer-Alicea, J.; Bommareddy, V.; Vega, A. R.; Ryder, B. D.; White, C. L.; Diamond, M. I.; Joachimiak, L. A. Network of Hotspot Interactions Cluster Tau Amyloid Folds. *Nature Communications* **2023**, *14* (1), 895.

87. Galvanetto, N.; Ivanović, M. T.; Chowdhury, A.; Sottini, A.; Nüesch, M. F.; Nettels, D.; Best, R. B.; Schuler, B. Extreme Dynamics in a Biomolecular Condensate. *Nature* **2023**, *619* (7971), 876–883.

# CHAPTER 5

# Conclusions and Future Perspectives

Cellular compartmentalization is a vital aspect of the cellular environment and plays a fundamental role in preserving the functional integrity of a cell. In this regard, the formation of membraneless biomolecular condensates formed via the physical process of phase separation has emerged as an essential paradigm in modulating the spatiotemporal coherence of the crowded cellular milieu. These non-canonical biological condensates have emerged at the forefront of most cellular activities and are often driven by transient, multivalent interactions amongst intrinsically disordered proteins or regions, both in the absence and presence of nucleic acids. Further, the network of interactions amongst the components of such condensates is essential in preserving their typically liquid-like nature. In this regard, the electrostatically-driven associative phase separation of single biomacromolecules (simple coacervation) or between two or more oppositely-charged species (complex coacervation) is particularly crucial for biological function, depending on the identity of the species recruited in such condensates. Notwithstanding, cellular stress-mediated aberrant phase transitions can modify the material properties of condensates, transforming them into solid amyloid-like aggregates in the process. The cascade of events that leads to such transformations is particularly typical for neuronal proteins implicated in neurodegenerative disorders that are often wholly or partially disordered.

The work described in this thesis dissects the molecular basis for the heterotypic phase transitions of one such neuronal IDP, the microtubule-associated protein tau. We have provided a structural description of the associative phase transitions of the tau protein, pertaining to its interactions with other critical cellular interactors that modulate its phase behavior, both in the context of disease and physiology. Briefly, I summarize:

- Heterotypic electrostatic interactions play a pivotal role in governing the complex phase separation of tau and the human prion protein, which can be modulated to form multiphasic condensates and co-aggregates. (Chapter 3)
- The mechanistic underpinnings governing the modulation of tau phase behavior by a critical component of the cellular protein quality machinery, Hsp40. (Chapter 4)

The emergence of overlapping neuropathological features in the etiology of several neurodegenerative diseases is indicative of the cross-talk between non-related amyloidogenic proteins. In this regard, the accumulation of tau with another IDP, α-synuclein (α-Syn), in the brains of patients afflicted by Parkinson's disease hints toward their synergistic interactions. Tau protein deposits have also been found in the brains of patients affected by Prion-Protein cerebral amyloid angiopathy (PrP-CAA). These patients displayed a highly unstructured PrP variant due to a nonsense mutation (Q160X) in the PRNP gene, leading to premature translation

termination. Additionally, Gerstmann-Sträussler-Scheinker (GSS) syndrome is also attributed partly to tau deposits, where a missense mutation in the PRNP gene leads to an amino acid switch at residue 198 (F198S) of PrP. Inspired by these findings and to investigate the effect of other neuronal proteins on tau phase separation, we studied the direct interaction between tau and the human prion protein. In this work, we dissected the domain-specific electrostatically controlled heterotypic phase separation of tau and PrP to form dynamic droplets that showed the perfect colocalization of both proteins (Chapter 3). Our results suggested the formation of a highly viscoelastic network amongst the two proteins upon condensation, suggesting an increase in the phase separation propensity of tau in the presence of PrP. We provided a molecular basis for the interactions of these proteins using domain-specific mutants, suggesting that this process is electrostatically driven. Additionally, our site-specific picosecond time-resolved fluorescence measurements revealed the formation of ordered electrostatic nano-clusters of tau and PrP. At a longer timescale, our single-droplet FCS and FRAP data further corroborate our measurements towards establishing a liquid-like nature of these condensates. Moreover, we show that the morphology of these droplets can be tuned in the presence of varying concentrations of RNA to form multiphasic condensates reminiscent of the nucleolar architecture. Further, with aging, we observed the co-aggregation of tau and PrP into hetero-aggregates comprising amyloid-like species. Collectively, our work reveals a fascinating interplay among molecular factors that facilitate and control the heterotypic phase transition, multiphasic coacervation, and maturation into intermixed ordered aggregates. This underscores the molecular foundation of intersecting neurodegenerative diseases that involve tau and PrP.

Disease-associated pathogenic amyloid aggregates of tau are involved in almost twenty-five different tau-related neuronal disorders, collectively termed tauopathies. Studies have shown that tau can misfold into multiple conformational states, each related to one or more of these diseases. In cells, a dedicated network of molecular chaperones forms the protein quality control machinery (PQC), which is responsible for aiding the proper folding of almost all proteins, including misfolded ones, in addition to clearing misfolded species that might prove to be toxic. Heat shock proteins are essential components of the PQC and are known to bind to different conformations of amyloid-forming IDPs, including tau. Tau aggregation is known to be accelerated several folds upon its phase separation, due to the densely concentrated environment of this condensate. However, the role of Hsps in this regard remains elusive. Here, using a combination of different biochemical and biophysical tools, we probed the structural

changes in phase-separated tau in the presence of a yeast homolog of Human Hsp40, Ydj1 (Chapter 4). Our work suggests the enhancement of tau phase separation in the presence of Hsp40 to form dynamic, perfectly miscible droplets. Additionally, tau-Ydj1 condensates display a thermoresponsive behavior and can be modulated by the presence of salt. Using domain-specific variants, we further delineated the role of a combination of hydrophobic and electrostatic interactions in driving this condensation. Moreover, we also characterized the role of two amyloid motifs in the tau repeat region in steering these interactions. Interestingly, we identified a role for the PHF6 amyloid motif present between the second and third repeats of tau ($^{306}$VQIVYK$^{311}$) in nucleating tau phase separation, potentially by the formation of transient beta-rich structures, which is abrogated upon the deletion of this motif. We also observed a typical reentrant behavior of tau-Ydj1 condensates in the presence of RNA. Using a combination of steady-state and time-resolved fluorescence measurements both at an ensemble and single-molecular level, we observed the opening of the tau MTBR region upon phase separation, leading to the exposure of the amyloid-motifs, which is responsible for augmenting material-change coupled amyloid-formation, in line with previous results. However, the binding of Hsp40 at this very region protects tau from establishing interchain contacts, consequently abrogating aggregation. Due to the fuzzy nature of this interaction, the transient tau interchain contacts that are established lead to the formation of small protein conglomerates instead of potentially pathogenic aggregates. Our results, therefore, establish that the conformational transition of tau from a closed paperclip to an open configuration is the structural basis for its interactions with Ydj1. This emphasizes the importance of the conformational plasticity of intrinsically disordered proteins in maintaining their functional state in biological systems.

We believe that the work carried out in this thesis represents a concerted effort to advance our current perspective on the underlying role of phase separation in promoting the molecular interaction networks orchestrated by intrinsically disordered proteins, exemplified by tau in the biological milieu. The extension of these investigations *in vivo* or to pertinent model systems can pave the way for delineating the role of associative phase transitions in the context of overlapping neuropathology and the functional aspects of the spatiotemporal regulation of biological condensates. Exploring these intricate pathways can provide empirical insights into the applicability and physiological relevance of phase separation phenomena. In conclusion, the work described in this thesis has implications in basic biology and offers prospects for the development of targeted therapeutic interventions.